FLOW RESISTANCE AND ASSOCIATED BACKWATER EFFECT DUE TO SPUR DIKES IN OPEN CHANNELS

A Thesis Submitted to the

College of Graduate Studies and Research

In Partial Fulfillment of the Requirements for the

Degree of Doctor of Philosophy

In the

Department of Civil and Geological Engineering

University of Saskatchewan

Saskatoon

By

Hossein Azinfar

PERMISSION TO USE

In presenting this thesis/dissertation in partial fulfillment of the requirements for a Postgraduate degree from the University of Saskatchewan, I agree that the Libraries of this University may make it freely available for inspection. I further agree that permission for copying of this thesis/dissertation in any manner, in whole or in part, for scholarly purposes may be granted by Dr. J.A. Kells who supervised my thesis/dissertation work or, in his absence, by the Head of the Department of Civil and Geological Engineering or the Dean of the College of Graduate Studies and Research in which my thesis work was done. It is understood that any copying or publication or use of this thesis/dissertation or parts thereof for financial gain shall not be allowed without my written permission. It is also understood that due recognition shall be given to me and to the University of Saskatchewan in any scholarly use which may be made of any material in my thesis/dissertation.

Requests for permission to copy or to make other uses of materials in this thesis/dissertation in whole or part should be addressed to:

Head of the Department of Civil and Geological Engineering

University of Saskatchewan

57 Campus Drive

Saskatoon, Saskatchewan S7N 5A9

Canada

OR

Dean

College of Graduate Studies and Research

University of Saskatchewan

107 Administration Place

Saskatoon, Saskatchewan S7N 5A2

Canada

Abstract

A spur dike is a hydraulic structure built on the bank of a river at some angle to the main flow direction. A series of spur dikes in a row may also be placed on one side or both sides of a river to form a spur dike field. Spur dikes are used for two main purposes, namely river training and bank protection. For river training, spur dikes may be used to provide a desirable path for navigation purposes or to direct the flow to a desirable point such as a water intake. For bank protection, spur dikes may be used to deflect flow away from a riverbank and thus protect it from erosion. It has also been observed that spur dikes provide a desirable environment for aquatic habitat. Despite the fact that spur dikes are useful hydraulic structures, they have been found to increase the flow resistance in rivers and hence increase the flow stage. The present study focuses on the quantification of the flow resistance and associated flow stage increase due to a single spur dike and also that of a spur dike field. Increased flow stage is referred to herein as a backwater effect.

In the first stage of the study, the flow resistance due to a single spur dike, expressed as a drag force exerted on the flow in an open channel, was studied and quantified. The work was carried out in a rigid bed flume, with the model spur dike being simulated using various sizes of a two-dimensional (2-D) rectangular plate. Several discharge conditions were studied. The drag force exerted by the spur dike for both submerged and unsubmerged flow conditions was determined directly from measurements made using a specially designed apparatus and also by application of the momentum equation to a control volume that included the spur dike. It was found that the unit drag force (i.e., drag force per unit area of dike) of an unsubmerged spur dike increases more rapidly with an increase in the discharge when compared with that of a submerged spur dike. The results also showed that an increase in the blockage of the open channel cross-section due to the spur dike is the main parameter responsible for an increase in the spur dike drag coefficient, hence the associated flow resistance and backwater effect. Based on these findings, relationships were developed for estimating the backwater effect due to a single spur dike in an open channel.

In the second stage of the study, the flow resistance due to a spur dike field expressed as a drag force exerted on the flow was quantified and subsequently related to the backwater

effect. The work was carried out in a rigid bed flume, with the model spur dikes simulated using 2-D, rectangular plates placed along one side of the flume. For various discharges, the drag force of each individual spur dike in the spur dike field was measured directly using a specially-designed apparatus. For these tests, both submerged and unsubmerged conditions were evaluated along with various numbers of spur dikes and various relative spacings between the spur dikes throughout the field. It was concluded that the configuration of a spur dike field in terms of the number of spur dikes and relative spacing between the spur dikes has a substantial impact on the drag force and hence the flow resistance and backwater effect of a spur dike field. The most upstream spur dike had the highest drag force amongst the spur dikes in the field, and it acted as a shield to decrease the drag force exerted by the downstream spur dikes. From the experiments on the submerged spur dikes, it was observed that the jet flow over the spur dikes has an important effect on the flow structure and hence the flow resistance.

In the third stage of the study, the flow field within the vicinity of a single submerged spur dike was modeled using the three-dimensional (3-D) computational fluid dynamic (CFD) software FLUENT. Application of the software required solution of the 3-D Reynolds-averaged Navier-Stokes equations wherein the Reynolds stresses were resolved using the RNG κ-ε turbulence model. One discharge condition was evaluated in a smooth, rectangular channel for two conditions, including uniform flow conditions without the spur dike in place and one with the spur dike in place. The CFD model was evaluated based on some experimental data acquired from the physical model. It was found that the CFD model could satisfactorily predict the flow resistance and water surface profile adjacent to the spur dike, including the resulting backwater effect. Furthermore, the CFD model gave a good prediction of the velocity field except for the area behind the spur dike where the effects of diving jet flow over the spur dike was not properly modeled.

Acknowledgements

I would like to give grace to God for giving me an opportunity to acquire an advanced level of education. I would like to thank my wife, Bita Moazed, for her unwavering support during the many long days of my Ph.D. program. I would like to thank God again for bringing an enjoyment to my life with my son, Armin, who was born during my Ph.D. program.

I wish to express my sincere gratitude and appreciation to my supervisor, Dr. James A. Kells, for his invaluable guidance, support and encouragement throughout the course of my Ph.D. program. His critical appraisal and suggestions have always been quite helpful at all stages of this research. I would like especially to thank him for being a patient listener to me.

I am greatly thankful to my advisory committee members, Dr. James Bugg, Dr. Kerry Mazurek and Dr. David Sumner, for their valuable suggestions and feedback. The time, encouragement and support of my advisory committee chair, Dr. Gordon Putz, is greatly appreciated.

I take this opportunity to thank Mr. Dale Pavier and Mr. Brennan Pokoyoway for their assistance and help throughout the laboratory program of my research. Also, I would like to thank Dr. Bruce Sparling for his help in the design of the drag force measurement apparatus, and the staff in Engineering Shops for fabricating the apparatus. Financial support from the Natural Sciences and Engineering Research Council of Canada through a grant to my supervisor and a scholarship from the University of Saskatchewan are also acknowledged.

Dedication

I dedicate this thesis to my loving wife, Bita Moazed, my precious son, Armin, my parents, Mohammad and Zahra, my brother and sisters

Table of Contents

List of Tables

List of Figures

Notation

$\bar{A}$	Average flow area in a spur dike field
a,…,d	Exponents in regression equation
A_r	Blockage ratio
A_s	Upstream projected area of spur dike /object
$A_{s\alpha}$	Upstream projected area of spur dike with orientation α
A_t	Cross-sectional area of a wind tunnel
B	Width of flume / open channel
b	Opening width of an open channel
C	Chezy coefficient
$c_{1...}c_4$	Constants in regression analysis
C_{base}	Base Chezy coefficient
C_D	Drag coefficient due to spur dike
C_{Do}	Base drag coefficient
$C_{D\alpha}$	Drag coefficient of angled spur dike
C_L	Coefficient of head loss
C_p	A function of h/P
C_s	Constant of the roughness function (= 0.5)
C_μ	Constant of turbulent viscosity (= 0.09)
D	Wind tunnel height
d	Diameter of a bridge pier / a plate length
E	Constant of the standard wall function (= 9.79)
e_p	Ratio of the total cross sectional area of a bridge piers to the total contracted area
e_r	Opening ratio

F	Force due to normal depth pressure distribution
F_1	Force due to upstream hydrostatic pressure distribution
F_2	Force due to downstream hydrostatic pressure distribution
F_3	Force due to upstream hydrostatic pressure distribution for a spur dike field
F_D	Drag force due to spur dike / object
F_{Da}	Drag force of the second spur dike beyond the critical spacing zone
F_{Db}	Drag force of the second spur dike in the critical spacing zone
F_{Df}	Total drag force due to a spur dike field
F_{Di}	Drag force due to i^{th} spur dike in a spur dike field
F_{Dt}	Total drag force due to all spur dikes in a spur dike field
$F_{D\alpha}$	Component of drag force in flow direction with orientation α
F_{ef}	Excess force (F_{wf} - F_{ff})
F_f	Force due to boundary friction
F_{ff}	Friction force due to boundary friction of a spur dike field
f_i	Function of
Fr	Froude number of the normal flow depth
Fr_1	Froude number of flow upstream of spur dike
Fr_2	Froude number of flow downstream from spur dike
F_u	Force due to upstream depth pressure distribution
F_{vof}	Volume of fluid
F_w	Component of weight of fluid in flow direction
F_{wf}	Component of weight of the fluid in flow direction for a spur dike field
g	Acceleration due to gravity (i.e., 9.81 m^2/s)
g^i	Gravitational acceleration in i-direction
H	Total flow head above the crest of the spur dike

h Normal flow depth

h_1 Depth of flow upstream of spur dike (approach flow depth)

h_2 Depth of flow downstream from spur dike (uniform flow depth)

h_3 Depth of flow upstream of a spur dike field

h_b Bridge deck thickness

H_G Total height of the flow relative to a reference elevation (hydraulic grade line)

h_g Flow depth in the spur dike field zone

h_L Energy loss due to an object

h_u Upstream flow depth

i Water surface slope

K Constant in regression analysis

k Turbulent kinetic energy

k_1 A function of flow conditions, channel and spur dike geometries for a spur dike field

k_2 $= 2Fr_2^{\ 2}$

K_D Relative drag force of a plate

K_s Physical roughness height

K_s^+ Non-dimensional roughness height

L Length of spur dike / plate

L_r Length of control volume of a spur dike field

L_o Distance between upstream and downstream of an object in a control volume

M Mass of standard weights

m Number of spur dikes in a spur dike field

P Height of spur dike / plate

P_t Total pressure

P_w Wetted perimeter of flow in control volume

Q Volumetric discharge

q Unit discharge (Q/B)

R Hydraulic radius

R^2 Square of the correlation coefficient

R_{e1} Reynolds number of flow upstream of spur dike (approach flow)

S Spacing between spur dikes in a spur dike field

s Thickness of bridge deck

S_f Energy slope of flow

$\overline{S}_f$ Average energy slope of the flow in an open channel

S_L Spacing of plates in succession

S_o Slope of an open channel

t Time

u Flow velocity in streamwise direction

u_{gr} Velocity in the spur dike field zone

u^i Velocity in x^i direction

uF_D Uncertainty of a single spur dike

uF_{Di} Uncertainty of i^{th} spur dike in a spur dike field

U_m Maximum velocity of the main flow zone adjacent to a spur dike

u_{mc} Main channel flow velocity in the presence of a spur dike field

U_o Maximum negative transverse velocity behind a spur dike

u_p Mean flow velocity at point p

uY Uncertainty of a dependent parameter

uX_i Uncertainty of the i^{th} independent parameter

$u\eta_i$ Uncertainty of the relative drag force due to i^{th} spur dike in a spur dike field

$u\eta_t$	Uncertainty of the total relative drag force in a spur dike field
u_*	Mean bed shear velocity
$u_*(z)$	Local bed shear velocity
V	Average velocity in normal depth region
v	Flow velocity in vertical direction
V_1	Average velocity upstream of spur dike
V_2	Average velocity downstream from spur dike
V_3	Average velocity upstream of a spur dike field
V_{imp}	Average impingement velocity
V_u	Average velocity in upstream depth region
W	Plate thickness
w	Flow velocity in transverse direction
x	Distance from the flume inlet
Xi	Cross-section i perpendicular to x coordinate
X_i	i^{th} independent parameter
Y	Dependent parameter in uncertainty analysis
y	Distance from channel bed
Yi	Cross-section i perpendicular to y coordinate
y_0	Distance from bed at which velocity is hypothetically equal to zero
y_p	Normal distance from the wall
Z	Side slope
z	Distance from channel wall
Zi	Cross-section i perpendicular to z coordinate
α	Angle between spur dike and channel wall
α_n	Energy correction factor in normal depth region

α_u Energy correction factor in upstream depth region

β_1 Momentum correction factor upstream of spur dike

β_2 Momentum correction factor downstream from spur dike

β_3 Momentum correction factor upstream of a spur dike field

β_n Momentum correction factor in normal depth region

β_u Momentum correction factor in upstream depth region

γ Specific weight of fluid

Δ Shape factor

ΔB A roughness function

Δh Backwater effect of a spur dike

δ Velocity deviation parameter

δh Backwater effect of an object

δ^{ij} Kronecker delta

ε Turbulence dissipation rate per unit mass

η_i Relative drag force for the i^{th} spur dike in a spur dike field

η_t Total relative drag force for a spur dike field

θ Impingement velocity parameter $\left(V_{imp}/V_1\right)^2$

κ von Karman constant

μ Dynamic viscosity

$\mu\varepsilon$ Micro-strain

ν Molecular kinematic viscosity

ν_t Turbulent kinematic viscosity

ξ A function of turbulence intensity and plate slenderness

ρ Fluid density

ρ_{air} Density of air

ρ_{water}	Density of water
τ	Average shear stress at flow boundary
τ^{ij}	Shear stress tensor
τ_o	Bed shear stress
τ_w	Side wall shear stress
φ_1	Drag coefficient expressed in terms of aspect ratio
φ_2	Drag coefficient expressed in terms of opening ratio
φ_3	Drag coefficient expressed in terms of submergence ratio
φ_4	Drag coefficient expressed in terms of Froude number
Ω_{air}	Volume of the computational cell filled with air
Ω_{cell}	Computational cell volume
Ω_{water}	Volume of the computational cell filled with water

Chapter 1. Introduction

1.1. Background

Spur dikes are hydraulic structures that project from the bank of a stream at some angle to the main flow direction. They are used for two purposes, namely river training and erosion protection of the riverbank. With respect to river training, the primary objective is to improve the navigability of a river by providing a sufficient depth of flow and a desirable channel alignment. Spur dikes also serve to increase the sediment transport rate through the diked reach, which decreases channel dredging costs. With respect to erosion protection, spur dikes can be designed to protect both straight reaches and channel bends. Compared with other methods, such as revetments, spur dikes are among the most economical structures that may be used for riverbank erosion protection (Shields, 1995).

There are several terms used for spur dikes in the literature, such as groins (or groynes), wing dams, transverse dikes, cross dikes, contracting dikes, spur dams, cross dams, spurs, navigational dikes, jetties, bendway weirs and barbs (e.g., USACE, 1980; Rajaratnam and Nwachukwu, 1983; Richardson and Simons, 1984; Ouillon and Dartus, 1997; Pinter et al., 2001; Minor et al., 2007). The term spur dike has been used throughout the present thesis document.

The construction of spur dikes on rivers creates a complicated bed profile, including local pools and riffles and also various flow features adjacent to the structure, which is often very valuable for aquatic habitat (e.g., Hendrickson and Schneider, 1999; Tamai et al., 1996; Shields, 1995). Spur dikes may be built as a single structure, namely a single spur dike, or as a series of spur dikes built in a row, along one or both sides of a river, as a spur dike field. Figure 1.1 shows an example of a single spur dike and Figure 1.2 shows two examples of spur dike fields.

Figure 1.1. Single spur dike on the South Saskatchewan River in the vicinity of the Pike Lake water intake (*Provided by Saskatchewan Watershed Authority*)

(a) (b)

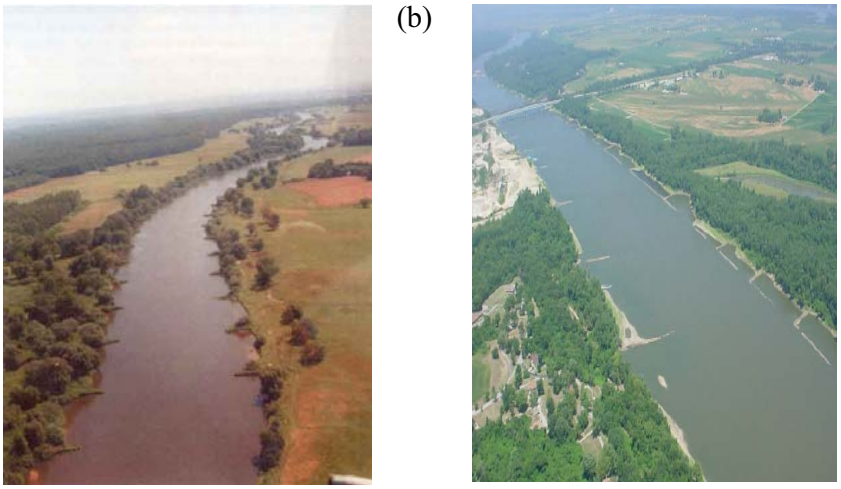

Figure 1.2. Spur dike fields; (a) Odra River in Poland (*Taken from iihr.uiowa.edu*), and (b) Missouri River, North of Saint Louis (*Taken from Criss, 2002*)

Despite their useful features, there is some concern that spur dikes may be responsible for increased flooding due to the associated backwater effect. Studies show that, over the past century, flood stages for given discharges at various locations along the Middle Mississippi and Lower Missouri rivers have increased by 2 m to 4 m (Criss and Shock, 2001). These river reaches are characterized by extensive river engineering works, including spur dikes and levees. Since levees are usually built to levels higher than the bankfull stage, Pinter et al. (2001) concluded that, for such rivers, observed stage increases for flows less than the bankfull discharge can be attributed to spur dikes. Stage increases due to spur dikes

have also been reported on the Rhine River in Europe. There, it has subsequently been decided to reduce the height of the spur dikes as a way of reducing their adverse effects during times of flooding (Belz et al., 2001; Yossef, 2002). In a study in China, Wu et al. (2005) have observed the backwater effect of long spur dikes constructed on the Lower Yellow River. Similarly, in a study on the Nile River in Egypt, it was concluded that the construction of spur dikes would have a considerable effect on upstream water levels (Soliman et al., 1997). In spite of the impact that the construction of spur dikes has on river flood stages, the backwater effect due to spur dikes is usually neglected in their design.

1.2. Spur dike design parameters

The most important parameters usually considered in the design of spur dikes include plan view shape, crest elevation, crest profile, length, spacing between adjacent spur dikes, angle of the spur dikes relative to the flow and bank, construction materials, cross section, depth of scour and riprap size (Franco, 1967; Richardson et al., 1975; Brown, 1984; Yossef, 2002). Figure 1.3 represents some of the most important spur dike design parameters.

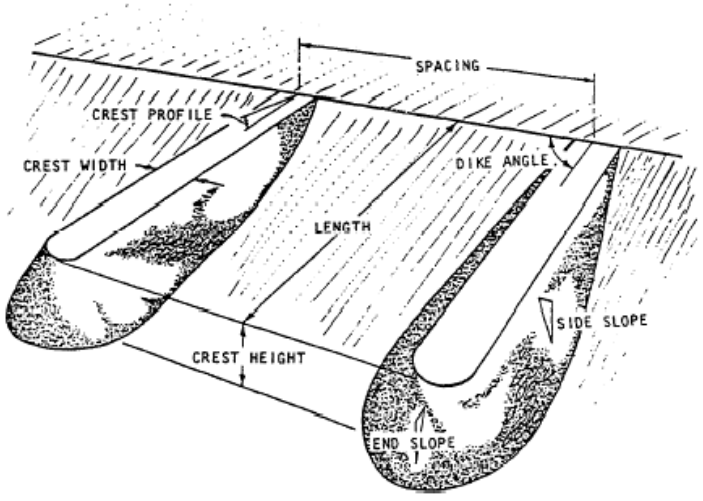

Figure 1.3. Schematic illustration of a spur dike field showing the most important design parameters (*Taken from USACE, 1980*)

The most widespread and cost efficient plan view shape of a spur dike is a straight line. Other shapes of spur dikes in plan view include an L-head shape, a T-head shape, and a J-shape or inverted T-shape (Ahmad, 1953; Fenwick, 1969; Richardson et al., 1975; USACE,

1980; Richardson and Simons, 1984; Shields, 1995). The basic design of a submerged spur dike requires that the crest of the dike is at a constant elevation equal to the low-water elevation (Franco, 1967). For bank protection, the crest elevation should be as high as the bank and also higher than any expected ice jam (Yossef, 2002). As noted by Klumpp and Baird (1991), spur dikes can be constructed with a sloped crest or a stepped-down crest in the longitudinal direction of the structure. The longitudinal slope is usually in the range of 0.1-0.25V:1H.

Spur dike length is usually determined based on the required river constriction and the desired constricted river depth (Richardson, 1975; USACE, 1980). For protection of straight reaches or reaches with long-radius bends in wide rivers, the minimum length of a spur dike should be 15 m while the maximum length should be less than 10-15% of the bankfull channel width (Richardson and Simons, 1984). Alvarez (1989) suggests that, in the case of straight reaches, the spur dike length is usually kept between h and 0.25B, where h and B are the mean depth and free surface width of the flow, respectively. The spacing between spur dikes is usually taken to be a function of the spur dike length (Brown, 1984). In order to obtain a well-defined, deep channel for navigation and flood control purposes, the recommended space between spur dikes is (1.5-2)L where L is the spur dike length. Greater spur dike spacings, (2-6)L, are used for riverbank protection (Richardson et al., 1975; USACE, 1980; Richardson and Simons, 1984; Klumpp and Baird, 1991; Watson et al., 1999; Yossef, 2002).

The orientation of a spur dike relative to the main flow direction has a substantial effect on the flow pattern as well as the scouring and sedimentation processes adjacent to the spur dike. The orientation of a spur dike is usually measured from the side of the bank located downstream from the spur dike. According to Richardson and Simons (1984), the orientation of a spur dike varies from 30° to 120° when measured from downstream. Spur dikes angled in a downstream direction are more useful for navigation purposes as they provide a greater depth of flow. Spur dikes having an orientation angle more than 90 degrees are more appropriate for bank protection. Sediment materials have a higher tendency to settle between these types of spur dikes so that they provide for a longer and more stabilized

riverbank protection (Franco, 1967; Jansen et al., 1979; USACE, 1980; Brown, 1984; Watson et al.; 1999; Kuhnle et al., 2002; Yossef, 2002).

The crest width of a spur dike usually varies from 1.5 to 6 m. For a rock or rock-covered spur dike, the minimum allowable width is controlled by the available construction equipment. The sideslopes of a spur dike vary from 1H:1.5V to 1H:5V depending on the angle of repose of the construction materials (Richardson et al.; 1975; USACE, 1980; Richardson and Simons, 1984). For determination of the spur dike base width, an estimate of the scour depth is required. For the construction of spur dikes, several types of material might be used, including rock, earth materials covered with rock, timber, steel or concrete piles, trees, sand bags, and automobile bodies (USACE, 1980). If a spur dike is made of erodible soil, it should be protected by riprap. For protection against local scour, a stone blanket may be placed at the outer edge around the spur dike nose (Richardson et al., 1975; Richardson and Simons, 1984).

Prediction of the scour depth adjacent to a spur dike is considered to be one of the most important design issues. It has been studied for decades, although there remains a lot of uncertainty in the prediction of scour depth. The scour depth is a function of the flow parameters, spur dike geometry, and bed material. The total scour depth adjacent to a spur dike is the sum of two scour components, namely contraction scour and local scour. The depth of local scour varies with time as a result of the presence or absence of dunes passing by the scour hole, with the maximum scour depth usually considered to be 30% greater than the equilibrium scour depth (Richardson and Simons, 1984).

Although, the backwater effect of spur dikes is not considered as a design parameter, the reported concerns about the impact of spur dike construction on river flood stages justify its quantification in the design of spur dikes. Quantifying the backwater effect is also important in flood management analysis for a riverine system having spur dikes. On this basis, a study was initiated on the backwater effects associated with spur dikes.

1.3. Objectives

The main objective of the research was to study and quantify the resistance and hence backwater effect due to spur dikes in a riverine flow field. In this context, the following issues were addressed:

- Quantification of the flow resistance due to a single spur dike having various geometries and subjected to various discharge conditions;
- Quantification of the flow resistance due to a spur dike field for various geometric arrangements (i.e., distance between spur dikes and number of spur dikes) and subjected to various discharge conditions;
- Development of a theoretical basis and relationships for assessing and predicting the backwater effect due to spur dikes;
- Obtaining a better understanding of the physics behind the resistance offered by spur dikes on the flow in an open channel; and
- Evaluating the application of a Computational Fluid Dynamics (CFD) model to predict the flow resistance and hence backwater effect due to spur dikes in a river and also the flow pattern around the spur dikes.

1.4. Scope

In general, this study of the backwater effect due to spur dikes was a laboratory work. However, a CFD model was also used for one of the experimental conditions (i.e., a single submerged spur dike) to evaluate the ability of such models to predict the flow resistance and hence backwater effect of a spur dike. Prediction of the flow pattern adjacent to the spur dike was also considered as a secondary objective of the CFD application. In the context of the laboratory work, the flow was uniform (i.e., constant depth throughout the entire flume length prior to installation of the spur dikes) and subcritical (i.e. Froude number < 1). The flume bed was rigid and smooth. The model spur dikes were smooth and two-dimensional in shape (i.e., 2-D plates). The spur dikes were studied for both submerged and unsubmerged

conditions. In the case of spur dike fields, all spur dikes were either submerged or unsubmerged. For single submerged spur dikes, four spur dike orientation angles relative to the flume wall were studied, including 45, 90, 112.5 and 135 degrees. However, in the case of a single unsubmerged dike and also for the spur dike fields, the spur dikes were placed perpendicular to the flume wall along only one side of the flume. The number of and distance between spur dikes in a spur dike field were dictated by the limitations of the flume length and of the spur dike dimensions. The dimensions of all spur dikes within the spur dike field were the same.

1.5. Overview of the thesis document

The format of the thesis document was approved by the advisory committee members to be a paper-based manuscript. In this respect, each part of the research is presented in an individual chapter, which includes the relevant literature review and associated list of references for that chapter. However, the second chapter of the thesis document was developed to present a short literature review about spur dikes in general. The second chapter also provides theoretical relationships that might be used to assess the flow resistance and associated backwater due to objects, including spur dikes, in an open channel. Chapters 3-5, which are the core of the thesis document, comprise three separate journal manuscripts that describe three distinct parts of the research, including: a) flow resistance due to a single spur dike in an open channel, b) drag force and associated backwater effect in a spur dike field in an open channel, and c) numerical modeling of the flow field within the vicinity of a single submerged spur dike (CFD model application). Chapter 6 of the thesis document provides general conclusions obtained from all parts of the research. Three appendices, including two additional journal manuscripts (now published) and a section on uncertainty analysis, form the last part of the document. The two manuscripts in the appendix were written during the theoretical development process for the research program. They are based on the backwater effect measurements made for a single submerged spur dike by Oak (1992) and some complimentary experiments by the Ph.D. candidate. These two manuscripts were not placed within the main body of the thesis to avoid confusion with the theoretical aspects of these papers versus that given in Chapter 3. The theoretical development for the flow resistance of a single spur dike in Chapter 3 evolved from the theoretical analysis presented

in the two manuscripts in Appendices A and B. The titles of the papers in appendix are: a) backwater effect due to a single spur dike, and b) backwater prediction due to the blockage caused by a single submerged spur dike in an open channel. The uncertainty analysis section gives a measure of the uncertainty that is expected for the relevant measured and calculated parameters in Chapter 3 and Chapter 4.

1.6. References

Ahmad, M. 1953. Experiments on design and behavior of spur dikes. Proc. of IAHR and ASCE Joint Meeting, University of Minnesota, MN, USA, pp. 145-159.

Alvarez, J.A.M. 1989. Design of groins and spur dikes. Proc. of the National Conference on Hydraulic Engineering, ASCE, New Orleans, LA, USA, pp. 14-18.

Belz, J.U., Busch, N., Engel, H. and Gasber, G. 2001. Comparison of river training measures in the Rhine catchment and their effects on flood behaviour. Water and Maritime Engineering, Proceedings of the Institution of Civil Engineers, London, 148(3): 123-132.

Brown, S.A. 1984. Design guidelines for spur-type flow-control structures. Transportation Research Record, Transportation Research Board, Washington, D.C., USA, 930(2): 193-201.

Criss, R.E. 2002. Rising flood stages on the lower Missouri River. Department of Earth & Planetary Sciences, Washington University in St. Louis, USA, 7 p. (http://www.ewgateway.org/pdffiles/library/wrc/rising_flood_stages.pdf)

Criss, R.E. and Shock, E.L. 2001. Flood enhancement through flood control. Geology, American Geophysical Union, 29(10): 875-878.

Fenwick, G.B. 1969. State of knowledge of channel stabilization in major alluvial rivers. USACE Committee on Channel Stabilization, Technical Report No. 7, 8 chapters.

Franco, J.J. 1967. Research for river regulation dike design. Journal of the Waterways and Harbors Division, ASCE, 93(WW3): 71-87.

Hendrickson, J.S. and Schneider, M.J. 1999. Hydraulic evaluation of discharge over submerged rock wing dams on the Upper Mississippi River. Water Quality Technical Notes Collections (WQTN PD-06), USACE, Research and Development Center, Vicksburg, MS, USA, 5 p.

Jansen, P.P., Van Bendegom, L., Van den Berg, J. and Zanen A. 1979. Principles of river engineering. Pitman Publishing Limited, London, 509 p.

Klumpp, C.C., and Baird, C.D. 1991. Design of groins on the Middle Rio Grande. Proc. of the National Conference on Hydraulic Engineering, ACSE, Nashville, TN, USA, pp. 148-153.

Kuhnle, R., Jia, Y. and Alonso, C. 2002. 3-Dimensional measured and simulated flow for scour near spur dikes. Proc. of the First International Conference on Scour of Foundations, ICSF-1, Texas A&M University, TX, USA, pp. 349-363.

Minor, B., Rennie, C.D. and Townsend, R.D. 2007. Barbs for river bend bank protection: application of a three-dimensional numerical model. Canadian Journal of Civil Engineering, NRC Press, 34(9): 1087-1095.

Oak, A.G. 1992. Backwater rise due to a submerged spur. M.Sc thesis, University of Saskatchewan, Saskatoon, SK, Canada, 63 p.

Ouillon, S. and Dartus, D. 1997. Three-dimensional computation of flow around groyne. Journal of Hydraulic Engineering, ASCE, 123(11): 962-970.

Pinter, N., Thomas, R. and Wlosinski, H. 2001. Assessing flood hazard on dynamic rivers. EOS, Transactions, American Geophysical Union, 82(31): 333-339.

Rajaratnam, N. and Nwachukwu, B.A. 1983. Flow near groin-like structures. Journal of Hydraulic Engineering, ACSE, 109(3): 463-480.

Richardson, E.V. and Simons, D.B. 1984. Use of spurs and guidebanks for highway crossing. Transportation Research Record, Transportation Research Board, 930(2): 184-193.

Richardson, E.V., Stevens, M.A. and Simons, D.B. 1975. The design of spurs for river training. Proc. of the 16th IAHR Congress, San Paulo, Brazil, pp. 382-388.

Shields, F.D. 1995. Fate of Lower Mississippi River habitats associated with river training dikes. Journal of Aquatic Conservation - Marine and Freshwater Conservation, 5(2): 97-108.

Soliman, M.M., Attia, K.M., Kotb, Talaat, A.M. and Ahmad, A.F. 1997. Spur dike effects on the river Nile morphology after High Aswan Dam. Proc. of 27th IAHR Congress, Managing Water, San Francisco, CA, USA, Vol. A, pp. 805-810.

Tamai, N., Kawahara, Y., Aoki, M., Matumoto, A., Ishikawa, Y. and Yasuda, M. 1996. Ecohydraulics of spur dikes in Ushizu River, Kyushu Region, Japan. Conference Proceedings of Ecohydraulics 2000, Quebec City, QC, Canada, Vol. B, pp. 631-642.

USACE. 1980. Engineering and design - Layout and design of shallow-draft waterways. Chapter 7: Improvement of Natural Stream Channels (last modified at 1997), Publication Number EM 1110-2-1611, 17 p.

Watson, C.C., Biedenharn, D.S. and Throne, C.R. 1999. Demonstration erosion control design manual. U.S. Army Corps of Engineers, Vicksburg, MS, USA, 274 p.

Wu, B., Wang, G., Ma, J. and Zhang, R. 2005. Case study: River training and its effects on fluvial processes in the Lower Yellow River, China. Journal of Hydraulic Engineering, ASCE, 131(2): 85-96.

Yossef, M. F. M. 2002. The effects of groynes on rivers (literature review). Delft Cluster Report No. DC1-334-4, Delft University, The Netherlands, 57 p.

Chapter 2. Overview of Spur Dikes

2.1. Introduction

The first part of the present chapter is a review of the available literature pertaining to the flow structure adjacent to spur dikes. The second part of the chapter is devoted to the methods used to evaluate the flow resistance and associated backwater effect due to objects, including spur dikes, in an open channel. The last part of the chapter reviews the numerical techniques used to model open channel flow, especially the free surface level.

An understanding of the flow structure adjacent to spur dikes is useful for explaining the flow resistance and associated backwater effect due to spur dikes. Based on the flow condition, a spur dike may operate in either an unsubmerged condition or a submerged condition. For unsubmerged conditions, the flow only passes around the end of the structure while, for submerged conditions, the flow passes both over and around the structure. The flow field adjacent to an unsubmerged spur dike is mostly two-dimensional except for a small area very near to the structure, while the flow adjacent to a submerged spur dike is fully three-dimensional. There is also a significant difference in the flow field near a single spur dike and a series of spur dikes (i.e., spur dike field). Interaction between the spur dikes in a spur dike field has a substantial effect on the flow structure in the zones between the spur dikes.

There are two methods that can be used to theoretically evaluate and quantify the flow resistance and hence the backwater effect of objects in open channels, namely the energy principle and the momentum principle. The second part of the present chapter starts with a theoretical explanation of the two principal approaches and it continues with a review of the available literature in which the flow resistance and backwater effect due to objects in open channels have been evaluated using the two approaches. In the present research, the momentum principle has been used to investigate and quantify the flow resistance and backwater effect due to spur dikes.

CFD models have been used for many years to investigate the flow structure in fluid mechanics. However, using CFD models in open channels, especially for free surface flow,

is relatively new. The last part of the present chapter is a review of the numerical methods that can be used to track the free surface level.

2.2. Flow field adjacent to a single unsubmerged spur dike

The flow pattern in the vicinity of a single unsubmerged spur dike can be divided into four main zones (Chen and Ikeda, 1997; Yossef, 2002), including the main flow zone, return flow zone, shear layer and reattachment point (Figure 2.1). The main flow zone is located between the spur dike tip and the opposite channel wall. In this area, the velocity increases as the spur dike reduces the effective width of the channel. Increased velocity in the main flow zone causes channel degradation due to scour, which results in an increase in the thalweg depth. The return flow zone, also known as the recirculation area, eddy zone or dead zone, is located downstream in the lee of the spur dike between the flow separation streamline and the right wall of the channel (viewing downstream). The difference in the flow velocities in the return zone and the main flow zone leads to a shear layer between the two zones. The shear layer is analogous to the separation streamline shown in Figure 2.1. According to Rajaratnam and Nwachukwu (1983), the shear layer is defined as the region downstream from the spur dike that lies between the outer plane of the deflected flow and the sidewall adjacent to the spur dike as shown in Figure 2.2. The outer edge of the shear layer on an arbitrary horizontal plane is a point where the velocity is equal to the velocity in the main flow zone, while the inner edge is a point where the absolute magnitude of the negative velocity reaches a maximum value.

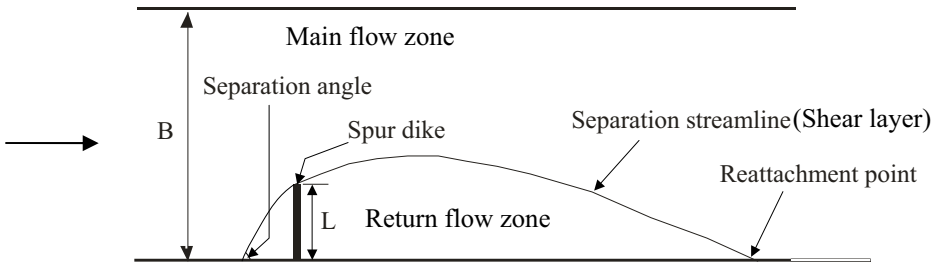

Figure 2.1. Schematic plan view of an unsubmerged spur dike showing the separation streamline, reattachment point, and separation angle (*Adapted from Rajaratnam and Nwachukwu, 1983*)

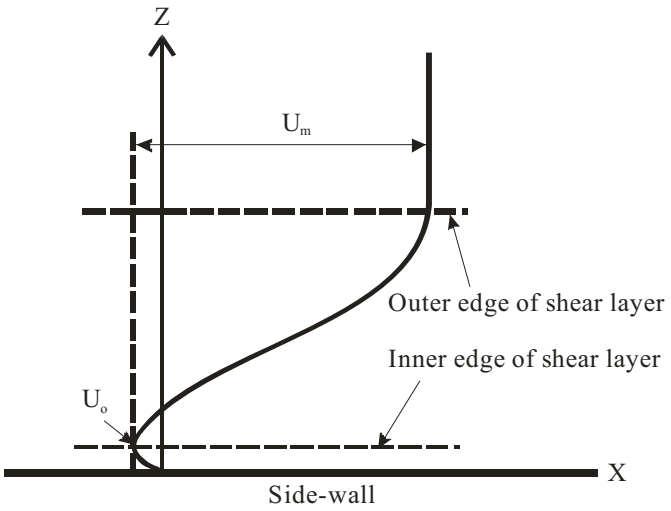

Figure 2.2 Typical plan view profile and definition sketch for the shear layer (*Adapted from Rajaratnam and Nwachukwu, 1983*)

The point at which the separation streamline attaches to the channel sidewall is known as the reattachment point, as shown in Figure 2.1. The total length of the return flow zone and hence the position of the reattachment point downstream from the spur dike is about 12 times the length of the spur dike. The separation streamline along the shear layer begins at the spur dike nose and extends outward from the wall to its maximum width of about two times the spur dike length before continuing downstream to the reattachment point. It has been observed that the shape of the separation streamline is negligibly affected by the Froude number in subcritical flow conditions (Ishii et al., 1983; Rajaratnam and Nwachukwu, 1983; Chen and Ikeda, 1997; Ouillon and Dartus, 1997).

Ishii et al. (1983) found that, as the spur dike angle varies from 30º to 150º (measured from downstream) with respect to the channel wall, the dimensionless reattachment length (i.e., ratio of the reattachment length to the projected length of the spur dike) remains almost constant. They mentioned, however, that the upstream separation angle, as is shown in Figure 2.1, is a function of the spur dike angle, which ranges from 30º to 60º as the spur dike angle changes from 30º to 60º. For spur dike angles greater than 60º, the upstream separation angle remains at 60º. Haltigin et al. (2007) studied the effects on pressure distribution and velocity of two angled spur dikes located on opposite sides of an open channel. The contraction ratio (i.e., projected length of the two spur dikes to the width of the open channel)

was about 0.25. The results of their work for the near-bed pressure distribution and velocities are shown in Figure 2.3. They observed that the pressure and velocities in the region upstream of the spur dikes increase with an increase in the spur dike angle (measured from downstream).

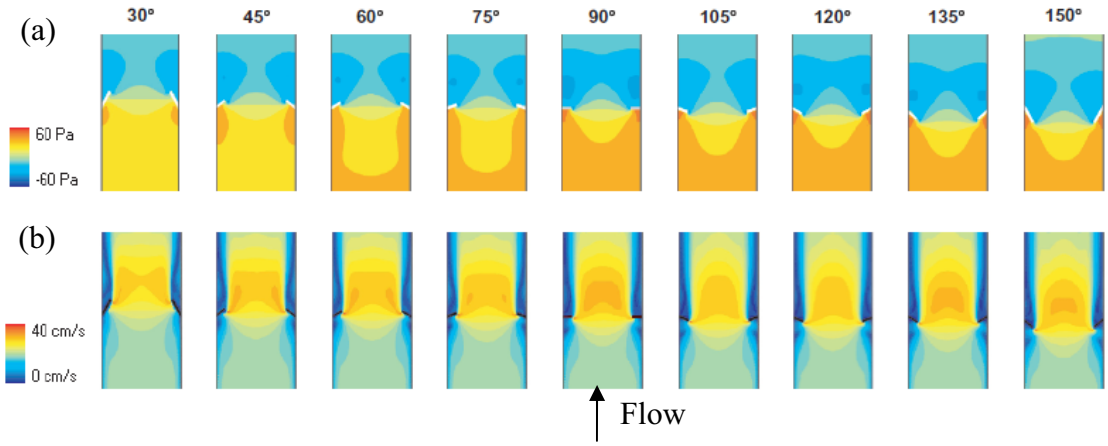

Figure 2.3. Effect of spur dike angle on the near bed distribution of (a) pressure, and (b) velocity (*Taken from Haltigin et al., 2007)*

The velocity field very close to an unsubmerged spur dike, especially adjacent to its nose, is three-dimensional. In a study by Rajaratnam and Nwachukwu (1983), it was observed that the streamwise velocity profile in the vertical direction, upstream of the spur dike, is logarithmic, while it is uniform around the nose of the structure. Downstream from the spur dike, velocity profiles showed that the flow forms a jet near the bed and that the deflected flow region can be considered as a skewed turbulent boundary layer.

The flow structure adjacent to a spur dike has also been characterized by identifying the system of vortices. As the flow reaches the spur dike, a strong downward flow is formed immediately upstream of the structure accompanied by a high pressure zone. Due to the high pressure zone in front of the spur dike, the flow is accelerated around the nose of the structure and forms horseshoe vortices. The spur dike nose serves to separate the flow and produce secondary currents (i.e., flow in planes normal to the longitudinal direction). The length of the secondary current zone is a function of the spur dike length to channel width ratio, flow depth and spur dike angle (Jia and Wang, 2000; Sukhodolov et al., 2004).

Marson et al. (2003) performed some experimental and numerical studies on the turbulent coherent structures caused by spur dikes in the presence of local scour. For the numerical studies, they used a CFD model (FLUENT) coupled with a standard k-ε turbulence closure model. It was observed that there are two distinct flow structures, namely the classical horseshoe vortex in front of the spur dike and a vortex located within the recirculation zone (i.e., return zone). Figure 2.4 shows fluid particle trajectories developed using the CFD model. It can be observed that the uppermost streamlines are only deviated by the spur dike in the horizontal plane. At intermediate depths, in addition to the horizontal deflection, the streamlines tend to deflect downward (i.e., vertical deflection). From their numerical model, Marson et al. (2003) also concluded that, in the initial phases of scour, the horseshoe vortex is mainly responsible for the scouring process, while in the later phases of the scouring process, the vertical vortex in the scoured hole becomes more significant.

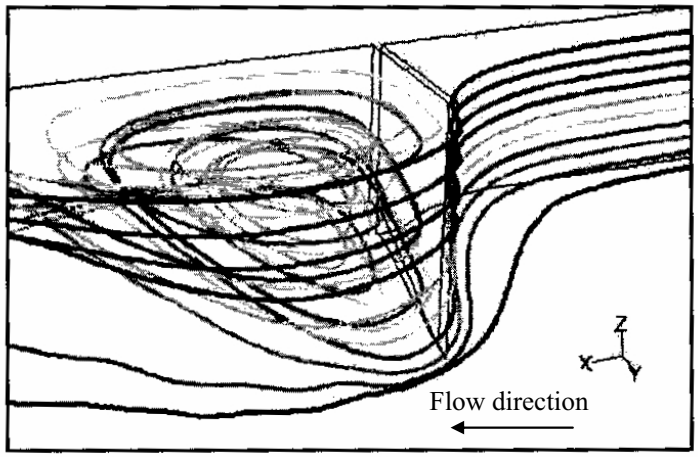

Figure 2.4. 3-D visualization streamlines near a spur dike (*Taken from Marson et al., 2003*)

Miller et al. (2003) simulated the flow around an unsubmerged spur dike using a 3-D CFD model. They used two types of spur dikes, including a vertical-walled spur dike and a spur dike with a side slope. In the case of the vertical-walled spur dike, they observed several flow structures, including: 1) a half horseshoe vortex in front of the spur dike (A in Figure 2.5); 2) a vortex flow consisting of: i) shedding vortices from the spur dike tip (vortices B), and ii) a recirculating zone downstream from the spur dike lee (vortex C in Figure 2.5); and, finally 3) contracted streamlines at the open side of the channel in front of the spur dike tip (D in Figure 2.5). This system of vortices is responsible for increasing the

sediment transport rate, resulting in local scour/deposition adjacent to the spur dike. In a study by Koken and Constantinescu (2008), it was observed that the intensity, position and structure of the horseshoe vortices vary considerably with time, although the intensity of the vortices was highest around the tip of the spur dike.

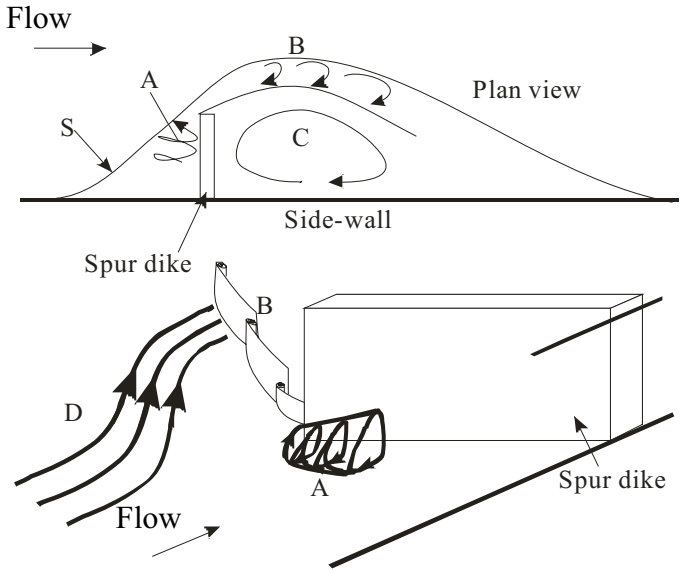

Figure 2.5. 3-D flow structure around a vertical-walled spur dike (*Adapted from Miller et al., 2003*)

Miller et al. (2003) also observed that the flow structure is notably different between the vertical-walled and side-sloped spur dikes. In the case of the sloped spur dike, the vortex A in Figure 2.5 is partially suppressed by the side-slope of the spur dike. The location of the upstream separation point was determined to be equal to the length of the spur dike. Paquier et al. (2003) measured the 3-D velocity distribution around a spur dike using a laser Doppler anemometer (LDA) in order to evaluate a 2-D numerical model that solves shallow water equations. It was observed that the spur dike redirects the flow toward the opposite bank and a recirculation zone (i.e., return flow zone) forms downstream from the spur dike. In front of the spur dike, the flow is redirected downward and a horseshoe vortex forms. These observations are similar to those reported by other researchers (e.g., Miller et al., 2003; Marson et al., 2003).

The effect of spur dikes on the bed shear stress distribution has also been studied. Computation of the bed shear stress adjacent to an unsubmerged spur dike showed that the magnitude of the bed shear stress increases with an increase in the spur dike length. The results also showed that the bed shear stress near the nose of the spur dike achieves a maximum value that is about five times greater than the bed shear stress of the approaching flow (Rajaratnam and Nwachukwu, 1983). In a numerical model study coupled with experimental work, Ouillon and Dartus (1997) concluded that the maximum bed shear stress, corresponding to the maximum scouring, is located at the upstream corner of the spur dike nose.

The pressure distribution adjacent to a spur dike was given consideration by some authors. Ouillon and Dartus (1997) observed that the vertical pressure profile around a spur dike is mainly hydrostatic except in an area very close to the nose of the structure. Moreover, the total pressure (i.e., static and dynamic pressures) was measured to be higher upstream of the spur dike than that downstream from the structure, which results in a net drag force exerted on the flow. In an experimental study, Mioduszewski et al. (2003) found that the pressure difference across a spur dike is due to the difference in water level from upstream to downstream. They also observed that the pressure difference across a spur dike is higher at the bottom of the spur dike than at the top. Paquier et al. (2003) measured the water surface elevation both upstream of and downstream from a spur dike. They observed that the water surface elevation is higher upstream of the spur dike.

Mioduszewski et al. (2003) studied the influence of the structure permeability on the flow pattern and local scouring near a spur dike. They concluded that there is a large difference between the flow patterns and scouring in the cases of permeable and impermeable spur dikes. This is expected as the emerging flow from the pores of the permeable spur dike affects the flow and sedimentation/scouring pattern downstream from the spur dike.

2.3. Flow field adjacent to a single submerged spur dike

The flow structure adjacent to a single submerged spur dike is more complicated than that for a single unsubmerged spur dike. The flow is highly three-dimensional adjacent to a submerged spur dike due to two types of vortices, namely vertical and transverse axis

vortices. Vertical axis vortices are due to the separation of the flow around the nose of the structure, while transverse vortices are due to the separation of the flow over the crest of the spur dike (Tominaga et al., 2001). Kuhnle et al. (2002, 2008) measured the velocity distribution within the vicinity of a submerged spur dike having a trapezoidal cross-section using an acoustic Doppler velocimeter (ADV). They also simulated flow pattern using a computer simulation model. The authors observed three vortices in three directions downstream from the spur dike, including vertical and transverse axis vortices, as shown in Figures 2.6a and 2.6b, and a horizontal axis vortex as shown in Figure 2.6c. The formation of the vertical and transverse axis vortices was discussed before. The formation of the horizontal axis vortex was due to the combined effects of the nose and crest of the spur dike. Figure 2.6 also shows that the dimensions of the vortices are in same the order as the spur dike dimensions.

The existence of secondary currents (i.e., flow in transverse direction) adjacent to submerged spur dikes has been also reported by Peng et al. (1997). Jia and Wang (2000) used a 3-D numerical model (CCHE3D) specifically designed for open channel flows. They reported that there is a secondary flow around the spur dike, including a horseshoe vortex in front of the spur dike. Both Kuhnle et al. (2002) and Jia and Wang (2000) reported that the downflow in front of a submerged spur dike having a trapezoidal cross-section is almost diminished and flow moves upward along the front surface of the spur dike. Kuhnle et al. (2002) also found increased streamwise velocities in the section of channel just beyond the end of the spur dike nose and decreased streamwise velocities immediately upstream of and downstream from the spur dike.

(a), Plan view

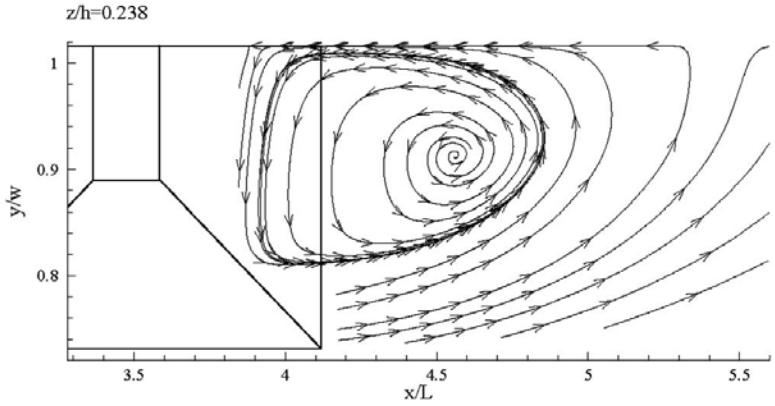

(b), Profile view

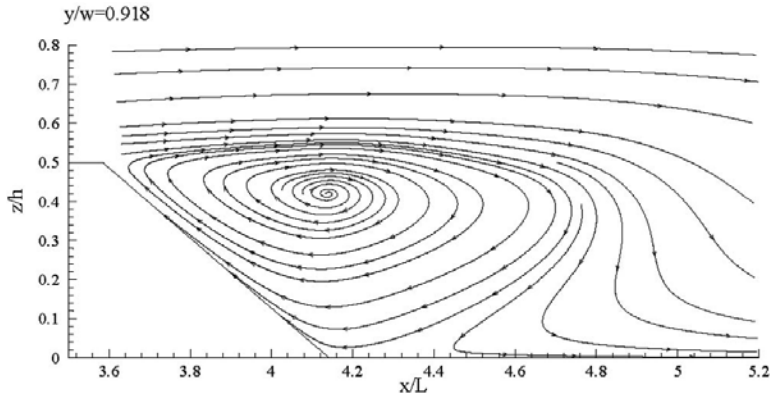

(c), Section view

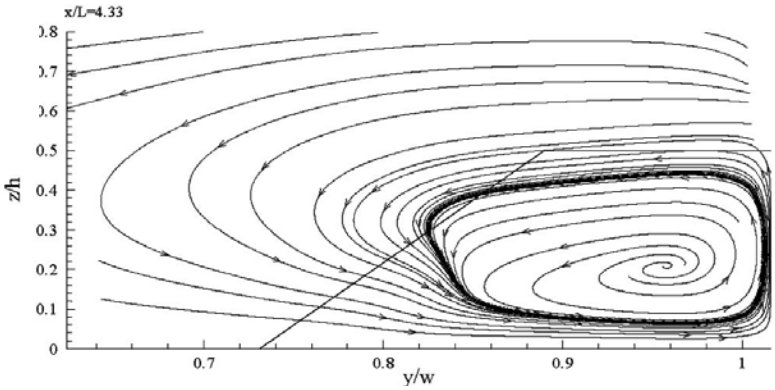

Figure 2.6. Path lines from simulated flow around a submerged spur dike; (a) vertical axis vortex, (b), transverse axis vortex, and (c) horizontal axis vortex (*Taken from Kuhnle et al., 2008)*

2.4. Flow field adjacent to an unsubmerged spur dike field

The flow pattern in an unsubmerged spur dike field is mainly two-dimensional except for areas in the interface layer which separates the main channel flow from the spur dike zone flow and also areas very close to the spur dikes where the flow is strongly three-dimensional

(McCoy et al., 2008). The interaction of the flow in the main channel and the spur dike field results in the formation of vortices between the spur dikes. The number and shape of these vortices are a strong function of the space to length ratio of the spur dikes. Sukhodolov et al. (2002) have categorized the vortex patterns between the spur dikes based on the spur dike spacing. At a very small spacing, as shown in Figure 2.7a, two small vortices with a transverse orientation occur inside the spur dike field. As shown in Figure 2.7b, one of these vortices disappears as the spacing between the spur dikes increase. With a larger spacing between the spur dikes, two vortices develop with a longitudinal orientation inside the spur dike field, as shown in Figure 2.7c.

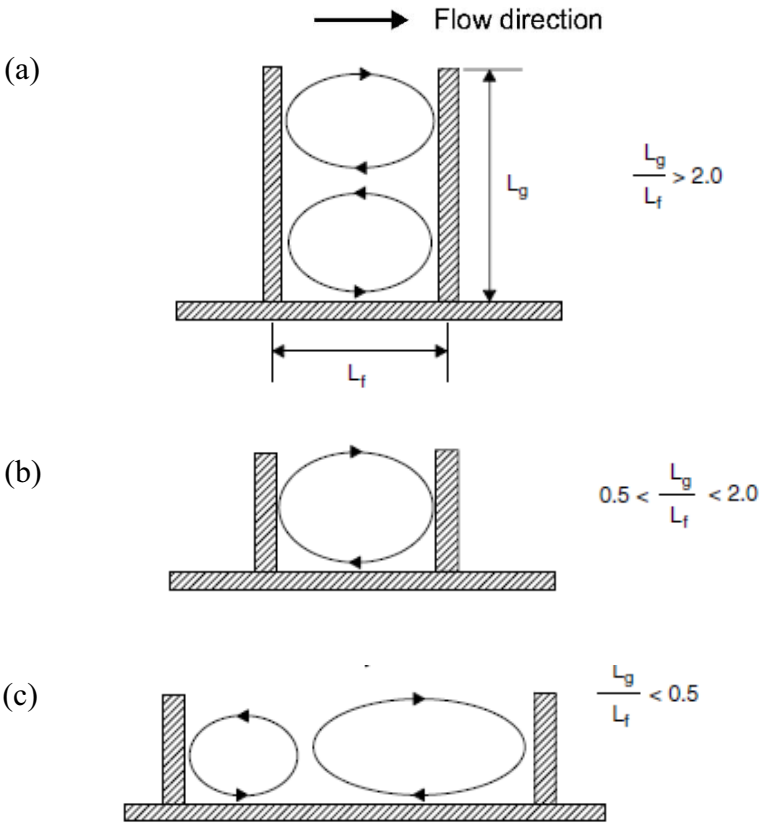

Figure 2.7. Conceptual schematic of the vortex patterns inside an unsubmerged spur dike field: (a) two transverse vortices, (b) a single vortex, and (c) two longitudinal vortices (*Taken from Sukhodolov et al.,2002)*

The conceptual model developed by Sukhodolov et al. (2002) has been confirmed by the velocity measurement in spur dike fields performed by Weitbrecht et al. (2008). They measured the velocity field using particle image velocimetry (PIV). They also concluded

that the pattern of the vortices is a dominant parameter controlling the mass flow exchange between the main current in a river and the flow within a spur dike field. Figures 2.8a, 2.8b and 2.8c show the vortex pattern for spur dike fields having relative spacings (i.e., ratio of spacing to length of spur dikes) of 0.5, 0.9 and 3, respectively.

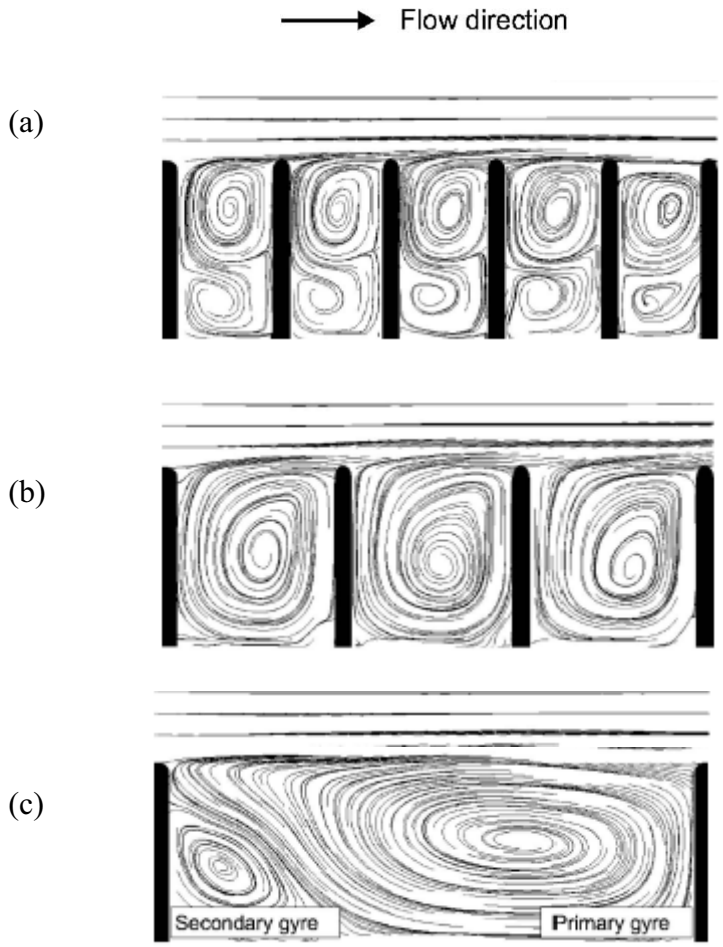

Figure 2.8. Measured flow patterns in unsubmerged spur dike fields for various relative spacings: (a) two transverse vortices, (b) a single vortex, and (c) two longitudinal vortices (*Taken from Weitbrecht et al. 2008*)

A Similar observation has also been made by Ujittewaal et al. (2001). They found that a space to length ratio of unity results in the formation of a strong single vortex between the spur dikes, which usually prevents the main flow from penetrating into the spur dike field zone. As the space to length ratio increases, a vortex system comprising two vortices is observed between the spur dikes. A large vortex forms in the downstream part of the spur dike field zone, while a small vortex forms in the upstream part of the spur dike field zone.

This system of vortices is strong enough to prevent the main flow from penetrating into the spur dike field zone. A further increase in the space to length ratio, in the order of six, causes the vortex system to weaken, with the penetration of the main flow into the spur dike field zone subsequently taking place. The weak vortex system is characterized by several smaller vortices between the spur dikes (Uijttewaal et al., 2001).

Figure 2.9, taken from Yossef (2002), distinguishes six types of flow pattern within a spur dike field that result from various spur dike spacing to length ratios. For bank protection purposes, the spacing to length ratio of the spur dikes is limited to a maximum value of six (i.e., type 2 flow) due to the characteristics of the vortex system described above (Klingeman et al., 1984; Uijttewaal, 1999, Yossef, 2002).

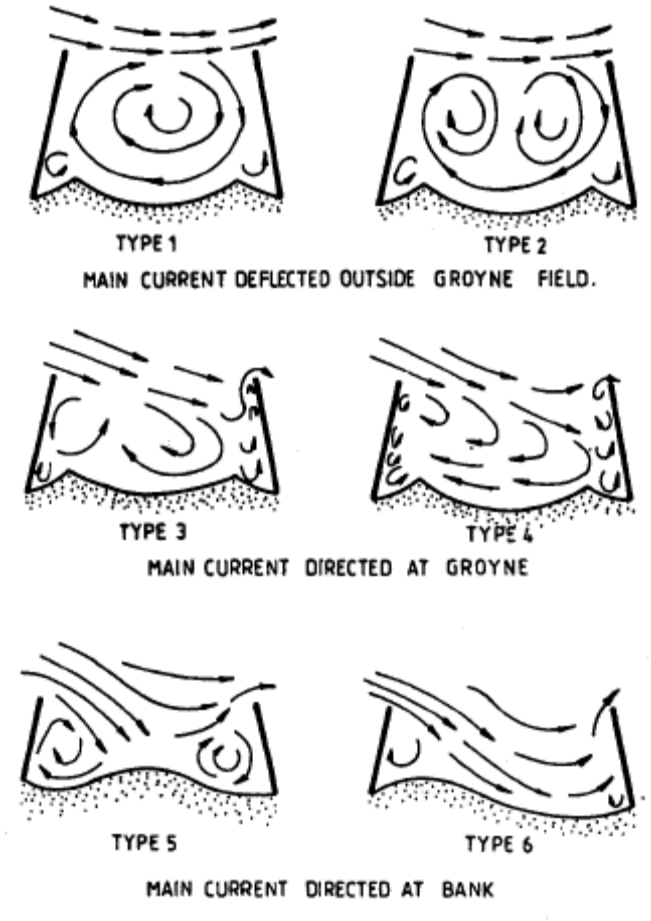

Figure 2.9. Effects of the spur dike spacing on the flow pattern of unsubmerged spur dike fields developed by Klingeman et al., 1984 (*Taken from Yossef, 2002*)

2.5. Flow field adjacent to a submerged spur dike field

The flow field adjacent to submerged spur dike fields is highly three-dimensional. Tominaga et al. (2001) have observed that there are two kinds of vortices adjacent to a submerged spur dike field, namely a vertical axis vortex due to the flow around the noses of the spur dikes and a transverse axis vortex due to the flow over the crests of the spur dikes Peng et al. (1997) observed that the size of the vertical axis vortex decreases from the bed to the free surface of the flow. The reason for this might be attributed to the suppression effect caused by the jet flow over the crests of the spur dikes. Secondary flows were also recognized upstream of and downstream from the spur dikes in a spur dike field. A recent study by Abad et al. (2008) shows the suppression effects of the jet flow on the vertical axis vortex inside the spur dike field. A single strong vertical axis vortex is observed in the case where the spur dike field is not submerged, as shown in Figure 2.10a. As the spur dike field becomes submerged, the jet flow penetrates inside the spur dike field and suppresses the vertical axis vortex, as shown in Figures 2.10b and 2.10c.

McCoy et al. (2007) used a numerical model to reveal the flow pattern and other turbulent flow characteristics adjacent to a submerged spur dike field. The results of their work for the flow pattern are shown in Figures 2.11 and 2.12. The relative spacing between the spur dikes is 2.4, while the submergence ratio (i.e., ratio of incoming flow depth to the spur dike height) is 1.4. Figure 2.11 shows the flow pattern and vertical vortices in plan view at various flow depths. It may be noted that the flow at the free surface above the spur dike crests is slightly deviated toward the bank opposite the field, as shown in Figure 2.11a. Moreover, a single vertical axis vortex forms inside the spur dike field at lower depths within the flow below the crest of the spur dikes, as shown in Figures 2.11b, 2.11c and 2.11d. It may also be noted that the center of the vortex moves toward the nose of the spur dike at the lower depths within the flow. A smaller vortex is observed behind the last spur dike, which is stronger in size at the mid-heights of the spur dikes. A very small vortex is also discernible upstream of the first spur dike and adjacent to the channel wall near to the spur dike field. The size of this vortex is also greater at the mid-height of the spur dikes.

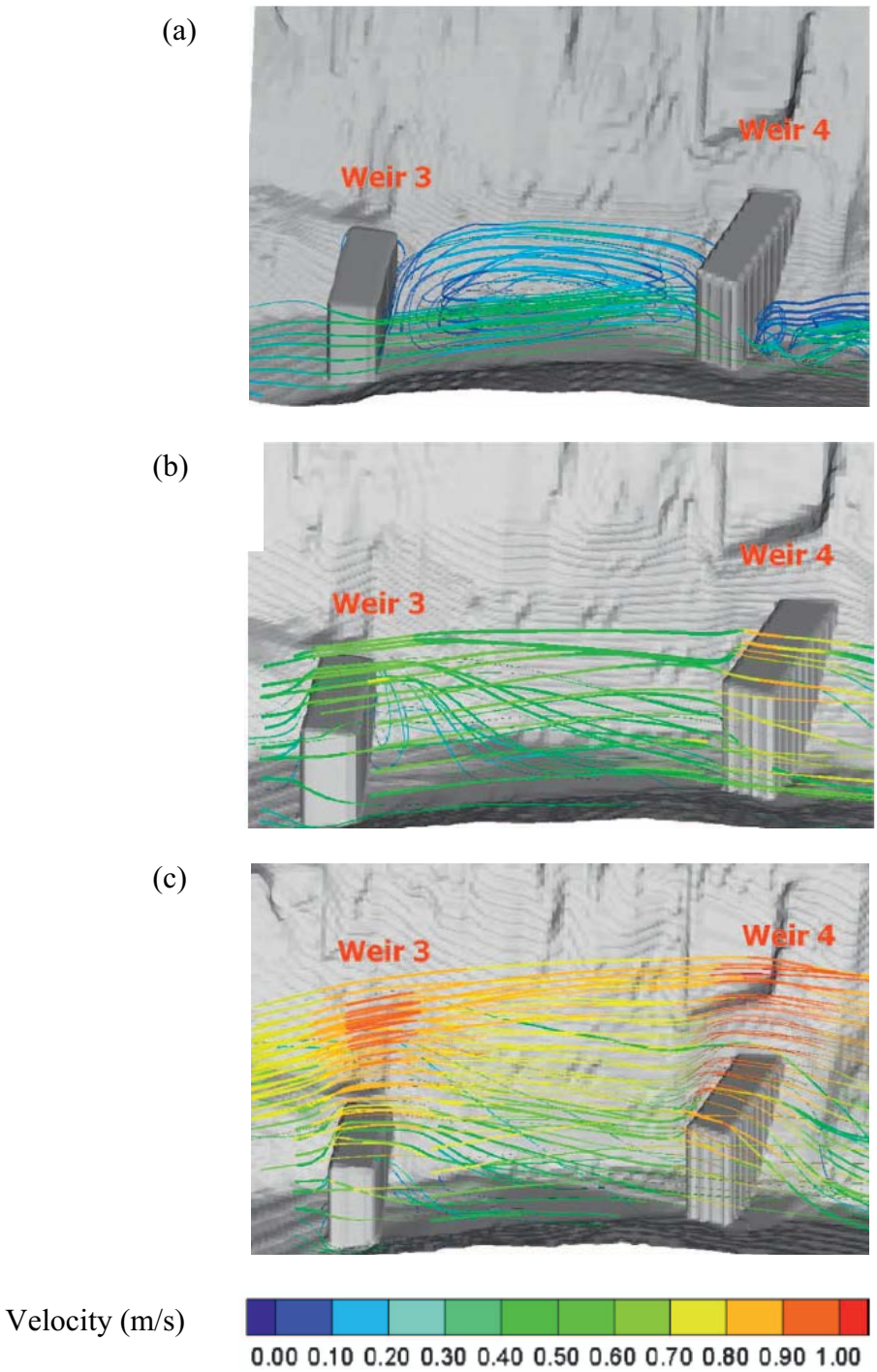

Figure 2.10. Vortex pattern inside a spur dike field: (a) no submergence, (b) low submergence ratio, and (c) high submergence ratio (*Taken from Abad et al., 2008)*

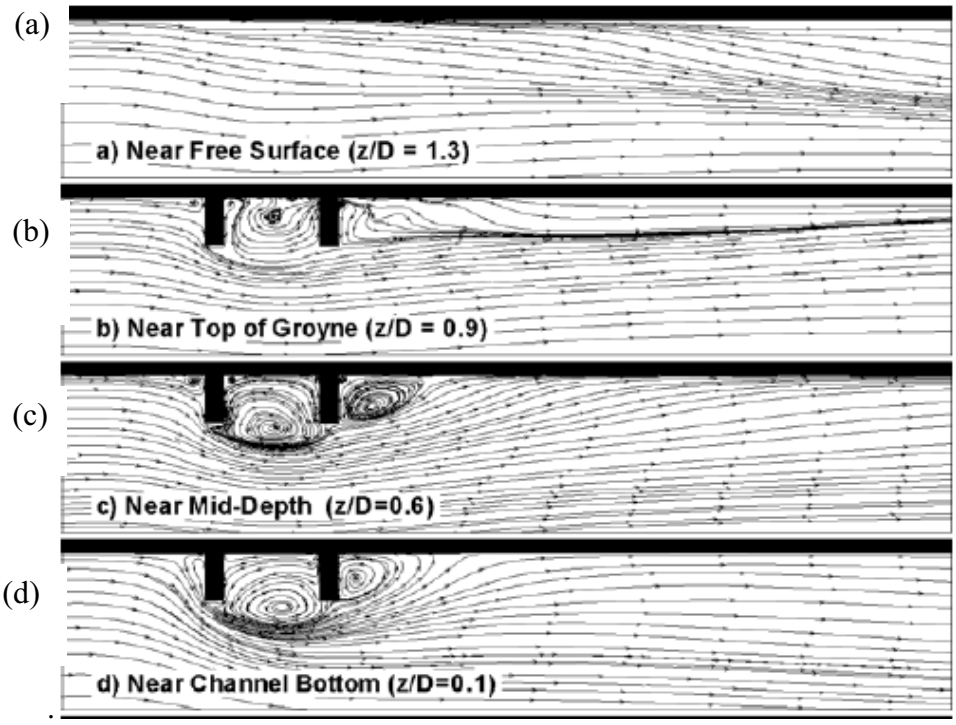

Figure 2.11. Flow pattern and vertical axis vortices adjacent to a submerged spur dike field at various depths of flow: (a) near to the free surface, (b) near to the crest of the spur dikes, (c) near to the mid-height of the spur dikes, and (d) near to the channel bed (*Taken from McCoy et al., 2007)*

Figure 2.12 shows the flow pattern and transverse axis vortices in profile view at various transverse locations. It is observed that a single transverse axis vortex forms between the spur dikes in the spur dike field. Figures 2.12a, 2.12b and 2.12c show the transverse locations near to the spur dike nose, close to the mid-length of the spur dikes and close to the channel wall inside the spur dike field, respectively. It may be observed that the center of the transverse axis vortex moves toward the crest of the spur dike as one moves from the spur dike nose to the channel wall. For all conditions, the existence of downflow is noticeable upstream of the first spur dike.

Tominaga et al. (2001) observed large tranverse axis vortices between spur dikes in a submerged spur dike field, with their centers located 10-15% of the spur dike height below the crest of each spur dike. An increase in the spur dike height resulted in moving the transverse axis vortex centers further downstream. Similar to Peng et al. (1997), they also observed large vertical axis vortices in which the strength decreased from the bed to the

surface of the flow. Here, the strength of the vortex is based on its size. Tominaga et al. (2001) compared the streamwise velocity of the flow in submerged and unsubmerged spur dike fields and concluded that the streamwise velocity is considerably smaller in the unsubmerged spur dike field. The reason for this might be attributed to the fact that the streamwise velocity is boosted by the jet flow over the crest of the spur dikes in the submerged condition. Peng et al. (1997) also studied the effect of the spur dike spacing on the bed shear stress between the spur dikes and concluded that an increase in the space between the spur dikes increases the overall bed shear stress between the spur dikes. They mentioned that the bed shear stress is small in the spur dike zone, while it is large adjacent to the spur dike noses. McCoy et al. (2008) estimated the bed shear stress adjacent to the most upstream spur dike to be an order of magnitude greater than the bed shear stress of the incoming flow. For downstream spur dikes, the increase in the bed shear stress is less than that for the most upstream dike.

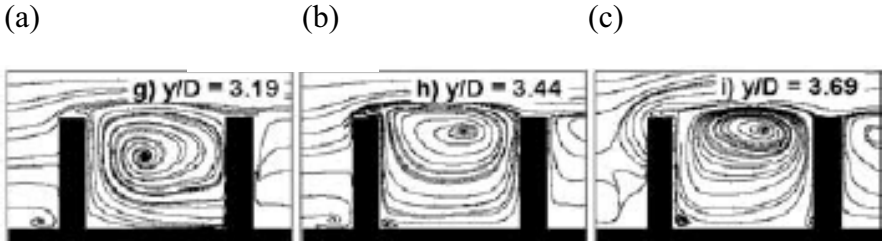

Figure 2.12. Transverse axis vortices adjacent to a spur dike field at transverse locations: (a) near to the spur dikes nose, (b) near to the mid-length of the spur dikes, and (c) near to the channel wall inside the spur dikes (*Taken from McCoy et al., 2007)*

2.6. Backwater effect

Placement of any object in an open channel flow results in an extra force, in the form of a drag force exerted on the flow, as well as associated energy losses. In open channels for subcritical flow conditions, as is the case for most rivers, the water level upstream of the object must increase to provide the extra force or the extra energy to overcome the drag force or the energy losses. The increased water level upstream of an object placed in an open channel such as a spur dike is called backwater effect, as shown in Figure 2.13.

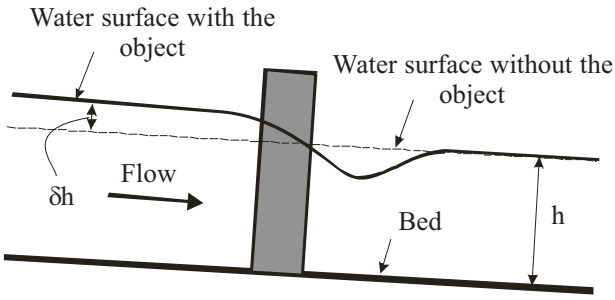

Figure 2.13. Definition of backwater effect, δh, due to an object in an open channel flow

The effect of an object in an open channel flow can either be expressed as a drag force or an energy loss in the flow. On this basis, the backwater effect problem can be analyzed using either the momentum equation or the energy equation. Application of the momentum equation results in the determination of the object drag coefficient, while application of the energy equation results in the determination of the object energy loss coefficient. In some instances, however, neither momentum nor energy equations have been used. Instead, the amount of the backwater effect has been related directly to the flow conditions and object characteristics using empirical relationships developed from experimental studies (e.g., Yarnell, 1934).

Figure 2.14 is a schematic illustration of an object in a control volume within an open channel flow. Flow parameters and corresponding forces have been shown both in the backwater effect area upstream of the object and in the normal flow region downstream from the object. Cross-sections 1 and 2 represent the control surfaces in the backwater effect area and normal flow region, respectively. F_u and F are the forces due to the pressure distribution at cross-sections 1 and 2, respectively. The average velocities of the flow in cross-sections 1 and 2 are shown by V_u and V, respectively. The depths of the flow in the backwater effect area and in the normal flow region are shown by h_u and h, respectively. The drag force due to the object, exerted on the flow, is shown by F_D, while the friction force and component of the fluid weight in the flow direction are shown by F_f and F_w, respectively.

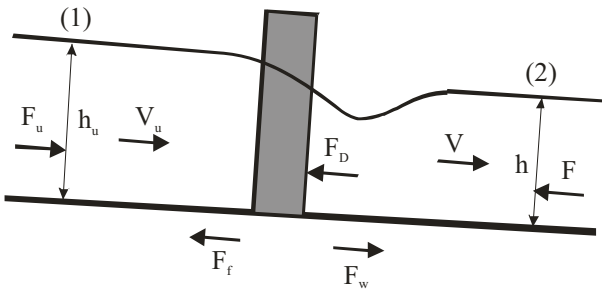

Figure 2.14. Schematic illustration of an object and corresponding flow parameters in a control volume within an open channel flow

Application of the linear momentum equation for the control volume in Figure 2.14 yields

$$[2.1] \quad F_u - F - F_D - F_f + F_w = \rho Q(\beta V - \beta_u V_u)$$

where β_u and β are the momentum correction factors applicable to the upstream and downstream flow conditions, respectively, ρ is the fluid density and Q is the volumetric discharge. The momentum correction factors are generally small and considered to be equal to unity. For subcritical flow conditions, F_f and F_w are assumed to be almost equal. The drag force of the object may be described by the basic drag equation

$$[2.2] \quad F_D = \frac{1}{2}\rho C_D A_s V_u^2$$

where A_s is the projected area of the object normal to the flow direction and C_D is the drag coefficient of the object. Substitution of Eq. [2.2] into Eq. [2.1] and the assumption of a hydrostatic pressure distribution at cross-sections 1 and 2, in conjunction with the continuity equation ($V_u = Q/Bh_u$ in a rectangular channel), yields

$$[2.3] \quad \frac{1}{2}\rho g B(h_u^{\,2} - h^2) - 1/2\rho C_D A_s \left(\frac{Q}{Bh_u}\right)^2 = \rho Q(\beta_n V - \beta_u V_u)$$

where B is the width of the open channel and g is the acceleration due to gravity. Knowing the downstream flow conditions and the geometry of the object, Eq. [2.3] shows that the drag

coefficient of the object must be determined in order to calculate the upstream flow depth and hence the backwater effect, $\delta h = h_u - h$. Many researchers have used the concept of a momentum balance to analyze the backwater effects due to objects in an open channel flow. They have obtained relationships to account for the resistance of objects in terms of a drag coefficient as a way of calculating the resulting backwater effect (e.g., Ranga Raju et al., 1983; Shields and Gippel, 1995; Wu et al., 1999; Uchida and Fukuoka, 2001; Fenton, 2003; Malavasi and Guadagnini, 2003; Morota and Tsuchiya, 2003).

Application of the energy equation between the backwater region and normal flow region adjacent to the object in Figure 2.6, on the other hand, yields

$$[2.4] \quad \left(h_u + \frac{\alpha_u V_u^{\,2}}{2g} \right) = \left(h + \frac{\alpha V^2}{2g} \right) + (S_f - S_\circ)L_\circ + h_L$$

where α_u and α are the energy correction factors, S_f is energy slope due to the channel boundary friction, S_o is the channel bed slope, L_o is the distance between sections 1 and 2, and h_L is the energy loss due to the existence of the object. The energy correction factors are generally small and maybe assumed to be equal to unity for purposes of further analysis. For a control volume with a relatively small length in an open channel and for subcritical flow conditions, it might be assumed that $(S_f - S_\circ)L_\circ \approx 0$ (which is exactly true for uniform flow). The head loss due to the object may be represented as

$$[2.5] \quad h_L = C_L \left| \frac{V_u^{\,2} - V^2}{2g} \right|$$

where C_L is the coefficient of head loss due to the existence of the object in the flow. Application of the continuity equation, $Q = Bh_u V_u = BhV$, in conjunction with Eqs. [2.4] and [2.5] can be used to calculate the upstream flow depth and hence the backwater effect provided that the head loss coefficient of the object is known *a priori*. The drag and head loss coefficients are usually a function of the flow parameters and the object geometry.

The backwater effect due to bridge abutments and piers has been studied for several decades. Bridge abutments and unsubmerged spur dikes are considered similar in terms of their hydraulic behavior (e.g. Melville, 1997; Lim, 1997; Molinas et al., 1998) so that the backwater effect due to a bridge abutment may be used to calculate the backwater effect of an unsubmerged spur dike. Yarnell (1934) was among the first researchers to present an empirical relationship to quantify the backwater effect of bridge piers and abutments. He obtained his empirical relationship on the basis of 2600 experiments of various pier shapes, which is still used in open channel flow packages such as HEC-RAS (HEC-RAS Reference Manual, 2002). Yarnell obtained the backwater effect as a function of downstream flow conditions, including the flow depth, h, Froude number, $Fr = V/\sqrt{gh}$, flow opening ratio, e_r, and pier or abutment shape factor, Δ. His relationship reads

$$[2.6] \qquad \frac{\delta h}{h} = \Delta\left(\Delta + 5Fr^2 - 0.6\right)\left(e_r + 15e_r^4\right)Fr^2$$

It can be observed from Eq. [2.6] that the opening ratio is an important parameter for the backwater effect. The opening ratio is the ratio of the contracted flow area to the total flow area downstream from the bridge. The shape factor is in the order of unity. There are other empirical relationships which have been developed for the backwater effect of bridge piers and abutments (e.g., Liu et al., 1957; Al-Nassri, 1994; Ghodsian and Shafieefar, 2001).

Some researchers quantify the backwater effect of bridge piers and abutments using the momentum equation arranged to give the drag coefficient of the bridge elements. Charbeneau and Holley (2001) carried out a study of the backwater effect due to circular bridge piers using the momentum equation. On this basis, they developed a relationship to relate the drag coefficient of bridge piers to the backwater effect, viz.

$$[2.7] \qquad C_D = \frac{1}{e_r Fr^2}\left(2\frac{\delta h}{h} + \left(\frac{\delta h}{h}\right)^2\right) - \frac{2}{e_r}\left(\frac{\delta h/h}{1+\delta h/h}\right)$$

They established a method to measure the drag force of bridge piers directly for various Froude numbers, opening ratios and pier diameters. Concurrent with the drag force

measurements, the amount of the backwater effect was also measured. They observed that the drag coefficient of bridge piers is a function of the opening ratio and Froude number although the variation of the drag coefficient with the Froude number was small.

In a similar study, conducted by Ranga Raju et al. (1983), the momentum equation was applied to quantify the backwater effect of circular bridge piers. They developed the following relationship from the momentum equation between the backwater effect and drag coefficient of a bridge pier, viz.

$$[2.8] \quad \frac{\delta h}{h} = \frac{\left(Fr^2 - 1\right) + \sqrt{\left(Fr^2 - 1\right)^2 + 3C_D \frac{d}{B} Fr^2}}{3}$$

where d is the diameter of the bridge pier. They measured the drag force of bridge piers for various flow conditions and opening ratios, the results of which were used to calculate the drag coefficient of the bridge piers. They proposed the following relationship to account for the effect of the blockage by the bridge piers, viz.

$$[2.9] \quad C_D = C_{Do} e_r^{-1.35}$$

where the base drag coefficient, C_{Do}, is the drag coefficient of a circular bridge pier in a very wide open channel in which the effect of the channel walls on the flow regime is negligible. The base drag coefficient was found to vary with the upstream Froude number and non-dimensional approach flow depth, h_u/d.

The momentum equation has also been used in HEC-RAS for bridge abutments and piers as an option for backwater effect calculation along with other methods. The blockage effects of the bridge are implicitly considered in the momentum equation. The base drag coefficient of bridge piers has been summarized for various pier shapes (HEC-RAS Reference Manual, 2002)

The energy method has been applied for the majority of the studies related to the backwater effect of bridge elements (e.g., Schneider et al., 1977; Shearman et al., 1986; Beffa, 1996). HEC-RAS has incorporated two methods based on the energy equation to

quantify the backwater effect of bridge elements including a standard method and a method developed by Federal Highway Administration (FHWA). The value of the head loss coefficient for bridge abutments, used in HEC-RAS, is given in Table 2.2.

Table 2.1. Base drag coefficients of various bridge pier shapes (*HEC-RAS Reference Manual, 2002*)

Pier shape	Base drag coefficient
Circular pier	1.20
Elongate pier with semi-circular ends	1.33
Elliptical piers with 2:1 length to width	0.60
Elliptical piers with 4:1 length to width	0.32
Elliptical piers with 8:1 length to width	0.29
Square nose piers	2.00
Triangular nose with 30 degree angle	1.00
Triangular nose with 60 degree angle	1.39
Triangular nose with 90 degree angle	1.60
Triangular nose with 120 degree angle	1.72

Table 2.2. Head loss coefficients for bridge abutments in subcritcial flow condition (*HEC-RAS Reference Manual, 2002*)

Transitional condition	Contraction	Expansion
Gradual transitions	0.1	0.3
Typical bridge sections	0.3	0.5
Abrupt transitions	0.6	0.8

As indicated in Table 2.2, the head loss coefficient at a bridge opening has been divided into two components, one for the flow contraction upstream of the bridge and one for the flow expansion downstream from the bridge. The total head loss coefficient due to the bridge abutments and piers is the summation of the two components. In a study performed by Seckin et al. (1998), the head loss coefficient of bridge abutments and piers for the expansion flow was found to be a function of the bridge opening ratio and the so called pier contraction ratio, e_p, viz.

[2.10] $C_{L(exp)} = -5.28\log(e_r) + 4.39e_p - 0.744$

where e_p is the ratio of the total cross-sectional area of the piers to the total contracted area. They found that the head loss coefficient for the contracting flow remains almost constant regardless of the opening ratios used in practice.

In spite of many years of study of the backwater effect due to bridge elements, there are a very limited number of studies reported in the literature about the backwater effect due to spur dikes. Backwater effect studies of spur dikes are even fewer in instances where the spur dikes are placed in series as in the case of spur dike fields. In a study performed by Chee (1979), the backwater effect of unsubmerged spur dikes was studied based on application of the energy equation. The study was limited to single spur dikes, double spur dikes with the same length located opposite to each other on either side of the channel (symmetrical), and double spur dikes with different lengths located opposite to each other on either side of the channel (unsymmetrical). It was concluded that the head loss coefficient, C_L, is mainly a function of the opening ratio. Table 2.3 represents the head loss coefficient for a single spur dike. Chee (1979) also introduced a correction factor for the backwater effect of double spur dikes. The correction factor was 1.20 and 1.30 for symmetrical and unsymmetrical double spur dikes, respectively.

Table 2.3. Head loss coefficients for a single unsubmerged spur dike (*Chee, 1979*)

Opening ratio, e_r	0.2	0.4	0.6	0.8	1.0
Head loss coefficient, C_L	0.74	0.72	0.55	0.20	0.0

An experimental study was performed by Oak (1992) to obtain the backwater effect due to a single spur dike for both submerged and unsubmerged conditions. The submergence of the spur dike was defined as ratio of the tailwater (i.e., downstream) depth to the height of the spur dike. Spur dikes having a rectangular shape and very small thickness (2-D) as well as those having a triangular cross section with a rounded nose (3-D) were investigated in the study. Based on Oak's experiments, Smith (1995) used regression analysis to develop two

empirical relationships for the prediction of the backwater effect due to 2-D spur dikes for both submerged and unsubmerged conditions, viz.

[2.11] $$\frac{h_u}{h} = 1 + 20(1 - e_r)^{1.8} Fr^{1.8};\ h_u / P \le 1$$

[2.12] $$\frac{h_u}{h} = 1 + C_p(1 - e_r)^{1.6} Fr^{1.5};\ h_u / P \ge 1$$

where P is the height of the spur dike. The opening ratio, e_r, for a spur dike is defined as the contracted width to the total width of the channel (b/B in Figure 2.15). Eq. [2.11] is applied for the unsubmerged condition, while Eq. [2.12] is applied for the submerged condition. In Eq. [2.12], the effects of the submergence are shown by the coefficient C_p, which is determined to be

[2.13] $$C_p = 3.9\left(\frac{h}{P}\right)^{-2.4}$$

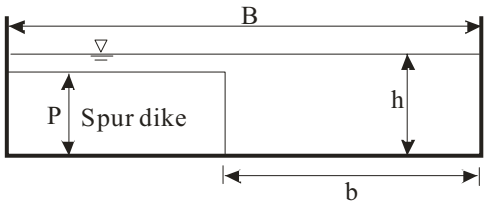

Figure 2.15. Schematic of a cross-section downstream from a single submerged spur dike

The two equations developed from Oak's (1992) study and reported by Smith (1995) (i.e., Eqs. [2.11] and [2.12]) show that the opening ratio and Froude number are considered the most important parameters in determining the backwater effect of a single spur dike. Since the relationships were obtained using regression analysis, their application is limited to the range of the experimental parameters evaluated in the study.

Using a physical model, a study was done by Krouzecky and Merlino (2003) to characterize the effects of unsubmerged spur dike fields on the backwater effect. The study was performed for two-dimensional PVC and three-dimensional stone spur dikes subjected to

various discharges, contraction ratios (i.e., spur dike length to channel width), channel longitudinal slopes and spur dike spacings. It was concluded that there is no significant difference between the two types of spur dikes (i.e., PVC and stone) on the backwater effect. Their results confirm the existence of a backwater effect for all experimental conditions. The backwater effect is higher for experimental conditions with higher discharges and higher contraction ratios. However, the relative spur dike spacing (i.e., ratio of the spur dike spacing to the spur dike length) had a negligible effect on the backwater effect. Despite the above results, no further analysis was made by the authors to develop a mathematical model for predicting the resistance or backwater effect due to unsubmerged spur dikes.

In a recent study carried out by Yossef (2004), the effect of the submergence level (defined by Yossef as the spur dike height to flow depth in the spur dike region) on the resistance of spur dikes was investigated. A physical model based on the dimensions of the Dutch River Waal was used and a spur dike field, composed of five successive spur dikes, was placed within the river model. Yossef used a momentum balance for a unit length of the flow and obtained a relationship for the resistance of the spur dikes, which was expressed in terms of a drag coefficient. The drag coefficient calculations for the spur dikes were based on flow depth and velocity measurements. The drag coefficient was obtained as a function of the Froude number of the flow and blockage (the blockage is considered by Yossef to be equal to the submergence level) caused by the spur dikes. He also related the resistance of the spur dikes to the overall resistance of the river in terms of an increased Chezy coefficient.

It is argued by the author of the present thesis that Yossef's model only provides an approximate estimation of the spur dike resistance. Many assumptions were made in calculating the drag coefficient of spur dikes in the spur dike field. Based on the momentum principle, Yossef (2004) used the following relationship to estimate the drag coefficient of a spur dike in the spur dike field, viz.

$$[2.14] \qquad ghi = \frac{g}{C_{base}^2} u_{gr}^2 + \frac{1}{2} C_D \left(\frac{h_g}{S} \right) u_{gr}^2$$

where g is the acceleration due to gravity, h is the local flow depth, i is the local water surface slope (assumed to be equal to the energy slope), C_{base} is the base Chezy coefficient

(which is considered to be equal to the Chezy coefficient in the main channel), u_{gr} is the velocity in the spur dike region away from the mixing layer (i.e., the interface between the spur dike and the main channel region), C_D is a representative drag coefficient for the spur dikes, h_g is the spur dike height and S is the spacing between adjacent spur dikes, which was taken to be constant in Yossef's work. In order to solve Eq. [2.14], it was assumed that the energy slope in the main channel is equal to that of the spur dike region. Based on the latter assumption, the left-hand side of Eq. [2.15] was obtained from the main channel parameters (i.e., Chezy coefficient and velocity), viz.

$$[2.15] \quad ghi = \frac{g}{C_{base}^2} u_{mc}^2$$

where u_{mc} is the main channel flow velocity. In order to obtain the spur dike drag coefficient, the velocity and depth of flow were measured at only one cross section, located upstream of the fifth spur dike. The author of the present thesis believes that the flow characteristics of a specific section is not representative of all flow regions in a spur dike field and hence the drag force exerted by each individual spur dike will vary. Moreover, the momentum balance must be established based on two sections (i.e., upstream and downstream of each spur dike). Not only must the energy slope be obtained for at least two sections, but also the energy slope in the main channel region may differ from that in the spur dike region. Nonetheless, the model gives an approximate indication of the overall effects of spur dikes on the resistance of rivers for preliminary analysis of flood stages.

2.7. Resistance and drag coefficient of a single two-dimensional plate

The resistance characteristic of rectangular spur dikes in a flow is similar to that of two-dimensional plates. The drag coefficient of a plate, C_{Do}, installed in a wind tunnel in free-stream conditions and having negligible blockage is a function of its aspect ratio (Hoerner, 1965) as shown in Table 2.4 in which P and L are the height and length of the plate normal to the flow direction, respectively.

Table 2.4. Drag coefficient of a rectangular plate in a wind tunnel (*Hoerner, 1965*)

Plate aspect ratio, P/L	0.0	0.05	0.10	0.20	1.0
Drag coefficient, C_{Do}	2.0	1.5	1.3	1.2	1.18

For cases where the plate is large in area compared to the test section of a wind tunnel, there is an effect due to the boundaries of the wind tunnel or flume on the flow pattern near the plate. This phenomenon is referred to as a blockage effect. Many studies have been conducted to investigate the effects of flow boundaries on the drag coefficient of plates and other objects. Shaw (1971) studied the effects of side walls on the flow passing over a two-dimensional plate. In that work, it was realized that there is a relationship between the drag coefficient of a two-dimensional plate and the opening ratio (opening width to channel width). As the opening ratio increases, and hence the effect of the channel walls decreases, the drag coefficient decreases accordingly. Ranga Raju and Singh (1976) studied the blockage effects on the drag of sharp-edged bodies. For a vertical square plate placed at the centre of a wind tunnel having a square cross-sectional shape, they proposed the following relationship:

$$[2.16] \quad C_D = C_{Do}\left(1 - \frac{A_s}{A_t}\right)^{-2.25}$$

where C_D is the drag coefficient of the plate with the existence of the blockage effects, C_{Do} is the drag coefficient of the plate without the existence of the blockage effects (given in Table 2.4), A_s is the projected area of the plate and A_t is the cross-sectional area of the wind tunnel. The blockage ratio is expressed as A_s/A_t. It was also found that an increase in the blockage increases the absolute magnitude of the pressure behind the plate (base pressure), while the pressure in front of the object remains almost constant.

In another study conducted by Laneville and Trepanier (1986) on two-dimensional plates, the observation of Ranga Raju and Singh (1976) about the effects of the blockage on base pressure was confirmed. They proposed the following relationship to correct for the blockage effect, viz.

$$[2.17] \quad C_D = \frac{C_{Do}}{1 + (L/P)^{-0.05/(A_s/A_t)} - \xi (A_s/A_t)^{1.4}}$$

where ξ is a function of W/P and turbulence intensity. Here, W is the thickness of the plate in the streamwise direction. The value of ξ increases with an increase in W/P and turbulence intensity. The proposed equation is limited to a blockage ratio of 6.5% to 13% and a turbulence intensity of 0.6 to 12%.

The effect of the free surface on the drag coefficient of two-dimensional plates has not been given much attention. Froude number, which is a ratio of the inertial force to the gravity force, represents the flow regime in free surface flows. Klaka et al. (2004) have measured the drag force of two-dimensional plates from which the drag coefficients of the plates were calculated. It was concluded that the Froude number has a marginal effect on the drag coefficient. In a study carried out by Malavasi and Guadagnini (2003) on the hydrodynamic forces exerted on bridge decks, it was shown that the Froude number affects the drag coefficient of bridge decks as shown in Figure 2.16. The Reynolds and Froude numbers were calculated based on the deck thickness, s. The effect of the Reynolds number was assumed to be negligible for a highly turbulent flow regime. Figure 2.16 represents the variation of the drag coefficient with the submergence ratio and the Froude number. In their work, the submergence ratio was defined as

$$[2.18] \quad h^* = \frac{h_u - h_b}{s}$$

where h_u and h_b are upstream flow depth and the distance between the channel bed and the deck bottom, respectively. It is observed that the drag coefficient of a bridge deck varies substantially with the submergence ratio, while the Froude number has only a moderate effect on the drag coefficient. It might also be observed that, for a constant Froude number, the maximum drag coefficient occurs for a submergence ratio slightly greater than unity.

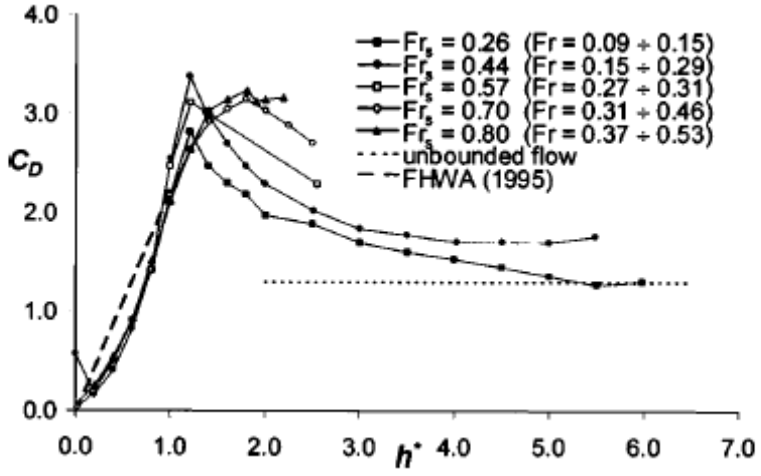

Figure 2.16. Variation of the drag coefficient of a bridge deck with the submergence ratio and the Froude number (*Taken from Malavasi and Guadagnini, 2003*)

2.8. Resistance and drag coefficient of two-dimensional plates placed in succession (i.e., tandem arrangement)

The drag coefficient of two plates placed in a tandem arrangement with various relative spcaings between the two plates has been measured by Hirano et al. (1983) and reported by Ohya et al. (1989). The relative spacing was defined as the ratio of the spacing to the length of the plates. It was observed that there is a steady decrease in the drag coefficient of the upstream plate with the relative spacing as the relative spacing varies from 0 to 4. The drag coefficient of the front plate increases as the relative spacing becomes greater than 4. Nonetheless, the drag coefficient of the upstream plate is very close to the drag coefficient of a single plate. The drag coefficient of the downstream plate is considerably less than the drag coefficient of a single plate and the upstream plate, and it is negative in some instances (for a relative spacing less than 1.8). The drag coefficient of the downstream plate experiences a steady decrease in magnitude as the relative spacing varies from 0 to 1.2. A sharp decrease in the downstream plate drag coefficient is observed for a relative spacing of about 1.2 after which the drag coefficient increases with the relative spacing. Regardless, the relative spacing of the downstream plate remains low even for high relative spacings. For example, the drag coefficient of the downstream plate is about half of that for a single plate at a relative spacing of about 10.

A study has been done by Ball and Cox (1978) for a series of plates placed in a group in an open channel. In their study, the Froude number and the plate lengths were held constant, while the distance between the plates was varied. The submergence ratio (approach flow depth to plate height) was held constant and equal to unity. For plates placed in succession, the relative drag force (the drag force of a specific plate in the row to the drag force of a single plate within the same flow condition) was the largest for the most upstream plate but was still less than unity. The relative drag force decreased for plates placed further downstream. It was also found that the variation in the spacing between the plates had an effect on the relative drag force of each individual plate. Their results also showed that there is a critical spacing to length ratio of about four where the relative drag force of the plate is a minimum.

Morris (1955) performed a study on the spacing effects of roughness elements on the flow regime and bed friction. He divided the flow regime into three categories, including isolated-roughness flow, wake-interference flow and skimming flow. If there is sufficient space between the roughness elements, there is no interaction between the elements. In this condition, the wake zone is completely developed and the vortices are completely dissipated before the next roughness element. If the spacing between the roughness elements is reduced to the point that the next downstream element is placed in the wake zone of the element just upstream, then an interaction will occur between the roughness elements. This type of flow is called wake-interference flow. For cases where the roughness elements are very close together, the separated flow from an upstream roughness element may skim over the next roughness element. This type of flow is called skimming or quasi-smooth flow.

Similar flow is probably valid for deeply submerged spur dikes, but the flow regime is likely to change if the free surface flow becomes a dominant parameter affecting the flow resistance. This is usually the case for spur dikes as they are either unsubmerged or the degree of submergence is not that high compared to roughness elements which are deeply submerged. On this basis, the backwater is not an issue for roughness elements, while it is an important parameter governing the flow regime in spur dikes. That said, there is a similarity between the effects of the spacing on the flow field and hence flow resistance between the roughness elements and spur dikes. As to the spacing between the spur dikes used in

practice, it is expected that the flow regime in a spur dike field would be categorized as wake interference.

2.9. Modeling of the flow field adjacent to spur dikes using CFD techniques

With the development of two- and three-dimensional numerical modeling techniques, several studies have been done in the past two decades to describe and model the flow pattern near single spur dikes and within spur dike fields (e.g., Richards, 1990; Molls et al., 1995; Ouillon and Dartus, 1997; Peng et al., 1997; Krebs et al., 1999; Jia and Wang, 2000; Zhou et al., 2000; Tominaga et al., 2001; Chang-bo et al., 2002; Miller et al., 2003; Minor et al., 2007). However, in all of the above studies, there is no systematic research about the effects of the spur dikes on the water surface profile including the backwater effect. In order to track the free surface flow including the backwater effect in a CFD model, it is necessary to introduce a free surface. There are two major methods (in the Eulerian system) for introducing the free surface flow into a numerical model, including the surface height method and the volume of fluid method. In both methods, the continuity equation is modified near to the free surface level in the form of a kinematic equation.

In the surface height method, the total height of the flow relative to a reference elevation (Hydraulic Grade Line), H_G, is introduced to the model to give the following relationship for the continuity equation, viz.

$$[2.19] \quad \frac{\partial H_G}{\partial t} + u\frac{\partial H_G}{\partial x} + v\frac{\partial H_G}{\partial y} = w$$

where u, v and w are the velocity components in the x, y and z directions, respectively and t is time. It must be noted that the above equation is used for incompressible fluids. The surface height equation is appropriate for free surface flow that does not deviate too much from the horizontal (Flow-3D, 2007).

In the volume of fluid method, the free surface flow is tracked by introduction of a variable into the computational cells, namely the volume fraction value (FLUENT, 2005). The volume fraction value in a cell identifies the ratio of two (or more) immiscible fluids in a

cell. For a free surface flow involving water and air, for example, the volume fraction, F_{vof}, is shown as

$$[2.20] \quad F_{vof} = \frac{\Omega_{water}}{\Omega_{cell}}$$

where Ω_{water} and Ω_{cell} are the volume of water in the computational cell and the total volume of the cell, respectively. It is realized that a cell completely filled with water has a volume fraction of unity, while a cell completely filled with air has a volume fraction of zero. The cells with a volume fraction between unity and zero contain a free surface. Based on the above definition, the continuity equation near to the cells with a free surface is modified to

$$[2.21] \quad \frac{\partial F_{vof}}{\partial t} + u\frac{\partial F_{vof}}{\partial x} + v\frac{\partial F_{vof}}{\partial y} + w\frac{\partial F_{vof}}{\partial z} = 0$$

The continuity equation is only solved for water, while the volume fraction of air is calculated from that of water ($\frac{\Omega_{air}}{\Omega_{cell}} = 1 - F_{vof}$). The volume of fluid method has been found to be very efficient and flexible for tracking complicated free surface patterns (Ouillon and Dartus, 1997).

2.10. Conclusions

In summary, although the very limited amount of available literature clarifies some aspects of spur dike resistance and backwater effect, there is still no exact and comprehensive method to quantify the amount of resistance for submerged spur dikes and spur dike fields. While some studies are limited due to the nature of the model development (e.g., regression analysis) and the narrow range of the effective parameters (e.g., the contraction ratio in Oak's work varies from 0.4 to 0.6), some others give a very approximate estimation for the resistance of spur dikes that may be used for initial assessments (Yossef, 2004). There is also a lack of an appropriate explanation about the effects of spur dikes on the overall resistance of a riverine system. Although some independent studies have been performed to obtain the resistance (in the form of a drag force) for objects that behave similar to spur dikes (but not

exactly the same), there is no systematic study to relate the resistance of these structures with the dimensions and arrangement of the objects as well as the flow characteristics in open channel flows.

2.11. References

Abad, J.D., Rhoads, B.L., Guneralp, I. and Garcia, M.H. 2008. Flow structure at different stages in a meander-bend with bendway weirs. Journal of Hydraulic Engineering, ASCE, 134(8): 1052-1063.

Al-Nassri, S. 1994. Effect of bridge pier shape and contraction ratios on backwater profile. Proc. of Hydraulic Engineering Conference, ASCE, Buffalo, NY, USA, pp. 563-568.

Ball, D.J. and Cox, N.J. 1978. Hydrodynamic drag forces on groups of flat plates. Journal of the Waterway, Port, Costal, and Ocean Division, ASCE, 104(WW2): 163-173.

Beffa. C. 1996 Backwater computation for transcritical river flows. Journal of Hydraulic Engineering, ASCE, 122(12): 745-748.

Chang-bo, J., Chen, Y.K., Bai, Y.C. and Zhao, Z.D. 2002. Numerical simulation of separated flow near groynes. Journal of Hydrodynamics, Elsevier, China, 14(4): 47-52.

Charbeneau, R.J. and Holley, E.R. 2001. Backwater effect on bridge piers in subcritical flow. Texas Department of Transportation, Research Report Number 0-1805-1, TX, USA, 102 p.

Chee, S.P. 1979. River training structures and its effect on the regime of waterways. Proc. of 4th National Hydrotechnical Conference, CSCE, Vancouver, BC, Canada, pp. 306-315.

Chen, F.Y. and Ikeda, S. 1997. Horizontal separation flows in shallow open channels with spur dikes. Journal of Hydroscience and Hydraulic Engineering, JSCE, 15(2): 15-30.

Fenton, J.D. 2003. The Effects of obstacles on surface levels and boundary resistance in open channel. Proc. of 30th IAHR Congress, Thessaloniki, Greece, Theme C, Hydraulic Resistance, pp. 9-16.

Flow-3D website. Accessed 2007. The basics of computational fluid dynamics (CFD) modeling. (http://www.flow3d.com/cfd101/cfd101_free_surf.html).

FLUENT. 2005. Fluent user's manual. Fluent Incorporated, Lebanon, NH, USA, 32 chapters.

Ghodsian, M. and Shafieefar, M. 2001. Afflux upstream of circular bridge pier. Proc. of 29th IAHR Congress, Beijing, China, Theme D, Design of Hydraulic Structures, pp. 108-112.

Haltigin, T.W., Biron, P.M. and Lapointe, M.F. 2007. Three-dimensional numerical simulation of flow around stream deflectors: The effect of obstruction angle and length. Journal of Hydraulic Research, IAHR, 45(2): 227-238.

HEC-RAS V. 3.1. 2002. HEC-RAS reference manual; River analysis system. US Army Corps of Engineers, Institute for Water Resources, Davis, CA, USA, 16 chapters.

Hoerner, S.F. 1965. Fluid-dynamic drag; practical information on aerodynamic drag and hydrodynamic resistance. Hoerner, S.F., Brick Town, NJ, USA, 20 chapters.

Ishii, C., Asada, H. and Kishi, T. 1983. Shape of separation region formed behind a groyne of non-overflow type in rivers. Proc. of 20th IAHR Congress, Moscow, USSR, pp. 405-412.

Jia, Y. and Wang, S.S.Y. 2000. Numerical study of turbulent flow around submerged spur dikes. 4th International Conference on Hydro-Science and Engineering, Korea Water Resources Association, Seoul, South Korea, 7 p.

Klaka, K., Penrose, J.D., Horsley, R.R. and Renilson, M.R. 2005. Hydrodynamic test on a fixed plate in uniform flow. Experimental Thermal and Fluid Science, Elsevier, 30(22): 131-139.

Klingeman, P.C., Kehe, S.M. and Owusu, Y.A. 1984. Streambank erosion protection and channel scour manipulation using rockfill dikes and gabions. WRRI-98, Oregon State University, Water Resources Research Institute, Corvallis, OR, USA, 169 p.

Koken, M. and Constantinescu, G. 2008. An investigation of the flow and scour mechanisms around isolated spur dikes in a shallow open channel: Conditions corresponding to the initiation of the erosion and deposition process. Water Resources Research, American Geophysical Union, 44, 19 p.

Krebs, M., Zanke, U. and Mewis, P. 1999. Hydro-morphodynamic modeling of groin fields. Proc. of 28th IAHR Congress, Graz, Austria, 7 p.

Krouzecky, N. and Merlino, L. 2003. Physical model tests for determination of pondage due to non-submerged groins. Proc. of 30th IAHR Congress, Thessaloniki, Greece, Theme C, Hydraulics of Groynes, pp. 369-376.

Kuhnle, R., Jia, Y. and Alonso, C. 2002. 3-Dimensional measured and simulated flow for scour near spur dikes. Proc. of the First International Conference on Scour of Foundations, ICSF-1, Texas A&M University, TX, USA, pp. 349-363.

Kuhnle, R., Jia, Y. and Alonso, C. 2008. Measured and simulated flow near a submerged spur dike. Journal of Hydraulic Engineering, ASCE, 134(7): 916-924.

Laneville, A. and Trepanier, J.Y. 1986. Blockage effects in smooth and turbulent flows: The case of two-dimensional rectangular cylinders. Journal of Wind Engineering and Industrial Aerodynamics, Elsevier, 22(2-3): 169-176.

Lim, S.Y. 1997. Equilibrium clear-water scour around an abutment. Journal of Hydraulic Engineering, ASCE, 123(3): 237-243.

Liu, H.K., Bradley, J.N. and Plate, E.J. 1957. Backwater effects of piers and abutments. Colorado State University, Report CER57HKLIO, Boulder, CO, USA, 364 p.

Malavasi, S. and Guadagnini, A. 2003. Hydrodynamic loading on river bridges. Journal of Hydraulic Engineering, ASCE, 129(11): 854-861.

Marson, C., Caroni, E., Fiorotto, V. and Deppo, L. 2003. Flow field analysis around a groyne. Proc. of 30th IAHR Congress, Thessaloniki, Greece, Theme C, Hydraulics of Groynes, pp. 377-384.

McCoy, A., Constantinescu, G. and Weber L. 2007. A numerical investigation of coherent structures and mass exchange process in channel flow with two lateral submerged groynes. Water Resources Research, American Geophysical Union, 43, 26 p.

McCoy, A., Constantinescu, G. and Weber L. 2008. Numerical investigation of flow hydrodynamics in a channel with a series of groynes. Journal of Hydraulic Engineering, ACSE, 134(2): 157-172.

Miller, R., Roulund, A., Sumer, B.M., Fredsoe, J., Truelsen, C. and Michelsen, J. 2003. 3-D numerical modeling of flow around a groin. Proc. of 30th IAHR Congress, Greece, Theme C, Hydraulics of Groynes, pp. 385-392.

Melville, B.W. 1997. Pier and abutment scour: Integrated approach. Journal of Hydraulic Engineering, ASCE, 123(2): 125-136.

Minor, B., Rennie, C.D. and Townsend, R.D. 2007. Barbs for river bend bank protection: application of a three-dimensional numerical model. Canadian Journal of Civil Engineering, NRC press, 34(9): 1087-1095.

Mioduszewski, T., Maeno, S. and Uema, Y. 2003. Influence of the spur dike permeability on flow and scouring during a surge pass. Proc. of International Conference on Estuaries and Coasts, Hangzhou, China, pp. 308-388.

Molinas, A., Kheireldin, K. and Wu, B. 1998. Shear stress around vertical wall abutments. Journal of Hydraulic Engineering, ASCE, 124(8): 822-830.

Molls, T., Chaudhry, M.H. and Khan, K.W. 1995. Numerical simulation of two-dimensional flow near a spur-dike. Advances in Water Resources, Elsevier, 18(4): 227-236.

Morota, K. and Tsuchiya, M. 2003. Study on the effect of placement of seigyu groins at confluence and curve. Proc. of 30th IAHR Congress, Thessaloniki, Greece, Theme C, Flood Control Works and Debris Flow, pp. 55-62.

Morris, H.M. 1955. Flow in rough conduits. Transaction of American Society of Civil Engineers, ASCE, Vol. 120, Paper No. 2745: 373-410.

Oak, A.G. 1992. Backwater rise due to a submerged spur. M.Sc. thesis, University of Saskatchewan, 63 p.

Ohya, Y., Okajima, A. and Hayashi, M. 1989. Encyclopedia of fluid mechanics; Volume 8: Aerodynamics and compressible flows; Section 1: Turbulence phenomena and modeling; Chapter 10: wake interference and vortex shedding. Gulf Publishing Company, Houston, TX, USA.

Ouillon, S. and Dartus, D. 1997. Three-dimensional computation of flow around groyne. Journal of Hydraulic Engineering, ASCE, 123(11): 962-970.

Paquier, A., Bristeau, M.O., Proust, S., Riviere, N. and Champagne, J.Y. 2003. Comparison of 2D flow modeling around a groyne. Proc. of 30th IAHR Congress, Thessaloniki, Greece, Theme C, Hydraulics of Groynes, pp. 393-400.

Peng, J., Kawahara, Y. and Tamai, N. 1997. Numerical analysis of three-dimensional turbulent flows around submerged groins. Proc. of 27th IAHR Congress, Theme A, Managing Water, San Francisco, CA, USA, pp. 829-834.

Pinter, N., Thomas, R. and Wlosinski, H. 2001. Assessing flood hazard on dynamic rivers. EOS, Transactions, American Geophysical Union, 82(31): 333-339.

Rajaratnam, N. and Nwachukwu, B.A. 1983. Flow near groin-like structures. Journal of Hydraulic Engineering, ACSE, 109(3): 463-480.

Ranga Raju, K.G. Rana, O.P.S., Asawa, G.L. and Pillai, A.S.N. 1983. Rational assessment of blockage effects in channel flow past smooth circular cylinders. Journal of Hydraulic Research, IAHR, 21(4): 289-302.

Ranga Raju, K.G. and Singh, V. 1976. Blockage effect on drag of sharp-edged bodies. Journal of Industrial Aerodynamics, Elsevier, 1: 301-309.

Richards, D.R. 1990. Flow separation around a solitary dike. Eddy viscosity and mesh considerations. Hydraulic Engineering, Proc. of the 1990 National Conference, ASCE, San Diego, CA, USA, pp. 867-872.

Seckin G., Yurtal R. and Haktann T. 1998. Contraction and expansion losses through bridge constriction. Journal of Hydraulic Engineering, ASCE, 124(5): 546-549.

Schneider, V.R., Board, J.W., Colson, B.E., Lee, F.N. and Druffel, L. 1977. Computation of backwater and discharge at width constrictions of heavily vegetated flood plains. U.S. Geological Survey, Water Resources Investigations, Bay St. Luis, MI, USA, pp. 76-129.

Shaw, T.L. 1971. Effect of side walls on flow past bluff bodies. Journal of Hydraulic Division, ASCE, 97(HY1): 65-79.

Shearman, J.O., Kirby, V.H., Schneider, V.R. and Flippo, H.N. 1986. Bridge waterways analysis model. U.S. Department of Transportation, Federal Highways Administration, Research Report FHWA/RD-86/108, Reston, VA, USA, 126 p.

Shields, F.D. and Gippel, C.J. 1995. Prediction of effects of woody debris removal on flow resistance. Journal of Hydraulic Engineering, ASCE, 121(4): 341-354.

Smith, C.D. 1995. Hydraulic structures. Published by University of Saskatchewan Printing Services, Saskatoon, SK, Canada, 11 chapters.

Sukhodolov, A., Engelhardt, C., Kruger, A. and Bungartz. 2004. Case study: Turbulent flow and sediment distribution in a groyne field. Journal of Hydraulic Engineering, ASCE, 130(1): 1-9.

Sukhodolov, A., Uijttewaal, W.S.J. and Engelhardt, C. 2002. On the correspondence between morphological and hydrodynamical patterns of groyne fields. Earth Surface Process and Landforms. John Wiley & Sons, 27: 289-305.

Tominaga, A., Ijima, K. and Nakano, Y. 2001. Flow structures around submerged spur dikes with various relative height. Proc. of 29th IAHR Congress, Beijing, China, Theme D, Hydraulic Structures, pp. 421-427.

Uchida, T. and Fukuoka, S. 2001. Two-dimensional analysis of shallow water flow with submersible large roughness elements. Proc. of 29th IAHR Congress, Hydraulic of Rivers, Water Works and Machinery, Beijing, China, Theme D, Hydraulic Structures, pp. 364-370.

Uijttewaal, W.S.J. 1999 Groyne field velocity patterns determined with particle tracking velocimetry. Proc. 28th IAHR Congress, Graz, Austria, 8 p.

Uijttewaal, W.S.J., Lehmann, D. and Mazijk, A. 2001. Exchange processes between a river and its groyne fields: Model experiment. Journal of Hydraulic Engineering, ASCE, 127(11): 928-936.

Weitbrecht, V., Socolofsky, S.A. and Jirka, G.H. 2008. Experiments on mass exchange between groin fields and main stream in rivers. Journal of Hydraulic Engineering, ASCE, 134(2): 173-183.

Wu, F.C., Shen, H.W. and Chou, Y.J. 1999. Variation of roughness coefficient for unsubmerged and submerged vegetation. Journal of Hydraulic Engineering, ASCE, 125(9): 934-942.

Yarnell D.L. 1934. Bridge piers as channel obstructions. U.S. Department of Agriculture, Report No. 442, Washington D.C., USA, 25 p.

Yossef, M.F.M. 2004. The effect of the submergence level on the resistance of groynes: an experimental investigation. The 6th International Conference on Hydroscience and Engineering, Brisbane, QL, Australia, 9 p.

Yossef, M.F.M. 2002. The effects of groynes on rivers (Literature Review). Delft Cluster Report No. DC1-334-4, Delft University, The Netherlands, 57 p.

Zhou, Y., Michiue, M. and Hinokidani, O. 2000. A numerical study on the comparison of 3-D flow properties around submerged spur-dikes. 4th International Conference on Hydro-Science and Engineering, Korean Water Resources Association, Seoul, South Korea, 9 p.

Chapter 3. Flow Resistance Due to a Single Spur Dike in an Open Channel

Contribution of the Ph.D. candidate

All work reported in this chapter, including design of the experimental program, implementation of the experiments, review of the literature, development of the theoretical framework, analysis and discussion of the results and writing of the text, has been carried out by the Ph.D. candidate.

As supervisor, Dr. J.A. Kells reviewed all parts of the work. A shortened version of this chapter has been published with the following citation:

> Azinfar H, and Kells, J.A. 2009. Flow resistance due to a single spur dike in an open channel. Journal of Hydraulic Research, IAHR, 47(6): 755-763.

This chapter contains additional details not found in the journal paper as published, including more explanation of the drag force measurement apparatus and drag force calculation (Figures 3.2 and 3.4 as well as Table 3.1), comments on the establishment of normal flow depth in the flume (Figures 3.5 and 3.6), inclusion of the velocity profile measurement (Figure 3.7), calculation of the impingement velocity (Equations 3.10 and 3.11), inclusion of the experimental results and measurements (Table 3.3) and explanation of bed shear stress effects (Figure 3.12).

Contribution of this chapter to the overall study

The work presented in this chapter quantifies the flow resistance and associated backwater effect due to a single spur dike in an open channel for various flow conditions, spur dike geometries, and submergence modes. In this chapter, a theoretical framework has been developed for assessing and predicting the flow resistance and backwater effect due to a single spur dike. The results of the research described herein also make a contribution toward improving the understanding of the role of the various physical parameters on the flow resistance and backwater effect of a single spur dike.

.

3.1. Abstract

A method for quantifying the resistance or drag force exerted on the flow in an open channel due to a single spur dike is presented. The work was carried out in a rigid bed flume, with the model spur dike being simulated using various sizes of a rectangular plate. The drag force exerted by the spur dike for both submerged and unsubmerged flow conditions was determined directly from measurements made using a specially-designed apparatus and also by application of the momentum equation to a control volume that included the spur dike. It was found that the drag force of an unsubmerged spur dike increases more rapidly with an increase in the discharge relative to that of a submerged spur dike. The results also show that an increase in the blockage due to the spur dike is the main parameter responsible for an increase in the spur dike drag coefficient, hence the associated flow resistance. Based on the experimental results obtained in this work, relationships are given for estimating the backwater effect due to a single spur dike in an open channel.

3.2 Introduction

Spur dikes are structures that project from the bank of a stream at some angle to the main flow direction. They are principally used for river training and for protection of the river bank from erosion. In the context of river training for river-based navigation, spur dikes may be used to provide for both a sufficient depth of flow and an improved channel alignment. They can also be used to deflect the flow toward a desirable point within a channel such as a water intake. With respect to erosion control, spur dikes can be used to deflect the high velocity flow away from an erodible bank and thereby protect the bank from erosion. Depending on the river discharge and height of the structure, spur dikes may operate in either a submerged or an unsubmerged mode.

Despite their useful features, there is concern that spur dikes may be responsible for increased flooding due to the associated increase in channel resistance in some instances. For example, studies show that, over the past century, flood stages for given discharges at various locations along the Middle Mississippi and Lower Missouri rivers have increased by 2 m to 4 m (Criss and Shock, 2001). Pinter et al. (2001) have attributed part of the observed stage

increases on these rivers to the construction of spur dikes. Stage increases due to spur dikes have also been reported on the Rhine River in Europe (Yossef, 2002; Belz et al., 2001). There, it has subsequently been decided to reduce the height of the spur dikes as a way of reducing their adverse effects during times of flooding. Wu et al. (2005) have observed the backwater effect of long spur dikes constructed on the Lower Yellow River in China and, similarly, in a numerical study of the Nile River in Egypt, it has been predicted that the construction of spur dikes would increase upstream water levels (Soliman et al., 1997).

In the present work, the increased water level in an open channel (i.e., backwater effect) due to a single spur dike is related to the spur dike resistance or drag force. This resistance has been determined experimentally for various sizes of spur dike, angles of orientation and discharge conditions within a rigid-bed flume. Both submerged and unsubmerged conditions are evaluated. The resistance is expressed in terms of a drag coefficient.

3.3 Theoretical considerations

The effect of a spur dike on an open channel flow can be considered to either induce an energy loss in the flow or a drag force exerted on the flow. On this basis, the flow around a spur dike (and hence backwater effect) can either be analyzed using an energy approach or a momentum approach. The energy loss around an unsubmerged spur dike is mostly due to flow separation, vortex generation and turbulence, as well as boundary friction associated with the increased local velocity around the structure. The vortex structure vortices adjacent to a spur dike is shown in Figure 2.5 (Miller et al., 2003) for unsubmerged spur dikes and Figure 2.6 (Kuhnle et al., 2008) for submerged spur dikes. Both figures show a large vertical axis vortex just downstream from the spur dike as well as transverse axis and horizontal axis vortices adjacent to the spur dike. For the submerged condition, the overtopping flow from the top edge of the spur dike may result in the development of a small hydraulic jump on the leeward side of the dike. This hydraulic jump, which is mostly suppressed by the side flow from the side edge of the spur dike, adds to the energy loss associated with the spur dike in such instances. All of these energy losses are difficult to quantify. Application of the momentum equation, on the other hand, avoids the need to consider energy losses in the

analysis. Instead, the drag force exerted on the flow by the spur dike, and other relevant forces, provide the basis for the analysis using the momentum approach. In the present study, the momentum approach was used in the analysis of the flow resistance due to a single spur dike in an open channel.

Application of the momentum equation to the flow field within a control volume involving a single spur dike yields the resistance or drag force of the spur dike exerted on the flow. The drag force due to a spur dike produces an increase in the upstream water level, which is in essence a backwater effect. With reference to Figure 3.1, the one-dimensional linear momentum equation can be written along the channel between section 1 upstream of the spur dike and section 2 downstream to give

[3.1] $$F_1 - F_2 - F_D - F_f + F_w = \rho Q(\beta_2 V_2 - \beta_1 V_1)$$

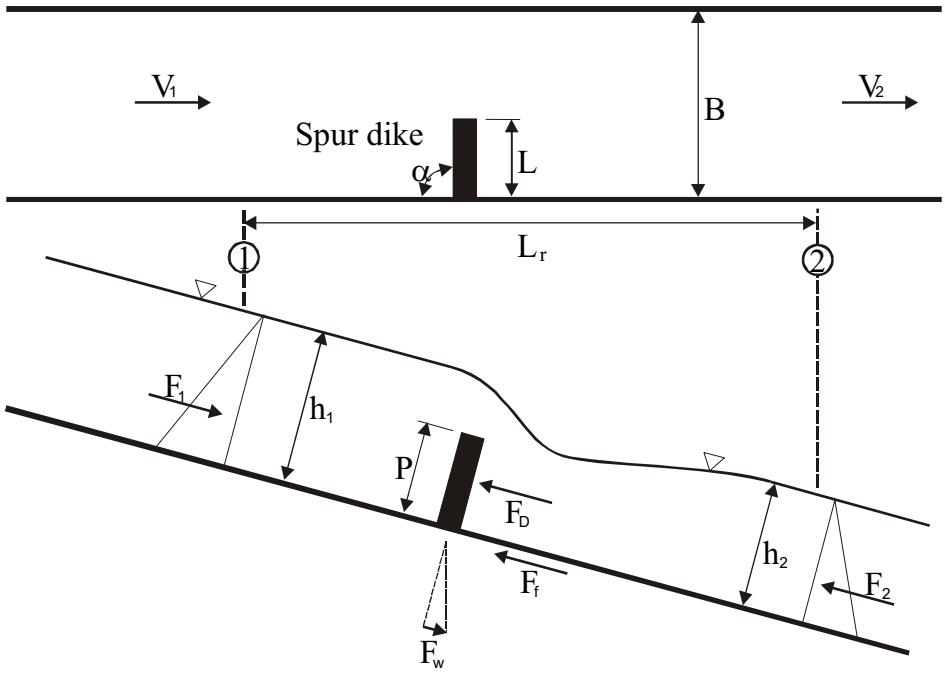

Figure 3.1. Schematic illustration (plan and profile) of a spur dike within a control volume (i.e., the region between sections 1 and 2)

where F_1 is the force due to the upstream hydrostatic pressure distribution, F_2 is the force due to the downstream hydrostatic pressure distribution, F_D is the drag force due to the spur dike, F_f is the force due to boundary friction between sections 1 and 2, F_w is the downstream component of the weight of the fluid within the control volume (i.e., between sections 1 and 2), ρ is the fluid density, Q is the discharge, V_1 and V_2 are the mean velocities at sections 1 and 2, respectively, and β_1 and β_2 are the momentum correction factors applicable at sections 1 and 2, respectively.

In the case of uniform flow in an open channel, the downstream component of the weight of the fluid within the control volume (i.e., between sections 1 and 2) is equal to the frictional resistance along the boundary (i.e., $F_f = F_w$). When a spur dike is placed within a uniform flow field, the water surface becomes distorted relative to the normal depth, as illustrated schematically in Figure 3.1. Herein, however, it has been assumed that $F_f = F_w$ is still approximately valid. Thus, for analysis purposes, both terms may be omitted from Eq. [3.1]. Rearranging the remaining terms in Eq. [3.1], the resistance or drag force of a single spur dike exerted on the flow is given by

$$[3.2] \quad F_D = \frac{1}{2}\rho g B h_1^2 - \frac{1}{2}\rho g B h_2^2 - \rho Q(\beta_2 V_2 - \beta_1 V_1)$$

where the hydrostatic pressure force terms have been expressed in terms of the flow depths. Here, B is the channel width, g is the acceleration due to gravity (i.e., 9.81 m/s^2), and h_1 and h_2 are the upstream and downstream flow depths, respectively. The backwater effect due to the spur dike is represented by the difference between the upstream and downstream flow depths (i.e., $\Delta h = h_1 - h_2$).

The drag force, F_D, which is exerted by the spur dike on the flow, can be expressed using the basic drag equation as

$$[3.3] \quad F_D = C_D A_s \frac{\rho V^2}{2}$$

where C_D is the drag coefficient, A_s is the upstream projected area of the spur dike, and V is a representative approach velocity. For a submerged spur dike, $A_s = PL$, where P is the height of the spur dike and L is the length of the spur dike normal to the flow direction. For an unsubmerged spur dike, P is replaced by the upstream flow depth, h_1 (i.e., $A_s = h_1 L$).

From a hydraulic point of view, it is usually convenient to relate an unknown parameter in a subcritical open channel flow to the known downstream flow conditions. However, for objects immersed within a flow field, it is usual to relate the drag force to the approach flow conditions. Moreover, the upstream flow depth is a more appropriate parameter for defining the submergence condition of a spur dike insofar as it reflects the condition at which overtopping of the spur dike occurs. In turn, it is felt that the submergence condition of a spur dike has a direct effect on the flow resistance that is experienced. Thus, for this study, the spur dike resistance has been expressed as a function of the approach (i.e., upstream) flow conditions. To this end, the representative approach velocity is taken to be the average impingement velocity, V_{imp}, which occurs just upstream of the face of the spur dike. The average impingement velocity represents the average velocity of the portion of the approach flow that is in line with the projected area of the spur dike. It was judged to be the physically relevant velocity parameter for drag computations as it represents the dynamic pressure that directly contributes to the drag force exerted on the spur dike.

From dimensional analysis, the drag coefficient of a submerged spur dike can be expressed in terms of a functional equation as

$$[3.4] \quad C_D = f_1(Re_1, Fr_1, A_r, P/L, h_1/P, \Delta, \alpha)$$

where Re_1 and Fr_1 are the Reynolds number and Froude number of the upstream flow, respectively. A_r is the blockage ratio of the spur dike defined by

$$[3.5] \quad A_r = \frac{A_s}{h_1 B}$$

Here, P/L is the aspect ratio of the submerged spur dike, h_1/P is the spur dike submergence ratio, Δ is the shape factor of the spur dike, and α is the angle between the spur dike and the stream bank or flow direction (Figure 3.1). For an unsubmerged spur dike, dimensional analysis leads to a slightly different functional relationship for the drag coefficient, viz.

$$[3.6] \quad C_D = f_2(Re_1, Fr_1, L/B, h_1/L, \Delta, \alpha)$$

where L/B is the blockage ratio of the spur dike, which is similar to A_r for a submerged spur dike, and h_1/L is the depth to length ratio of an unsubmerged spur dike. In the case of angled spur dike, the projected area (submerged conditions) or length (unsubmerged conditions) of the spur dike normal to the main flow direction is used in calculating the blockage ratio.

Some of the independent parameters in Eqs. [3.4] and [3.6] can be omitted from the further analysis due to the fact that they are either insignificant compared to others or because they were held fixed in the experimental program of this study. For example, it is well known that fluid viscosity in high Reynolds number flows has an insignificant effect on the drag coefficient of a two-dimensional rectangular plate (2-D plate) in a flow field (Munson et al., 1998). As such, Reynolds number effects are not considered further in this work. In the present study, spur dikes with a fixed shape (i.e., 2-D plates) have been used so that the shape factor, Δ, may also be omitted from further analysis. The shape factor might be thought as a ratio of the drag coefficient of a spur dike having an arbitrary shape (e.g., one having a trapezoidal cross section) to the drag coefficient of a spur dike having a more basic shape (e.g., 2-D spur dike plate), all other things being equal.

In contrast to independent parameters that can be omitted from further analysis, it is known that the blockage of an object immersed in a flow field has a substantial effect on the drag coefficient (Shaw, 1971). Ranga Raju and Singh (1976) conducted a series of experiments to study the effects of blockage on the drag coefficient of sharp-edged, 2-D plates placed within a wind tunnel. They proposed the following relationship to account for the blockage effects of a 2- D plate having negligible thickness, viz.

[3.7] $$C_D = C_{Do}(1 - \frac{P}{D})^{-2.25}$$

where C_{Do} is the drag coefficient of a 2-D plate without blockage effects, P is the height of the plate and D is the height of the wind tunnel. In Eq. [3.7], C_{Do} may be thought of as a base drag coefficient. The parameter P/D represents the blockage ratio.

Combining Eqs. [3.2] and [3.3], along with the continuity equation and the assumption that the momentum correction factors are equal to unity, leads to

[3.8] $$2Fr_1^2\left(\frac{h_1}{h_2}\right)^3 - \left(2Fr_1^2 - C_D\theta A_r Fr_1^2 + 1\right)\left(\frac{h_1}{h_2}\right)^2 + 1 = 0$$

where θ is the impingement velocity parameter, which is defined as

[3.9] $$\theta = \left(\frac{V_{imp}}{V_1}\right)^2$$

Eq. [3.8] can be solved implicitly for the upstream flow depth and hence the backwater effect if the downstream flow conditions (i.e., depth and discharge), spur dike and channel geometry (which, in some respects, are both implicit in the variable A_r), the impingement velocity parameter and the drag coefficient are known.

For a given projected area of a submerged spur dike, A_s, an increase in the flow depth results in a decrease in the blockage ratio, A_r. Eq. [3.8] shows that, as the blockage ratio decreases to a limiting value of zero, the ratio h_1/h_2 approaches a value of unity, which corresponds to a condition of no backwater effect, as it should. In the case of an unsubmerged spur dike, A_r is given by L/B, which is independent of the flow depth, h_1 (i.e., A_r is constant in this instance). As such, there is no similar effect in respect of the impact on the backwater effect. Further discussion on the backwater effect due to an unsubmerged spur dike is provided later. It is also evident from Eq. [3.8] that, as the projected area of either a submerged or an unsubmerged spur dike approaches a limiting value of zero, the blockage ratio approaches zero, which results in a condition of no backwater effect.

3.4 Experimental program

An experimental program was established to quantify the flow resistance due to a single spur dike within an open channel flow. Plates representing 2-D spur dikes of various geometries were installed in a tilting flume located in the Hydrotechnical Laboratory at the University of Saskatchewan. The flume width, height and length are 800 mm, 600 mm and 10 m, respectively. The drag force exerted by the spur dike plate on the flow was obtained using two different methods. For the first method, the drag force was calculated using the momentum equation (Eq. [3.2]). The second method involved direct measurement of the drag force using a specially-designed apparatus. The calculated and measured drag forces were compared to assess the assumptions used in the momentum equation. The discharge and flow depths were measured using an electromagnetic flow meter and a point gauge, respectively. A tailgate was used to regulate the flow depth. A micro-propeller current meter was used for the velocity measurements, which included measuring several vertical velocity profiles within the flow field. The diameter of the micro-propeller was 15 mm. The velocity profiles were used in determining the impingement velocity and the momentum correction factor.

The drag force measurement apparatus consists of three streamlined and cantilevered aluminum bars projecting from a rigid top plate. At the bottom, the bars are connected to an aluminum base plate (50 mm$\times$100 mm) by ball joints. The design allowed for aluminum plates of various dimensions to be subsequently attached to the base plate. The drag force exerted on the plate is equal to the sum of the three reaction forces exerted at the ends of the three cantilevered bars. The reaction forces create three moments at the fixed ends of the cantilevered bars. The strains due to the moments are detected using six strain gauges, two on each cantilevered bar. In turn, the strain gauges are connected to a data acquisition system and finally to a computer for recording the strains.

For calibration purposes, the drag force apparatus was clamped in a horizontal position and the base plate was detached from the three cantilevered bars. For each cantilevered bar, a series of standard weights were hung from the bar using a fine wire connected to the point where the ball joint would be fastened to the bar. The strains from the

two strain gauges of each particular bar were recorded for each standard weight both before and after the placement of the standard weight. The difference between the two sets of strain gauge readings with and without the standard weight was correlated to the standard weight. The procedure was repeated for several standard weights for the first cantilevered bar and in turn for the two other bars. Figure 3.2 shows the correlation between the standard weights (in mass units, M) and the net micro-strain (strain $\times 10^6$) for each cantilevered bar. After calibration of each individual cantilevered bar, the base plate was connected to the bars using the ball joints. The combined performance of the cantilevered bars was then tested using three different loads (i.e., drag forces) exerted at various locations on the base plate, with the apparatus still held in a horizontal position.

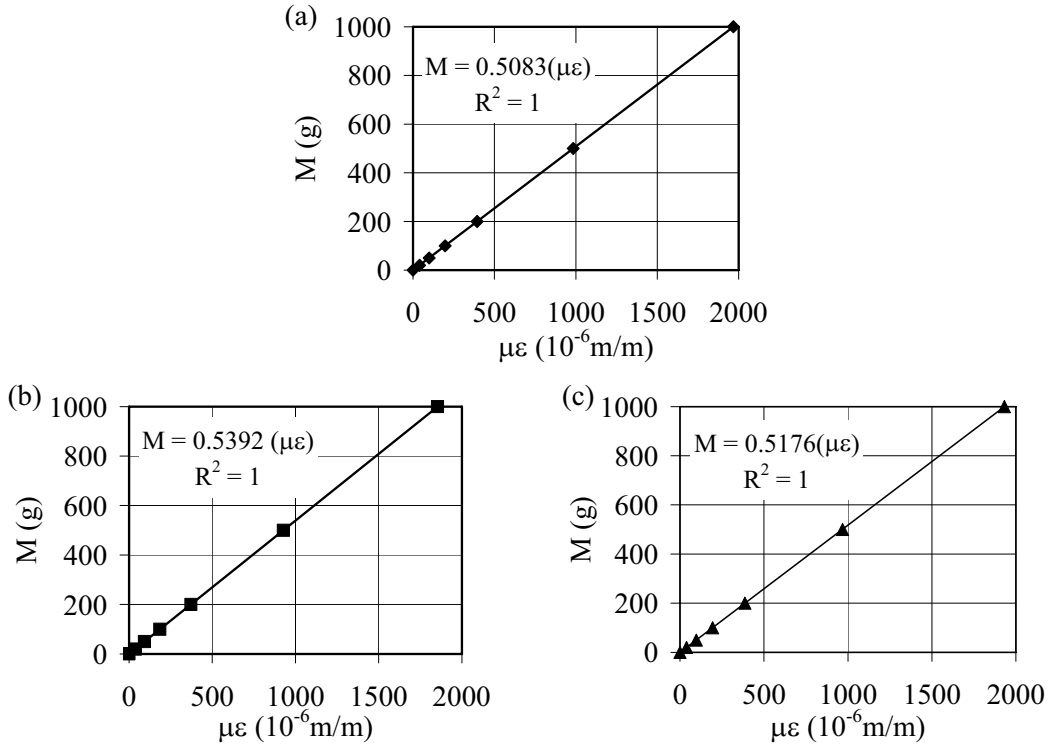

Figure 3.2. Correlation between the mass of standard weights and the micro-strain in the cantilevered bars; (a) left bar, (b) middle bar, and (c) right bar (left and right as viewed downstream)

Table 3.1 shows the results of the calibration measurements. It is to be noted that, over the range of the measurements made, the maximum average error is about 2%. Photographs of the drag force measurement apparatus are shown in Figure 3.3.

Table 3.1. Combined performance of the calibrated cantilevered bars for drag force measurement

Applied mass (g)	Measured mass (g)	Mean (g)	Average error (g)
500	504, 502, 500, 516, 497, 498, 498, 511	504	5
200	199, 201, 198	199	1
100	104, 102, 101	102	2

Figure 3.3. Apparatus for drag force measurement of 2-D spur dike plates

The apparatus was fastened into the study flume by means of a simple frame. The design was such that it was possible to adjust the position of the various sizes of spur dike plates both vertically and horizontally so as to allow for only a very small gap, in the order of 1 mm, between the plate and the flume wall and floor. During the experimental program, it was observed that the drag force due to the spur dike plate is not sensitive to the gap size, at least for gaps up to a value of about 3 mm. Moreover, for comparison purposes, some tests were done with a PVC spur dike plate attached directly to the bed and wall. For the same size of spur dike plate and discharge condition, the backwater effect was observed to be

exactly equal to the backwater effect when the plate was attached to the drag force measurement apparatus and located about 1 mm from the bed and wall of the flume.

For each spur dike plate configuration and for each discharge condition, the strains of the three cantilevered bars were recorded for a period of time so that a time-mean strain could be used in the subsequent force analysis. To evaluate the test duration needed to produce acceptable mean drag force results, the force-strain results for one test condition were obtained over a 1.5-hr recording period. The results are shown in Figure 3.4.

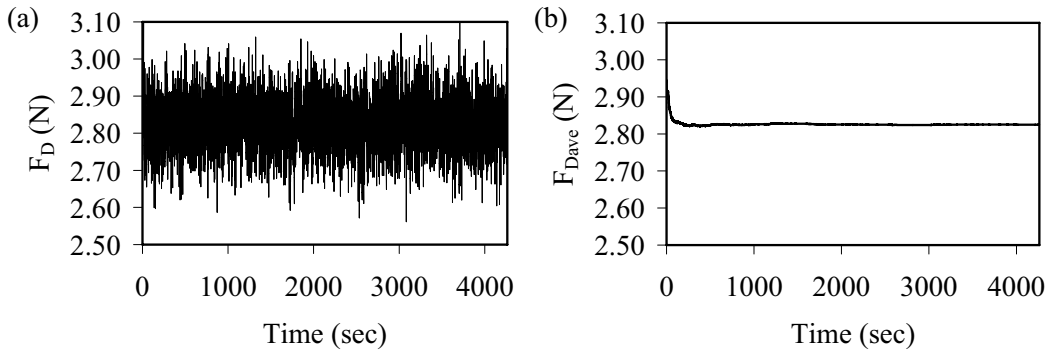

Figure 3.4. Variation of the drag force with time for one of the experiments: (a) instantaneous drag force, and (b) cumulative average drag force

For this test, the spur dike plate height and length were 50 mm and 200 mm, respectively, the discharge was 30.2 L/s and the upstream and downstream water depths were measured as 86 mm and 78 mm, respectively. Figure 3.4a shows the variation of the instantaneous drag force with time, while Figure 3.4b shows the variation of the cumulative average drag force with time. As the results indicate, there is no systematic oscillation in the drag force with time and that the average drag force becomes quite stable within a period of less than about five minutes (i.e., 300 sec). The standard deviation of the measured drag force was calculated to be about 0.075 N, which gives a 5.2% variation from the average drag force within 95% confidence limits. That the measured drag force was relatively stable with time is indicative of the relatively low turbulence intensity of the incoming flow. On the

basis of this test result, a five-minute recording period was used for the strains used in calculating the drag force exerted by the spur dike plate on the flow.

Even though the cantilevered bars were designed with a streamlined shape, the drag force exerted on the bars was nonetheless determined separately (i.e., a "tare" force) so that a net drag force due to the spur dike plate could be determined for subsequent analysis purposes. This was done for each test condition throughout the study. Typically, the tare force was in the order of 0.1 N.

The flume slope was set to 0.000975 m/m. By setting a variety of discharges and through adjustment of the downstream tailgate, it was possible to experimentally establish the stage-discharge relationship for uniform flow conditions in the flume. The stage-discharge relationship is shown in Figure 3.5.

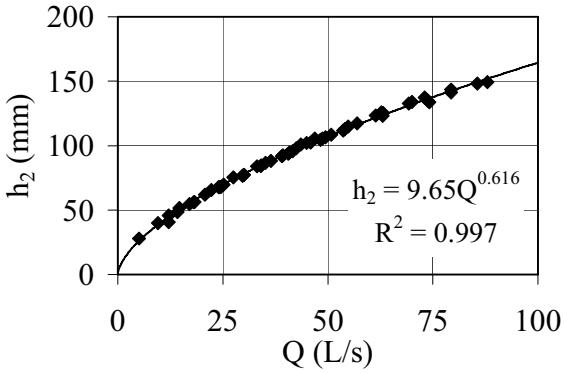

Figure 3.5. Stage-discharge relationship for uniform flow conditions in the laboratory flume (S_o = 0.000975 m/m)

For each test, uniform flow conditions were established in the flume prior to the installation of the spur dike plate. As such, the backwater effect was defined as being the difference between the uniform flow depth without any spur dike plate in place and the resulting upstream depth with the spur dike plate in place as shown in Figure 3.6.

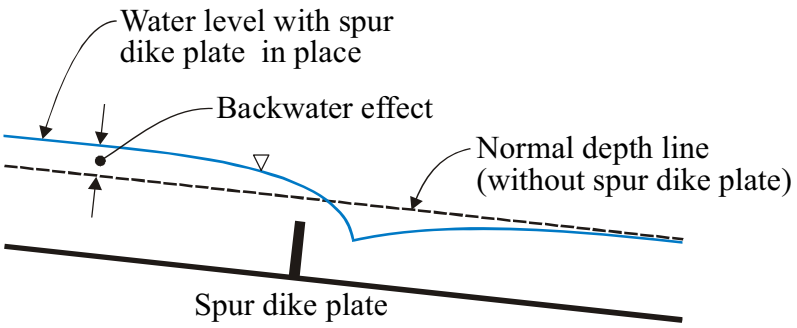

Figure 3.6. Schematic illustration showing the backwater effect due to a single spur dike

As a precursor to the study, it was necessary to assess the flow development in the flume (i.e., boundary layer development, existence of uniform flow conditions) so that the model spur dike was appropriately placed in a region of fully established, uniform flow. For a discharge of 30.4 L/s, the vertical velocity profile was measured along the centerline of the flume. The resulting vertical velocity profiles along the centerline of the flume are shown in Figure 3.7, where the longitudinal distances, x, are shown from the flume inlet (i.e., x = 0). On the basis of these results, it was concluded that the flow was fully established a short distance from the flume inlet and well before the place where the spur dike plates were located (x = 5.0 m) and the upstream flow depths were measured. This finding is in agreement with an analytical assessment of the boundary layer development.

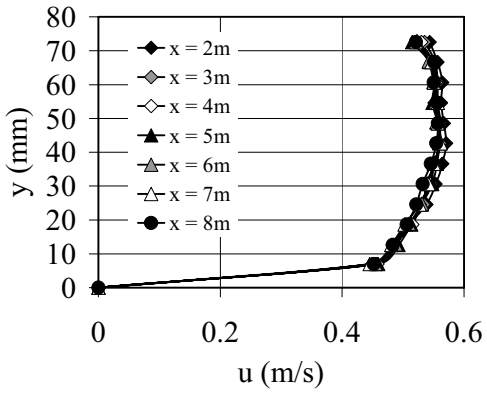

Figure 3.7. Vertical velocity profiles along the centerline of the flume (Q = 30.4 L/s, h_2 = 79 mm)

For subcritical flow conditions in which the Froude number exceeds 0.1, it has been found that the Froude number has minimal effect on the drag coefficient of a thin 2-D plate (Naudascher and Medlarz, 1983; Klaka et al., 2005; Azinfar and Kells, 2007). Ettema and Muste (2004) also found that there is no pronounced effect on the flow structure around a single spur dike, including in the separation region, for Froude numbers in the range 0.2 - 0.6. The drag coefficient of a spur dike is usually governed by the flow structure and especially by the separation region in the lee of the spur dike. As the Froude numbers of the flow evaluated in this work exceeded a value of 0.1, the effect of the Froude number on the drag coefficient has not been considered further in this study.

Two-dimensional spur dike plates of various dimensions were installed along the right side (looking downstream) of the flume, midway along its length (i.e., at x = 5.0 m). For each size of spur dike plate, a range of discharges was set. For each discharge, the uniform flow depth and the flow depth at a location about 0.5 m upstream of the spur dike plate were measured in the centerline of the flume. Both submerged and unsubmerged flow conditions were evaluated. Table 3.2 shows the range of the parameters evaluated in the study.

Table 3.2. Range of experimental parameters evaluated in the study

Submerged spur dikes		**Unsubmerged spur dikes**	
Parameter	**Range**	**Parameter**	**Range**
Aspect ratio, P/L	0.083-0.50	Flow depth to length ratio, h_1/L	0.128-1.62
Blockage ratio, A_r	0.042-0.65	Blockage ratio, L/B	0.12-0.50
Submergence ratio, h_1/P	1.03-3.18	Orientation angle, α	90°
Orientation angle, α	45°-135°	Channel aspect ratio, h_1/B	0.051-0.20
Channel aspect ratio, h_1/B	0.068-0.20	U/S Froude number, Fr_1	0.25-0.55
U/S Froude number, Fr_1	0.15-0.58		

Figures 3.8a and 3.8b show the model in operation for the case of both submerged and unsubmerged flow conditions, respectively. The difference between the water levels upstream and downstream for each of the two spur dike plates is clearly evident.

(a) 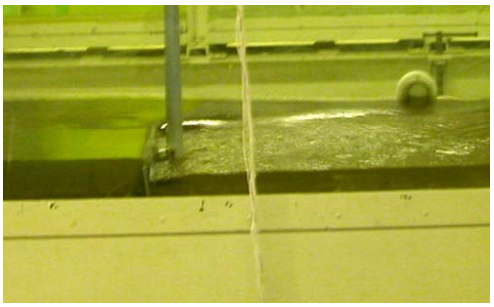 (b) 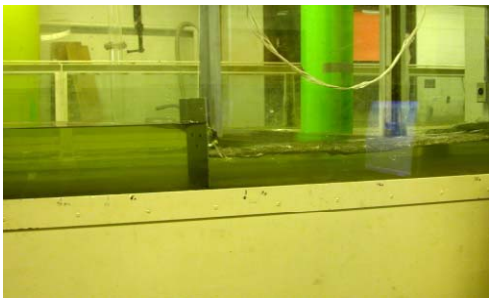

Figure 3.8. Model in operation for (a) a submerged spur dike plate, and (b) an unsubmerged spur dike plate

Assessment of the impingement velocity was done in the backwater region at a location where the upstream flow depth was measured, which was just beyond the region immediately upstream of the spur dike where the velocity distribution of the flow was altered due to the presence of the spur dike. Upstream of this area (i.e., within the M1 profile), the horizontal velocity distribution is symmetrical about the centerline of the flume (i.e., z = 0.40 m). Velocity distribution measurements show that, in a cross-section as close as 0.5 m upstream of the spur dike plate, the vertical velocity profiles are symmetrical about the centreline of the flume cross-section. On this basis, the upstream flow depth measurements and assessment of the impingement velocity were done about 0.5 m upstream of the spur dikes plate.

Velocity distribution measurements were not performed for all test conditions. Thus, to assess the impingement velocity for other test conditions, recourse was made to the model developed by Yang et al. (2004). The model was calibrated using the available velocity distribution measurements. In their model, Yang et al. postulated that the velocity at any location within a rectangular open channel flow in a fully-developed flow region can be described by

$$[3.10] \quad \frac{u}{u_*} = \frac{1}{\kappa}\ln\left(\frac{y}{y_0}\right) + \frac{\delta}{\kappa}\ln\left(1 - \frac{y}{h}\right)$$

where u is the longitudinal time-averaged velocity at a distance y from the channel bed and a distance z from the channel wall, u_* is the overall bed shear velocity, $(gRS_f)^{0.5}$, for the

channel, R is the hydraulic radius of the flow, S_f is the energy slope of the flow, $y_0 = \upsilon/u_*(z)$ is the distance above the bed at which the velocity is hypothetically equal to zero, υ is the kinematic viscosity of the fluid, $u_*(z)$ is the local bed shear velocity at distance z from the wall, κ is the von Karman constant, and h is the flow depth. In the present study, the energy slope was taken to be equal to the flume slope. The parameter δ, which is related to the dip phenomenon common in open channel flows, particularly those having a narrow aspect ratio (i.e., channel width to flow depth ratio), represents the deviation of the vertical velocity profile from the classical log-law profile.

The velocity profiles used for the calibration of the Yang et al. (2004) model were taken both for uniform flow conditions without any spur dike plate in place and at a location a short distance upstream of a spur dike plate. The plate used here had dimensions of 50 mm high by 400 mm long and was located midway along the length of the flume (i.e., x = 5.0 m). For uniform flow conditions without the spur dike plate in place, velocity distribution measurements were made at x = 5.0 m for several discharges, which varied from 9.7 L/s to 67.2 L/s. This range of discharge covers most of the experiments as shown in Tables 3.3 and 3.4. With the spur dike plate in place, the measurements were taken upstream of the plate at x = 4.5 m, also for several discharges. On the basis of all of the velocity measurements made, two relatively simple equations were determined for Yang et al.'s δ parameter and the local bed shear velocity, viz.

$$[3.11a]\ \delta = 0.23\left(\frac{z}{h}\right)^{-0.48} + 0.29$$

$$[3.11b]\ \frac{u_*(z)}{u_*} = 1 - \exp\left(-4.85\frac{z}{h}\right)$$

The major difference between the calibrated relationships given by Eqs. [3.11a] and [3.11b] and those presented in Yang et al. (2004) is the position of the maximum velocity in the vertical profile relative to the location of the free surface (i.e., the dip phenomenon). The Yang et al. (2004) relationships show that the dip phenomenon disappears for the transverse points for z/h > 5 (i.e., the maximum velocity occurs at the free surface of the flow) while the

dip phenomenon was observed for all velocity profiles measured in this work, including for $z/h > 5$. Eqs. [3.10] and [3.11], along with velocity-area-integration using MATHCAD 2000, were used to calculate the impingement velocity. The average impingement velocity was then used in the subsequent drag force analysis.

3.5 Results and discussion

3.5.1. Direct measurement of the drag force due to a single spur dike

The results of the drag force and flow depth measurements associated with each spur dike plate geometry are shown in Tables 3.3 and 3.4 for both the submerged and unsubmerged modes of operation, respectively.

Table 3.3. Experimental results of drag force measurements for submerged spur dike plate

Spur dike dimensions (height, mm × length, mm and angle of orientation)																	
50 × 100 (90°)						50 × 200 (90°)						50 × 250 (90°)					
Q (L/s)	h_1 (mm)	h_2 (mm)	F_D (N)	Fr_1	Re_1	Q (L/s)	h_1 (mm)	h_2 (mm)	F_D (N)	Fr_1	Re_1	Q (L/s)	h_1 (mm)	h_2 (mm)	F_D (N)	Fr_1	Re_1
14.6	54.0	51.6	0.55	0.47	6.45E+04	15.1	59.0	49.5	2.18	0.34	6.56E+04	12.1	54.4	40.6	2.46	0.38	5.32E+04
20.8	64.6	62.0	0.76	0.50	8.94E+04	20.1	69.2	59.9	2.61	0.35	8.58E+04	18.0	67.2	56.0	3.08	0.41	7.72E+04
40.8	97.4	94.6	1.09	0.54	1.64E+05	25.2	78.6	69.4	2.78	0.37	1.05E+05	24.6	78.2	68.0	3.81	0.45	1.03E+05
41.7	97.8	95.6	1.04	0.54	1.67E+05	30.4	86.0	78.4	3.16	0.39	1.25E+05	30.1	87.6	77.4	3.92	0.46	1.23E+05
43.6	103.2	100.8	1.11	0.52	1.73E+05	35.0	96.8	85.9	2.87	0.37	1.41E+05	34.1	94.0	84.6	4.14	0.47	1.38E+05
49.4	109.2	106.6	1.27	0.55	1.94E+05	44.2	106.8	100.1	3.45	0.40	1.75E+05	40.6	103.6	93.8	4.32	0.49	1.61E+05
50.8	110.2	108.4	1.36	0.55	1.99E+05	49.5	116.4	107.8	3.38	0.40	1.92E+05	48.3	114.0	104.6	4.65	0.50	1.88E+05
61.4	124.4	123.4	1.43	0.56	2.34E+05	59.3	127.4	121.2	3.76	0.42	2.25E+05	54.0	121.4	112.8	4.75	0.51	2.07E+05
69.3	134.6	132.8	1.38	0.56	2.59E+05							63.1	131.8	123.2	5.14	0.53	2.37E+05
79.4	148.0	143.4	1.56	0.56	2.90E+05							73.8	144.8	134.8	5.37	0.53	2.71E+05
79.4	144.0	141.2	1.65	0.58	2.92E+05							88.0	159.2	149.4	5.90	0.55	3.15E+05
50 × 400 (90°)						50 × 600 (90°)						75 × 150 (90°)					
Q (L/s)	h_1 (mm)	h_2 (mm)	F_D (N)	Fr_1	Re_1	Q (L/s)	h_1 (mm)	h_2 (mm)	F_D (N)	Fr_1	Re_1	Q (L/s)	h_1 (mm)	h_2 (mm)	F_D (N)	Fr_1	Re_1
12.1	64.0	45.8	5.27	0.30	5.20E+04	5.1	57.6	28.0	7.97	0.15	2.22E+04	23.9	75.6	67.8	2.58	0.46	1.01E+05
17.1	74.4	54.6	6.22	0.34	7.19E+04	9.6	68.8	39.8	9.72	0.21	4.07E+04	25.2	77.4	69.8	2.80	0.47	1.06E+05
22.2	83.6	65.6	7.34	0.37	9.19E+04	14.2	78.8	48.4	11.44	0.26	5.92E+04	29.9	85.4	77.2	3.16	0.48	1.23E+05
27.5	92.4	75.4	7.70	0.39	1.12E+05	18.2	86.4	56.2	12.59	0.29	7.50E+04	35.2	95.0	86.6	3.55	0.48	1.42E+05
33.1	101.0	84.0	7.98	0.41	1.32E+05	24.2	97.2	67.8	14.03	0.32	9.75E+04	39.1	100.6	91.8	3.78	0.49	1.56E+05
36.4	105.8	88.2	8.51	0.42	1.44E+05	29.7	105.8	76.6	14.74	0.34	1.17E+05	45.0	110.2	102.2	3.91	0.49	1.76E+05
42.4	114.6	97.8	8.95	0.44	1.65E+05	34.1	112.8	84.2	15.45	0.36	1.33E+05	48.7	113.2	105.6	4.29	0.51	1.90E+05
46.9	120.4	105.4	8.97	0.45	1.80E+05	39.3	120.4	92.6	15.89	0.38	1.51E+05	54.9	123.4	114.8	4.22	0.51	2.10E+05
57.0	132.6	117.2	9.96	0.47	2.14E+05	45.9	129.2	102.4	16.84	0.39	1.73E+05	62.7	133.4	125.8	4.53	0.51	2.35E+05
63.1	140.8	125.4	9.88	0.48	2.33E+05	53.6	139.0	111.6	17.53	0.41	1.99E+05	70.1	142.0	133.8	4.56	0.52	2.58E+05
73.0	152.4	137.4	10.23	0.49	2.64E+05							74.2	144.2	133.6	4.95	0.54	2.73E+05
												85.6	157	148.0	5.60	0.55	3.07E+05

Note: Drag force, F_D, was measured using the drag force measurement apparatus.

Table 3.3.(cont'd.)

Spur dike dimensions (height, mm × length, mm and angle of orientation)																	
50 × 400 (45°)						50 × 400 (112.5°)						50 × 400 (135°)					
Q (L/s)	**h_1 (mm)**	**h_2 (mm)**	**F_D (N)**	**Fr_1**	**Re_1**	**Q (L/s)**	**h_1 (mm)**	**h_2 (mm)**	**F_D (N)**	**Fr_1**	**Re_1**	**Q (L/s)**	**h_1 (mm)**	**h_2 (mm)**	**F_D (N)**	**Fr_1**	**Re_1**
12.0	56.6	44.7	3.92	0.35	5.24E+04	12.1	62.2	45.1	5.38	0.31	5.25E+04	12.0	57.0	44.8	3.88	0.35	5.26E+04
15.4	63.6	52.2	4.36	0.38	6.64E+04	15.6	68.6	52.6	6.01	0.35	6.66E+04	16.1	65.0	53.6	4.58	0.39	6.92E+04
19.2	70.4	59.7	4.73	0.41	8.15E+04	19.3	76.2	60.1	6.62	0.37	8.12E+04	19.3	70.8	59.9	5.00	0.41	8.19E+04
24.4	78.8	69.3	5.11	0.44	1.02E+05	24.2	84.4	68.9	7.13	0.39	9.99E+04	24.3	79.4	69.2	5.39	0.43	1.02E+05
30.4	89.2	79.3	5.45	0.46	1.24E+05	29.9	93.4	78.6	7.54	0.42	1.21E+05	30.4	89.6	79.4	5.69	0.45	1.24E+05
36.1	97.4	88.1	5.74	0.47	1.45E+05	36.1	102.8	88.2	7.95	0.44	1.44E+05	36.3	98.2	88.4	5.93	0.47	1.46E+05
42.7	108.0	97.8	6.07	0.48	1.68E+05	41.9	111.4	96.7	8.31	0.45	1.64E+05	43.7	109.2	99.1	6.30	0.48	1.71E+05
50.1	120.0	108.0	6.81	0.48	1.93E+05	50.2	122.4	108.1	8.81	0.47	1.92E+05	49.9	117.4	107.6	6.50	0.50	1.93E+05
57.8	128.4	117.8	7.35	0.50	2.19E+05	58.1	132.0	118.2	9.31	0.48	2.19E+05	57.4	128.0	117.3	6.79	0.50	2.17E+05
66.4	138.8	128.3	8.00	0.51	2.46E+05	66.0	141.2	127.8	9.56	0.50	2.44E+05	66.5	138.8	128.5	7.06	0.51	2.47E+05
74.6	148.8	137.9	8.50	0.52	2.72E+05	74.6	150.8	137.9	10.20	0.51	2.71E+05	74.5	148.2	137.8	7.45	0.52	2.72E+05
88.4	163.0	153.0	9.52	0.54	3.14E+05	87.9	166.6	152.5	10.51	0.52	3.10E+05	88.3	163.0	152.9	8.16	0.54	3.14E+05

Table 3.4. Experimental results of drag force measurements for unsubmerged spur dike plate

Spur dike dimensions (height, mm × length, mm and angle of orientation)																	
100 × 200 (90°)						200 × 200 (90°)						200 × 400 (90°)					
Q (L/s)	**h_1 (mm)**	**h_2 (mm)**	**F_D (N)**	**Fr_1**	**Re_1**	**Q (L/s)**	**h_1 (mm)**	**h_2 (mm)**	**F_D (N)**	**Fr_1**	**Re_1**	**Q (L/s)**	**h_1 (mm)**	**h_2 (mm)**	**F_D (N)**	**Fr_1**	**Re_1**
9.5	40.6	38.8	0.32	0.46	4.31E+04	9.6	45.4	39.0	0.99	0.40	4.30E+04	7.1	51.2	32.5	3.06	0.25	3.16E+04
14.4	51.2	50.1	0.61	0.50	6.39E+04	14.4	58.8	50.1	1.92	0.40	6.28E+04	12.0	71.4	44.8	8.42	0.25	5.09E+04
19.1	60.2	59.6	0.84	0.52	8.29E+04	19.2	69.4	59.8	2.99	0.42	8.18E+04	15.6	82.6	52.6	11.32	0.26	6.45E+04
23.8	70.4	68.3	1.11	0.51	1.01E+05	24.5	81.6	69.5	4.82	0.42	1.02E+05	15.7	82.6	52.9	11.83	0.26	6.52E+04
30.8	82.0	80.0	1.68	0.52	1.28E+05	29.6	93.0	78.1	6.40	0.42	1.20E+05	19.2	95.4	59.8	16.44	0.26	7.76E+04
35.5	90.0	87.2	2.02	0.52	1.45E+05	35.5	104.6	87.3	7.85	0.42	1.41E+05	24.3	109.0	69.1	24.66	0.27	9.53E+04
42.1	100.2	96.9	2.60	0.53	1.68E+05	39.5	112.8	93.2	9.27	0.42	1.54E+05						
49.1	111.2	106.6	3.30	0.53	1.92E+05	46.4	124.2	102.9	12.04	0.42	1.77E+05						
54.5	119.2	113.6	3.78	0.53	2.10E+05	55.3	139.0	114.7	15.52	0.43	2.05E+05						
62.9	130.0	124.1	4.62	0.54	2.37E+05	65.6	154.8	127.3	22.00	0.43	2.36E+05						
73.6	143.6	136.7	5.85	0.54	2.71E+05												
88.3	160.6	152.9	7.99	0.55	3.15E+05												

Note: Drag force, F_D, was measured using the drag force measurement apparatus.

The drag force exerted on both a submerged and an unsubmerged spur dike plate is shown plotted against the discharge in Figure 3.9. In the figure, the dimensions of the spur dike plate are shown in code form in the legend. The first two digits (submerged conditions) or three digits (unsubmerged conditions) of the code indicates the height of the spur dike plate, while the last three digits of the code indicate the length of the spur dike plate (e.g., 50100 implies a plate 50 mm in height and 100 mm in length). The values in parentheses indicate the orientation of the spur dike plate with respect to the flume wall, α, as indicated in Figure 3.1.

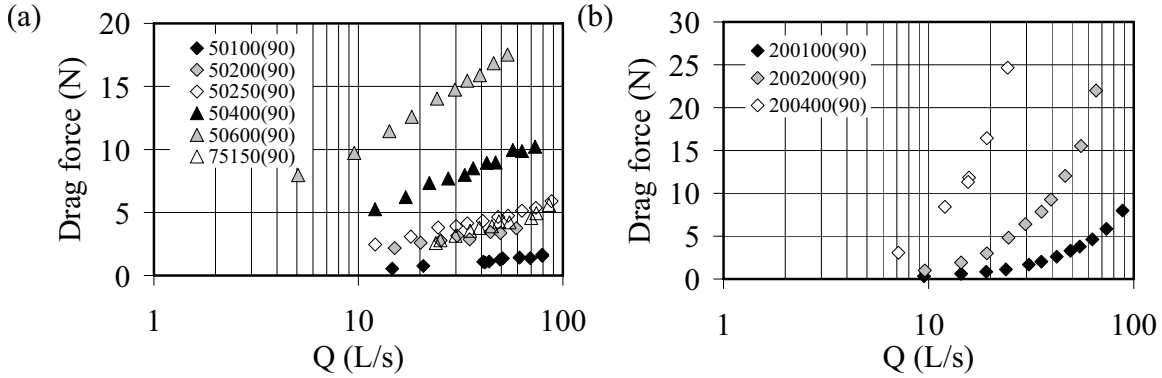

Figure 3.9. Drag force due to spur dike plates of various dimension versus discharge for (a) submerged conditions and (b) unsubmerged conditions

As the results in Figure 3.9 show, for a given discharge, an increase in the size of the spur dike plate results in an increase in the drag force exerted by the plate on the flow. Moreover, this is also true even when the force is normalized by the plate area, thus indicating some additional underlying phenomena affecting the force exerted by the plate. Here, the latter effect is evidenced by comparing the results for a specific size of spur dike plate, wherein the results in Figure 3.9 show that an increase in the discharge results in an increase in the drag force exerted by the plate on the flow. However, there is an apparent difference in the observed trend depending on whether the plate is submerged or unsubmerged. The rate of increase in the drag force with an increase in the discharge for an unsubmerged spur dike plate is much greater than that for a submerged spur dike plate. This outcome shows that there is an apparent difference between the flow structures and hence flow resistance around submerged and unsubmerged spur dike plates.

The effect of the angle of orientation on the drag force of submerged spur dike plates is shown in Figure 3.10. As shown, for a particular size of spur dike plate, the drag force decreases as the orientation of the plate deviates from 90°. This reduction in the drag force is essentially independent of whether the plate is angled upstream or downstream.

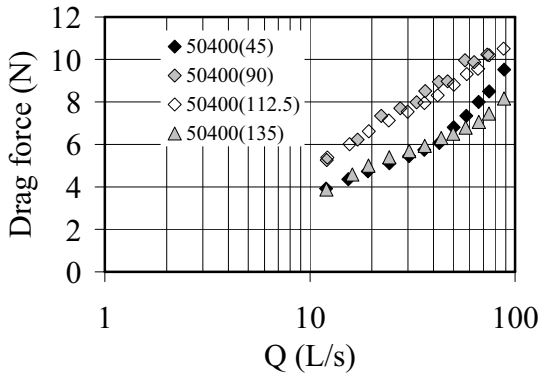

Figure 3.10. Drag force of the submerged spur dike plates with various angles of orientation

3.5.2. Application of the momentum equation for calculating the drag force due to a single spur dike

The drag force exerted by various sizes of spur dike plates inserted into the flow was calculated using Eq. [3.2] for each discharge and for both submerged and unsubmerged modes of operation. For this analysis, the approach flow depth h_1 was taken to be the water depth measured immediately upstream of the spur dike plate but beyond the local drawdown region (i.e., about 0.50 m upstream), while h_2 (i.e., the nominal tailwater condition) was taken to be the uniform depth of flow for the imposed discharge as shown in Figure 3.6. For angled spur dike plates, the measured drag force was taken to be the component of total measured drag force in the streamwise direction. The momentum correction factors in Eq. [3.2] were taken to be equal to unity. Figure 3.11 shows the drag force calculated using Eq. [3.2] versus the drag force measured using the drag force measurement apparatus. The results for both the submerged and unsubmerged conditions are included in the figure. The mean absolute relative error (MRE) is 24.6%.

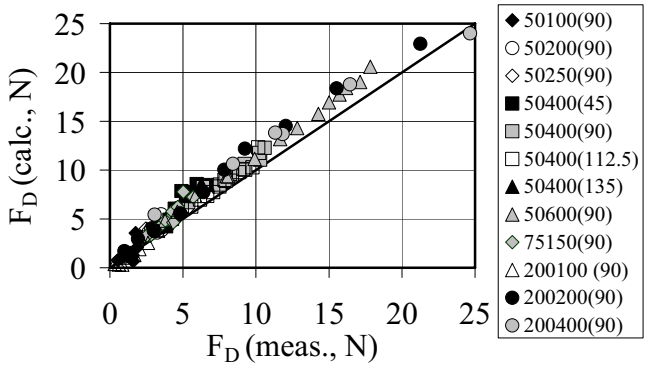

Figure 3.11. Calculated drag force versus measured drag force for both submerged and unsubmerged spur dike plates

As indicated in Figure 3.11, the calculated drag force is, in most cases, greater than the measured drag force. A possible reason for this difference may be partially attributed to the increased bed shear stress that is experienced around the nose of the spur dikes. The latter effect has also been reported by others (e.g., Rajaratnam and Nwachukwu, 1983b; Ouillon and Dartus, 1997). An increased bed shear stress leads to an increase in the boundary friction force on the control volume containing the spur dike. In applying the momentum equation, the boundary friction force was assumed to be equal to the component of the fluid weight acting in the flow direction, such that any increase in the boundary friction force is inherently lumped into the calculated drag force, which results in a higher computed drag force when compared with the measured value.

The average bed shear stress in a control volume containing a spur dike was estimated using the results from a numerical modeling study for one of the experimental test conditions. The results from the study are shown in Figure 5.12. It was found that the average bed shear stress in the control volume containing the spur dike was about 80% greater than the bed shear stress of the incoming flow. The increased friction force (~2 N) due to the increased bed shear stress was calculated to be almost equal to the difference between the calculated (~10 N) and measured (~8 N) drag forces. This finding confirms that the difference between the calculated and measured drag forces is largely related to the increased bed shear stress around spur dikes.

The increase in bed shear stress is not the same for all experimental conditions. Figure 3.12 shows the relationship difference between the calculated and measured drag forces versus the measured drag force. Although the scatter in data is high, it is observed that there is a direct relationship between the measured drag force and the difference between the calculated and measured drag forces. On this basis, one may conclude that the increase in bed shear stress is greater for spur dikes with a greater drag force.

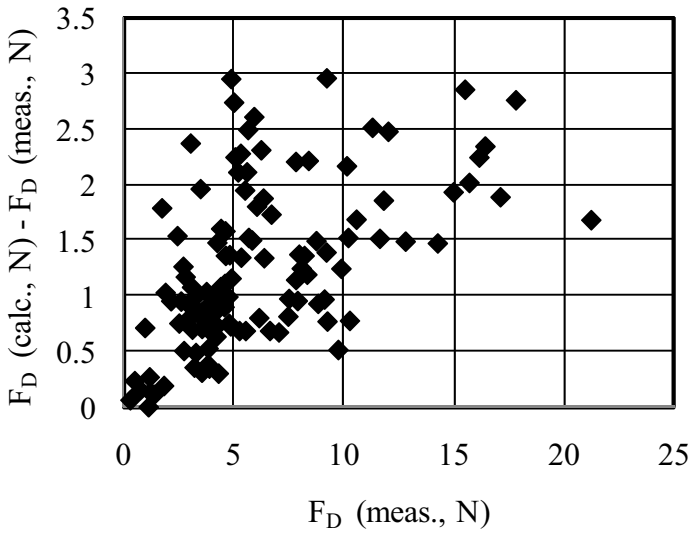

Figure 3.12. Difference between the calculated and measured drag forces versus the measured drag forces

The momentum correction factor was estimated to evaluate its effect on the computed spur dike plate drag force. The velocity distribution measurements for the uniform flow conditions and that in the flow upstream of a spur dike plate (50 mm × 400 mm), as described earlier, were used to estimate the momentum correction factor. The momentum correction factor was found to vary from 1.04 to 1.07 for all flow conditions, with or without the spur dike plate in place. The drag force was re-calculated using Eq. [3.2] with best estimates of the momentum correction factor incorporated into the equation for each test condition. The results showed a slight improvement between the measured and calculated drag forces with an MRE of about 21.8%. From this, one may conclude that the assumption of the momentum correction factor equal to unity is reasonable.

3.5.3. Drag coefficient of a single spur dike in an open channel – submerged conditions

Based on the drag force values determined from the drag force measurement apparatus, and using the computed impingement velocities for the imposed flow conditions, it was possible to use Eq. [3.3] to calculate spur dike plate drag coefficients for the submerged flow conditions. Figure 3.13 shows the drag coefficient for various sizes of submerged spur dike plate plotted against the passage ratio (= 1 - blockage ratio) for a 90° spur dike orientation and for all discharges used in the study. As the results show, there is a strong inverse relationship between the drag coefficient and the blockage ratio. It is also evident that, given the small amount of scatter in the data, the effects of the other independent parameters on the drag coefficient, including the aspect ratio and the submergence ratio, are relatively small.

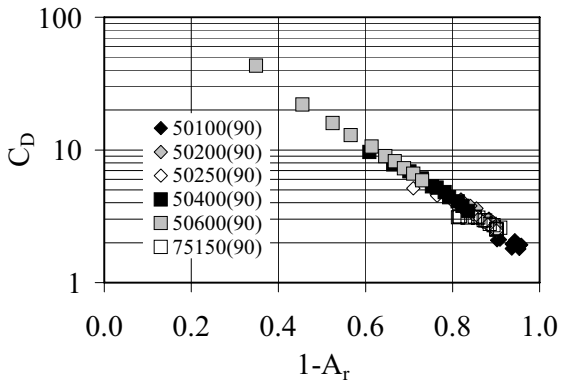

Figure 3.13. Drag coefficient of submerged spur dikes versus the passage ratio for various spur dike plate dimensions (90° orientation)

Using the computer program Statistical Package for the Social Sciences (SPSS), v9, a non-linear, multivariable regression analysis was performed on the drag coefficient for a 90° submerged spur dike and the three independent, influencing parameters, namely the blockage ratio, the submergence ratio and the aspect ratio. The results reveal the following relationship, viz.

$$[3.12] \quad C_D = 1.62(1 - A_r)^{-2.40}\left(\frac{P}{L}\right)^{-0.32}\left(\frac{h_1}{P}\right)^{-0.19}$$

for which the coefficient of determination, R^2, was found to be equal to 0.998. It is to be noted that the exponent for the blockage ratio is about an order of magnitude greater than that for the other two independent parameters. The exponent –2.40 for the blockage ratio is close to the exponent -2.25 obtained by Ranga Raju and Singh (1976) for the effects of blockage in a wind tunnel. From this, it may be concluded that the effects of blockage for a submerged spur dike in an open channel are similar to the blockage created by a plate in a wind tunnel.

Ranga Raju and Singh (1976) studied the effects of blockage on the drag coefficient of a vertical square plate placed in a wind tunnel having a square cross-section. They observed that, as the blockage ratio increases, the pressure behind the plate decreases, while the pressure distribution on the upstream side of the plate remains constant. The decrease in the pressure behind the spur dike plate inherently results in an increase in the drag coefficient. This observation supports the results of the present study wherein it was found that, as the blockage ratio increases, the drag coefficient increases accordingly. An increase in the blockage ratio is expected to increase the local velocity around the end (both submerged and unsubmerged conditions) and over the top (submerged conditions) of the spur dike. The increased velocity in the vicinity of the spur dike plate results in a decrease in the pressure behind the plate, hence an increase in the drag coefficient.

In order to compare the drag coefficient results with those found in the literature, and to assist in providing a physical interpretation of the effects of the aspect and submergence ratios on the drag coefficient, a base drag coefficient was determined for the spur dike plates. The base drag coefficient represents the drag coefficient of a spur dike plate for negligible blockage conditions, such as in the case of a relatively small spur dike in a relatively large open channel. The base drag coefficient was calculated from

$$[3.13] \quad C_{Do} = \frac{C_D}{(1 - A_r)^{-2.40}}$$

where, it may be noted, the denominator is the same as the blockage ratio term shown in Eq. [3.12].

Figure 3.14 shows the base drag coefficient calculated from Eq. [3.13] plotted against the submergence ratio for various spur dike plate aspect ratios. It is observed that the base drag coefficient of a submerged spur dike plate increases with a decrease in the plate aspect ratio. This finding is in accordance with the classical variation of the drag coefficient for a 2-D plate with the aspect ratio in a wind tunnel (Hoerner, 1965).

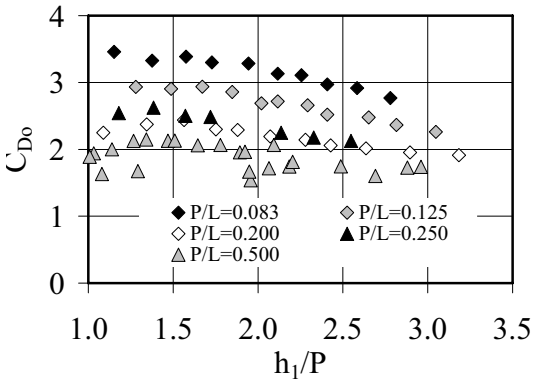

Figure 3.14. Base drag coefficient versus the submergence ratio for various aspect ratios (submerged spur dike)

The results shown in Figure 3.14 indicate that, for a given aspect ratio, the maximum base drag coefficient occurs for a submergence ratio between unity and 1.5. This finding is to be contrasted with that obtained from Eq. [3.12], wherein it is evident that the maximum base drag coefficient for a given aspect ratio is obtained for a submergence ratio of unity. Similar to the results of the present study, Malavasi and Guadagnini (2003) observed that the maximum drag coefficient of a bridge deck occurs when the submergence ratio is slightly greater than the unity. It may also be observed from the results given in Figure 3.14, albeit the effect being only slight, that the submergence ratio corresponding to the maximum base drag coefficient is closer to unity for higher aspect ratios. Malavasi and Guadagnini (2003) also observed that the drag coefficient of a bridge deck is independent of the submergence ratio for ratios greater than about four to five. Similarly, the results shown here for submerged spur dike plates indicate that for high submergence ratios the base drag coefficient becomes almost independent of the submergence ratio and approaches a value of two, which is a classical drag coefficient for a 2-D plate in a wind tunnel.

In order to analyze the effect of orientation angle on the spur dike plate drag coefficient, the drag coefficients obtained from tests on angled spur dike plates (i.e., $C_{D\alpha}$) were normalized by the drag coefficients obtained from 90° spur dike plates (i.e., C_{D90}) for the same test conditions in terms of the blockage, submergence and aspect ratios. The component of the drag force in the streamwise direction (i.e., $F_{D\alpha} = F_D \sin\alpha$) and the projected area of the spur dike plate normal to the streamwise direction (i.e., $A_{s\alpha} = A_s \sin\alpha$) were used in calculating $C_{D\alpha}$. The projected areas of the spur dike plates normal to the streamwise direction were also used in calculating the blockage ratio for the angled spur dike plates. C_{D90} corresponding to each $C_{D\alpha}$, on the other hand, was calculated from Eq. [3.12] with the blockage, aspect and submergence ratios being equal to that of the angled spur dike plate having an angle of orientation α. The results of the averaged, normalized drag coefficients are shown in Figure 3.15. Error bars showing two standard deviations are also shown in the figure.

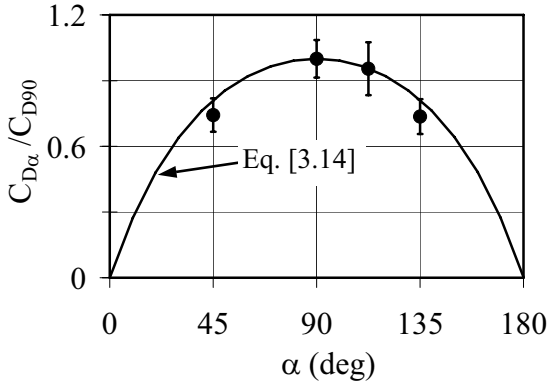

Figure 3.15. Normalized drag coefficient of an angled spur dike plate versus the plate angle of orientation

In Figure 3.15, it may be observed that the drag coefficient of an angled spur dike is less than that of a 90° spur dike. Moreover, the drag coefficients are essentially the same regardless of whether the spur dike plate is angled upstream or downstream. The results agree with those reported by Lindenburg (2001). In that case, he cited a theoretical relationship developed by Hoerner (1975) to account for the orientation of a 2-D plate having a small aspect ratio placed in a wind tunnel, viz.

[3.14] $$C_{D\alpha} = C_{D90}\left(\frac{\sin\alpha}{0.56 + 0.44\sin\alpha}\right)$$

Equation [3.14] is shown plotted in Figure 3.15. It is evident that there is a good match between the results of the present study and those given by Eq. [3.14]. The slight difference between the experimental data and the relationship expressed by Eq. [3.14] is perhaps due to the difference in the flow conditions (free surface flow in the present study vs. wind tunnel in Hoerner's work) and the effect of the aspect ratio (i.e., the aspect ratios in the work reported herein are greater than those of Hoerner's wind tunnel plates). The issue of a free surface and aspect ratio effects on the drag coefficient of angled spur dikes is an area in need of further study.

3.5.4. Drag coefficient of a single spur dike in an open channel – unsubmerged conditions

For unsubmerged conditions, the spur dike drag coefficient was analyzed with respect to two independent parameters, namely the blockage ratio, L/B, and the depth-to-length ratio, h_1/L. It is noted here that the experiments for the unsubmerged spur dike plates were limited to a 90° orientation angle. With the force apparatus designed for this study, it was not possible to properly adjust the gap between the spur dike plate and the flume wall concurrent with the angle of orientation of the plate. Figure 3.16 shows the variation of the drag coefficient versus the depth-to-length ratio for various blockage ratios. As the results in Figure 3.16 show, the drag coefficient increases significantly with an increase in the blockage ratio. Moreover, there is an increase in the drag coefficient of the spur dike with an increase in the depth-to-length ratio, such increase being small for small blockage ratios and vice versa.

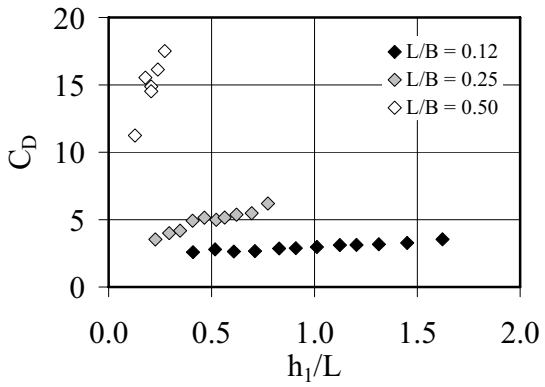

Figure 3.16. Variation of the drag coefficient for unsubmerged spur dikes versus the depth to length ratio for various blockage ratios

Using SPSS, v9, a non-linear, multivariable regression analysis was performed on the drag coefficient of an unsubmerged spur dike plate and the two independent influencing parameters, namely the blockage ratio and the depth to length ratio. The resulting regression equation, with R^2 value of 0.988, is given as

$$[3.15] \quad C_D = 2.02\left(1-\frac{L}{B}\right)^{-3.83}\left(\frac{h_1}{L}\right)^{0.40}$$

As with the submerged spur dike plates, Eq. [3.15] shows that the blockage ratio is the main factor governing the drag coefficient for an unsubmerged spur dike (i.e., largest exponent). In order to compare the drag coefficient results with those found in the literature and to observe the trend of the drag coefficient with the ratio of flow depth to spur dike plate length (i.e., depth-to-length ratio), the base drag coefficient for the unsubmerged spur dike plates was calculated in a manner similar to that for the submerged spur dike plates (but with the exponent of –3.83 for the blockage ratio as per the regression results shown in Eq. [3.15]). The results are shown in Figure 3.17.

Whereas Eq. [3.15] indicates that there is no limit to the increase in the drag coefficient of an unsubmerged spur dike plate with an increase in the depth to length ratio, the results shown in Figure 3.17 suggest that the base drag coefficient approaches a limiting value of about 2.0 to 2.5. This finding suggests that a power law relationship does not

necessarily model the influence of the depth to length ratio very well. Moreover, there are three distinct patterns or trends in the base drag coefficients shown in Figure 3.17, one each for the three blockage ratios. Further study is required to obtain a more full understanding of the effects of the blockage and depth-to-length ratio on the drag coefficient of unsubmerged spur dike plates.

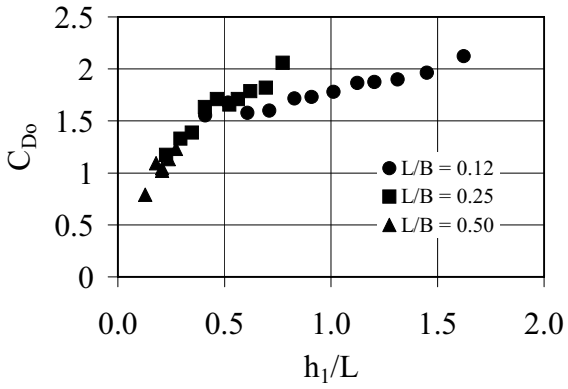

Figure 3.17. Base drag coefficient (unsubmerged spur dike) versus the depth to length ratio

A comparsion of Eqs. [3.12] and [3.15] for submerged and unsubmerged spur dike plates, respectively, shows that the exponent for the blockage ratio of an unsubmerged spur dike plate is –3.83 compared to –2.40 for a submerged spur dike plate. This finding indicates that the blockage ratio has a greater effect on the drag coefficient of an unsubmerged spur dike plate than it does for a submerged spur dike plate. This difference is likely due to the difference in the flow pattern between the two cases. For an unsubmerged spur dike plate, the flow is confined between the end of the plate and the opposite side of the channel. As such, any increase in the blockage ratio, which is due to the increase in the length of the plate and hence decrease in the area between the tip of the plate and the opposite side of the channel (constricted zone), is expected to be accompanied by a considerable increase in the local velocity of the flow in the constricted zone as there is no other means for the flow to pass by the spur dike. For a submerged spur dike, however, in addition of the constricted zone, flow also occurs over the top of the spur dike. This “freedom” to pass both over and around the spur dike reduces the impact of the spur dike on the flow as the blockage ratio increases. As such, the possible increase in the local velocity around and over the submerged

spur dike plate with an increase in the blockage ratio is less than that experienced around the end of an unsubmerged spur dike plate. A smaller increase in the local velocity with the blockage ratio around a submerged spur dike plate relative to that of an unsubmerged spur dike plate results in less decrease in the pressure behind the submerged spur dike plate. This relative difference in the change in pressure on the backside of the plates for the two conditions (i.e., submerged vs. unsubmerged) translates to a less than proportional increase of the drag coefficient for the submerged spur dike plate.

3.5.5. Backwater effect of submerged and unsubmerged spur dikes

An increase in the discharge in the case of an unsubmerged spur dike plate of a given geometry is accompanied by an increase in the flow depth which, as shown by Eq. [3.15], results in an increase in the drag coefficient of the plate. An increase in the drag coefficient results in an increase in the depth ratio (i.e., h_1/h_2 as given by Eq. [3.8]) and hence an increase in the backwater effect. However, for high discharges, when the spur dike is submerged, an increase in the discharge is accompanied by an increase in the flow depth and hence a decrease in the blockage ratio and the corresponding drag coefficient (Eq. [3.12]). As shown by Eq. [3.8], a decrease in the blockage ratio and drag coefficient is accompanied by a decrease in the depth ratio and hence a decrease in the backwater effect.

3.5.6. Calculation of the backwater effect due to a single spur dike in an open channel

The results of the present study may be used to estimate the backwater effect due to a single spur dike in an open channel. To do this, the geometry of the spur dike and the open channel, the flow conditions downstream from the spur dike, the impingement velocity parameter θ, and the drag coefficient must be known in order to solve Eq. [3.8] for the upstream flow depth and hence the backwater effect due to the presence of the spur dike. The impingement velocity parameter θ may be estimated from the velocity distribution in the open channel, although in the case of a wide channel, where the velocity distribution is more-or-less uniform, it may be taken to be equal to unity. The drag coefficient for a submerged and an unsubmerged spur dike may be obtained using Eqs. [3.12] and [3.15], respectively. However, as the drag coefficients are expressed in terms of the upstream flow conditions,

which are not known *a priori*, a trial and error procedure is required. As a first step, a trial value may be selected for the upstream flow depth, h_1. From this, the spur dike drag coefficient may be calculated and, finally, the calculated drag coefficient may be used to compute a new upstream depth using Eq. [3.8]. The procedure is repeated until convergence of the upstream flow depth is achieved.

Subsequent to the work presented above, geometry of the spur dike plates, geometry of the flume, measured discharges and measured tailwater depths were used to calculate the backwater effect using Eq. [3.12] or Eq. [3.15] (for submerged or unsubmerged spur dike plates, respectively) and Eq. [3.8]. The magnitude of the backwater effect computed in this way is compared with the measured values of the backwater effect as shown in Figure 3.18. In this analysis, the velocity impingement factor, θ, and momentum correction factor, β, were taken to be equal to unity.

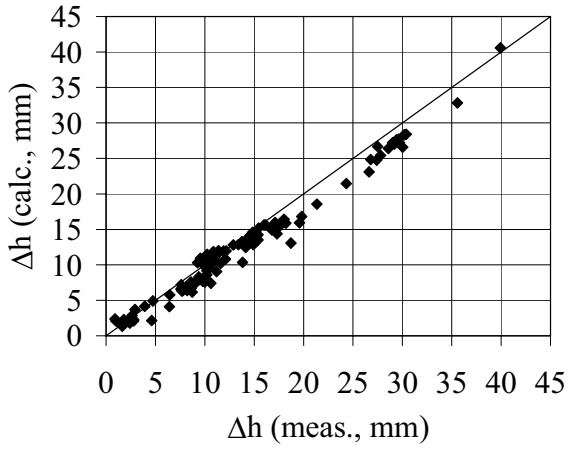

Figure 3.18. Calculated versus measured backwater effect of spur dike plates

The calculated backwater effect has been underestimated by about 18.4% on average. The results in Figure 3.18 are in agreement with those in Figure 3.11 where the calculated drag force obtained from the flow depth measurements is greater than the measured drag force. To account for the underestimate, it is suggested that the backwater effect calculated from Eqs. [3.8] and [3.12] or [3.15] be increased by about 25%. In this context, it is suggested that the work presented herein only be used as a way of giving a first estimate of

the backwater effect. In an erodible boundary channel, a scour hole will develop around the nose of a spur dike, which effectively decreases the blockage ratio. As per the results of the present study, a decrease in the blockage ratio is accompanied by a decrease in the drag coefficient and hence the drag force and backwater effect. It is also noted that spur dikes having a trapezoidal cross-sectional shape, which are typical of those used in practice, are more streamlined when compared with the 2-D plates used in this work. As such, it is likely that the drag coefficients for the 2-D spur dike plates used in this work are higher than those for spur dikes shapes used in practice, which suggests that the results reported herein are likely conservative (i.e., greater backwater effect than might occur in practice). Thus, the calculated backwater effect using the relationships presented herein likely represents a worst-case scenario.

3.6. Conclusions

The flow resistance of both submerged and unsubmerged spur dikes in terms of the drag force exerted on the flow in an open channel was studied. In this work, the drag force due to spur dikes in the flow was represented by a drag coefficient, which was subsequently related to the backwater effect due to the presence of the spur dikes.

The drag force exerted on an open channel flow due to a 2-D single spur dike plate was obtained using two methods. In the first method, the drag force was measured directly using a specially-designed cantilevered bar system. In the second method, the drag force was calculated using a momentum analysis in conjunction with the measured flow parameters. It was shown that the calculated drag force is somewhat greater than the measured drag force. The reason for this difference may be attributed to the increased bed shear stress around the end of the spur dike plate, which is implicitly accounted for in the direct measurement approach but not in the momentum analysis.

For both a submerged and an unsubmerged spur dike plate, the drag force increases with an increase in the discharge. However, the drag force for an unsubmerged spur dike plate increases more rapidly with an increase in the discharge than it does for a submerged spur dike plate. The increase in the drag force with discharge may be attributable to the

increase in the average velocity of the flow, while the difference between the submerged and unsubmerged cases is undoubtedly due to the difference in response to a change in the flow conditions for the two cases (e.g., completely different vortical flow structures).

It is concluded that the drag coefficient is a strong function of the blockage ratio for both submerged and unsubmerged spur dike plates. This finding implies that the flow resistance and corresponding backwater effect due to a spur dike plate is strongly affected by the blockage caused by the plate. For submerged spur dike plates, the drag coefficient decreases with an increase in the submergence ratio and it increases with the decrease in the aspect ratio. For unsubmerged spur dike plates, the drag coefficient increases with an increase in the depth to length ratio. It is also observed that angled spur dikes, regardless of their orientation (i.e., angled upstream or downstream), produce smaller drag coefficients than do those oriented normal to the streamwise direction. The reduction in the drag coefficient with the spur dike angle is in accordance with a theory developed by Hoerner (1975) for angled 2-D plates placed in a wind tunnel.

Based on the momentum equation, relationships were developed to estimate the backwater effect for both submerged and unsubmerged spur dikes. These relationships are directly applicable to 2-D spur dikes in a rigid bed rectangular channel, which is expected to yield a conservative result for the backwater effect relative to that likely to be experienced in an erodible boundary channel. As such, the results obtained from the relationships presented herein should be considered as conservative, first-order estimates of the backwater effect.

3.7. Acknowledgements

Financial support for this research was provided by the Natural Sciences and Engineering Research Council of Canada through a grant to the second author, as well as by a University of Saskatchewan graduate scholarship to the first author. This support is gratefully acknowledged. Also, the authors thank Dr. Bruce Sparling for his help in the design of the drag force measurement apparatus, the staff in Engineering Shops for fabricating the apparatus, and the lab technicians, Mr. Dale Pavier and Mr. Brennan Pokoyoway, for their assistance in conducting the experiments.

3.8. References

Azinfar, H. and Kells, J.A. 2007. Backwater effect due to a single spur dike. Canadian Journal of Civil Engineering, NRC Press, 34(1): 107-115.

Belz, J.U., Busch, N., Engel, H. and Gasber, G. 2001. Comparison of river training measures in the Rhine catchment and their effects on flood behavior. Water and Maritime Engineering, Thomas Telford, 148(3): 123-132.

Criss, R.E. and Shock, E.L. 2001. Flood enhancement through flood control. Geology, The Geological Society of America, 29(10): 875-878.

Ettema, R. and Muste, M. 2004. Scale effects in flume experiments on flow around a spur dike in flatbed channel. Journal of Hydraulic Engineering, ASCE, 130(7): 635-646.

Hoerner, S.F. 1965. Fluid-dynamic drag, practical information on aerodynamic drag and hydrodynamic resistance. Hoerner Fluid Dynamics, Brick Town, N.J., USA, 20 chapters.

Klaka, K., Penrose, J.D., Horsley, R.R. and Renilson, M.R. 2005. Hydrodynamic test on a fixed plate in uniform flow. Experimental Thermal and Fluid Sciences, Elsevier, 30(22): 131-139.

Kuhnle, R., Jia, Y. and Alonso, C. 2008. Measured and simulated flow near a submerged spur dike. Journal of Hydraulic Engineering, ASCE, 134(7): 916-924.

Lindenburg, C. 2001. Stall coefficients, aerodynamic airfoil coefficients at large angles of attack. Energy Research Centre of Netherlands, Report No. ECN-RX-01-004, 18 p.

Malavasi, S. and Guadagnini, A. 2003. Hydrodynamics loading on river bridges. Journal of Hydraulic Engineering, ASCE, 129(11): 854-861.

Miller, R., Roulund, A., Sumer, B.M., Fredsoe, J., Truelsen, C. and Michelsen, J. 2003. 3-D numerical modeling of flow around a groin. Proc. of 30th IAHR Congress, Greece, Theme C, Hydraulics of Groynes, pp. 385-392.

Munson, B.R., Young, D.F. and Okishi, T.H. 1998. Fundamentals of fluid mechanics. John Wiley & Sons, Third Edition, 877 p.

Naudascher, E. and Medlarz, H.J. 1983. Hydrodynamic loading and backwater effect of partially submerged bridges. Journal of Hydraulic Research, IAHR, 12(3): 213-232.

Ouillon, S. and Dartus, D. 1997. Three-dimensional computation of flow around groyne. Journal of Hydraulic Engineering, ASCE, 123(11): 962-970.

Pinter, N., Thomas, R. and Wlosinski, H. 2001. Assessing flood hazard on dynamic rivers. EOS, Transactions, American Geophysical Union, 82(31): 333-339.

Rajaratnam, N. and Nwachukwu, B.A. 1983. Flow near groin-like structures. Journal of Hydraulic Engineering, ACSE, 109(3): 463-480.

Ranga Raju, K.G. and Singh, V. 1976. Blockage effects on drag of sharp-edged bodies. Journal of Industrial Aerodynamics, Elsevier, 1(3): 301-309.

Shaw, T.L. 1971. Effect of side walls on flow past bluff bodies. Journal of the Hydraulics Division, ASCE, 97(HY1): 65-79.

Soliman, M.M., Attia, K.M., Kotb, Talaat, A.M., and Ahmad, A.F. 1997. Spur dike effects on the river Nile morphology after High Aswan Dam. Proc. of 27th IAHR Congress, Managing Water, Vol. A, San Francisco, CA, USA, pp. 805-810.

Wu, B., Wang, G., Ma, J., and Zhang, R. 2005. Case study: River training and its effects on fluvial processes in the Lower Yellow River, China. Journal of Hydraulic Engineering, ASCE, 131(2): 85-96.

Yang, S.Q., Tan, S.K. and Lim, S.Y. 2004. Velocity distribution and dip-phenomenon in smooth uniform open channel flows. Journal of Hydraulic Engineering, ASCE, 130(12): 1179-1186.

Yossef, M.F.M. 2002. The effects of groynes on rivers (Literature Review). Delft Cluster Report No. DC1-334-4, Delft, The Netherlands, 57 p.

Chapter 4. Drag Force and Associated Backwater Effect Due to a Spur Dike Field in an Open Channel

Contribution of the Ph.D. candidate

All work reported in this chapter, including design of the experimental program, implementation of the experiments, review of the literature, development of the theoretical framework, analysis and discussion of the results and writing of the text, has been carried out by the Ph.D. candidate.

As supervisor, Dr. J.A. Kells reviewed all parts of the work. A shortened version of this chapter, co-authored by the Ph.D. candidate and supervisor, was submitted to the Journal of Hydraulic Research (IAHR) for possible publication. This chapter contains additional details not included in the journal paper manuscript as submitted (i.e., the manuscript is currently in review), including comparison of the present work with the work done by Morris (1955), inclusion of experimental measurements and results (Tables 4.3 and 4.4) and comparison of the findings of Ball and Cox (1978) with those of the present study. Of course, the journal manuscript is subject to revision prior to publication, so further differences may be evident once the manuscript has been approved for publication.

Contribution of this chapter to the overall study

Following a study on quantifying the flow resistance and backwater effect due to a single spur dike in Chapter 3, the work presented in this chapter quantifies the flow resistance and associated backwater effect due to a spur dike field in an open channel flow. Various flow conditions and spur dike field configurations in terms of the number of spur dikes and spacing between them have been considered. In this chapter, a theoretical framework has been developed for assessing and predicting the flow resistance and backwater effect due to a spur dike field. The results of the research described herein also make a contribution toward improving our understanding of the role of various parameters including configuration of spur dikes in a field and submergence conditions on the flow resistance of individual spur dikes in a spur dike field.

4.1. Abstract

The study focuses on quantifying the flow resistance and the associated backwater effect of a spur dike field in an open channel flow. The work was carried out in a rigid bed flume. The model spur dikes were simulated using 2-D, rectangular plates, which were placed in an array along one side of the flume. The results showed that the arrangement of a spur dike field has a substantial impact on the drag force and hence the backwater effect that is experienced. In general, the total drag force of a spur dike field increases with an increase in the number of spur dikes and the relative spacing between them in the spur dike field. The most upstream spur dike experienced the greatest drag force amongst the spur dikes in the field, essentially acting as a shield to decrease the drag force of the downstream spur dikes. For submerged flow conditions, the drag forces of all individual spur dikes increased with an increase in the submergence ratio. It was observed during the experiments that the jet flow across the crest of the submerged spur dikes has a substantial impact on the flow structure when compared with the flow structure associated with unsubmerged spur dikes.

4.2. Introduction

A spur dike is a hydraulic structure that extends outward from a river bank and into the channel at some angle to the main flow direction. A number of spur dikes built in series along one or both banks of a river is known as a spur dike field. The arrangement of a spur dike field may vary by the number, the geometry and the relative spacing between the spur dikes. Spur dike fields may be used to protect the river bank from erosion or to facilitate river training for navigation purposes. In some cases, it has been observed that the construction of spur dikes has improved the aquatic habitat and fish populations between the spur dikes (Shields, 1995).

Despite their useful features, there is some concern that spur dikes may be responsible for increased flooding due to the associated flow resistance. For example, studies show that, over the past century, flood stages for given discharges at various locations along the Middle Mississippi and Lower Missouri rivers have increased by 2 m to 4 m (Criss and Shock, 2001). Pinter et al. (2001) have attributed a part of the observed stage increases to the

construction of spur dikes. Stage increases due to spur dikes have also been reported on the Rhine River in Europe (Belz et al., 2001). Wu et al. (2005) have observed a stage increase due to long spur dikes constructed on the Lower Yellow River in China. Here, the stage increase or backwater effect is defined as the increased water level above the normal stage upstream of a spur dike or a spur dike field in an open channel.

In the present study, the momentum equation was applied to relate the backwater effect due to a spur dike field to the flow resistance expressed in the form of a drag force. A physical model study was used to quantify the drag force associated with spur dike fields of various arrangements (i.e., number of spur dikes and relative spacing between the spur dikes) and for various discharges in a rigid bed flume. The study was limited to the single size spur dikes being placed along one side of the flume only. The drag force of each individual spur dike in the spur dike field was measured for both submerged and unsubmerged conditions. In turn, the drag force of the entire spur dike field was analyzed and related to the spur dike arrangement and flow conditions.

4.3. Theoretical considerations

With reference to Figure 4.1, the one-dimensional linear momentum equation can be applied to the flow field within a control volume containing a single spur dike, viz.

$$[4.1] \quad F_1 - F_2 - F_D - F_f + F_w = \rho Q(\beta_2 V_2 - \beta_1 V_1)$$

where F_1 is the force due to the upstream hydrostatic pressure distribution, F_2 is the force due to the downstream hydrostatic pressure distribution, F_D is the drag force due to the spur dike, F_f is the force due to boundary friction between sections 1 and 2, F_w is the downstream component of the gravity force within the control volume (i.e., between sections 1 and 2), ρ is the fluid density, Q is the discharge, V_1 and V_2 are the average velocities at sections 1 and 2, respectively, and β_1 and β_2 are the momentum correction factors applicable at sections 1 and 2, respectively.

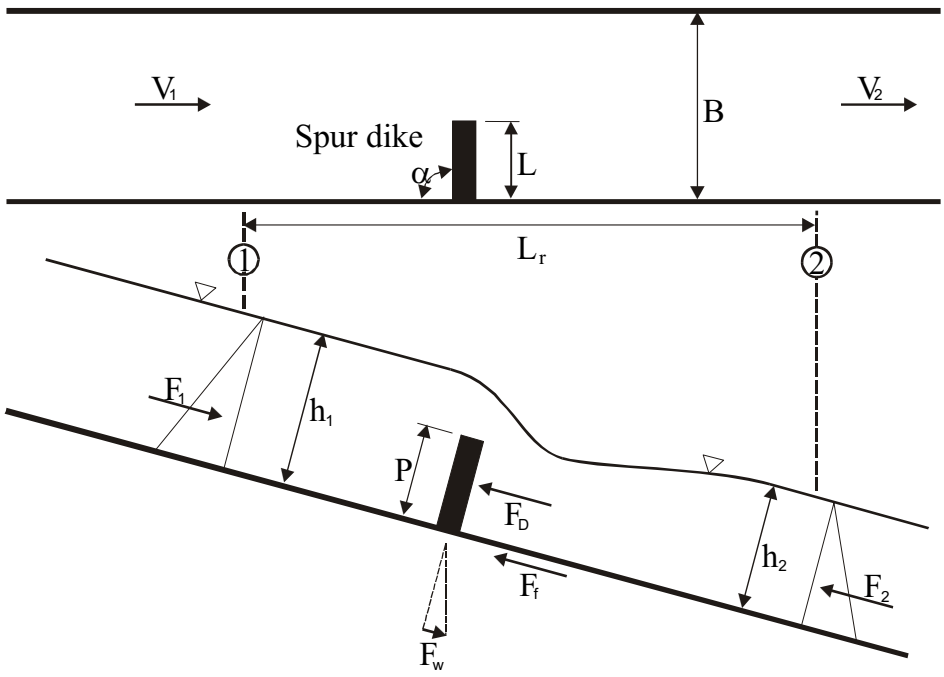

Figure 4.1. Schematic illustration (plan and profile) of a single spur dike within an open channel control volume

For a single spur dike, the downstream component of the gravity force within the control volume (i.e., between sections 1 and 2 in Figure 4.1) may be assumed to be equal to the frictional resistance at the boundaries (i.e., $F_f \approx F_w$). Thus, for analysis purposes, both terms may be omitted from Eq. [4.1]. Expressing the force due to the hydrostatic pressure distribution upstream of and downstream from the spur dike more explicitly, Eq. [4.1] reads:

$$[4.2] \quad \frac{1}{2}\rho g B h_1^2 - \frac{1}{2}\rho g B h_2^2 - F_D = \rho Q(\beta_2 V_2 - \beta_1 V_1)$$

Here, B is the channel width, g is the acceleration due to gravity (i.e., 9.81 m/s^2), and h_1 and h_2 are the upstream and downstream flow depths, respectively.

The drag force of a single spur dike, F_D, which is exerted by the spur dike on the flow, can be expressed using the basic drag equation as:

[4.3] $$F_D = C_D A_s \frac{\rho V_1^2}{2}$$

where C_D is the spur dike drag coefficient and A_s is the upstream projected area of the single spur dike. For a submerged spur dike, $A_s = PL$, where P is the height of the spur dike and L is the length of the spur dike perpendicular to the flow direction. For an unsubmerged spur dike, on the other hand, $A_s = h_1 L$.

Combining Eqs. [4.2] and [4.3], along with the continuity principle and the assumption that the momentum correction factors are equal to unity, leads to the following equation, viz.

[4.4] $$2Fr_1^2\left(\frac{h_1}{h_2}\right)^3 - \left(2Fr_1^2 - C_D A_r Fr_1^2 + 1\right)\left(\frac{h_1}{h_2}\right)^2 + 1 = 0$$

where Fr_1 is the upstream Froude number, and A_r is the blockage ratio of the spur dike, viz.

[4.5] $$A_r = \frac{A_s}{h_1 B}$$

Equation [4.4] can be solved implicitly for the flow depth upstream of a single spur dike if the downstream flow conditions and drag coefficient are known.

For a given channel slope, discharge and Manning's resistance coefficient, it can be expected that adding more spur dikes into the channel will result in an increase in the upstream flow depth. With reference to Figure 4.2, as the single spur dike is replaced by a field of spur dikes (i.e., two or more spur dikes), the flow depth upstream of the spur dike field will increase from h_1 to h_3, while the flow depth far downstream from the spur dike field will remain constant and equal to the tailwater depth, h_2 (as in the case of a single spur dike). Application of the one-dimensional linear momentum equation between sections 3 and 2, upstream and downstream of the spur dike field, respectively, yields:

[4.6] $$F_3 - F_2 - F_{Df} - F_{ff} + F_{wf} = \rho Q(\beta_2 V_2 - \beta_3 V_3)$$

Similar to the case of a single spur dike, F_3 is the force due to the upstream hydrostatic pressure distribution, F_2 is the force due to the downstream hydrostatic pressure distribution, F_{Df} is the total drag force due to the spur dike field, F_{ff} is the force due to the boundary friction between sections 3 and 2, and F_{wf} is the downstream component of the gravity force within the control volume (i.e., between sections 3 and 2).

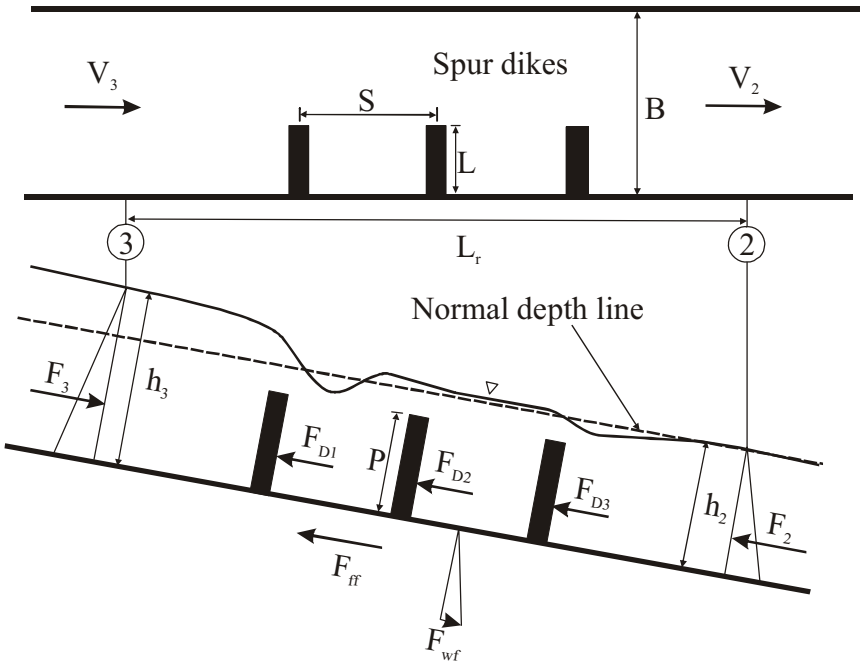

Figure 4.2. Schematic illustration (plan and profile) of a spur dike field within an open channel control volume

The drag force of a spur dike field with "m" number of spur dikes can be expressed as

[4.7] $$F_{Df} = F_{D1} + F_{D2} + ...F_{Di} + ... + F_{Dm}$$

where F_{Di} is the drag force of the i^{th} spur dike in the spur dike field and F_{Dm} is the drag force of the last spur dike in the field. The relative drag force, η_i, for each individual spur dike may be defined as

[4.8] $$\eta_i = \frac{F_{Di}}{F_D}$$

where F_D is the drag force of a single spur dike for the same flow conditions (e.g., discharge and tailwater depth). Based on the above definition, it is apparent that:

$$[4.9] \quad \frac{F_{Df}}{F_D} = \eta_1 + \eta_2 + ... + \eta_i + ... + \eta_m = \eta_t$$

where η_t is the total relative drag force of all spur dikes in the field. If the geometry of all spur dikes in the spur dike field is the same, then

$$[4.10] \quad F_{Df} = \eta_t C_D A_s \frac{\rho V_1^2}{2}$$

The friction force in the control volume containing a spur dike field may be estimated from

$$[4.11] \quad F_{ff} = \gamma \overline{A} L_r \overline{S}_f$$

where γ is the specific weight of the fluid, $\overline{A}$ is the average flow area in the control volume, L_r is the length of the control volume and $\overline{S}_f$ is the average energy slope of the flow in the control volume containing the spur dike field. Similarly, the downstream component of the gravity force of the fluid within the control volume may be estimated from

$$[4.12] \quad F_{wf} = \gamma \overline{A} L_r S_o$$

where S_o is slope of the channel bed. An excess force, F_{ef}, for a spur dike field may be defined as

$$[4.13] \quad F_{ef} = F_{wf} - F_{ff} = \gamma \overline{A} L_r \left(S_o - \overline{S}_f \right)$$

The excess force is the difference between the friction force along the control volume boundaries and the component of the fluid weight in the flow direction. This force is zero for uniform flow conditions ($S_o = \overline{S}_f$).

It is known that an M1 water surface profile is developed upstream of a spur dike field for subcritical flow conditions. If cross-section 3 in Figure 4.2 is moved to the upstream end of the M1 profile where the flow depth becomes equal to the normal depth, the drag force would be equal to the excess force. This can be easily shown by applying the momentum equation between cross-sections 3 and 2. From this analysis, it is apparent that the relative magnitude of the excess force to the total spur dike drag force depends on the spacing between the spur dikes, S, shown in Figure 4.2. For small relative spacings, the relative magnitude of the excess force to the drag force is small, while for large relative spacings, this ratio is large. The maximum relative magnitude of the excess force to the drag force is equal to unity when the spacing between the spur dikes is greater than the total length of the M1 water surface profile. For this condition, the drag force of a downstream spur dike is balanced by the excess force before reaching the next upstream spur dike such that each spur dike in the spur dike field essentially acts as a single spur dike.

The total resistance and hence backwater effect of a spur dike field is equal to that of a single spur dike for two limiting values of spacing. For a spacing value of zero, a spur dike field essentially behaves as a single spur dike. In this case, the total drag force of the spur dike field is equal to the drag force of a single spur dike and the excess force is close to zero. For the spacing value equal to the M1 water surface profile length, the total resistance and hence backwater of the spur dike field is also equal to that of a single spur dike. In such a spur dike field with m spur dikes, each spur dike acts as a single spur dike so that the total drag force and excess force are equal to mF_D and $(m-1)F_D$, respectively. The difference between the total drag force and the excess force represents the total resistance of the spur dike field, which in this case is equal to that of a single spur dike. Between the two spacing limits, the total resistance and hence backwater of a spur dike field is expected to have a peak value, which is greater than that for a single spur dike.

In a study performed by Morris (1955), the effect of spacing of a series of roughness elements on an open channel flow regime was studied. In that work, Morris classified the flow regime in three categories including isolated-roughness flow, wake-interference flow and skimming flow. It was shown that the total resistance of flow increases with an increase in the spacing of elements in wake-interference zone due to the interaction effects of

elements. The flow resistance is reduced for small relative spacings in the skimming flow regime and also for large relative spacings in the isolated roughness flow regime in which each element acts as a single entity. Although, there is a difference between Morris' experimental conditions for deeply submerged roughness elements and those for spur dikes where the dike is either unsubmerged or the degree of submergence is low, the maximum resistance of the flow for both conditions should occur in the wake-interference zone.

In most spur dike fields, the spacing between the spur dikes is much less than the length of the M1 water surface profile so the excess force is small compared to the drag force due to the spur dikes. Moreover, the flow in an open channel with a spur dike field can be classified as wake-interference flow. In the present study, the spacing between the spur dikes was much smaller than the length of the M1 profile so that the excess force was neglected from further analysis and hence the total resistance of a spur dike field was considered to be equal to its total drag force. On this basis and by combining Eqs. [4.2] and [4.10] in conjunction with the continuity equation, the following relationship can be obtained, viz.

$$[4.14]\quad \left(\frac{h_3}{h_1}\right)^3 - \left[2Fr_1^2 + 1 + C_D A_r(\eta_t - 1)Fr_1^2\right]\left(\frac{h_3}{h_1}\right) + 2Fr_1^2 = 0$$

Equation [4.14] is solved for the ratio of the upstream flow depth due to a spur dike field to that due to a single spur dike, $\left(\frac{h_3}{h_1}\right)$. This ratio is in accordance with the definition of the total relative drag force which was the ratio of the total drag force of a spur dike field to the drag force of a single spur dike. The upstream flow depth due to a single spur dike can be obtained from Eq. [4.4] if the drag coefficient of the single spur dike is known. The drag coefficient of the single spur dike is also required to solve Eq. [4.14]. Azinfar and Kells (2009) (see Chapter 3) have obtained relationships for determining the drag coefficient and upstream flow depth (hence backwater effect) of a single spur dike for various flow conditions and spur dike geometries. In addition to the above-mentioned information, to solve Eq. [4.14] it is necessary to have the total relative drag force, η_t, which is the subject of

the present work. It is of interest to note that, if the total relative drag force is equal to unity (i.e., the case of a single spur dike), then Eq. [4.14] gives $h_3 = h_1$ as expected.

4.4. Experimental program

An experimental program was developed to measure the drag force of each individual spur dike in a spur dike field. The spur dikes were modeled using thin rectangular plates fabricated from Poly Vinyl Chloride (PVC). Various numbers of spur dikes with various relative spacings between the spur dikes were installed in a laboratory flume located in the Hydrotechnical Laboratory at the University of Saskatchewan. The flume width, height and length are 800 mm, 600 mm and 10 m, respectively. The flume has an adjustable slope system and tailgate that allows for uniform flow conditions to be established throughout the length of the flume. In order to quickly change the configuration of a spur dike field, a false floor made of PVC was installed on the flume bed. It was possible to attach the model spur dike plates on the false floor very quickly at pre-determined locations using screws. The discharge and depth were measured using an electromagnetic flow meter and a point gauge, respectively.

The spur dike drag force was measured using a specially designed apparatus. The apparatus consisted of three streamlined cantilever aluminum beams projecting from a rigid top plate. At the bottom end, each beam was connected to an aluminum base plate (50 mm × 100 mm) by means of a ball joint. Two aluminum plates, one for submerged condition and the other for unsubmerged condition, could subsequently be attached to the base plate. The drag force exerted on each plate was equal to the sum of the moment reaction forces exerted at the top ends of the three cantilever beams. The strains due to the moments were detected using six strain gauges, two on each cantilever beam. In turn, the strain gauges were connected to a data acquisition system and computer for recording the strains. Using standard weights, each of the three cantilever beams was calibrated individually and in combination so that it was possible to obtain the drag force from the measured strains. The apparatus was fastened into place in the flume by means of a simple frame such that a 1 mm gap was left between the plate and the flume wall and floor.

Uniform flow conditions were established in the flume prior to the installation of the PVC spur dike plates. For such conditions, the backwater effect is the difference between the uniform flow depth without any spur dike plate in place and the resulting upstream flow depth with the plate in place. The flume slope was set to 0.000975 m/m. At the outset of the work, a stage-discharge curve was established by setting a variety of discharges, and through adjustment of the downstream tailgate, a variety of uniform flow depths was established for each discharge. Figure 4.3 shows the resulting stage-discharge relationship.

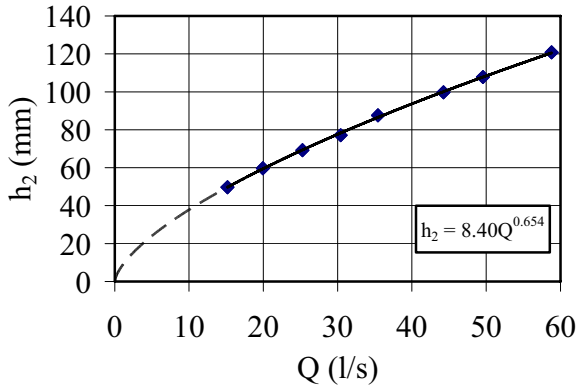

Figure 4.3. Stage-discharge relationship for uniform flow conditions in the laboratory flume (S_o = 0.000975 m/m)

After setting a particular discharge, the drag force of the single spur dike plate attached to the apparatus was measured thus giving F_D as shown in Eq. [4.8]. Then, a series of PVC spur dike plates was attached to the false floor at desired locations, leaving a vacant position for only one spur dike in which the drag force measurement apparatus was subsequently positioned. The apparatus was installed in the designated position for about five minutes to collect the measured strains at a sampling rate of about 1 Hz. After completing the measurement of the drag force at one location, one of the PVC spur dikes was removed from its location and replaced with the drag force measurement apparatus for the next set of measurements. In this manner, it was possible to quantify the drag force of all individual spur dikes in the spur dike field. Three discharges for submerged flow conditions (44.3 L/s, 30.2 L/s and 20.2 L/s) and one discharge for an unsubmerged flow condition (20.1 L/s) were evaluated. Table 4.1 shows the range of the parameters used in the present

study. The Froude number of the uniform subcritical flow was limited to a narrow range as shown in Table 4.1.

Figure 4.4 shows two examples of the physical model for submerged and unsubmerged conditions in which the drag force measurement apparatus is located in the position of the third spur dike plate position within the spur dike field. For the setup shown, the relative spacing between the spur dike plates is equal to one.

Table 4.1. Range of the experimental parameters used in the study

Submerged conditions		Unsubmerged conditions	
Parameter	Range	Parameter	Range
Spur dike length, L (mm)	200	Spur dike length, L (mm)	200
Spur dike height, P (mm)	50	Spur dike height, P (mm)	N/A
Number of spur dikes, m	2-16	Number of spur dikes, m	2-4
Relative spacing, S/L	1-15	Relative spacing, S/L	1-16
Submergence ratio, h_2/P	1.2-2.0	Submergence ratio, h_2/P	N/A
Orientation angle, α°	90	Orientation angle, α°	90
Channel aspect ratio, h_2/B	0.075-0.125	Channel aspect ratio, h_2/B	0.075
D/S Froude number, Fr_2	0.53-0.56	D/S Froude number, Fr_2	0.53

(a)

(b)

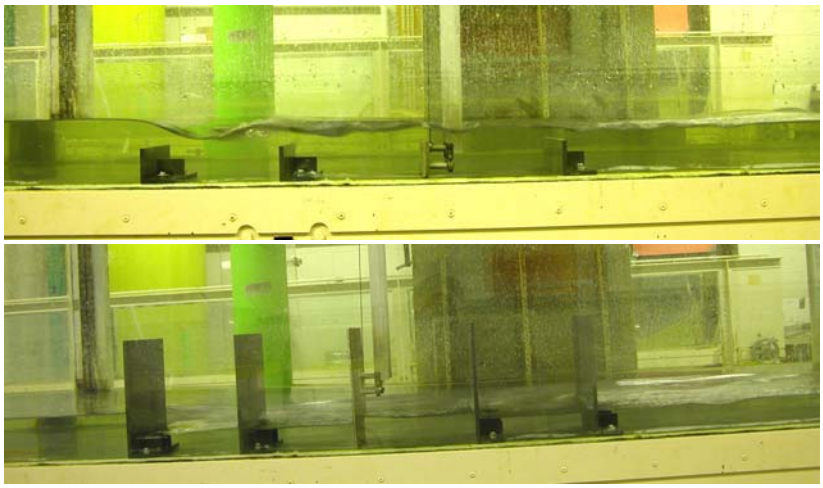

Figure 4.4 Model in operation for two spur dike fields:(a) submerged conditions and, (b) unsubmerged conditions

4.5. Results and discussion

The drag force and backwater effect of a single spur dike plate having the same geometry and for similar discharges as used for the spur dike plates in the spur dike field tests were measured, with the results as shown in Table 4.2. The drag force of a single spur dike plate is used in calculating the relative drag force of a field of spur dike plates as expressed by Eq. [4.8].

Table 4.2. Drag force and backwater effect due to a single spur dike plate of the same size used in the spur dike field tests

Q (L/s)	F_D (N)	h_1-h_2 (mm)	Spur dike condition
44.3	3.5	7.4	submerged
30.2	3.0	8.3	submerged
20.2	2.6	9.5	submerged
20.1	4.2	13	unsubmerged

Table 4.2 shows that the drag force due to a single submerged spur dike plate increases with an increase in the discharge, while the corresponding backwater effect decreases. This is in agreement with the analysis of Eq. [4.4]. With an increase in the discharge, and hence the flow depth, the blockage ratio decreases so that the ratio h_1/h_2 in Eq. [4.4] decreases, which means that the associated backwater effect is reduced accordingly. The relative drag force of each submerged spur dike plate within a spur dike field has been calculated by dividing the measured drag force for each individual plate by the drag force of a single submerged spur dike plate for the same flow conditions as given in Table 4.2. Table 4.3 shows the relative drag force results for the various plates in a submerged spur dike field. In this table, the relative drag force, η_i, of the i^{th} plate from upstream in a spur dike field having m plates is shown for various submergence ratios, h_2/P and spacing ratios, S/L. From Table 4.3, the total relative drag force, η_t, of a specific submerged spur dike field is obtained by summing the relative drag forces of all individual spur dikes in the field. The total relative drag force is subsequently used in Eq. [4.14] to calculate the backwater effect of the spur dike field.

Table 4.3. Relative drag force due to submerged spur dike plates

η_i (h_2/P=2.00)														
m	**2**		**3**			**4**				**5**				
i	1	2	1	2	3	1	2	3	4	1	2	3	4	5
S/L														
1	0.848	0.420	0.806	0.360	0.220	0.783	0.266	0.179	0.267	0.778	0.223	0.171	0.230	0.275
2	0.874	0.482	0.821	0.410	0.370	0.777	0.336	0.358	0.328	0.770	0.297	0.347	0.299	0.308
3	0.879	0.533	0.838	0.507	0.390	0.783	0.447	0.394	0.331	0.776	0.386	0.368	0.323	0.359
4	0.888	0.565	0.852	0.557	0.393	0.789	0.482	0.406	0.380	0.781	0.457	0.383	0.349	0.407
5	0.891	0.571	0.838	0.571	0.425	0.792	0.494	0.442	0.410					
6	0.885	0.583	0.840	0.587	0.460									
7	0.899	0.601	0.846	0.584	0.481									
8	0.888	0.604	0.846	0.596	0.499									
9	0.897	0.619												
10	0.897	0.652												
11	0.902	0.655												
12	0.911	0.646												
13	0.894	0.664												
14	0.905	0.685												
15	0.899	0.690												

Table 4.3 (cont'd.)

η_i (h_2/P=2.00)																
m		**6**			**7**		**8**		**9**	**10**	**11**	**12**	**13**	**14**	**15**	**16**
i	**S/L**	1	2	3	1	2	1	2	1	1	1	1	1	1	1	1
1		0.695	0.784	0.839	0.736	0.710	0.725	0.691	0.708	0.694	0.694	0.702	0.686	0.680	0.674	0.662
2		0.200	0.289	0.397	0.139	0.264	0.133	0.233	0.109	0.067	0.061	0.074	0.055	0.049	0.055	0.052
3		0.132	0.297	0.308	0.163	0.303	0.157	0.302	0.154	0.155	0.136	0.157	0.166	0.154	0.151	0.151
4		0.243	0.327	0.357	0.208	0.307	0.202	0.251	0.202	0.188	0.191	0.127	0.175	0.169	0.178	0.172
5		0.267	0.319	0.365	0.295	0.330	0.213	0.237	0.198	0.185	0.185	0.209	0.206	0.212	0.203	0.209
6		0.259	0.338	0.417	0.250	0.264	0.192	0.234	0.195	0.173	0.176	0.168	0.165	0.165	0.153	0.153
7					0.244	0.290	0.212	0.264	0.196	0.173	0.167	0.126	0.120	0.108	0.099	0.096
8							0.239	0.325	0.196	0.163	0.151	0.164	0.148	0.142	0.136	0.127
9									0.230	0.151	0.133	0.170	0.158	0.167	0.161	0.158
10										0.178	0.142	0.170	0.161	0.161	0.152	0.139
11											0.178	0.194	0.179	0.161	0.142	0.149
12												0.213	0.183	0.162	0.152	0.137
13													0.268	0.235	0.168	0.155
14														0.213	0.184	0.163
15															0.228	0.191
16																0.219

Table 4.3 (cont'd.)

η_i (h_2/P=1.56)															
m		**2**		**4**				**8**							
S/L	**i**	1	2	1	2	3	4	1	2	3	4	5	6	7	8
1		0.728	0.668	0.705	0.404	0.155	0.209	0.649	0.205	0.130	0.132	0.128	0.061	0.096	0.212
2		0.799	0.524	0.741	0.387	0.024	0.253	0.649	0.218	0.188	0.141	0.132	0.115	0.156	0.313
3		0.852	0.490	0.741	0.342	0.093	0.310								
4		0.859	0.479	0.734	0.336	0.162	0.370								
5		0.859	0.503	0.741	0.315	0.192	0.414								
6		0.869	0.517												
7		0.876	0.531												
8		0.869	0.551												
9		0.862	0.565												
10		0.866	0.592												
11		0.866	0.610												
12		0.859	0.661												
13		0.848	0.675												
14		0.859	0.678												
15		0.855	0.692												

Table 4.3. (cont'd.)

η_i (h_2/P=1.20)																	
m	**2**		**3**			**4**				**8**							
i	1	2	1	2	3	1	2	3	4	1	2	3	4	5	6	7	
S/L																	
1	0.749	0.488	0.754	0.347	0.084	0.675	0.333	0.198	0.121	0.694	0.289	0.059	0.004	0.008	0.058	0.105	0.
2	0.839	0.441	0.824	0.300	0.153	0.749	0.222	0.103	0.371	0.687	0.150	0.024	0.035	0.047	0.128	0.186	0.
3	0.863	0.426	0.809	0.320	0.271	0.749	0.175	0.129	0.422								
4	0.871	0.453	0.809	0.238	0.317	0.745	0.147	0.198	0.496								
5	0.890	0.461	0.789	0.265	0.427	0.741	0.151	0.259	0.516								
6	0.882	0.484	0.797	0.253	0.477												
7	0.871	0.543	0.809	0.277	0.508												
8	0.867	0.582	0.793	0.288	0.557												
9	0.863	0.574															
10	0.863	0.590															
11	0.863	0.629															
12	0.855	0.668															
13	0.863	0.684															
14	0.863	0.676															
15	0.859	0.730															

The results shown in Table 4.3 are plotted in Figure 4.5. The position of each plate in the field is indicated in the legend, herein "1" represents the most upstream plate, "2" the second plate, and so on. The total relative drag force for the spur dike field, which is shown as T in the legend, was obtained by summing the individual relative drag forces. The submergence ratio is shown in the top left corner of each figure. The relative spacing for the spur dike fields having a large number of plates was limited to smaller values due to a flume length limitation.

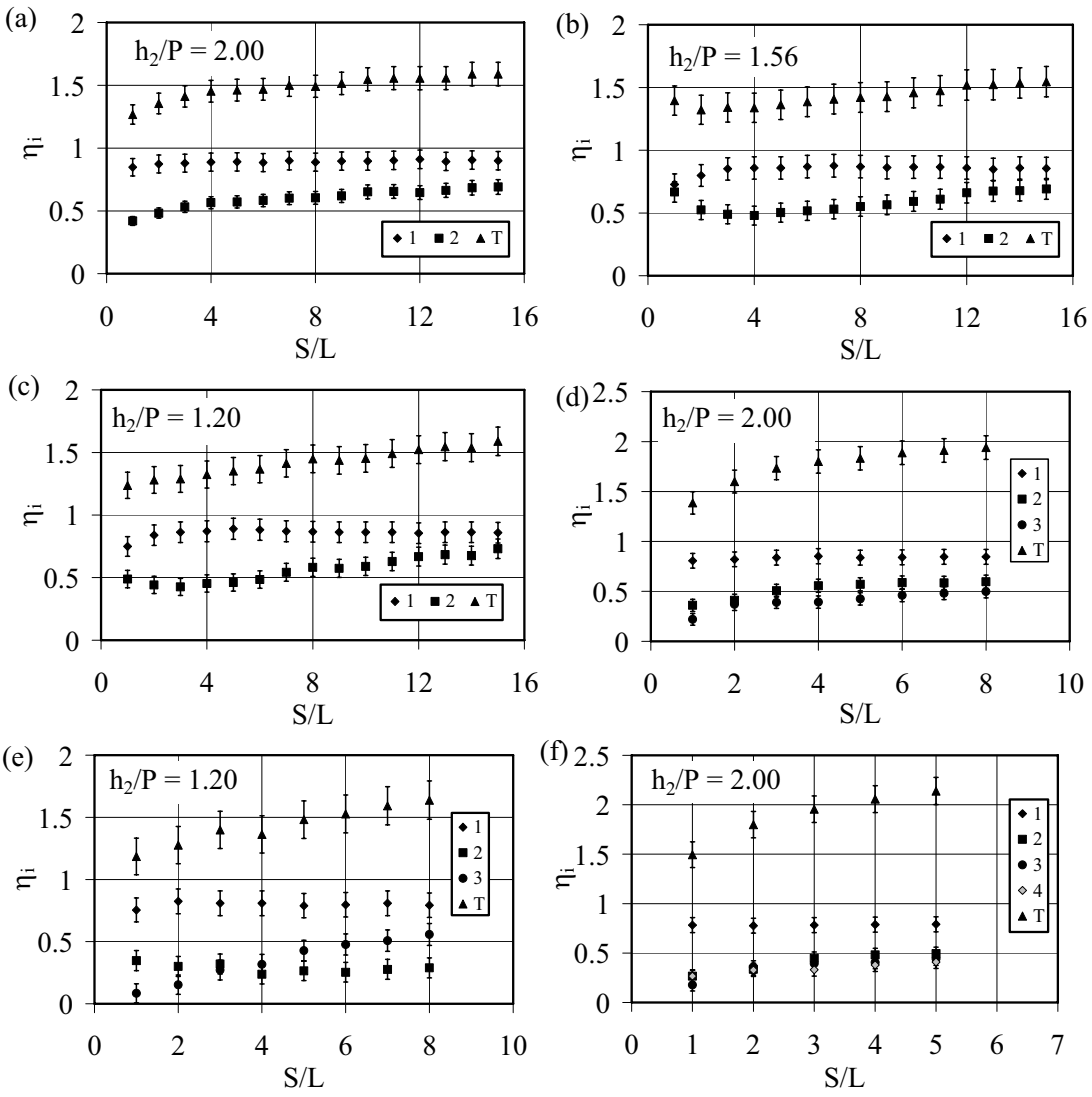

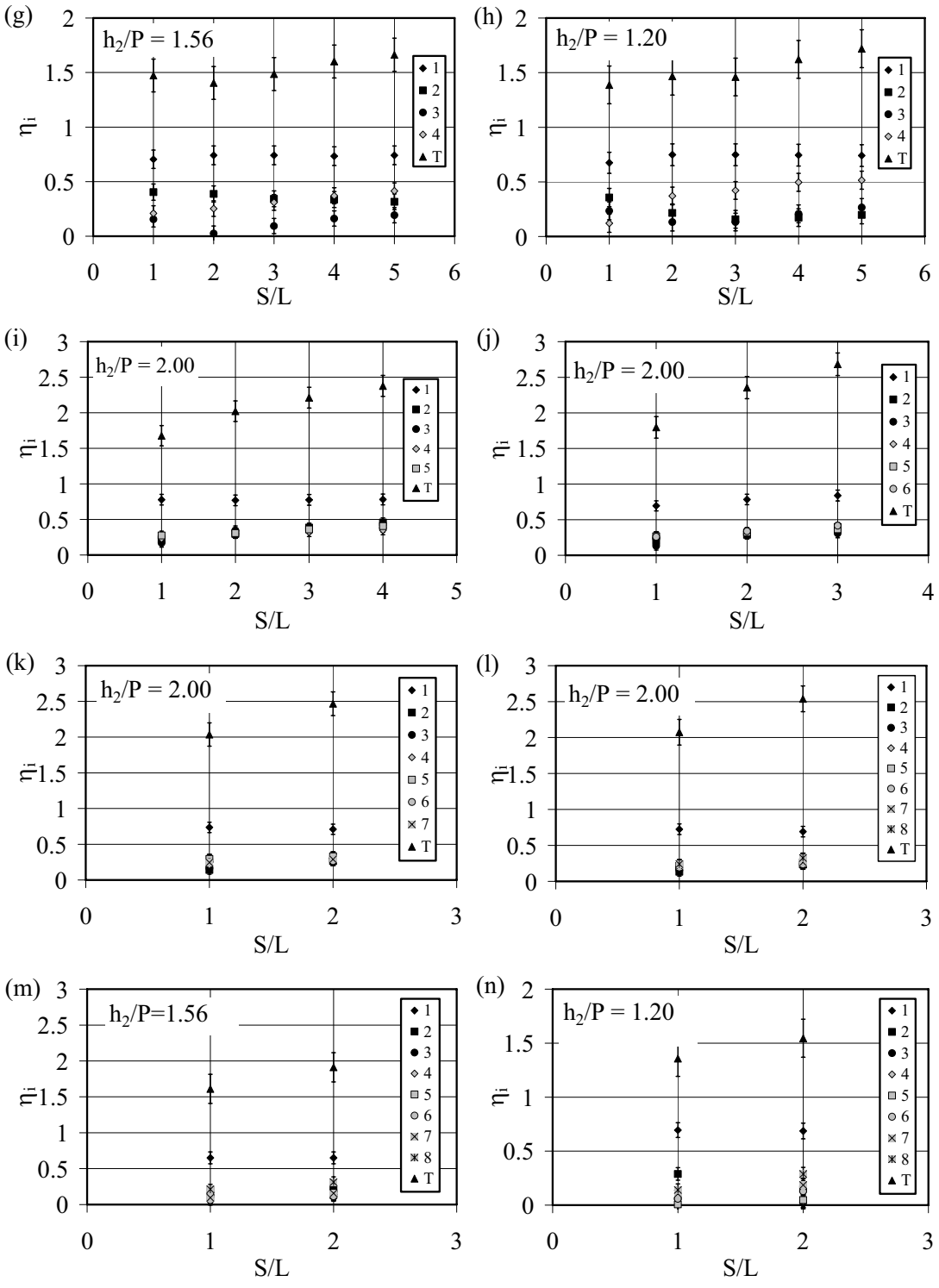

Figure 4.5. Variation in the relative spur dike plate drag force versus the relative spacing in a field for various numbers of plates for submerged flow conditions

The results in Figure 4.5 consistently show that the relative drag force of the most upstream or leading spur dike plate ("1" in the legend) is greater than that of the others in the spur dike field. This finding is as expected, due to the shielding effect of the leading spur dike plate on those placed downstream. The leading plate invariably experiences a greater streamwise velocity and associated dynamic pressure than do those located in the downstream wake region. It can also be seen that, in most cases, there is an increase in the total relative drag force with an increase in the relative spacing between the spur dike plates. This finding confirms that the flow in the spur dike field may be classified as wake-interference flow as suggested by Morris (1955). The relative drag force of the various individual plates does not show a consistent trend with the relative spacing, presumably due to the development of a complex flow structure adjacent to each plate. For high relative spacings (greater than four), nonetheless, the relative drag force of the downstream plates does show a consistent increase with an increase in the relative spacing. On this basis, it may be concluded that, for high relative spacings, the effect of the wake due to the upstream spur dike plates on those placed downstream is reduced as the spacing between the plates increases.

Comparison of the results for the various submergence ratios shown in Figure 4.5 indicates that, as the submergence ratio increases, the total relative drag force of the spur dike field increases accordingly. Tominaga et al. (2001) measured the velocity distribution around submerged spur dikes having various submergence ratios which were obtained from spur dikes having various heights placed in a constant flow depth. They observed that the strength of the reverse flow (vertical vortex) formed by the side edge (tip) of the spur dikes becomes weaker with a decrease in the spur dike height (i.e., increase in the submergence ratio). From this observation, it might be argued that an increase in the submergence ratio increases the jet flow velocity over the top and hence between the spur dikes, which in turn suppresses the reverse flow. An increase in the jet flow velocity is accompanied by an increase in the streamwise velocity toward the upstream face of the next downstream spur dike. This outcome leads to a greater dynamic pressure and hence a greater relative drag force for the downstream spur dike. The rate of increase in the total relative drag force with submergence ratio is greater for spur dike fields having a larger number of spur dikes. For

example, there is no apparent variation in the total relative drag force with the submergence ratio for a spur dike field having only two spur dikes (Figures 4.5a, 4.5b and 4.5c), while a spur dike field with eight spur dikes (Figures 4.5l, 4.5m and 4.5n) shows a substantial increase in the total relative drag force with an increase in the submergence ratio.

The effect of the submergence ratio for submerged spur dike fields comprising two spur dike plates (Figures 4.5a, 4.5b and 4.5c) on the relative drag force indicates that there may be dissimilarity in the flow structure adjacent to the spur dike plates for the various submergence ratios studied. For the lower submergence ratios (Figs. 4.5b and 4.5c), the relative drag force of the second spur dike decreases with an increase in the relative spacing to a minimum value at $S/L \approx 3$ and then it increases for larger S/L values. The minimum value of the relative drag force due to the second spur dike occurs at a so-called critical relative spacing, which is about 3 and 4. This finding is in general agreement with the drag characteristics of two bluff bodies having a tandem arrangement (e.g., Ohya et al., 1989, Auteri et al., 2008). It is speculated that, at a relative spacing less than the critical value, the vortex from the first spur dike plate induced from the tip of the plate (i.e., side-induced vortex) rolls up behind the second spur dike plate. As the trailing edge of the vortex is near to the downstream face of the second plate, it suppresses the negative pressure behind the plate (i.e., the pressure increases behind the second plate). However, at relative spacings above the critical value, the vortex induced from the first spur dike plate rolls up in front of the upstream face of the second plate. Figure 4.6 is a plan view schematic that illustrates the critical spacing effects. The drag force exerted on the second spur dike plate in Figure 4.6a, F_{Da}, is higher than that exerted on the second spur dike plate, F_{Db}, in Figure 4.6b.

For large submergence ratios (e.g., Figure 4.5a), the jet flow over the leading spur dike plate serves to suppress the vertical vortex so that a steady increase in the relative drag force experienced by the second spur dike plate is observed. The effects of the first plate on the second one decreases as the relative spacing increases, resulting in an increase in the relative drag force experienced by the second plate. Based on the premise that the two spur dikes are independent at very high relative spacings, it is expected that the relative drag force

of both spur dikes will approach a value of unity while the total relative drag force approaches a value of two.

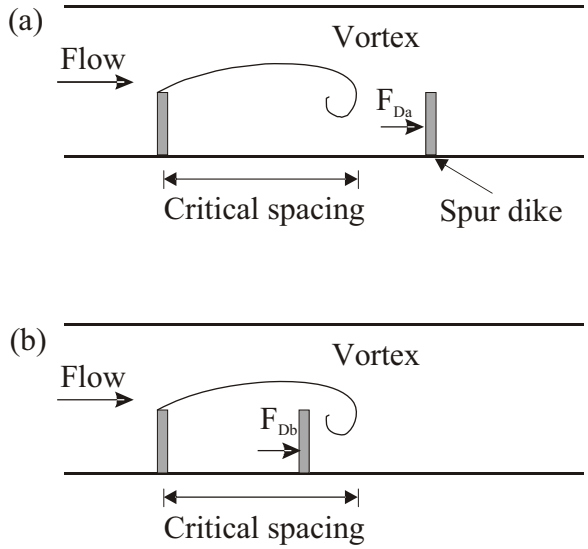

Figure 4.6. Schematic illustration of the critical spacing in which (a) the relative spacing is greater than the critical spacing, and (b) the relative spacing is less than the critical spacing

For submerged spur dike fields with three spur dikes and for a low submergence ratio (Figure 4.5e), the relative drag force of the second spur dike plate is greater than that of the third spur dike plate for S/L < 3. However, for S/L > 3, the relative drag force of the third plate becomes greater than that of the second one. For relative spacings where the third spur dike plate is located at a spacing less than the critical spacing, it is expected that the vortex induced from the side edge of the first plate will roll up at the downstream face of the third plate so that the drag force of the third plate is less than that of the second one. For large relative spacings, the third spur dike plate does not have any downstream plate to interfere with its wake, which could be the reason for the third spur dike showing a greater drag force compared to that of the second one. This trend is not observed for the higher submergence ratio (Figure 4.5d) as the effect of the stronger jet flow (compared to that for the lower submergence ratios) suppresses the vortex effect induced from the side edge of the first plate. The latter effect is also shown in Figure 2.10 (Abad et al., 2008).

There is a similar behaviour between spur dike fields having three and four plates in terms of the relative spacing and submergence ratio effects. For the lowest submergence ratio (Figure 4.5h), the minimum drag force occurs for the plates immediately upstream of the critical spacing point. The minimum drag force for plate numbers four and three occurs for the relative spacings of one and two, respectively. For larger relative spacings, the fourth plate shows a larger drag force compared to the second and third ones. Similar behaviour, as explained previously, is observed for spur dike fields having five, six, seven, and eight spur dike plates (Figures 4.5i, 4.5j, 4.5k, 4.5l, 4.5m and 4.5n). The drag forces of the middle plates for a particular spacing ratio in the spur dike fields with a large number of plates are similar in magnitude and they increase with the relative spacing.

Figure 4.7 shows the relative drag force of each individual plate in a spur dike field for two submergence ratios and three relative spacings. The legend in the figure represents the number of plates in each individual spur dike field. The figure shows that, for a particular submergence ratio, in general, the relative drag force of an individual plate in a field decreases with an increase in the number of plates. This is more pronounced for the most upstream spur dike plate and also for the lowest submergence ratio. The reason for this finding is partly related to the increased upstream flow depth for a given discharge and hence decreased approach velocity as the number of plates in the field increases. The decreased velocity results in a decrease in the dynamic pressure and hence drag force for each plate in the field.

Figure 4.7a shows the relative drag force of each spur dike plate in a field having a large submergence ratio and a small relative spacing. It can be observed that the relative drag force experienced by the second or third plate is the least among the group. Similar to the argument of critical spacing associated with the effects of the side-induced vortex, it is also to be expected that there is a critical spacing associated with the relative position of the jet flow reattachment point on the channel bed. A plate located upstream of the reattachment point experiences a smaller drag force compared with those located downstream from the reattachment point where their upstream face is in direct contact with the jet flow. On the basis of this argument, one can conclude that all plates in Figure 4.7b having a relative

spacing of four are located downstream from the jet flow reattachment point. For spur dikes fields with large number of plates, the relative drag force of the middle plates is essentially constant, as shown in Figure 4.7a.

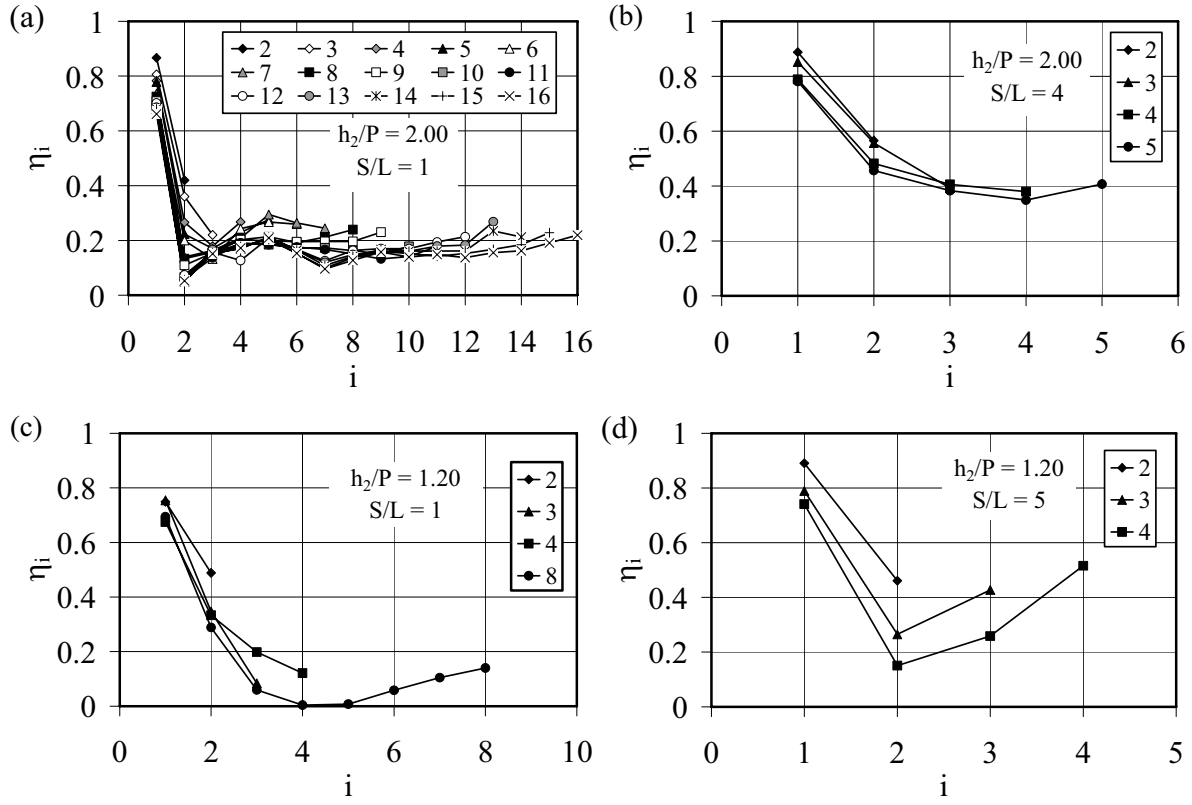

Figure 4.7. Relative drag force of each individual spur dike plate in a submerged spur dike field for two submergence ratios and three spacing ratios

From Figure 4.7c, for the lowest submergence and spacing ratios, it can be observed that the minimum relative drag force occurs for plate number four. However, for a relative spacing equal to five, as shown in Figure 4.7d, the minimum relative drag force occurs for plate number two. As noted previously, the critical relative spacing primarily due to the tip-induced vortices of the spur dike plates occurs at a relative spacing of about three to four, so it is expected that a plate located at about the critical relative spacing location would experience the least relative drag force. In the cases shown in Figures 4.7c and 4.7d, the plates experiencing the least relative drag force are nearest to the critical relative spacing when compared to the other plates in the field. In this context, Ball and Cox (1978)

measured the drag force of a series of 2-D plates located along the centerline of an open channel. The submergence ratio was adjusted to be near to unity. The results of their work are shown in Figure 4.8 where *d, S_L*, and K_D are the length, spacing and relative drag force of plates, respectively. Their findings in the context of the relative drag force are similar to those found in the present study as shown in Figures 4.7. The shielding effects of the first spur dike in both Figures 4.8a, and 4.8b have caused the relative drag force of downstream spur dikes decreases. The minimum relative drag force in Figure 4.8b occurs for a relative spacing of about four which is similar to the results of this study.

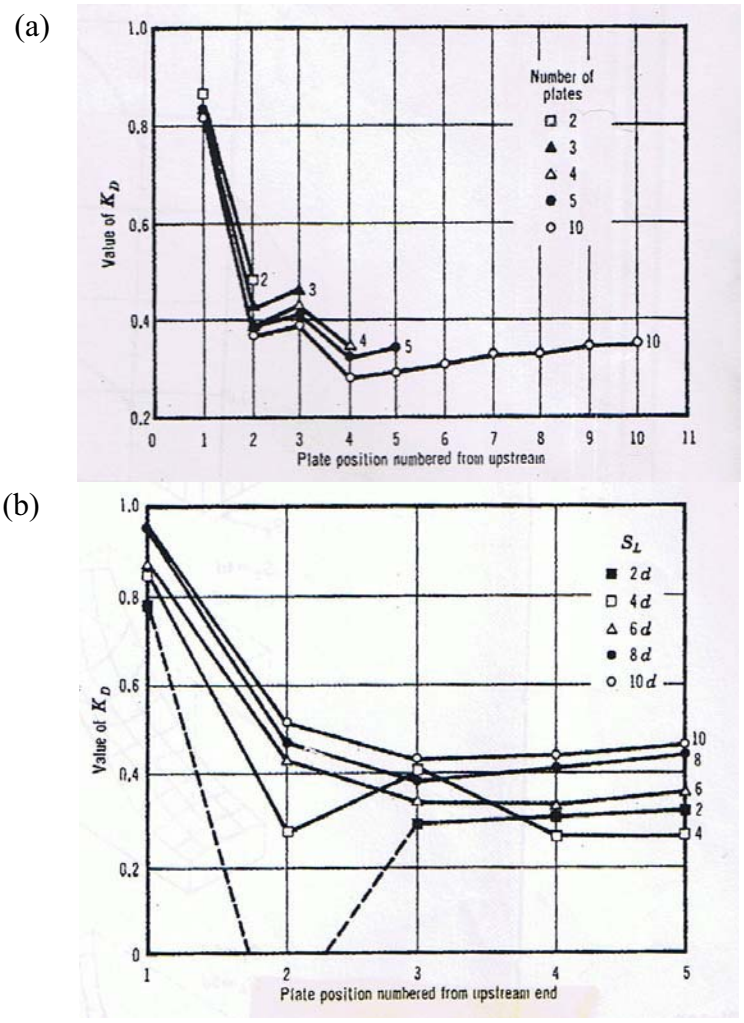

Figure 4.8. Relative drag force of 2-D plates placed in succession versus the spacing and position of plates: (a) various number of plates for S_L=5*d*, and (b) plate spacing for n=5 (*Taken from Ball and Cox, 1978*)

Figure 4.9 shows the total relative drag force versus the number of plates in a spur dike field for various relative spacings and a submergence ratio of two. The relative spacing between the spur dikes is shown in the legend of the figure along with the 45 degree line, which represents the total drag force of a spur dike field having an equivalent number of single spur dike plates. The results show that the total relative drag force increases with an increase in the number of spur dike plates in a spur dike field. The rate of increase is greater for spur dike fields having a larger relative spacing. However, the total relative drag force of a spur dike field with "m" number of plates is much smaller than the total relative drag force exerted by the same number of single spur dike plates. It can be concluded that the interaction between the plates, and mainly the shielding effect provided by the most upstream plate in a spur dike field, substantially decreases the total drag force exerted by the field when compared to the total drag force of an equivalent number of single plates.

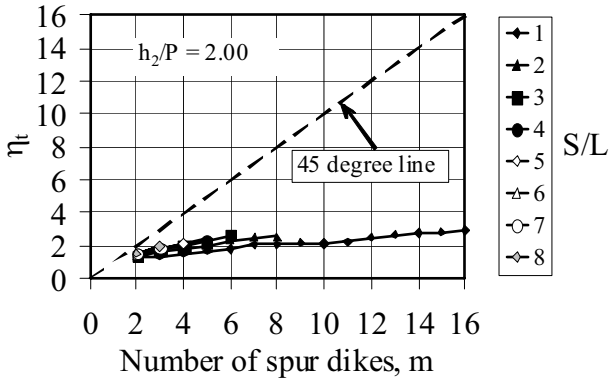

Figure 4.9. Variation in the total relative drag force with the number of spur dike plates in a spur dike field for various relative spacings between the plates (the relative spacing is shown in the legend)

A regression analysis was performed to relate the total relative drag force due to submerged spur dikes in a spur dike field to the number of spur dikes in the field, the relative spacing between the spur dikes, and the submergence ratio. This relationship is given by

$$[4.15] \quad \eta_t = 0.78 m^{0.38} \left(\frac{h_2}{P}\right)^{0.28} \left(\frac{S}{L}\right)^{0.11}$$

The coefficient of determination, R^2 was found to be 0.93. Based on the exponents of each of the variables in Eq.[4.15], it is concluded that the number of spur dikes has the most effect on the total relative drag force of submerged spur dike fields. Equation [4.15] is only valid in the range of values used in the present study, as reported in Table 4.1. Moreover, the value of the relative spacing must be equal to or greater than unity.

Similar to submerged spur dikes, the relative drag force of unsubmerged spur dike plates within a spur dike field has been calculated by dividing the measured drag force for each individual spur dike plate by the drag force for a single unsubmerged spur dike plate as shown in Table 4.2. Table 4.4 shows the results for unsubmerged spur dike fields.

Table 4.4. Relative drag force of unsubmerged spur dike plates

Unsubmerged mode									
m	**2**		**3**			**4**			
i	1	2	1	2	3	1	2	3	4
S/L									
1	1.010	-0.044	-0.065	0.984	-0.024	1.123	-0.082	-0.143	0.147
2	1.114	-0.019	-0.148	0.995	0.160	1.058	-0.233	-0.025	0.175
3	1.014	0.104	-0.129	0.963	0.203	0.972	-0.228	0.099	0.218
4	0.964	0.228	-0.012	0.897	0.217	0.863	-0.166	0.141	0.246
5	0.966	0.235	0.024	0.890	0.238	0.844	-0.141	0.126	0.303
6	0.932	0.269	0.019	0.869	0.295				
7	0.911	0.240	0.029	0.848	0.344				
8	0.913	0.223	-0.072	0.839	0.406				
9	0.915	0.235							
10	0.928	0.260							
11	0.923	0.301							
12	0.908	0.345							
13	0.911	0.410							
14	0.896	0.439							
15	0.894	0.410							
16	0.879	0.454							

In Table 4.4, the relative drag force of the i^{th} plate in a row, η_i, in a particular spur dike field having m number of plates is shown for various spacing ratios, S/L. In some cases, as the table shows, the relative drag force is negative. The negative drag force is usually

referred to as thrust force and spur dike plates experiencing thrust are exhibiting a net force opposite to the streamwise direction.

The results of Table 4.4 are plotted in Figure 4.10 to represent the variation of the relative drag force of spur dike plates in unsubmerged conditions versus the relative spacing. The position of each plate in the field is indicated in the legend. In this figure, similar to that for submerged spur dike plates, "1" represents the most upstream plate, "2" the second plate, and so on. The total relative drag force for the spur dike field, which is shown as T in the legend, was obtained by summing the individual relative drag forces.

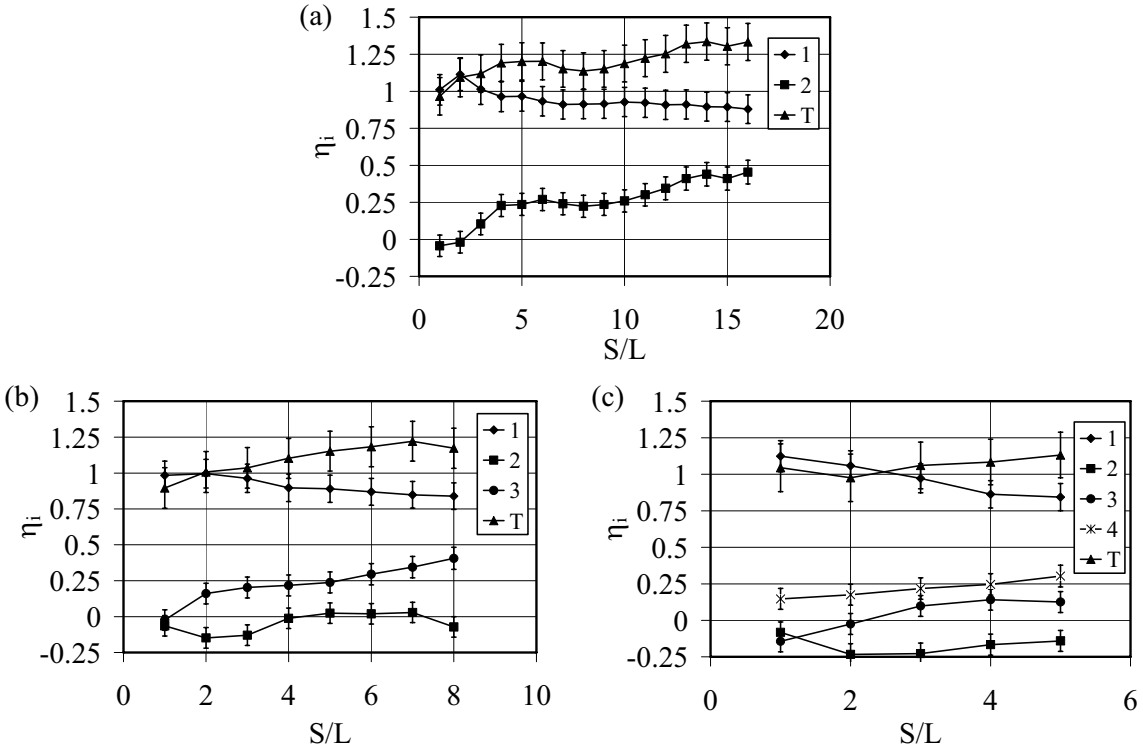

Figure 4.10. Relative drag force of unsubmerged spur dike plates versus relative distance for spur dike fields having (a) two plates, (b) three plates, and (c) four plates

It is to be noted that, in general, the total relative drag force of a spur dike field increases with an increase in the relative spacing between the spur dike plates. This trend is similar to that for a submerged spur dike field, which suggests that spur dike fields perform in the wake-interference zone as per Morris' (1955) flow classification. The total relative

drag force of an unsubmerged spur dike field is considerably less than that for a submerged spur dike field, most likely due to the lack of surface jet flow effects. Jet flow considerably increases the flow momentum by increasing the streamwise velocity between the spur dike plates which results in an increase in the drag force experienced by the plates in a spur dike field. Figures 4.10a, 4.10b and 4.10c show that, as the number of plates in the spur dike field increases, the drag force of the middle plates decreases. In some instances, where the relative spacing between the plates is small, there is a negative drag force or thrust force experienced by the middle plates. The drag force of the second plate is always negative in the case of an unsubmerged spur dike field having four plates (Figure 4.10c). The relative drag force of the second plate is lowest at a relative spacing of about two to three (Figures 4.10b and 4.10c), most likely due to the effects of vortex generated from the tip of the most upstream plate. This critical spacing differs from that for submerged spur dike fields, which occurs at relative spacing of about three to four. It seems that wake interference has a substantial role in influencing the drag force of unsubmerged plates.

Figure 4.10 shows that the relative drag force of the leading spur dike plate for all unsubmerged spur dike fields decreases with an increase in the relative spacing between the plates. This trend is in contrast to that observed for submerged spur dike fields. This reduction might be explained using the flow pattern classification described by Klingeman et al. (1984) for unsubmerged spur dikes, as shown in Figure 2.9. Depending on the relative spacing between the plates, they have categorized unsubmerged spur dike fields based on the types of eddy patterns. For small relative spacings, there is a single large eddy structure that forms between the spur dikes (i.e., spur dike zone). This single large eddy is separated from the main flow in the channel and thereby the main flow is prohibited from penetrating the spur dike zone. However, as the relative spacing between the spur dikes increases, the single strong eddy between the spur dikes decomposes into two smaller eddies. The eddies between the spur dikes wane in size and strength and the main flow from the channel penetrates further into the spur dike zone.

As the relative spacing between the spur dike plates increases, there is no significant change in the pressure upstream of the leading plate. However, as the flow in the main

channel adjacent to the spur dike penetrates further into the downstream area (wake) of the leading spur dike plate in accordance with the finding of Klingeman et al. (1984), the pressure in the wake region of the plate becomes greater and hence the drag force is reduced. The increased flow depth upstream of the spur dike field and hence a decreased velocity (for a given discharge) is also a factor that decreases the relative drag force of the leading plate as the relative spacing increases.

As for submerged spur dikes, a regression analysis was performed to relate the total relative drag force of unsubmerged spur dikes to the number of spur dikes in the spur dike field and the relative spacing between the spur dikes. The results showed that the number of spur dikes has minimal effect on the total relative drag force. As such, the regression analysis was repeated to relate the total relative drag force to the relative spacing alone, as shown in Eq. [4.16]. The coefficient of determination, R^2, was found to be 0.91. Of course, Eq.[4.16] is only valid over the range of values used in the present study, as reported in Table 4.1.

$$[4.16] \quad \eta_t = \left(\frac{S}{L}\right)^{0.09}$$

In general, the results of the study shows that the total relative drag force and hence total drag force of a spur dike field increases with an increase in the relative spacing, although the total drag force is considerably lower than the total drag force of a spur dike field with the same number of single spur dikes. This outcome suggests that the spur dike plates are in the wake-interference region. It is expected that for a very high relative spacing where the excess force effect becomes considerable, the total resistance of the spur dike field will decrease. Figure 4.10 shows the measured backwater effect variation of a spur dike field with two spur dike plates with relative spacing. The legend in Figure 4.11 represents the three submergence ratio cases and the case of unsubmerged one (shown by Unsub.). It is observed that the backwater effect and hence the total resistance of the spur dike fields increases with an increase in the relative spacing. However, the backwater effect shows a very small variation in higher submergence ratios. This stability in the backwater effect is

reached in lower spacing ratios for submerged conditions. The backwater effect of the spur dike fields will decrease to that of a single spur dike for a very high relative spacing.

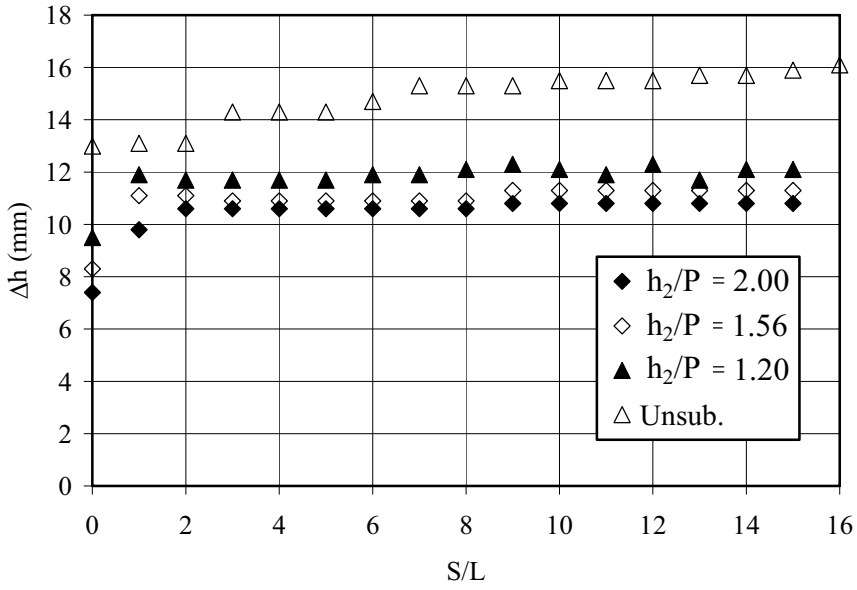

Figure 4.11. Backwater effect variation of a spur dike field having two spur dike plates versus relative spacing

The results also show that there is a considerable variation in the relative drag force of spur dike plates in a field which is attributed to various flow structures experienced by the plates. The interaction of the jet flow with the vertical vortices is responsible for various observed flow structures in a spur dike field. Arrangement of spur dikes and also the flow conditions (i.e., submergence ratio) govern the vertical vortices and jet flow characteristics. The critical spacing, which reasonably explains the location of a plate having the minimum relative drag force, seems to almost remain unaffected by the flow structure.

In order to evaluate the results obtained from the direct measurement of drag force, the backwater effect was calculated from Eq. [4.14] and compared with that measured in the experiments. Figure 4.12 shows the calculated versus the measured backwater effect due to spur dike fields for both submerged and unsubmerged conditions. The legend shows the number of spur dikes in the spur dike field and, in parentheses, the submergence ratio. The "Unsub." in parentheses means that the spur dike field is unsubmerged.

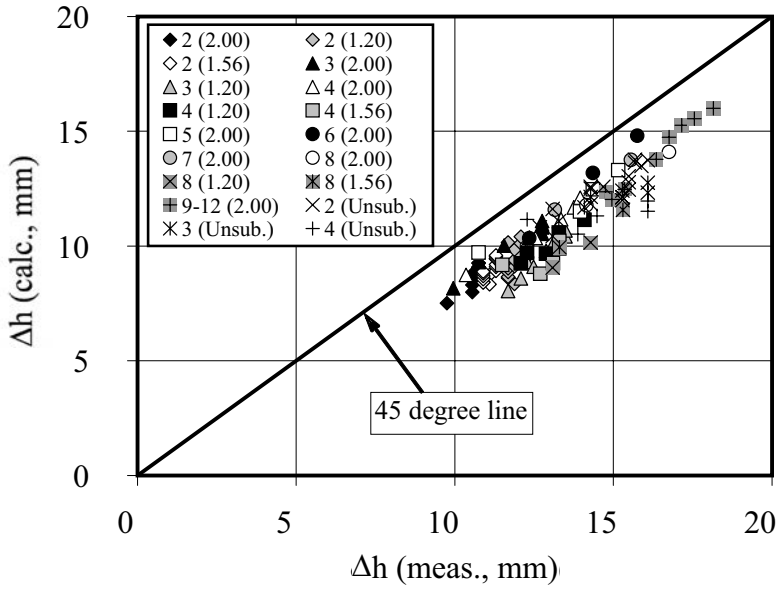

Figure 4.12. Calculated versus measured backwater effect for submerged and unsubmerged spur dike fields

The results show that the calculated backwater effect is less than that measured. The reason for the difference might be partially related to the high bed shear stress in the vicinity of the nose of the spur dikes where the velocity is relatively high. In the theoretical analysis of the backwater effect, it may be recalled that it was assumed that the mean bed shear stress is offset by the downslope component of the weight of water in the control volume. As such, any underestimate in the bed shear stress will result in an underestimate of the backwater effect. The average difference between the calculated and measured backwater effect is about 19%, so the backwater effect calculated using the total drag force of a spur dike field must be increased by about 23% in order to yield the actual backwater effect likely to be experienced.

4.6. Summary and conclusions

The flow resistance expressed in terms of a drag force exerted by spur dikes in a spur dike field was studied using a physical model. By applying the momentum equation, relationships were developed to estimate the backwater effect of a spur dike field. The drag

forces due to individual spur dike plates in a spur dike field for various geometric arrangements and flow conditions were measured directly using a specially designed apparatus. The geometric arrangements of the spur dike fields varied in terms of the number of spur dike plates in the field and the relative spacing between them. In this work, the spur dike length and channel width were held constant.

It is concluded that the number and spacing of spur dike plates in a spur dike field and the flow conditions have a substantial effect on the flow resistance and hence backwater effect that is experienced. In general, the total drag force exerted by a spur dike field increases with an increase in the number of plates and also with an increase in the relative spacing between the plates. This was more prominent for submerged flow conditions than for unsubmerged flow conditions. The drag force of the first spur dike plate is the greatest amongst the group, as it acts as a shield to reduce the drag force experienced by the downstream plates. For submerged flow conditions, the spur dike plate drag force increases with an increase in the submergence ratio. For unsubmerged flow conditions, the drag force of the middle spur dike plates is quite small, even showing some negative values.

It is concluded that the flow structure is quite different between submerged and unsubmerged flow conditions. The difference is related to the effect of the jet flow over the submerged spur dike plates, which influences the dynamic pressure in front of the downstream plates. The flow resistance and hence the backwater effect of spur dike fields is strongly affected by the flow structure.

The outcomes of the present study are directly applicable to 2-D spur dike fields in a rigid bed rectangular channel, which is expected to yield a conservative result for the backwater effect relative to that likely to be experienced in an erodible boundary channel. As such, the results due to the present work should be considered as conservative, first-order estimates of the backwater effect.

4.7. Acknowledgements

Financial support for this research has been provided by the Natural Sciences and Engineering Research Council of Canada through a grant to the second author, as well as by a University of Saskatchewan graduate scholarship to the first author. This support is gratefully acknowledged. Also, the authors thank Dr. Bruce Sparling for his help in the design of the drag force measurement apparatus, the staff in Engineering Shops for fabricating the apparatus, and the lab technicians, Mr. Dale Pavier and Mr. Brennan Pokoyoway, for their assistance in conducting the experiments.

4.8. References

Abad, J.D., Rhoads, B.L., Guneralp, I. and Garcia, M.H. 2008. Flow structure at different stages in a meander-bend with bendway weirs. Journal of Hydraulic Engineering, ASCE, 134(8): 1052-1063.

Auteri, F., Belan, M., Gibertini, G. and Grassi, D. 2008. Normal flat plates in tandem: An experimental investigation. Journal of Wind Engineering and Industrial Aerodynamics, Elsevier, 96(6-7): 872-879.

Azinfar H, and Kells, J.A. 2009. Flow resistance due to a single spur dike in an open channel. Journal of Hydraulic Research, IAHR, 47(6): 755-763.

Ball, D.J. and Cox, N.J. 1978. Hydrodynamic drag forces on groups of flat plates. Journal of the Waterway, Port, Costal, and Ocean Division, ASCE, 104(WW2): 163-173.

Belz, J.U., Busch, N., Engel, H. and Gasber, G. 2001. Comparison of river training measures in the Rhine catchment and their effects on flood behavior. Water and Maritime Eng., Thomas Telford, 148(3): 123-132.

Chow, V. T. 1959. Open-channel hydraulics. McGraw-Hill, Inc., New York, NY, USA, 680 p.

Criss, R.E. and Shock, E.L. 2001. Flood enhancement through flood control. Geology, The Geological Society of America, 29(10): 875-878.

Klingeman, P.C., Kehe, S.M. and Owusu, Y.A. 1984. Streambank erosion protection and channel scour manipulation using rockfill dikes and gabions. WRRI-98, Oregon State University, Water Resources Research Institue, Corvallis, Oregon, 169 p.

Morris, H.M. 1955. Flow in rough conduits. Transaction of American Society of Civil Engineers, ASCE, Vol. 120, Paper No. 2745: 373-410.

Ohya, Y., Okajima, A. and Hayashi, M. 1989. Encyclopedia of fluid mechanics, Wake interference and vortex shedding. Gulf Publishing Company, Houston, Texas, USA, Volume 8, Chapter 10: 324-389.

Pinter, N., Thomas, R. and Wlosinski, H. 2001. Assessing flood hazard on dynamic rivers. EOS, Transactions, American Geophysical Union, 82(31): 333-339.

Shields, F.D. 1995. Fate of lower Mississippi River habitats associated with river training dikes. Journal of Aquatic Conservation: Marine and Freshwater Conservation, John Wiley & Sons, Ltd., 5(2): 97-108.

Tominaga, A., Ijima, K. and Nakano, Y. 2001. Flow structures around submerged spur dikes with various relative heights. Proceedings of 29th IAHR Congress, Beijing, China, pp. 421-427.

Wu, B., Wang, G., Ma, J. and Zhang, R. 2005. Case study: River training and its effects on fluvial processes in the Lower Yellow River, China. Journal of Hydraulic Engineering, ASCE, 131(2): 85-96.

Chapter 5. Numerical Modeling of the Flow Field within the Vicinity of a Single Submerged Spur Dike

Contribution of the Ph.D. candidate

All work reported in this chapter, including the review of the literature, selection of the appropriate CFD modeling software, adapting of the CFD model to the present study, running of the CFD model, analysis of the CFD model results, design of the experimental program, conducting of the experiments, presentation and discussion of the results, and writing of the text, has been carried out by the Ph.D. candidate.

As supervisor, Dr. J.A. Kells reviewed all parts of the work. A similar version of this chapter, co-authored by the Ph.D. candidate and supervisor, was submitted to the Canadian Journal of Civil Engineering for possible publication. This chapter differs from the manuscript as submitted for possible publication insofar as there has been additional detail provided herein about the flow pattern adjacent to the spur dike (Figure 5.11). Of course, the journal manuscript is subject to revision prior to publication, so further differences may be evident once the manuscript has been approved for publication.

Contribution of this chapter to the overall study

In Chapters 3 and 4 of the thesis, the flow resistance and associated backwater effect due to spur dikes was assessed using an experimental study. The work presented in this chapter assess the capability of the 3-D CFD model FLUENT for evaluating the resistance and associated backwater effect due to a spur dike in an open channel flow. Moreover, the flow structure in terms of the velocity distribution adjacent to a single submerged spur dike has been investigated. This work provides evidence that a general 3-D CFD model (i.e., FLUENT) is reasonably capable of simulating the flow resistance and backwater effect due to hydraulic structures (in this case a single submerged spur dike in an open channel flow). This work also serves to extend the available literature in the application of VOF modeling to simulate free surface flow and also in the assessment of a turbulence model (RNG k-ε) for simulating anisotropic turbulence conditions in a flow field.

5.1. Abstract

The flow field within the vicinity of a submerged spur dike was modeled using the commercial three-dimensional (3-D) CFD model FLUENT. Application of the model required solution of the 3-D Reynolds-averaged Navier-Stokes equations wherein the Reynolds stresses were resolved using the RNG k-ε turbulence model. The model was run with one discharge for two channel geometries, one comprising a smooth, rectangular channel that resulted in uniform flow conditions and the other a smooth, rectangular channel in which a single spur dike was installed that resulted in non-uniform flow conditions. The CFD model results were evaluated using experimental data acquired from a flume study utilizing a physical model. The CFD model was first tested on the basis of uniform flow conditions, after which it was applied to the prediction of the flow field characteristics with the spur dike in place. It was found that the CFD model could satisfactorily predict the water surface profile adjacent to the spur dike, including the backwater effect. Furthermore, the CFD model gave good prediction of the velocity field except for an area immediately behind the spur dike where the effects of diving jet flow over the top of the spur dike were experienced.

5.2. Introduction

A spur dike is a type of hydraulic structure often constructed on the bank of a river at some angle to the main flow direction. Such a structure may be used for river training or for the protection of the river bank from erosion. With respect to river training for navigation purposes, a series of spur dikes may be used to provide for both a sufficient depth of flow and an improved channel alignment. A single spur dike can also be used to deflect the flow toward a desirable point within a channel such as a water intake. In the context of erosion control, spur dikes can be used to deflect the flow away from the river bank and thereby protect the bank from erosion. It has also been found that the construction of spur dikes on rivers creates a complex bed profile, including local pools and riffles and various other flow features adjacent to the structure, which may be very valuable for aquatic habitat (Hendrickson and Schneider, 1999; Shields, 1995; Tamai et al., 1996).

It is to be expected that improved understanding of the flow field adjacent to a spur dike would be of benefit in the design of such a structure. Among other things, this improved understanding would extend to the impact of spur dikes on sediment transport, river water quality, and river water levels. When a spur dike is placed in an open channel, the flow becomes highly disturbed. In the case of a submerged spur dike, there are two kinds of vortices formed within the vicinity of the spur dike, including both vertical and transverse vortices (Tominaga et al. 2001). The vertical vortices are formed due to the lateral flow along the length of the spur dike peeling off the nose within the mid-channel region, while the transverse vortices are formed due to the flow over the top of the spur dike. The interaction of the two types of vortices produces a highly three-dimensional flow field adjacent to the spur dike. Due to the three-dimensional flow, it is expected to observe vertical and transverse or secondary currents adjacent to the spur dike. Developments of the secondary currents in the vicinity of spur dikes have been observed by Peng et al. (1997) and Kuhnle et al. (2002). Kuhnle et al. (2002) measured the velocity distribution within the vicinity of a trapezoidal submerged spur dike using an acoustic Doppler velocimeter (ADV). They found increased streamwise velocities in the section of channel just beyond the end of the spur dike nose and decreased streamwise velocities immediately upstream of and downstream from the spur dike. Negative streamwise velocities were also reported in the lee of the structure. Two transverse vortex patterns were observed as the flow converged and diverged over the top of the structure.

In a subcritical flow, the water surface elevation upstream of a spur dike increases. The difference between the water surface elevations upstream of and downstream from a submerged spur dike has been reported by Aya et al. (1997). The increased water surface elevation upstream of a spur dike (i.e., backwater effect) may be cause for concern during high flow periods. For example, studies show that, over the past century, flood stages for given discharges at various locations along the Middle Mississippi and Lower Missouri rivers have increased by 2 m to 4 m (Criss and Shock, 2001). Pinter et al. (2001) have attributed part of the observed stage increase to the construction of spur dikes. Wu et al. (2005) have observed the backwater effect of long spur dikes constructed on the Lower Yellow River in China. Stage increases due to spur dikes have also been reported on the Rhine River in

Europe. There, it has subsequently been decided to reduce the height of the spur dikes as a way of reducing their adverse effects during times of flooding (Yossef, 2002; Belz et al., 2001).

Several CFD model studies of the flow field adjacent to submerged spur dikes have been reported in the literature. Peng et al. (1997) used a three-dimensional CFD model to study the flow field near to a series of submerged spur dikes. They found a strongly three-dimensional flow structure adjacent to the spur dikes. Moreover, they obtained the turbulence characteristics of the flow and the bed shear stress distribution. It was concluded that the Reynolds stresses, which represent the influence of turbulence motion on the mean flow, have a high gradient near to the spur dikes. Moreover, the maximum bed shear stress occurred near the tip of the spur dikes. Jia and Wang (2000) used a CFD model to simulate the flow field adjacent to a submerged trapezoidal cross-section spur dike. They observed a three-dimensional flow structure including a horseshoe vortex in front of and a large size recirculation zone behind the spur dike. They also reported a high bed shear stress zone in the channel just beyond the spur dike nose and slightly downstream from the structure. A CFD model was used by Kuhnle et al. (2002) to simulate the three-dimensional flow around a submerged trapezoidal cross-section spur dike. A small vortex at the front corner and a large recirculation zone behind the spur dike were observed. The flow field predicted by the CFD model matched reasonably well with their experimental data. Nonetheless, the CFD model under-estimated the velocities in the recirculation region behind the structure. In all of the studies reported, however, prediction of the water surface profile, including the backwater effect within the vicinity of the spur dike, has not been given adequate consideration.

The work presented herein is directed toward an application of the commercial 3-D CFD software FLUENT v6.2 to the prediction of the flow resistance and associated backwater effect due to a single submerged spur dike in an open channel flow. It is also intended to show the utility of FLUENT in quantifying the velocity and shear stress distribution within the vicinity of the spur dike. FLUENT is widely used for solving 3-D turbulent flows for complex flow fields, including some recently successful use in the analysis of open channel flows (Salaheldin et al., 2004; Dargahi, 2004; Marson et al., 2003;

Ma et al., 2002). In the work described herein, FLUENT has been applied to a uniform flow field with no spur dike in place and to a flow field containing a single spur dike. The CFD model results are compared with those from an experimental study carried out using a physical model set up in the Hydrotechnical Laboratory at the University of Saskatchewan.

5.3. Description of the physical model and associated measurements

A physical model study was undertaken to establish quantitatively the flow field characteristics and flow resistance of a single spur dike in an open channel. The fixed-bed flume used in the study had a width of 800 mm, a height of 600 mm and a length of 10 m. The flume slope was set to 0.000975 m/m, which allowed for the establishment of the uniform flow depth of 84 mm for the corresponding test discharge of 33.1 L/s by adjustment of the tailgate located at the downstream end of the flume. The discharge and flow depth were measured using an electromagnetic flow meter and a point gauge, respectively. As part of the model study, a two-dimensional spur dike made of PVC material was attached to the flume bed and right sidewall midway along the length of the flume. The spur dike had a height and length of 50 mm and 400 mm, respectively. The same discharge and tailgate setting, used for the case of uniform flow conditions, were also used for the tests in which a single spur dike was installed in the flume. The longitudinal water surface profile was measured at three transverse locations, namely at 50 mm, 400 mm and 750 mm from the flume right sidewall (as viewed from upstream). The drag force associated with the spur dike was also measured using a specially-designed cantilever beam apparatus as reported in Azinfar and Kells (2006). The streamwise and transverse vertical velocity profiles at several cross sections along the length of the flume were measured for both uniform flow conditions with no spur dike and non-uniform flow conditions with the spur dike installed in the flume. The cross sections indicated in Figure 5.1 show the locations where the velocity profiles were measured. The distance between the dashed lines is shown in meters from the upstream end of the flume. The number of measurement points for each vertical velocity profile varied from three to six with the spur dike in place. For uniform flow conditions, the number of measurements was seven for each vertical velocity profile.

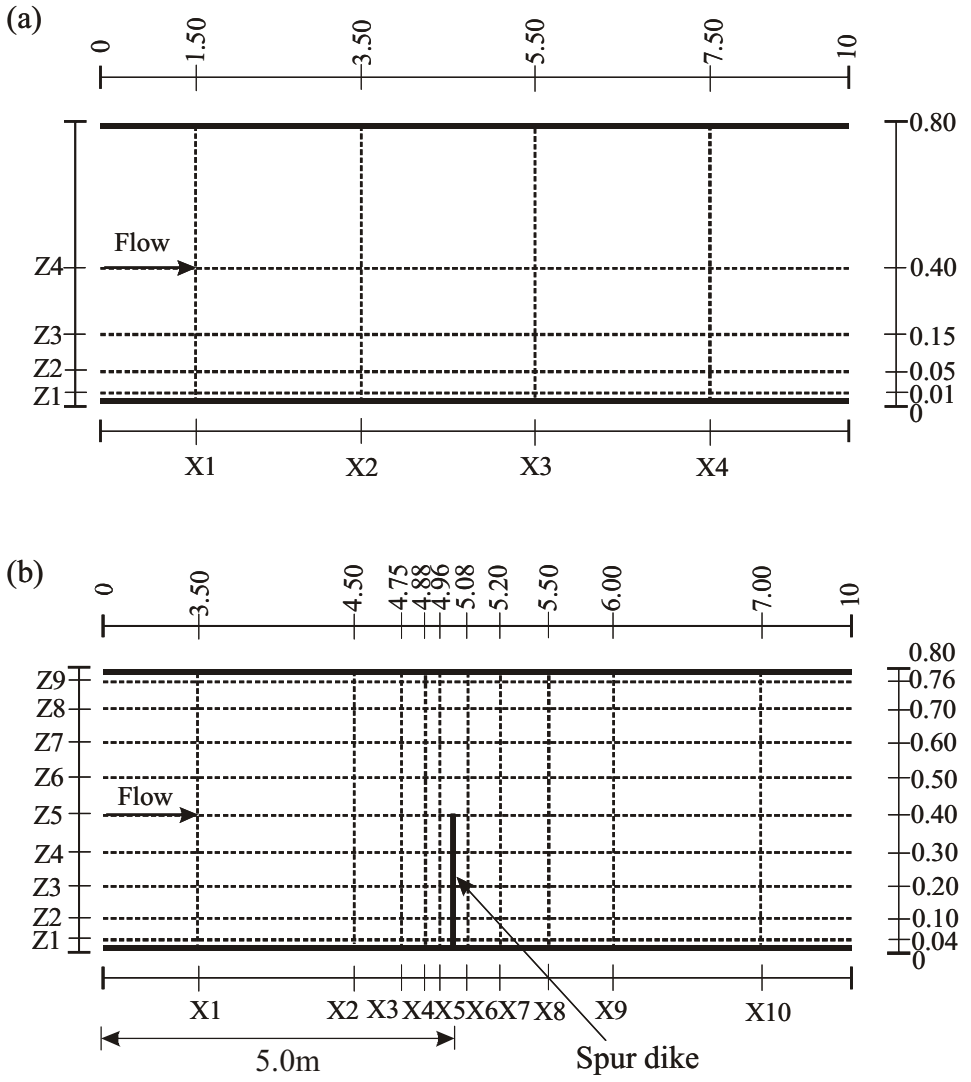

Figure 5.1. Velocity profile measurement locations for (a) uniform flow conditions, and (b) flow conditions with the spur dike installed. All dimensions shown are in meters.

A 2-D side-looking 16 MHz micro-ADV developed by SonTek was used for the velocity measurements. The micro-ADV measures the velocity components within a very small volume of water (0.09 cc), so it is considered as a single-point measurement apparatus. The ADV operates on the basis of a pulse-to-pulse coherent Doppler shift. The ADV probe has a single transmitter located at the centre of the probe head and either two (2-D probe) or three (3-D probe) receivers, one for each velocity component. The transmitter sends a sound beam through the body of water which is reflected back by the moving particles in the flow. In turn, the reflections due to the moving particles, 50 mm from the transmitter, are taken by

the receivers with a high sampling frequency. For the present study, the 2-D micro-ADV with a 50 Hz sampling rate was used to measure the velocity components in the streamwise and transverse directions (ADV operations manual, 2001). The ADV was positioned for five minutes at each specific data collection point. Post-processing software (WinADV v32), developed by The U.S. Department of Interior, was used to filter the data and to obtain the timed-averaged velocities. Two quality control parameters were applied to the ADV data, including the signal to noise ratio (SNR) and correlation coefficient (COR). The filtering criteria were based on SNR and COR values greater than 15 and 70, respectively, as suggested in the ADV operation's manual (ADV operations manual, 2001).

5.4. General description of the CFD model

The 3-D CFD model, FLUENT v6.2 was used in the present study to solve the Reynolds-averaged Navier-Stokes equations for incompressible flow. FLUENT uses the finite-volume method in which the governing equations are integrated and discretized over individual control volumes to derive algebraic equations. In turn, the algebraic equations are linearized and solved sequentially to obtain the updated solution (FLUENT User's Guide, 2005). The Navier-Stokes equations for incompressible turbulent flow in a Cartesian coordinate system may be written as

$$[5.1] \quad \rho\frac{\partial u^i}{\partial t} + \rho u^j \frac{\partial u^i}{\partial x^j} = -\frac{\partial P_t}{\partial x^i} + \frac{\partial \tau^{ij}}{\partial x^j} + \rho g^i$$

$$[5.2] \quad \tau^{ij} = \left[\rho(\nu + \nu_t)\left(\frac{\partial u^i}{\partial x^j} + \frac{\partial u^j}{\partial x^i}\right)\right] - \left[\frac{2}{3}\rho(\nu_t + k)\frac{\partial u^i}{\partial x^i}\delta^{ij}\right]$$

$$[5.3] \quad \frac{\partial u^i}{\partial x^i} = 0$$

where ρ is fluid density, u^i is the velocity component in the x^i direction, t is time, P_t is total pressure, τ^{ij} is the stress tensor, g^i is gravitational acceleration in the i-direction, ν and ν_t are the kinematic molecular and turbulent viscosities, respectively, k is the turbulent kinetic

energy and δ^{ij} is the Kronecker delta. Equations [5.1] and [5.3] show the momentum and continuity equations, respectively, and Eq. [5.2] represents the shear stress tensor in the momentum equation.

In order to track the position of the free surface, FLUENT uses a multiphase technique called the volume of fluid (VOF). For two-phase flow (i.e., air and water), the volume fraction of water in a computational cell, F_{vof}, is defined as

$$[5.4] \quad F_{vof} = \frac{\Omega_{water}}{\Omega_{cell}}$$

where Ω_{cell} is the computational cell volume and Ω_{water} is the volume of the computational cell filled with water. The value of F_{vof} varies from zero (computational cell is full of air) to unity (computational cell is full of water). For the cases where the value of F_{vof} is between zero and unity, the computational cell has a free surface. For the present study, however, as is usual in practice, the volume fraction of 0.5 was considered as the average free surface of the flow. The continuity equation (i.e., Eq. [5.3]) is modified to account for the volume fraction of water, viz.

$$[5.5] \quad \frac{\partial F_{vof}}{\partial t} + u^i \frac{\partial F_{vof}}{\partial x^i} = 0$$

There is no continuity equation for the air flow as the volume fraction of air is calculated from the volume fraction of water. The momentum equation does not change in the VOF model, although fluid properties such as density are inherently shared between the two phases. For example, the density in a cell filled with both air and water is calculated from

$$[5.6] \quad \rho = F_{vof}\rho_{water} + (1 - F_{vof})\rho_{air}$$

where ρ_{water} is the density of water and ρ_{air} is the density of air. More information about the governing equations and the VOF model is provided in the FLUENT v6.2 User's Guide (2005).

There are several turbulence models available in FLUENT for computing the turbulence stresses. One of the most widely used two-equation turbulence models is the standard k-ε model. This semi-empirical model solves two transport equations, including one for turbulent kinetic energy, k and one for its dissipation rate, ε. The model is recommended for recirculating flows (Rodi, 1984). A relatively newer version of the k-ε model, the RNG k-ε model, has been developed from theoretical principles in contrast to the semi-empirical approach used in the case of the standard k-ε model. The model is believed to give improved performance for separated and curvilinear flows as well as flows with moderate swirls (Dargahi, 2004). For the present study, the RNG k-ε model was used.

5.5. Application of the CFD model

In order to apply the VOF model for flow in an open channel, it is necessary to introduce two separate immiscible flows (two-phase flow), namely water and air in which the air flows on top of the water. One inlet and one outlet were considered for the model to be shared by both the flow of water and air. Although the flow characteristics of the air flow are not of interest, the passage area of the air flow should be large enough so that it does not have any effect on the flow of the water. Nonetheless, it is an advantage to minimize the air flow area in order to minimize the size of the model and hence the time required to complete the numerical calculations. By using several trials and the guidance provided by Salaheldin et al. (2004), the air flow area was taken to be one-third of that for the water flow. The solid boundaries of the model including the spur dike were considered as walls. At the top surface of the air flow, a symmetry boundary condition was specified in order to produce zero normal gradients for all variables. GAMBIT v.2 was used to produce the geometry of the model and to generate the required hexahedral mesh elements. Two model geometries were assembled using GAMBIT, including a plain channel for modeling the uniform flow conditions and a plain channel including a spur dike. After several trials, the mesh size was revamped to have dimensions of 5 mm and 10 mm in the vertical and transverse directions, respectively. Similarly, the average mesh size in the streamwise direction was selected to be 100 mm with a smaller mesh size near to the boundary of the spur dike in order to capture the high gradients of the flow parameters in this region. Although a formal mesh-convergence

study was not performed as a part of this work, use of a smaller mesh size was assessed for comparison purposes both with and without the spur dike in place. It was found that the velocity profiles did not change significantly despite a considerable increase in the required computation time. As such, the original mesh size was assumed to be adequate for the modeling process. The Cartesian coordinate system was defined as x, y and z for the streamwise, vertical and transverse directions of the flow, respectively, which originated at the inlet (x = 0 m), bed (y = 0 m) and right sidewall (z = 0 m) of the flume. Figure 5.2 shows the mesh geometry produced by GAMBIT for the case of the plain channel with the spur dike in place.

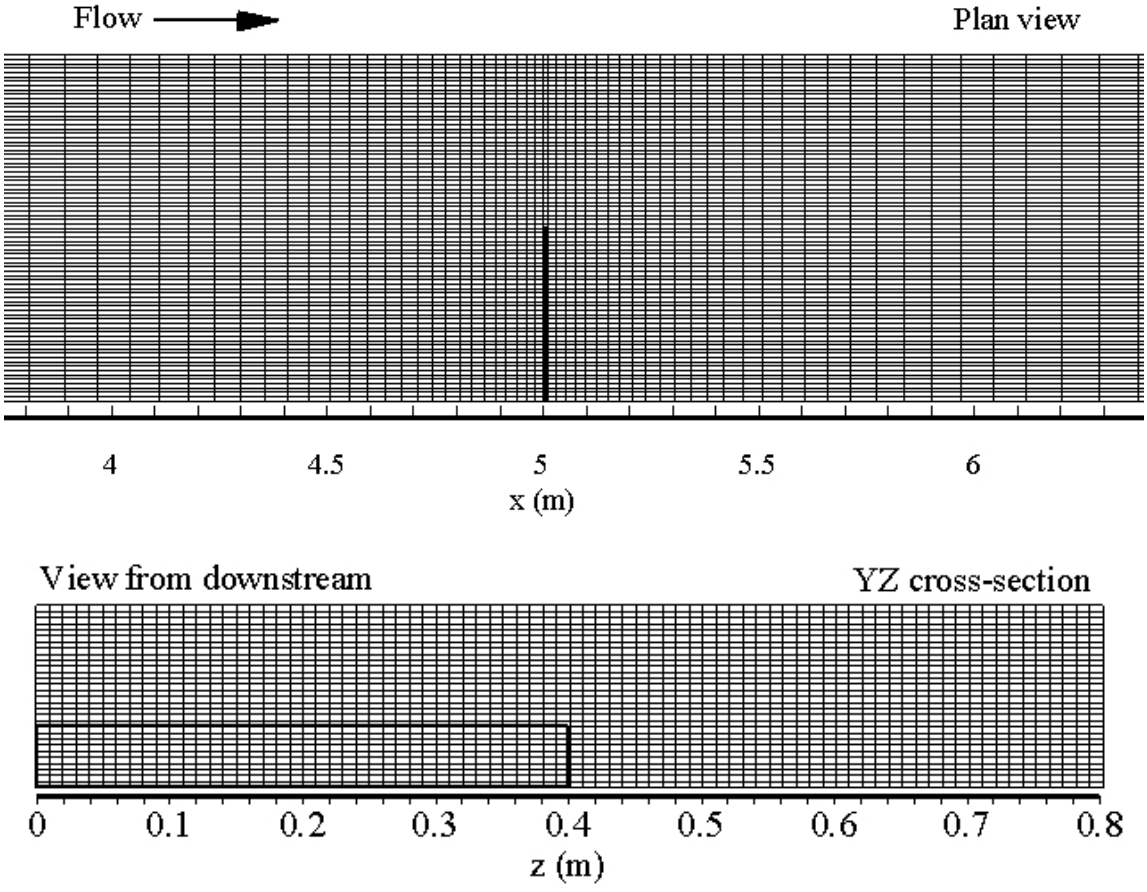

Figure 5.2. Geometry of the mesh produced by GAMBIT for the case of the plain channel with a single spur dike in place

The mass-flow-inlet option of FLUENT was selected for the inlet boundary condition. The open channel option of the inlet boundary condition was selected so that a hydrostatic pressure distribution could be adopted for the water flow. For this type of inlet boundary condition, it is necessary to provide the mass flow rate, flow depth and turbulence properties. Two mass flow rates, one for the water flow and one for the air flow, were specified in the model. It was assumed that the discharge of the air flow was one-third of that for the water flow so the mass flow rate of the air flow was calculated accordingly. For the uniform flow conditions without the spur dike in place, an arbitrary flow depth (i.e., 100 mm), which was near to that measured in the physical model, was used as part of the inlet boundary conditions. This depth is adjusted in the process of numerical simulation which it would be equal to the normal flow depth upon the calibration of the model. In the case of the non-uniform flow conditions with the spur dike in place, the flow depth upstream of the structure was not known *a priori*. In fact, a primary purpose of the model was to allow prediction of the flow depth upstream of the spur dike given a particular downstream condition involving subcritical flow. On this basis, for the applied discharge, the downstream uniform flow depth (i.e., normal flow depth) was specified at the inlet as a starting point for the numerical simulation. During the subsequent model iterations, the CFD model updated and adjusted the flow depth upstream of the spur dike.

Turbulence properties were input to the model by specifying the turbulence intensity and hydraulic diameter. The hydraulic diameter was used by FLUENT to internally calculate the flow length scale. In turn, the flow length scale and the turbulence intensity were utilized by FLUENT to determine k and ε at the inlet. The incoming flow turbulence intensity was estimated to about 5%, which was confirmed from the experimental results, and this was specified for the inlet conditions. The inflow depth was used to represent the hydraulic diameter in FLUENT. For the outlet boundary condition, the outlet option of FLUENT was selected to let the model calculate the flow parameters (e.g., flow depth) at the downstream end of the model. The no-slip boundary condition was specified for the walls so that the velocity was set to zero at the solid boundaries. The law-of-the-wall modified for roughness was adopted for the solid boundaries of the model using the standard wall function option of

FLUENT. The law-of-the-wall modified for roughness is given as (FLUENT User's Guide, 2005)

$$[5.7] \quad \frac{u_p u^*}{\tau_w / \rho} = \frac{1}{\kappa} \ln\left(E \frac{\rho u^* y_p}{\mu} \right) - \Delta B$$

$$[5.8] \quad u^* = C_\mu^{1/4} k^{1/2}$$

where u_p is the mean flow velocity at point p, u^* is the shear velocity, τ_w is shear stress due to the solid wall, κ is von-Karman's constant (= 0.418), E has a constant value of 9.79, C_μ is equal to 0.09, y_p is the normal distance from the wall, μ is the dynamic viscosity and ΔB is a roughness function. The roughness function, ΔB, depends on the non-dimensional roughness height, K_s^+, which is defined as

$$[5.9] \quad K_s^+ = \frac{\rho K_s u^*}{\mu}$$

where K_s is the physical roughness height. For hydrodynamically smooth regimes, where $K_s^+ \le 2.25$, ΔB is equal to zero. For fully rough regimes, where $K_s^+ \ge 90$, the roughness function is given as

$$[5.10] \quad \Delta B = \frac{1}{\kappa} \ln\left(1 + C_s K_s^+\right)$$

where C_s is the roughness constant with a default value of 0.5.

Gravitational acceleration components in both the streamwise and vertical directions were adopted in the CFD model to account for the slope of the flume. The model uses the SIMPLE algorithm to couple the velocity and pressure fields. The upwind first order discretization scheme was used for the convective terms in the momentum equations, turbulence parameters and continuity, while the upwind QUICK scheme was used for the VOF model. More information about the discretization schemes is provided in Versteeg and

Malasekera (1995). The body weighted force scheme was used for the pressure discretization as is suggested for gravity dominated flows such as open channel flows. In this discretization scheme, the pressure is considered to be balanced locally by the gravity forces and the effects of other parameters (i.e., convective and shear stress terms) are neglected from the momentum equation. This treatment of the pressure term is useful for achieving quick convergence of the solution (FLUENT User's Guide, 2005). Under-relaxation factors for the various parameters of the CFD model were selected to be between 0.2 and 0.5. The convergence criteria were based on the normalized residual wherein the normalized changes between successive iterations were equal to or smaller than 10^{-3}.

5.6. Results and discussion

The CFD model was initially applied to the case of uniform flow conditions in the flume with no spur dike in place. The primary calibration parameter for the CFD model was the roughness height. It was found that, by assigning of a zero roughness height to the solid boundaries, the CFD model was able to predict correctly the measured uniform flow depth profile in the flume. This finding confirmed that the solid boundaries of the flume were smooth as expected. Figure. 5.3 shows a comparison of the flow depth profile predicted by the CFD model and that measured in the experiment. The average difference between the predicted and the measured flow depths is less than 1%. As a simple case in open channel flow, the condition of uniform flow in the flume was also used to facilitate adjustments to some of the model parameters, including the mesh size, under-relaxation factor and convergence time.

Figure 5.4 shows the vertical profiles of streamwise velocity predicted by the CFD model and the experimental data for various locations within the flow. The symbols "Xi" and "Zi" represent cross-sections perpendicular to the x and z coordinates, respectively, as shown in Figure 5.1a.

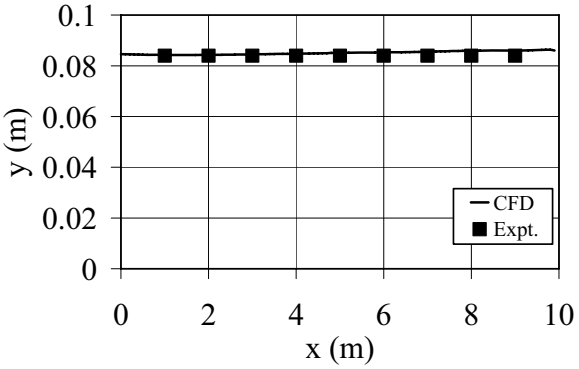

Figure 5.3. Predicted and measured flow depth profiles for uniform flow condition (Q = 33.1 L/s)

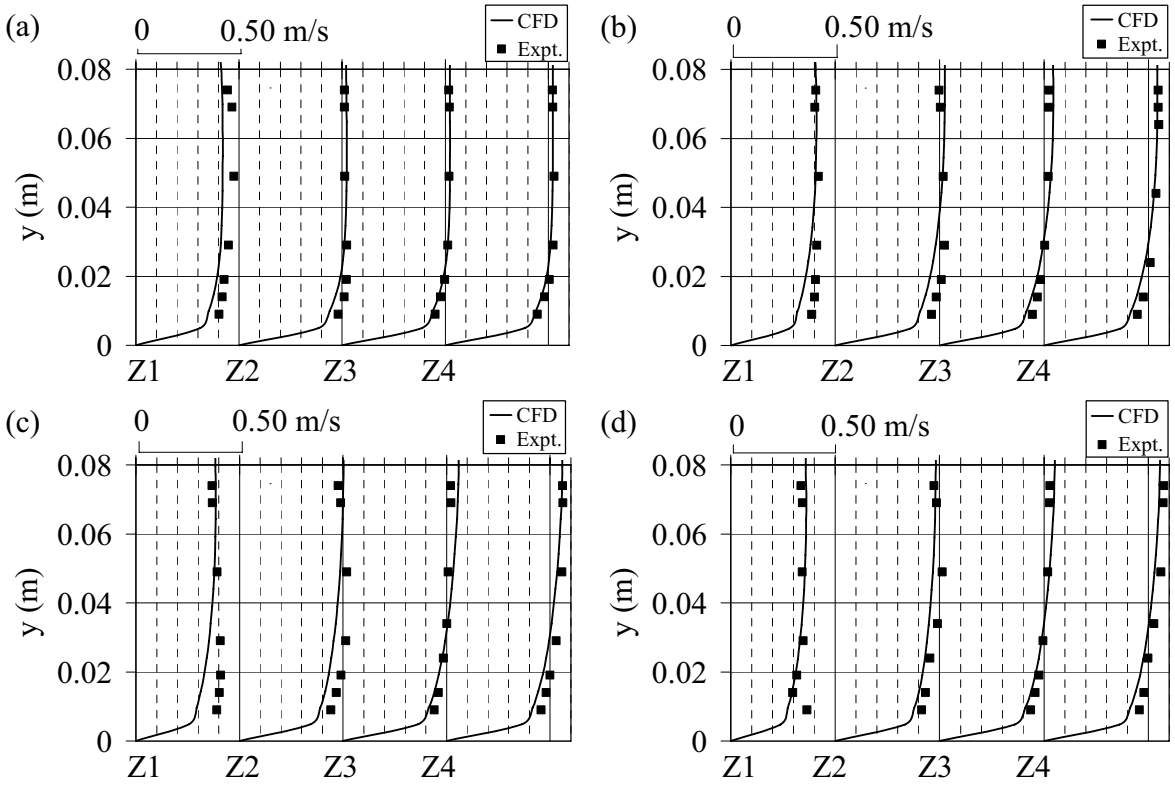

Figure 5.4. Predicted and measured streamwise vertical velocity profiles under uniform flow condition for various locations within the flow field (a) X1, (b) X2, (c) X3, and (d) X4

Similarity of the velocity profiles shown in Figure 5.4 indicates that the flow became established at X2 (i.e., x=3.50 m), which is upstream of the mid-point length of the flume where the spur dike was subsequently positioned. In general, there is good agreement

between the CFD results and those obtained experimentally. However, there is a small difference between the predicted and measured velocities in the lower portion of each profile in the near-wall region, which could partly be related to the uncertainty of the model results due to model approximations such as mesh configuration, truncation error, convergence criteria, etc. The uncertainty of the results due to model approximations was not estimated in the present study. The experimental results also show that the maximum velocity within the profile adjacent to the wall occurs somewhat below the water surface. This phenomenon is known as the dip phenomenon, which is related to the effects of secondary currents in open channel flow due to the existence of sidewalls (Yang et al., 2004). The CFD model has predicted the dip at greater distance above the channel bed compared to that measured experimentally. The reason for the above differences is speculated to be attributable to the applied wall function (i.e., law of the wall), which does not sufficiently convey the wall turbulence effects into the flow. Thus, the CFD model results might be improved through the use of more advanced wall functions (i.e., non-equilibrium wall functions) as described in the FLUENT User's Guide (2005), although this treatment has not been evaluated in the current study.

Given the relatively good results obtained for uniform flow conditions, the CFD model was applied to the case of a single spur dike being placed in the channel. Figure 5.5 shows the predicted water surface profiles (depth) from both the CFD model and those measured experimentally for three transverse locations, namely z = 0.05 m, 0.40 m and 0.75 m. The flow depth measurement locations adjacent to the flume walls (i.e., z = 0.05 m and 0.75 m) are slightly different from those where the velocity was measured (i.e., z = 0.04 m and 0.76 m). This is due to fact that the point gauge could not be moved closer than 50 mm to the flume walls. It can be observed that the CFD model has, in general, successfully predicted the water surface profile in the vicinity of the spur dike. However, the flow depth upstream of the spur dike, and hence the backwater effect, has been slightly under-estimated.

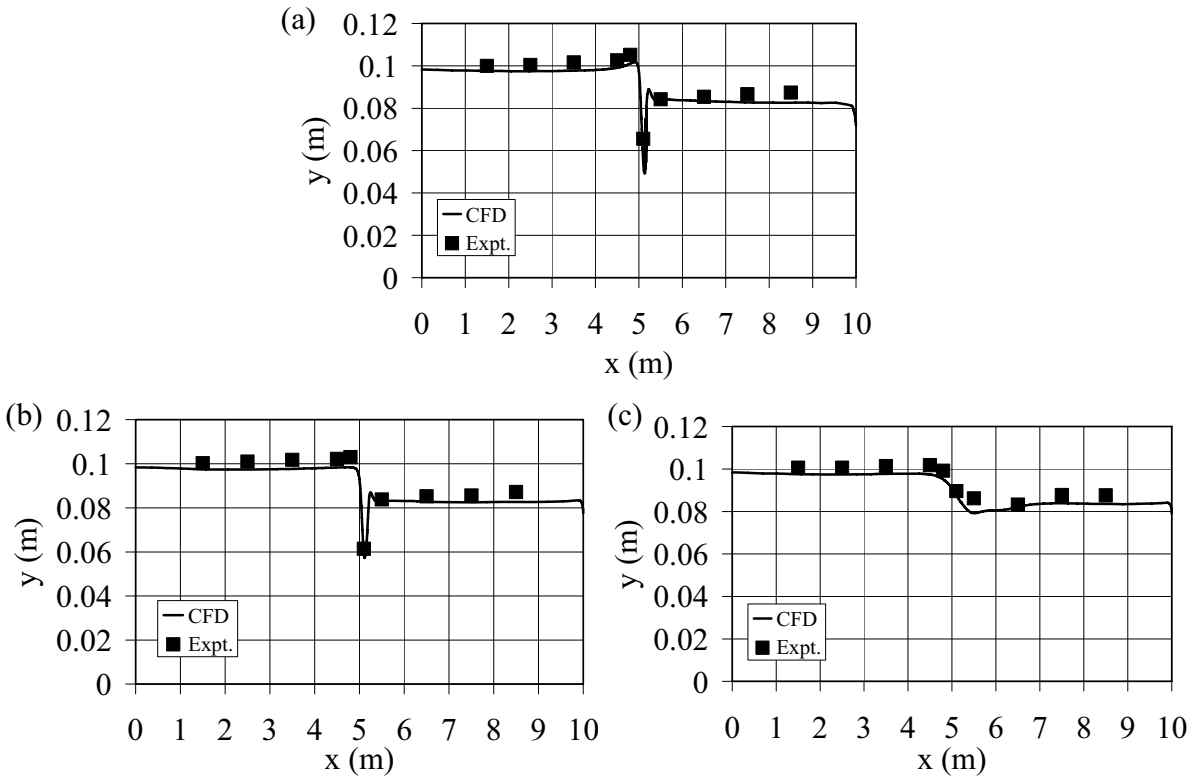

Figure 5.5. Predicted and measured water surface profiles with the spur dike in place (x = 5.0 m): (a) z = 0.05 m, (b) z = 0.40 m, and (c) z = 0.75 m (Q = 33.1 L/s)

Table 5.1 shows the spur dike backwater effect determined from the CFD model results and from the experimental data. Here, it may be noted that the mean difference in the predicted and measured backwater effects is approximately 21%. The drag force exerted by the spur dike on the flow was also obtained from the CFD model and compared with that directly measured from the physical model. For Q = 33.1 L/s, the measured drag force due to the spur dike was 8.0 N, while the CFD model predicted a value of 7.1 N, which yields an underestimation of about 11%. The underestimation of the predicted drag force is in agreement with the underestimation of the backwater effect by the CFD model. It is evident from Table 5.1 that the CFD model better predicts the backwater effect along the right sidewall. From both the experimental data and the CFD model results, it can be observed that the flow depth upstream of the spur dike is greater along the right sidewall where the spur dike is located than it is along the left sidewall, while downstream from the spur dike the flow depth is greater along the left sidewall.

Table 5.1. Predicted backwater effect from the CFD model results and from the experimental data.

Transverse location, z (m)	Backwater effect (mm), Q = 33.1 L/s		Difference (%)
	CFD model	Experiment	
0.05	17.8	21.2	16.0
0.40	14.4	19.0	24.2
0.75	13.8	17.8	22.4

The predicted and measured streamwise vertical velocity profiles at various locations upstream of the spur dike are shown in Figure 5.6. Similar to the symbols used for uniform flow conditions, the symbols "Xi" and "Zi" represent cross-sections perpendicular to the x and z directions, respectively, as shown in Figure 5.1b. It may be observed that the velocity profiles have been predicted reasonably well for all locations upstream of the spur dike.

Both the CFD model results and the experimental data show that, at cross-section X1 located 1.50 m upstream of the spur dike, the flow structure has not been affected by the spur dike (despite the fact that cross section X1 is located in the backwater zone upstream from the spur dike). At this cross-section, the velocity profiles are almost symmetrical about the centerline (i.e., z = 0.40 m). The local effects due to the spur dike start to appear at cross-section X2, located 0.50 m upstream of the spur dike (which is of the same order as the spur dike length), where the velocity increases adjacent to the left sidewall and decreases adjacent to the right sidewall due to the blocking effect of the spur dike. As the results indicate, the velocity profiles become more skewed from their uniform distribution around the centerline of the cross-section as one moves nearer to the spur dike (i.e., as indicated by the results for cross-sections X3, X4 and X5).

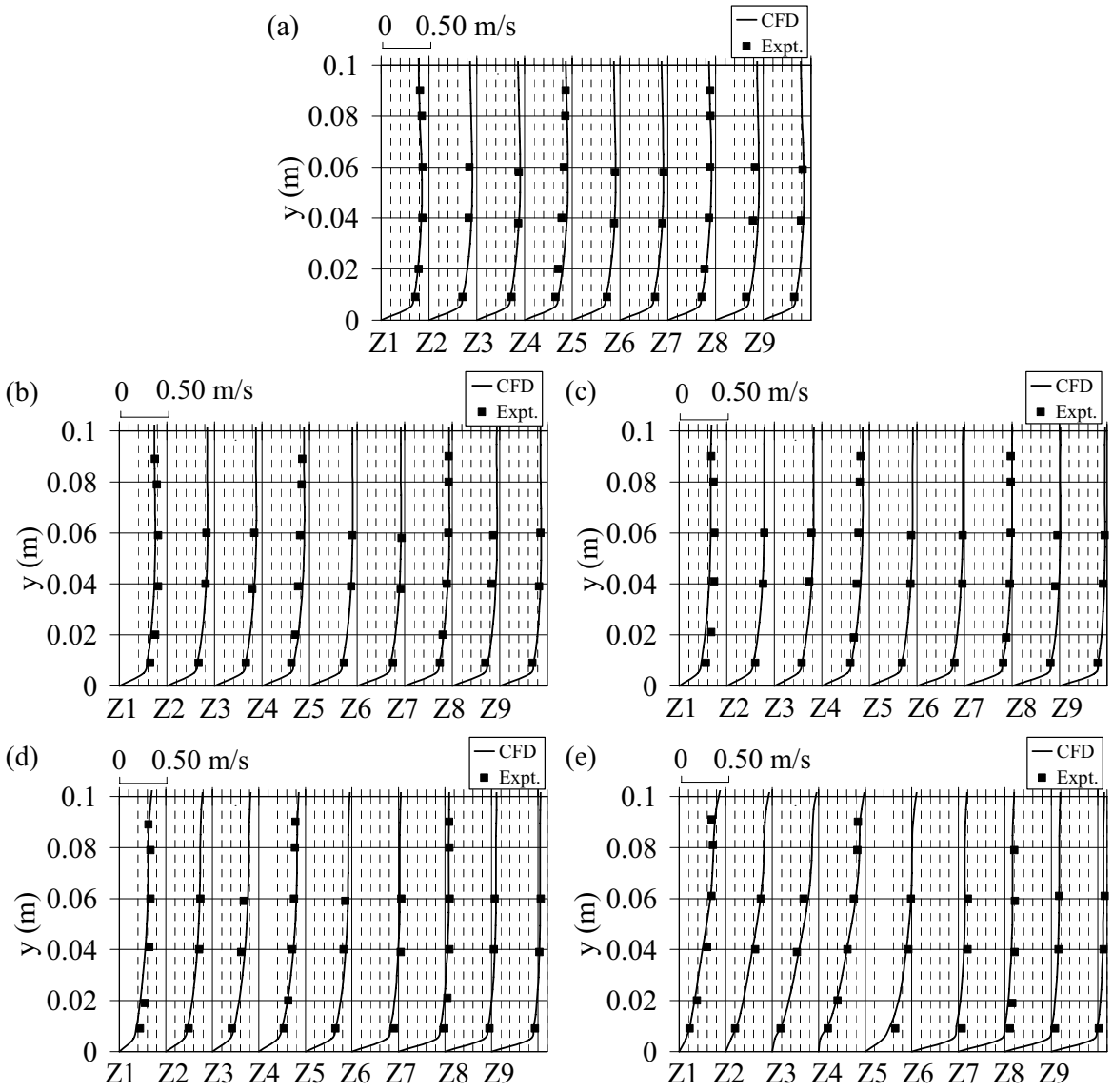

Figure 5.6. Predicted and measured streamwise vertical velocity profiles for various locations upstream of the spur dike (a) X1, (b) X2, (c) X3, (d) X4, and (e) X5

The predicted and measured streamwise vertical velocity profiles at various locations downstream from the spur dike are shown in Figure 5.7. As the results indicate, the flow passing over the crest of the spur dike behaves similar to that of a diving jet flow spreading out into the flow core downstream from the spur dike. The existence of two transverse vortices is evident on the basis of the negative streamwise velocities shown in some of the profiles downstream from the spur dike. One of the two vortices is located near to the channel bed and below the jet flow off the crest, immediately downstream from the spur dike

(adjacent to cross-section X6), while the other vortex is located above the jet flow at the free surface (adjacent to cross-section X7). Both the CFD model results and the measurements show that there is a high velocity zone in the open region between the tip and left wall (constricted zone of the channel), while a low velocity zone is evident starting at a distance of about 1.0 m downstream from the spur dike (i.e., cross-section X9) where the jet flow effect is diminished.

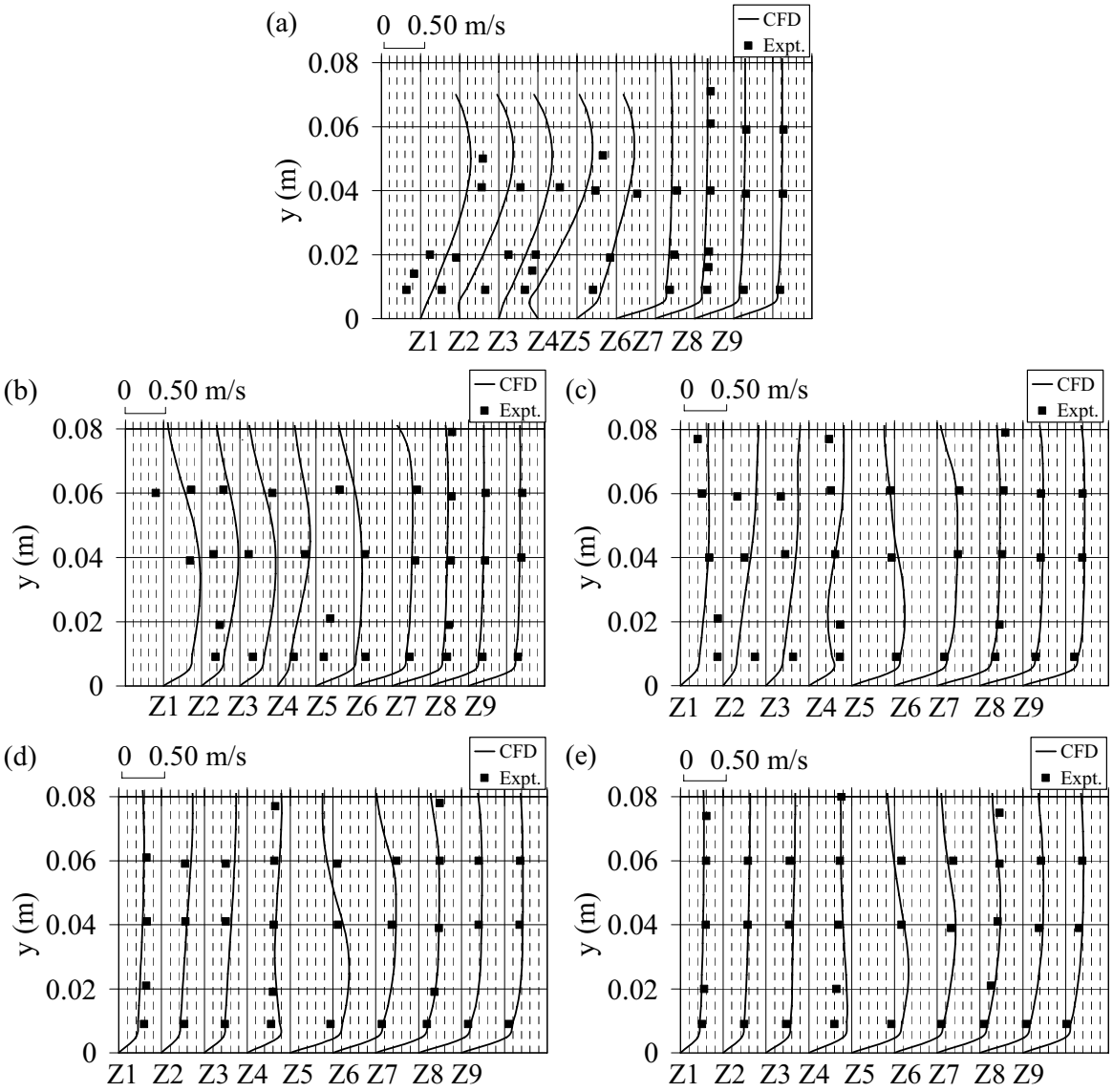

Figure 5.7. Predicted and measured streamwise vertical velocity profiles for various locations downstream from the spur dike (a) X6, (b) X7, (c) X8, (d) X9, and (e) X10

It can be observed that the largest discrepancy between the results of the CFD model and those determined experimentally occurs at cross-sections X6, X7 and X8 immediately downstream from the spur dike. While the general structure and shape of the jet flow has been predicted reasonably well by the CFD model, the interaction of the jet flow with the downstream flow core has not been modeled very well. Indeed, it appears that the CFD model over-dissipated the jet flow into the flow core immediately downstream from the spur dike. Aside from the numerical uncertainties, the error could also be related to the over-dissipation of turbulence by the turbulence model, especially at the beginning of the jet flow. The turbulence model uses an isotropic turbulence mixing rate, while for the highly asymmetric flow downstream from the spur dike the turbulence mixing rate is likely quite different in each direction. The difficulty associated with turbulence models capturing the initial stages of jet flow growth is reported in the literature (Georgiadis et al., 2006; Khosronejad et al., 2007; Abad et al., 2008). The performance of the CFD model might be improved by adjusting the coefficients of the diffusion terms or by introducing anisotropic diffusion terms into the turbulence model. Aside from the CFD model deficiencies, the difficulties associated with acquiring ADV velocity measurements in a highly-skewed and turbulent flow can also be a factor in difference between the measured and simulated velocity pattern immediately downstream from the spur dike.

Both the CFD model results and the velocity measurements made using the ADV showed that the transverse velocities (secondary currents) increase in magnitude adjacent to the spur dike and also near to the flume bed. Figure 5.8 represents the transverse velocity profiles, w, about 10 mm above the flume bed for the two cross-sections located immediately upstream of and downstream from the spur dike. It may be observed that the transverse velocities have been predicted reasonably well by the CFD model. However, the maximum transverse velocity, which occurs near the tip of the spur dike ($z = 0.40$ m), has been over-estimated upstream of the spur dike and under-estimated downstream from the spur dike.

The velocity vectors obtained from the experiments in three various horizontal planes, including $y = 9$ mm, $y = 40$ mm, and $y = 60$ mm, are shown in Figure 5.9. A high velocity zone is shown immediately downstream from the spur dike in Figures 5.9a and 5.9b. This

high velocity zone represents the position of the jet flow behind the spur dike in each specific plane. However, this high velocity zone is not shown in the most upper plane (y = 60 mm). The reason is that the velocity was not measured in this plane just downstream from the spur dike due to the fact that the flow depth was not high enough (nappe of the jet flow downstream from the spur dike) to be measured by the ADV apparatus. As expected, the location of the jet flow is closer to the spur dike at higher positions of the flow depth. Figure 5.9 shows that there is a vertical-axis recirculation zone downstream from the spur dike near to the bed of the channel. Moreover, in the upper-most plane (i.e., y = 60 mm) there is another vertical axis vortex above the jet flow at a short distance downstream from the spur dike. The results also show that there is a high velocity zone adjacent to the tip of the spur dike close to the left wall. This high velocity is due to the constriction effects of the spur dike on the channel as explained before. This finding has also been observed by Peng et al. (1997).

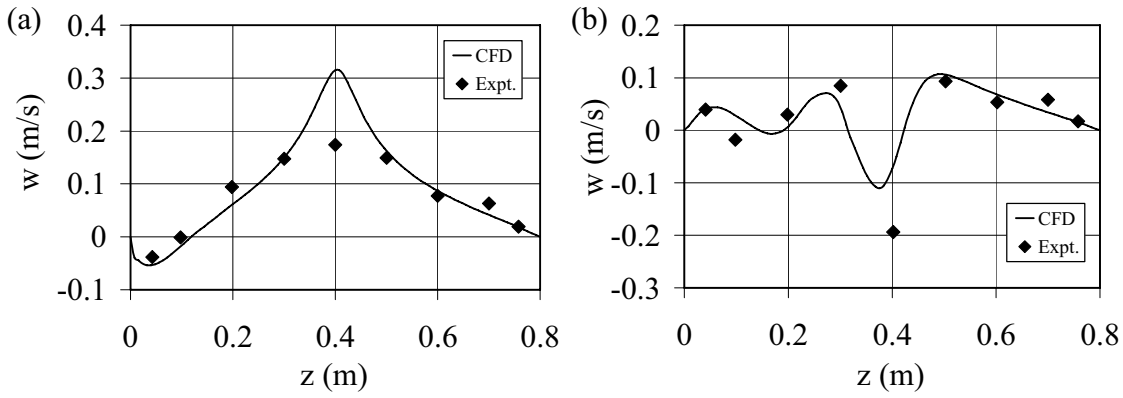

Figure 5.8. Predicted and measured transverse velocity profiles for two locations 10 mm above the flume bed adjacent to the spur dike (a) X5, and (b) X6

Similar results shown in Figure 5.9 are obtained from the CFD model and plotted in Figure 5.10. There is a relatively good agreement between the measurements and the CFD model results. The high velocity of the jet flow immediately downstream from the spur dike at all planes is captured by the CFD model. The results from the CFD model also show the vertical-axis recirculation zone immediately downstream from the spur dike near to the bed as well as the high velocity in the constricted zone of the channel similar to the experiments.

However, the vertical axis vortex in the upper-most plane (i.e., y = 60 mm) and above the jet flow is not shown by the CFD model.

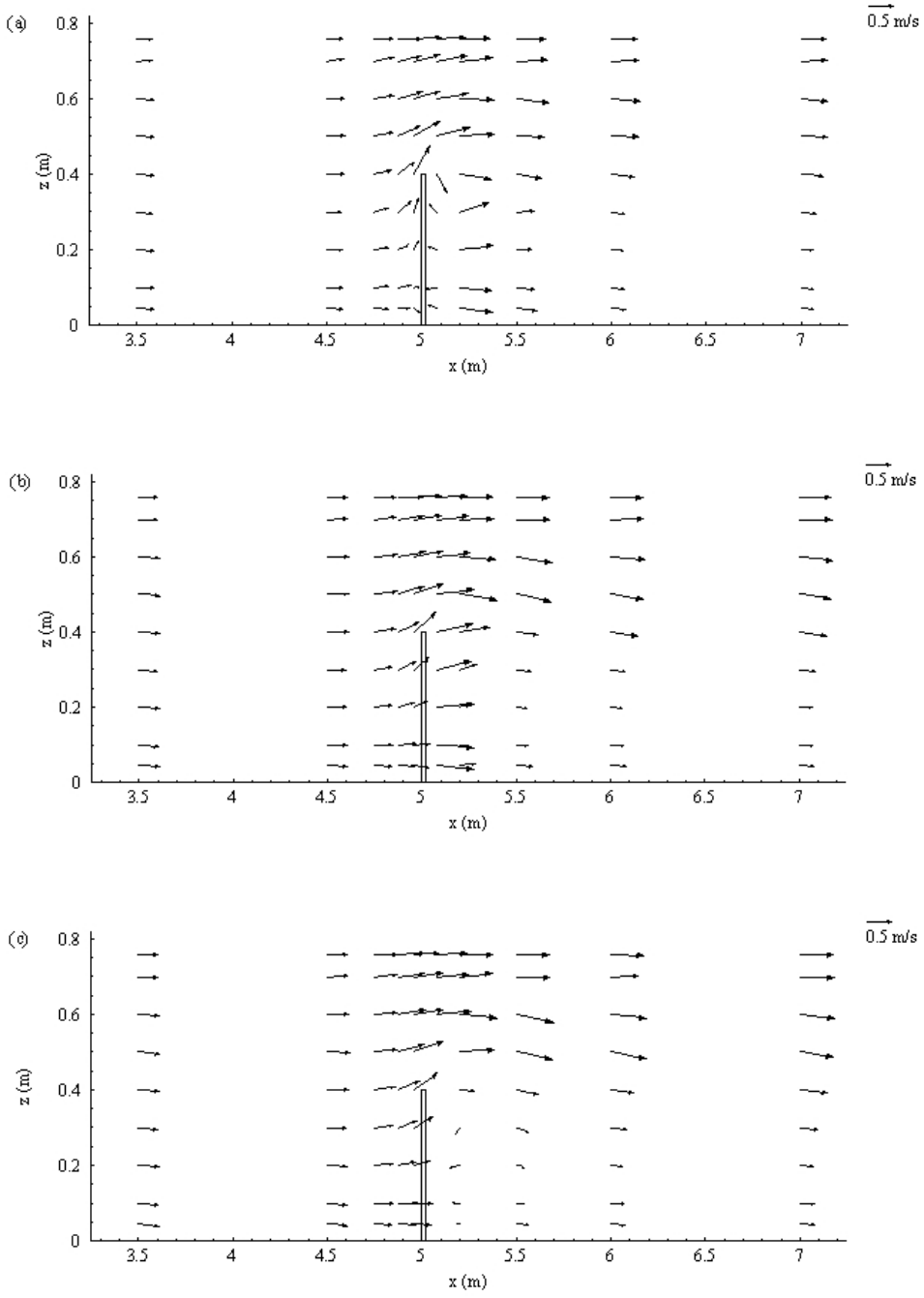

Figure 5.9. Velocity vectors in the vicinity of the spur dike as obtained from the experiments for (a) 9 mm from the flume bed, (b) 40 mm from the flume bed, and (c) 60 mm from the flume bed

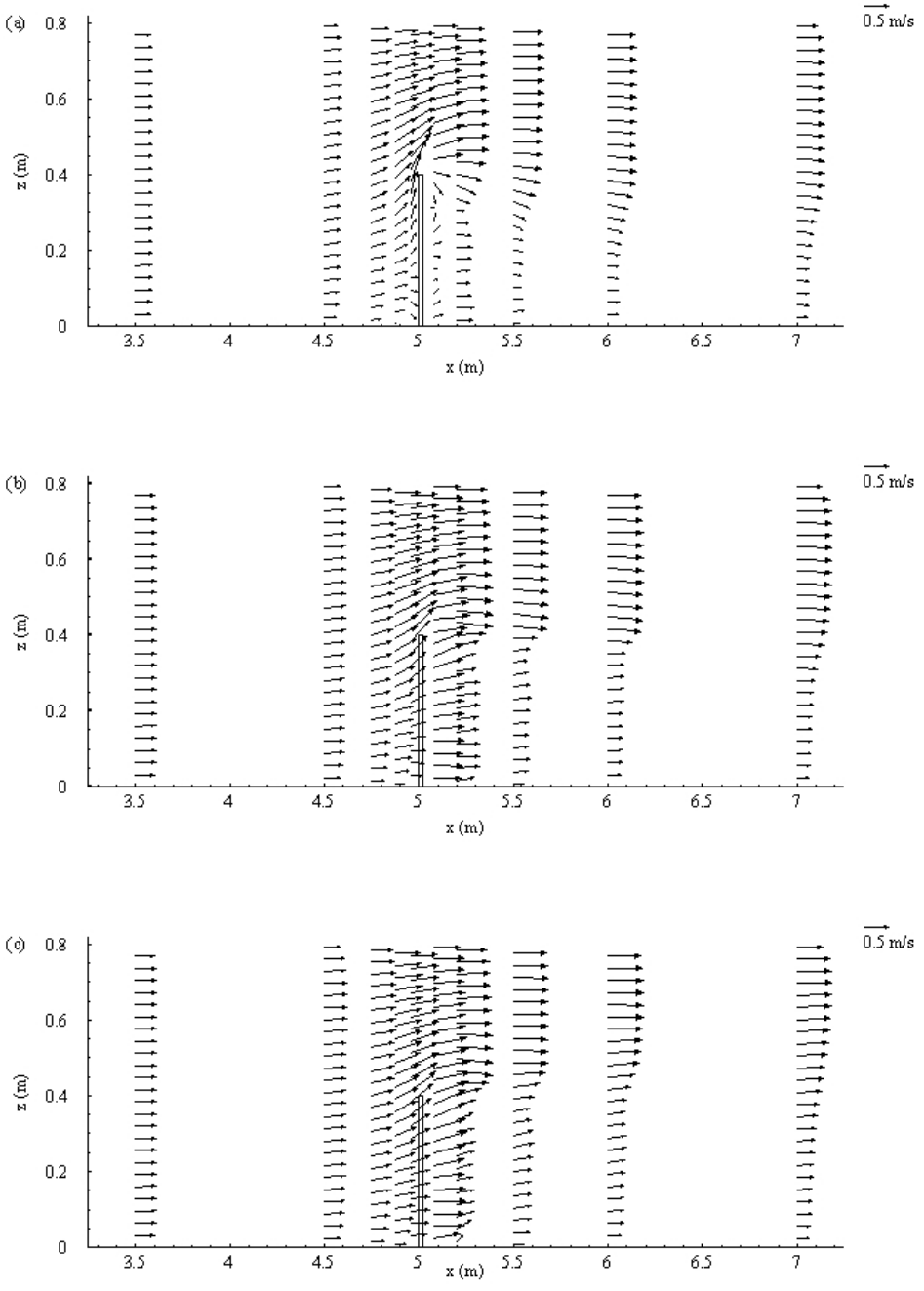

Figure 5.10. Velocity vectors in the vicinity of the spur dike as obtained from the CFD model for (a) 9 mm from the flume bed, (b) 40 mm from the flume bed, and (c) 60 mm from the flume bed

On the basis of the present study and previous observations of the flow field adjacent to submerged spur dikes given in the literature as outlined in Chapter 2, a schematic

illustration of the flow pattern in the vicinity of a submerged spur dike is shown in Figure 5.11. Three transverse vortices are shown in Figure 5.11a, including a small one in the upstream corner of the spur dike near the flume bed as well as one above and one below the jet flow located downstream from the spur dike. Two vertical vortices are shown in Figure 5.11b, including a small one upstream of the spur dike near to the flume wall and a larger one downstream from the spur dike.

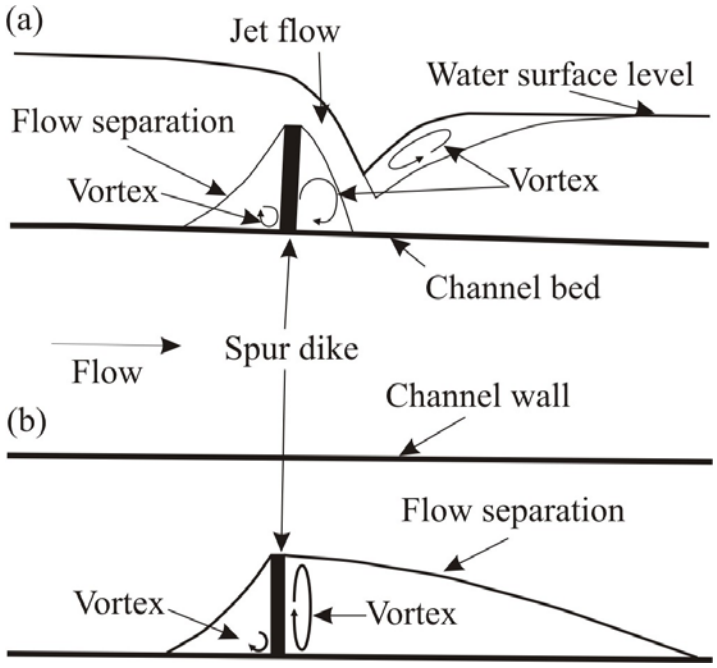

Figure 5.11. Flow pattern adjacent to a submerged spur dike; (a) profile view, and (b) plan view

The bed shear stress distribution from the CFD model is plotted and shown in Figure 5.12. This figure shows a high concentration of the shear stress along the main channel flow zone and adjacent to the tip of the spur dike. A low shear stress zone immediately upstream and also downstream from the spur dike is also predicted by the CFD model. The high shear stress zone near to the tip of the spur dikes has been reported by several researchers (e.g., Peng et al., 1997; Jia and Wang, 2000). The high bed shear stress near to the tip and main channel flow zone represent possible areas of scouring, while the low bed shear stress zones behind the spur dike represents possible areas of sedimentation.

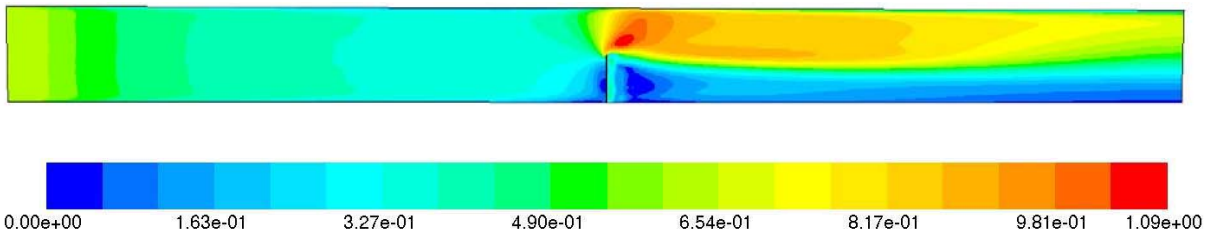

Figure 5.12. Bed shear stress distribution (Pascal) adjacent to the spur dike

In Chapters 3 and 4 of the thesis, it was argued that an increased bed shear stress adjacent to the tip of the spur dike and also in the constricted zone of the channel is the main reason for having a higher calculated drag force using the flow depth measurement compared to that of direct measured drag force using the drag force measurement apparatus. The results of the bed shear stress distribution by the CFD model support this argument.

5.7. Conclusions

The flow field within the vicinity of a submerged spur dike has been studied using both the commercial 3-D CFD software FLUENT v6.2 and a physical hydraulic model. In the work, two flow conditions were studied, one involving uniform flow in a plain channel and the other non-uniform flow in a channel containing a single spur dike. For the flow conditions studied, the spur dike was submerged. The experimental data were primarily intended to provide a basis for evaluating the performance of the CFD model. The CFD model was tested on the basis of uniform flow conditions to check the roughness of the flume walls and bed. The calibrated model, based on the roughness of solid boundaries of the open channel, was then used to predict the flow field characteristics for the non-uniform flow conditions in which the spur dike was present.

Application of the VOF multiphase modeling technique in FLUENT resulted in the successful prediction of the water surface profile and hence backwater effect in the vicinity of the submerged spur dike. Compared with the velocity measurements acquired using an ADV, it was concluded that the CFD model was able to predict the velocity field reasonably well in the vicinity of the spur dike. However, the diving jet flow emerging over the crest of

the spur dike was not modeled very well probably due to the over-dissipation of the turbulence, especially at the beginning of the jet flow. The CFD model results might be improved by adjusting the coefficients of the turbulence model diffusion terms or by introducing anisotropic diffusion terms into the turbulence model.

It was observed that, at a distance of about one length of the spur dike upstream, the flow conditions are locally affected by the presence of the spur dike. The existence of two transverse vortices were observed downstream from the spur dike, one located near to the bed of the channel and immediately adjacent to the spur dike and one located near to the free surface above the diving jet flow. Both the CFD model and experimental results showed that there is a high velocity zone in the open region between the tip of the spur dike and left wall of the channel and a low velocity zone in the region starting at a distance of about 1.0 m downstream from the spur dike where the effect of the jet flow is diminished. The CFD model and experimental results also showed that the transverse velocities (secondary currents) increase near to the channel bed and also in the vicinity of the spur dike, reaching a maximum value around the tip of the spur dike.

5.8. Acknowledgements

Financial support for this research has been provided by the Natural Sciences and Engineering Research Council of Canada through a grant to the second author and the gradate scholarship from the University of Saskatchewan to the first author. This support is gratefully acknowledged.

5.9. References

Abad, J.D., Rhoads, B.L., Guneralp, I. and Garcia, M.H. 2008. Flow structure at different stages in a meander-bend with bendway weirs. Journal of Hydraulic Engineering, ASCE, 134(8): 1052-1063.

Acoustic Doppler Velocimeter (ADV). 2001. Operations manual SonTek/YSI Inc., San Diego, CA, USA, 110 p.

Aya, S., Fujita, I. and Miyawaki, N. 1997. 2-D Models for flows in river with submerged groins. Proceedings of 27th IAHR Congress, San Francisco, CA, USA, pp 829-837.

Azinfar, H. and Kells, J.A. 2006. Resistance of a single spur dike in an open channel. Proceedings of 34th Annual General Conference of the Canadian Society for Civil Engineering, Calgary, AB, Canada, GC-056, CD-ROM, 10 p.

Belz, J.U., Busch, N., Engel, H. and Gasber, G. 2001. Comparison of river training measures in the Rhine catchment and their effects on food behavior. Water and Maritime Engineering, Proceedings of the Institution of Civil Engineers, London, UK, 148(3): 123-132.

Criss, R.E. and Shock, E.L. 2001. Flood enhancement through flood control. Geology, American Geophysical Union, 29(10): 875-878.

Dargahi, B. 2004. Three-dimensional flow modeling and sediment transport in the River Klaraven. Earth Science Process and Landforms, John Wiley & Sons, Ltd., 29(7): 821-852.

FLUENT 6.2. 2005. User's guide. Fluent Inc., Centerra Resource Park, Lebanon, NH, USA, 32 chapters.

Georgiadis, N.J., Yoder, D. A. and Engblom, W.A. 2006. Evaluation of modified two-equation turbulence models for jet flow predictions. The American Institute of Aeronautics and Astronautics Journal, 44(12): 3107-3114.

Hendrickson, J.S. and Schneider, M.J. 1999. Hydraulic evaluation of discharge over submerged rock wing dams on the Upper Mississippi River. Water Quality Technical Notes Collections (WQTN PD-06), U.S. Army Engineer Research and Development Center, Vicksburg, MS, USA, 5 p.

Jia, Y. and Wang, S.S.Y. 2000. Numerical study of turbulent flow around submerged spur dikes 4th International Conference on Hydro-Science and Engineering, Korea Water Resources Association, Seoul, South Korea, CD-ROM, 7 p.

Khosronejad, A., Rennie, C.D., Salehi Neyshabouri, S.A.A. and Townsend, R.D. 2007. 3D numerical modeling of flow and sediment transport in laboratory channel bends. Journal of Hydraulic. Engineering, ASCE, 133(10): 1123-1134.

Kuhnle, R., Jia, Y. and Alonso, C. 2002. 3-dimensional measured and simulated flow for scour near spur dikes. Proceedings of the First International Conference on Scour of Foundations, ICSF-1, Texas A&M University, TX, USA, pp. 349-363.

Ma, L., Ashworth, P.H., Best, J.A., Elliott, L., Ingham, D.B. and Whitcombe, J.L. 2002. Computational fluid dynamics and the physical modeling of an upland urban river. Geomorphology, Elsevier, 44(3-4): 375-391.

Marson, C., Caroni, E., Fiorotto, V. and Deppo, L. 2003. Flow field analysis around a groyne. Proceedings of 30th IAHR Congress, Thessaloniki, Greece, Theme C, Hydraulics of Groynes, pp. 377-384.

Peng, J., Kawahara, Y. and Tamai, N. 1997. Numerical analysis of three-dimensional turbulent flows around submerged groins. Proceedings of 27th IAHR Congress, San Francisco, CA, USA, Managing Water, pp. 829-834.

Pinter, N., Thomas, R. and Wlosinski, H. 2001. Assessing flood hazard on dynamic rivers. EOS, Transactions, American Geophysical Union, 82(31): 333-339.

Rodi, W. (1984). Turbulence models and their application in hydraulics - A state of the art review. International Association of Hydraulic Research, Delft, The Netherlands, 104 p.

Salaheldin, T.M., Imran, J. and Chaudhry, M.H. 2004. Numerical modeling of three-dimensional flow field around circular piers. Journal of Hydraulic Engineering, ASCE, 130(2): 91-100.

Shields, F.D. 1995. Fate of Lower Mississippi River habitats associated with river training dikes. Journal of Aquatic Conservation, Marine and Freshwater Conservation, Wiley InterScience, 5(2): 97-108.

Tamai, N., Kawahara, Y., Aoki, M., Matumoto, A.,Ishikawa, Y. and Yasuda, M. 1996. Ecohydraulics of spur dikes in Ushizu River, Kyushu Region, Japan. Conference Proceedings of Ecohydraulics 2000, Québec City, QC, Canada, Vol. B, pp. 631-642.

Tominaga. A., Jjima, K. and Nakano, Y. (2001). "Flow structures around submerged spur dikes with various relative height. Proceedings of 29th IAHR Congress, Beijing, China, Vol. D, pp. 421-427.

Versteeg, H.K. and Malasekera, W. 1995. An introduction to computational fluid dynamics - The finite volume method. Longman Scientific & Technical, Essex, England, 257 p.

Wu, B., Wang, G., Ma, J. and Zhang, R. 2005. Case study: River training and its effects on fluvial processes in the Lower Yellow River, China. Journal of Hydraulic Engineering, ASCE, 131(2): 85-96.

Yang, S. Q., Tan, S.K. and Lim, S.Y. 2004. Velocity distribution and dip-phenomenon in smooth uniform open channel flows. Journal of Hydraulic Engineering, ASCE, 130(12): 1179-1186.

Yossef, M. F. M. 2002. The effects of groynes on rivers (literature review). Delft Cluster Report No. DC1-334-4, Delft University, The Netherlands, 57 p.

Chapter 6. Conclusions

6.1. Major research conclusions

The research comprises three main parts. The first part is devoted to studying and quantifying the flow resistance and associated backwater effect due to a single spur dike. This part is described in Chapter 3. The second part is devoted to the studying and quantifying the flow resistance and associated backwater effect due to a spur dike field. This part is described in Chapter 4. In the third part of the work, a 3-D CFD model was developed for a single submerged spur dike. The intention of the CFD work was to provide an opportunity to evaluate the ability of such models to predict the flow resistance in terms of drag force and associated backwater effect and to study the flow field in the vicinity of spur dikes. This part is described in Chapter 5.

In Chapter 3, the flow resistance due to a single spur dike in a physical model study was measured, with the results expressed in terms of a drag force exerted on the flow in an open channel. Various spur dike geometries for both submerged and unsubmerged flow conditions were studied. In this work, the drag force due to a single 2-D spur dike plate was obtained using two methods. With the first method, the drag force was measured directly using a specially-designed cantilevered bar system. With the second method, the spur dike plate drag force was calculated using a momentum analysis in conjunction with the measured flow parameters. An important outcome of the study for a single spur dike is that the blockage ratio for both submerged and unsubmerged conditions has a prominent effect on the spur dike drag coefficient and associated backwater effect. It was also found that angled spur dikes, regardless of their orientation (i.e., angled upstream or downstream), produce smaller drag coefficients. For all flow conditions and spur dike geometries, it was concluded that a spur dike may have a greater backwater effect for a modest discharge in which the spur dike is just overtopped by the flow. For high discharges during which a spur dike will be highly submerged, the backwater effect is small. Comparison of direct and indirect measurement of the drag force showed that the directly-measured drag force was less than that indirectly-measured using the momentum equation. This difference is attributed to the increased bed

shear stress that occurs in the vicinity of the spur dike, which can not be accounted for in the analysis.

In Chapter 4, the flow resistance associated with each individual spur dike in a spur dike field in terms of the drag force exerted on the flow in an open channel was measured. The physical model study involved various arrangements of spur dike fields, in terms of the number of spur dikes and the relative spacing of the dikes, and various flow conditions (i.e., both submerged and unsubmerged modes of operation). It was concluded that the spur dike arrangement and the flow conditions have a substantial effect on the flow resistance and hence the backwater effect due to a spur dike field. In general, the total drag force due to a spur dike field increases with an increase in the number of dikes and also with an increase in the relative spacing between the dikes. The drag force of the leading spur dike was found to be the greatest amongst the spur dikes in the field, essentially acting as a shield to reduce the drag force of the downstream dikes. For submerged conditions, the drag force due to a spur dike field increases with an increase in the submergence ratio. For unsubmerged flow conditions, the drag force of the middle spur dikes within the field was quite low, including some measurement of negative values (i.e., drag force acting downstream on the flow). Regarding the drag force measurements, it was concluded that the flow structure is quite different for the two cases of submerged and unsubmerged modes of operation. The difference in the flow structure arises from the effect of the jet flow emerging from the crest of an upstream submerged spur dike influencing the dynamic pressure along the upstream face of a downstream spur dike. The comparison between the calculated backwater effect, using the measured drag force, and the measured backwater effect suggests that the overall bed shear stress may be larger in a spur dike field compared to that for normal flow conditions with no spur dike in place.

In Chapter 5, the ability of a 3-D CFD model to predict the flow field, including the flow resistance and backwater effect, due to a submerged spur dike in an open channel flow was studied. The 3-D CFD software FLUENT v6.2 along with experimental data obtained from a physical model, including flow depth and velocity data, were used in the work. Two flow conditions were studied, one involving uniform flow conditions in a plain channel and

the other non-uniform flow conditions in a channel containing a submerged spur dike. The CFD model was calibrated for uniform flow conditions. The calibrated model was then used to predict the flow field characteristics for the non-uniform flow conditions in which a spur dike was present. Application of a multiphase technique, VOF, using FLUENT to predict the free surface flow resulted in successful prediction of the water surface profile, and hence backwater effect, within the vicinity of the submerged spur dike. When compared with the experimental velocity data, it was concluded that the CFD model was able to satisfactorily predict the velocity field adjacent to the spur dike. However, the development of diving jet flow emerging over the crest of the spur dike was not modeled well, particularly in the region immediately downstream from the spur dike, due to the over-dissipation of the jet turbulence within the downstream flow region.

6.2. Research contribution

The present research contributes to the literature in both hydraulic engineering and fluid mechanics. In the field of hydraulic engineering, it serves to enhance available design criteria for spur dikes in rivers. In this regard, two major features are worth mentioning. The results of the study can be used to evaluate the contribution of spur dike resistance to the overall resistance of a river system, which may be important in flood management planning. The present research also helps to provide for better structural design of spur dikes as the drag force exerted on the structure can now be determined. In the fluid mechanics field, the study increases the available knowledge with respect to the hydrodynamic behaviour of objects (2-D plates) immersed in a free surface flow. Most studies in this context have been done in wind tunnels. For a series of 2-D plates in a field, the research provides improved understanding of the effects of the plate interactions and their effects on the drag force experienced by the plates. In the context of hydraulic engineering, the results of the CFD model show that the VOF technique is an efficient method to simulate and predict the free surface flow and hence backwater effect due to spur dikes within an open channel. In the context of the fluid mechanics, it is concluded that the turbulence model needs to be improved to capture the 3-D flow structure downstream from a spur dike.

6.3. Possible extensions to the research

The scope of the present work can be extended by studying a wider range of the influencing parameters applied in the present work, including flow conditions, spur dike geometry and shape, spur dike arrangement, and channel geometry. The flow resistance, expressed in terms of a drag coefficient, was shown to be a function of the submergence ratio in the case of a single submerged spur dike and of the flow depth to length ratio in the case of a single unsubmerged spur dike. In the present study, the submergence ratio and flow depth to length ratio were limited to about 3.5 and 1.7, respectively. The results of the present study show that the base drag coefficient (i.e., drag coefficient of a spur dike with a negligible blockage effect) seems to reach to some constant values as the submergence ratio in the case of a submerged spur dike and length to depth ratio in the case of an unsubmerged spur dike reaches values greater than those tested in the present study (see Figures 3.13 and 3.16, respectively). It would be beneficial to confirm this observation by using higher values of submergence and flow depth to length ratios. As suggested in Chapter 3, an experimental study to extend the above parameters would also enhance understanding of the behavior of a single spur dike in an open channel for large flow depths. From the literature review, it was postulated that the effect of Froude number is negligible on the drag coefficient for 2-D rectangular spur dikes as used in this study. However, the drag coefficient of other shapes of spur dikes, such as those having a trapezoidal cross-section, may show greater sensitivity to the Froude number. This issue needs to be explored in more detail.

As described in Chapter 4, it was concluded that the submergence ratio strongly affects the flow resistance of a submerged spur dike field. Only three submergence ratios were studied, including values of 1.2, 1.56 and 2.0. This range could be extended to higher values. Moreover, in the present study, 2-D rectangular plates were used to simulate the spur dikes. The effects of the flow regime, expressed in terms of the Froude number, might vary with the spur dike shape. Furthermore, the number of spur dikes and their spacing were limited in this study. It would be useful to extend the number of spur dikes and the spacing between dikes in a spur dike field for both submerged and unsubmerged modes of operation to improve and extend the results of this research.

The channel shape and bed materials may also have substantial effects on the flow resistance of a spur dike or spur dike field. In the present study, an inerodible boundary, rectangular open channel was used. However, natural rivers usually have irregular shapes and erodible bed and bank materials. Furthermore, the wake region behind a spur dike in an open channel having an irregular shape could be different from that in a rectangular open channel, which could affect the flow resistance due to the spur dikes. Moreover, the scouring and sedimentation that tends to occur around spur dikes changes the flow conditions and geometry of the open channel, which in turn is likely to affect the flow resistance due to the spur dikes.

The CFD model was shown to be very useful in predicting the flow pattern in the vicinity of a spur dike and also the backwater effect. Although the prediction of the overall flow pattern around a submerged spur dike was satisfactory, the development of the diving jet into the downstream flow core was not modeled well. The results of the CFD model might be improved by adjusting the coefficients of the diffusion terms or by introducing anisotropic diffusion terms into the turbulence model. Moreover, application of the CFD model could be extended to more complicated scenarios, such as the case of a spur dike field or spur dikes with various geometry as well as cases where the open channel has an irregular cross-sectional shape.

6.4. Limitations of the study

The results of the present study are limited to the range of parameters evaluated in the physical model. In the physical model, spur dikes were simulated using 2-D rectangular plates, while a laboratory flume with a rectangular cross-section and rigid bed was used to simulate an open channel. Based on the nature of the physical model, the developed relationships are directly applicable to 2-D spur dike and spur dike fields in a rigid bed rectangular channel, which is expected to yield a conservative result for the backwater effect relative to that likely to be experienced in an erodible boundary channel. As such, the results due to the present work should be considered as conservative, first-order estimate of the backwater effect. Moreover, in the case of a spur dike field, configuration of the field in

terms of the number and spacing between spur dikes as well as the angle of spur dikes to the main flow direction is bounded by the range of parameters evaluated in the study.

Appendices

Appendix A. Backwater Effect Due to a Single Spur Dike

This paper, which comprises part of the Ph.D. program reported herein, was developed on the basis of experimental results obtained by Oak (1992) and a series of experiments performed by the Ph.D. candidate. All parts of the paper including writing of the text, review of the literature, development of the theory, analysis of the results and discussion have been implemented by the Ph.D. candidate.

Dr. J.A. Kells has reviewed all parts of the work as mentioned above. This paper has been published with the following citation:

Azinfar, H. and Kells, J.A. 2007. Backwater effect due to a single spur dike. Canadian Journal of Civil Engineering, NRC Press, 34(1): 107-115.

The manuscript presented in this appendix is identical in content to that published in the Canadian Journal of Civil Engineering.

A.1. Abstract

Spur dikes, which are river engineering structures that project from the bank of a stream at some angle to the main flow direction, are principally used for two purposes: river training and protection of the river bank from erosion. In some respects, a spur dike might be considered a form of macro-scale boundary roughness, which results in increased resistance to the flow in a stream. As such, a spur dike produces an upstream backwater effect and energy loss in the reach immediately downstream. In spite of these effects, spur dike design often proceeds without regard to the impact that the spur dike might have on the overall stream system. The work presented in the paper is on the backwater effect due to a single, vertical-walled spur dike. It is centered around a theoretical framework based on the momentum principle in which the resistance offered by the spur dike is represented by a drag equation. In this, the key parameter is the drag coefficient for the spur dike. Experimental data acquired for various configurations of a single spur dike within fixed bed flumes have been used to calibrate and validate the proposed backwater model. The results show that the spur dike drag coefficient, hence the computed backwater effect, depends on the channel contraction caused by the spur dike, the degree of spur dike submergence, the aspect ratio of the spur dike, and the Froude number of the flow.

A.2. Introduction

Spur dikes are hydraulic structures that project from the bank of a stream at some angle to the main flow direction. They are principally used for two purposes, namely river training and erosion protection of a river bank. River training applications of spur dikes frequently involve improving the navigability of a river by increasing the flow depth, straightening the channel alignment, and increasing the sediment transport rate through the improved reach. The latter feature results in reduced costs for channel dredging. In the case of bank protection, spur dikes deflect the flow away from the bank, thereby reducing the near-bank flow velocity and often creating a region of deposition. Relative to other approaches, such as revetments, spur dikes are among the most economical structures that may be used for river bank protection (Shields 1995). However, despite their useful features, there is some concern that spur dikes may be responsible for increased flooding due to the

associated backwater effect. For example, studies show that, over the past century, flood stages for given discharges at various locations along the Middle Mississippi and Lower Missouri rivers have increased by 2 m to 4 m (Criss and Shock 2001). These river reaches are characterized by extensive river engineering works, including spur dikes and levees. Pinter (2004) confirms the reported increase in flood stage due to the presence of engineering works on the two rivers.

The relative increase in a river's stage and attendant flooding can be due to a modified hydrologic regime, changes in the hydraulic regime, or both. In order to separate the effects of the two factors, Criss and Shock (2001) and Pinter et al. (2001) tracked the changes in the stages of the Mississippi and Missouri river stages over time for constant discharge conditions. With the discharge being held constant, the variations in a river's stage can be attributed solely to changes in the channel hydraulics, while the effects of a modified hydrologic regime are eliminated. Based on their analysis, Criss and Shock and Pinter et al. observed that the relative stages of the Mississippi and Missouri rivers have increased over the last century. These findings suggest that the channel roughness of the rivers has increased, which the researchers attribute to the construction of river engineering works such as spur dikes. They also observed that the increase in channel roughness is more important for higher discharge conditions. At low discharges, in the case of an erodible boundary channel, there may even be a decrease in the river's stage, which can be attributed to main channel degradation due to channel confinement resulting from spur dike construction. As well, many rivers with river engineering works, such as the Mississippi River, contain both spur dikes and levees. Since levees are usually built to levels higher than the bankfull stage, Pinter et al. also concluded that, for such rivers, observed stage increases for flows less than bankfull can be attributed solely to spur dikes.

Stage increases due to spur dikes have also been reported on other rivers too. For example, for the Rhine River in Europe, it has subsequently been decided to reduce the height of the spur dikes as a way of reducing their adverse effects during times of flooding (Yossef 2002; Belz et al. 2001). Similarly, in a numerical study of the Nile River in Egypt, it was concluded that the construction of spur dikes has had a considerable effect on upstream

water levels (Soliman et al. 1997). These increases in flood stage often endanger buildings, infrastructure (roadways, cables, bridges, etc.), farmland, hydraulic structures (e.g. pump stations, intakes, etc.) and people who live near the river.

Since it has now been demonstrated that the construction of spur dikes can significantly increase the stage of a river, especially during times of flooding, it is then prudent to quantify the amount of backwater effect that occurs so that the impacts of spur dike construction can be determined by those charged with managing the river system. For this reason, a study on the backwater effects associated with spur dikes was recently initiated at the University of Saskatchewan. The purpose of the study was to explore the various parameters that affect the resistance characteristics of spur dikes in open channels and to develop a model for quantifying the amount of backwater effect experienced. The work reported herein, which is part of a larger study on the backwater effect due to spur dikes, was based on a single spur dike having a basic geometric configuration (i.e., rectangular flat plates arranged perpendicular to the channel wall). In this paper, a theoretical framework based on the momentum principle is developed as a way of relating the backwater effect to the drag force exerted by a single spur dike, wherein the spur dike drag force is represented by a drag coefficient. Using the results from two physical models, experimental data acquired for various dimensions of a single spur dike within fixed bed flumes have been used to calibrate and validate the proposed spur dike backwater model.

A.3. Theoretical framework

Any obstacle located within a flow field exerts a drag force on the flow, which invariably results in some type of energy loss. In free surface flow, such as the flow in a river, the energy loss is overcome by a rise in the upstream water level, herein termed backwater effect. For non-streamlined objects or bluff bodies, the approach flow separates from the boundaries of the object, producing a wake zone behind the object, which is characterized by eddies and a high rate of energy dissipation. The resulting difference in pressure from the upstream side of the object to the downstream side results in a net upstream force being exerted by the object on the flow. This force is known as form drag. In addition to form drag, there is often a small amount of drag resulting from the increased shear stress

associated with the relatively high velocity flow over the surface of the object. This latter drag is called viscous drag or skin friction drag. The total drag force is the sum of the two types of drag. For bluff bodies, form drag is typically dominant. As spur dikes can be classified as bluff bodies, the drag resulting from a spur dike is primarily due to form drag. This drag is principally responsible for the energy loss and backwater effect at a spur dike.

The analysis of the backwater effect due to a spur dike in an open channel can be done using either an energy approach or a momentum approach. A momentum approach has been used in this work. With reference to Figure A.1, the one-dimensional linear momentum equation can be written between section 1 upstream of the spur dike and section 2 downstream to give

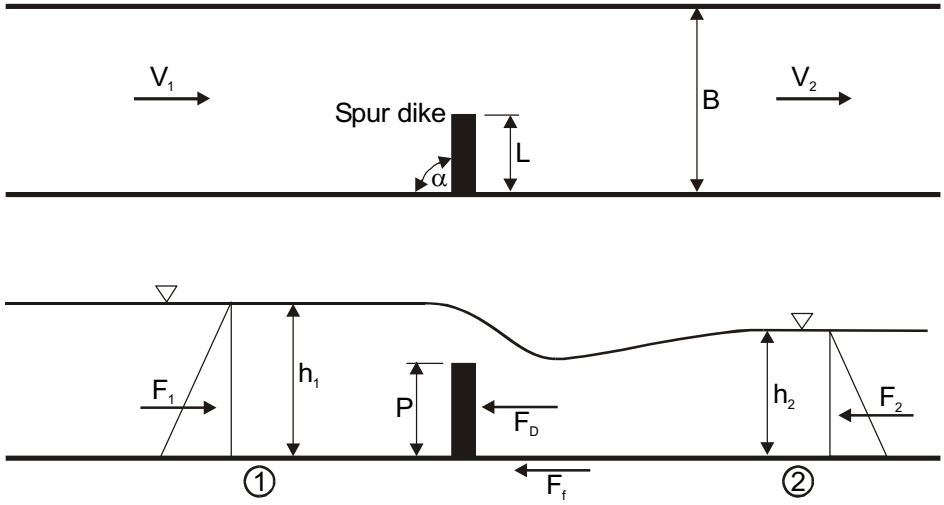

Figure A.1. Schematic (plan and profile) of a spur dike within a control volume.

[A.1] $$F_1 - F_2 - F_D - F_f = \rho Q(\beta_2 V_2 - \beta_1 V_1)$$

where F_1 is the force due to the upstream hydrostatic pressure distribution, F_2 is the force due to the downstream hydrostatic pressure distribution, F_D is the drag force due to the spur dike, F_f is the friction force due to boundary friction between sections 1 and 2, ρ is the fluid density, Q is the discharge, V_1 and V_2 are the average velocities at sections 1 and 2, respectively, and β_1 and β_2 are the momentum correction factors applicable at sections 1 and

2, respectively. In this analysis, the channel is horizontal and thus there are no effects due to bed slope to be considered.

For this analysis, it is assumed that the friction force is negligible and that the momentum correction factors are equal to unity. These assumptions are common with many types of momentum analyses and are somewhat compensatory in nature (i.e., the effects of the two assumptions tend to offset each other). Furthermore, it might be noted that, if the channel bed had a slope and the flow was uniform, the downstream component of the weight of the fluid within the control volume (i.e., between sections 1 and 2) would exactly offset the frictional resistance at the boundary. The drag force, F_D, can be expressed as

$$[A.2] \quad F_D = C_D A_s \frac{\rho V_r^{\,2}}{2}$$

where C_D is the drag coefficient and A_s is the upstream projected area of the spur dike (i.e., A_s = PL, where P is the height of the spur dike and L is the length of the spur dike perpendicular to the flow). The velocity, V_r, is a representative velocity, which for this work has been taken to be the approach velocity, V_1. On this basis, Eq. [A.1] can be revised to read

$$[A.3] \quad \frac{1}{2}\rho g B h_1^2 - \frac{1}{2}\rho g B h_2^2 - C_D A_s \rho \frac{V_1^2}{2} = \rho Q (V_2 - V_1)$$

where the hydrostatic pressure force terms have been expressed in terms of the flow depth. Here, B is the channel width, g is the acceleration due to gravity (i.e., 9.81 m/s^2), and h_1 and h_2 are the upstream and downstream flow depths, respectively. The backwater effect, which is the subject of this investigation, is represented by the difference between the upstream and downstream flow depths (i.e., h_1 - h_2).

Further manipulation of Eq. [A.3] in conjunction with the continuity equation leads to

$$[A.4] \quad 2Fr_1^2 \left(\frac{h_1}{h_2}\right)^3 - \left(2Fr_1^2 - C_D A_r Fr_1^2 + 1\right)\left(\frac{h_1}{h_2}\right)^2 + 1 = 0$$

where the area ratio, A_r, is given by A_s/Bh_1 and Fr_1 is the Froude number of the approach flow. If the tailwater conditions, spur dike geometry and drag coefficient are known, Eq. [A.4] can be solved implicitly for h_1/h_2 to obtain the upstream water depth and the corresponding backwater effect resulting from the spur dike. If Newton's method is used in the solution procedure, it is required to find the first derivative of Eq. [A.4], which is given by

$$[A.5] \quad f'\left(\frac{h_1}{h_2}\right) = 2\left(\frac{h_1}{h_2}\right)\left(Fr_1^2 - C_D A_r Fr_1^2 - 1\right)$$

Even so, the key issue requiring resolution at this stage is the determination of the spur dike drag coefficient.

From dimensional analysis, the drag coefficient can be expressed in terms of a functional equation as

$$[A.6] \quad C_D = f(Re_1, Fr_1, L/B, P/L, h_1/P, \Delta, \alpha)$$

where Re_1 is the Reynolds number of the approach flow, Δ is the spur dike shape factor and α is the angle between the spur dike and the stream bank as measured from upstream. The Reynolds number represents the effects of viscosity, which are assumed to be insignificant in the case of a flow field involving a spur dike. Moreover, since only a vertical-walled spur dike is considered in this study, the spur dike shape factor can be omitted from the analysis. Similarly, only one spur dike orientation was used in this work, with the spur dike being oriented normal to the stream bank (i.e., $\alpha = 90°$). Thus, for this work, the spur dike drag coefficient can be expressed by a simplified functional equation as

$$[A.7] \quad C_D = f(Fr_1, L/B, P/L, h_1/P)$$

In turn, Eq. [A.7] can be expressed in a more useful mathematical form as

$$[A.8] \quad C_D = K(P/L)^a (1 - \frac{L}{B})^b (\frac{h_1}{P})^c (Fr_1)^d$$

where K, a, b, c and d are assumed to be constants, which must be determined by experiment. The parameter P/L is the spur dike aspect ratio, the parameter L/B is the spur dike contraction ratio, and the parameter h_1/P is the spur dike submergence ratio. In this work, the drag coefficient in Eq. [A.8] has been expressed using values representative of the upstream flow conditions.

It will be noted that a parameter referred to as the opening ratio, defined herein as 1 – L/B, has been used instead of the contraction ratio, L/B, in Eq. [A.8]. The reason for this is that use of the opening ratio avoids the problem of the drag coefficient approaching zero as the contraction ratio approaches zero. Thus, as the opening ratio approaches unity (i.e., there is little to no contraction of the channel due to the spur dike), the opening ratio also approaches unity, which means that there is negligible effect of the parameter on the computed drag coefficient as is to be expected.

A.4. Experiment and model development

In order to calibrate Eq. [A.8], the data obtained from a series of experiments carried out by Oak (1992) have been used. An 800 mm wide, horizontal, fixed-bed flume containing smooth, blunt end (i.e., rectangular), vertical-walled spur dikes of various length and height was used in Oak's work. The test conditions included evaluation of both submerged and unsubmerged spur dikes. Table A.1 shows the range of parameters studied by Oak.

Table A.1. Range of experimental parameters used in Oak's (1992) experiments

Parameter	Range	Parameter	Range
Spur dike height, P (mm)	100, 150, 200	D/S depth, h2 (mm)	100 - 254
Spur dike length, L (mm)	320, 400, 480	D/S Froude number, Fr2	0.05 - 0.40
Channel width, B (mm)	800	Submergence ratio, h1/P	1.03 - 1.77
Channel slope, S_o (m/m)	0	Discharge, Q (L/s)	13.9 - 42.3

In addition to the above experiments for vertical-walled spur dikes, Oak (1992) also conducted experiments for spur dikes having a triangular cross-section and a rounded nose and both smooth and rough boundaries. These latter spur dikes were also tested for both submerged and unsubmerged modes of operation. However, only the data for Oak's smooth,

blunt end, vertical-walled, submerged spur dikes have been considered in this study. In this regard, two points are worth noting. First, the most critical condition with respect to the backwater effect due to a spur dike is for flood conditions, during which time the spur dike is likely to be submerged. Second, as found by Oak and Smith (1994), the backwater effect associated with a spur dike having a triangular cross-section and a rounded nose is less than that for one having a blunt end and vertical orientation. The streamlining associated with the former geometry results in a reduced backwater effect. As such, the results of the work reported herein can be considered to be somewhat conservative with respect to the predicted backwater effect.

In Oak's (1992) experiments, both the upstream and downstream water levels were measured for each of several spur dike geometries and flow conditions. Thus, it is possible to re-analyze Oak's data using Eq. [A.3] expressed in terms of the drag coefficient as

$$[A.9] \quad C_D = \frac{2q^2\left(\frac{1}{h_1} - \frac{1}{h_2}\right) + g\left(h_1^2 - h_2^2\right)}{\left(\frac{A_s}{B}\right)\left(\frac{q}{h_1}\right)^2}$$

where q is the unit discharge (i.e., Q/B). Using Eq. [A.9] to determine the drag coefficient for 540 tests from Oak's work, and applying multiple variable regression analysis to the data set for an equation expressed in the form of Eq. [A.8], resulted in

$$[A.10] \quad C_D = 4.00\left(\frac{P}{L}\right)^{-0.431}\left(1-\frac{L}{B}\right)^{-0.849}\left(\frac{h_1}{P}\right)^{-1.676}\left(Fr_1\right)^{-0.221}$$

The software SPSS (Statistical Package for the Social Sciences, v.9) was used for this analysis. The resulting R^2 value was found to be 0.88. In this work, the combination of Eqs. [A.4] and [A.10] is referred to as the regression backwater model.

On the basis of the exponent values given in Eq. [A.10], it is evident that the submergence ratio has the greatest effect on the drag coefficient (i.e., largest exponent) while the Froude number has the least effect (i.e., smallest exponent). In doing the analysis for Eq.

[A.10], at least three of the parameters used to describe the drag coefficient are physically independent, including the aspect ratio, P/L, the opening ratio, 1-L/B, and the submergence ratio, h_1/P. However, it was suspected that there may be a relationship between the submergence ratio, h_1/P, and the Froude number, Fr_1, given that both variables depend on the flow rate. However, covariance analysis using SPSS applied to Oak's (1992) data showed that there is no significant relationship between the two variables. Thus, on the basis of variable independence, it is possible to define the drag coefficient as

[A.11] $C_D = \varphi_1\varphi_2\varphi_3\varphi_4$

where the various φ terms, which are each a type of drag coefficient, can be defined as

[A.12] $\varphi_1 = f_1(\frac{P}{L}), \quad \varphi_2 = f_2(1-\frac{L}{B}), \quad \varphi_3 = f_3(\frac{h_1}{P}), \quad \varphi_4 = f_4(Fr_1)$

Equations [A.4] and [A.11] are referred to herein as the multiple function backwater model. This model is discussed further in the following paragraphs.

To develop the various φ relationships described in Eq. [A.12], recourse was again made to Oak's (1992) data and the results of the multiple variable regression analysis expressed by Eq. [A.10]. In doing this, each φ term was individually evaluated by dividing the computed drag coefficient by all of the remaining parameters in Eq. [A.10], one by one. For example, in the case of φ_1, which represents the aspect ratio term in Eq. [A.10] (i.e., the P/L term), the data were expressed as

[A.13] $$\varphi_1 = \frac{C_D}{4.00\left(1-\frac{L}{B}\right)^{-0.849}\left(\frac{h_1}{P}\right)^{-1.676}\left(Fr_1\right)^{-0.221}}$$

The same procedure was applied to all other φ terms. Equation [A.13] in essence reveals the nature of the variation of the drag coefficient with the aspect ratio, P/L, as the effects of the other variables have essentially been factored out. In this way, comparison can be made to the literature in respect of this parameter (and, in turn, the other three parameters

too). As well, it is also possible to gain some insight to the physics of the problem, largely because the analysis procedure allows one parameter to be evaluated at a time.

The results of the analysis described above, which quantify the functional relationships expressed by Eq. [A.12], are shown in Figure A.2. In each of the four figures (i.e., Figures A.2a – A.2d), it may be noted that the graphical relationship has been expressed in three ways: by a simple plot of the data (data points), by a power law least squares regression fit to the data (solid line), and by a curve fitted to an extended range of the data (dashed line). In the case of the curve fitted to an extended range of the data, recourse was made to a review of the trend expressed by Oak's (1992) data, by applying simple logic to the basic physics of the problem (e.g., recognition of the physical limits of applicability), and by comparison with the results of related work in the published literature. The specific details applicable to each of the four φ parameters are discussed below.

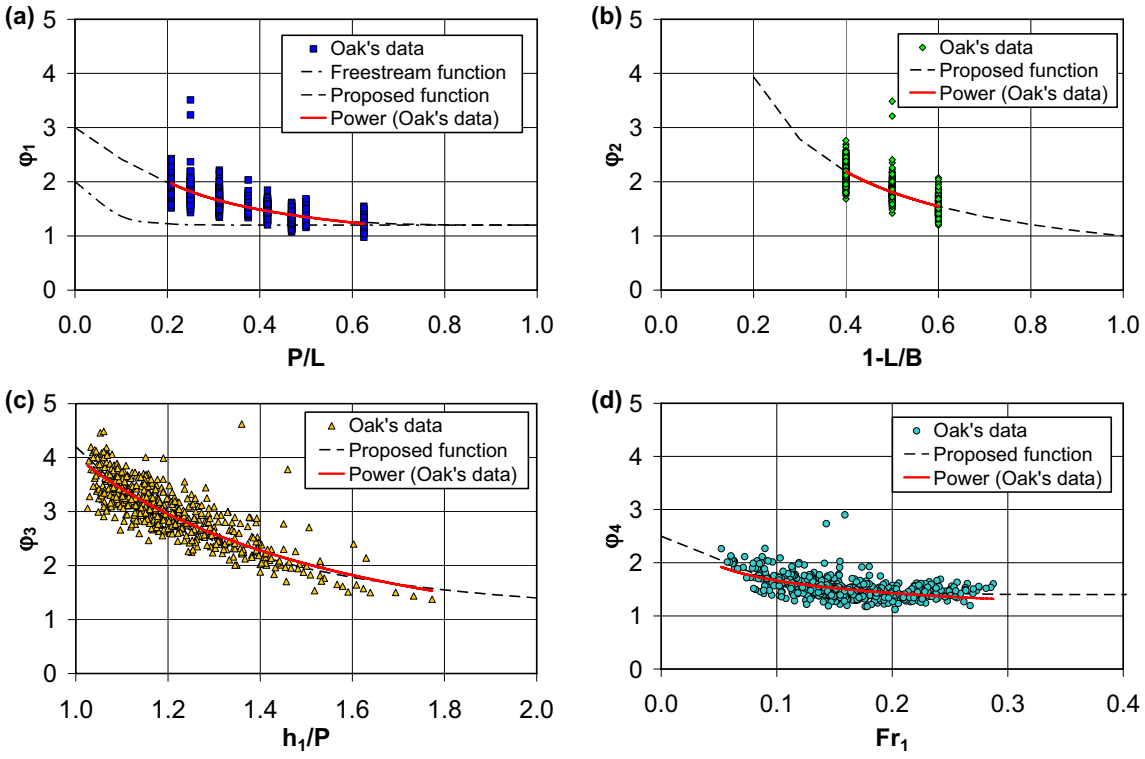

Figure A.2. Contribution of the various parameters to the drag coefficient: a) spur dike aspect ratio; b) spur dike opening ratio; c) spur dike submergence ratio; and d) upstream Froude number.

Figure A.2a shows the variation of φ_1 with the spur dike aspect ratio, P/L. Also included in this figure is the relationship for the drag coefficient of a rectangular flat plate positioned within a free-stream flow as given by Hoerner (1965). The upper range of the parameter φ_1 has been extended to lower values of P/L based on the trend expressed by Oak's data, while its lower range has been limited to a value of 1.2 on the basis of both the trend expressed by Oak's data and the drag coefficient of a rectangular flat plate for large aspect ratios as given by Hoerner. The resulting relationship for φ_1 as a function of P/L can then be expressed by

$$[A.14] \quad \varphi_1 = 1.8(1 - \frac{P}{L})^{3.7} + 1.2$$

As indicated in the figure, except for aspect ratios greater than about 0.6, the experimental results for the drag coefficient from this study are greater than those for a rectangular plate located within a free-stream flow. It is postulated that the difference can be explained by the limited "ventilation" of the flow around the plate in the case of a spur dike, which is fastened to both the bed and one sidewall, versus the free-stream situation in which flow can access the backside of the plate from all sides. This explanation is supported by the work of Ranga Raju et al. (1983), who measured the drag coefficient of circular cylinders in an open channel. In that work, it was observed that the drag coefficient for a circular cylinder fastened to the floor of a flume is greater than that for the case of the same cylinder located within a free-stream environment. Dalton and Masch (1968) make a similar observation. In their case, Dalton and Masch argued that the horseshoe vortex near the flume bottom increases the stagnation pressure in front of the cylinder, which in turn results in an increase in the drag coefficient.

Figure A.2b shows the variation of φ_2 with the spur dike opening ratio, 1-L/B. A power law equation has been used to describe the φ_2 relationship, as with Eq. [A.10], viz.

$$[A.15] \quad \varphi_2 = (1 - \frac{L}{B})^{-0.85}$$

Two observations are readily apparent with Eq. [A.15] and as shown in Figure A.2b. First, in the limit as L/B approaches zero, which means that there is no spur dike present, the value of φ_2 approaches unity. In essence, this means that there is no effect of the opening ratio on the drag coefficient for this situation, as expected. Second, the trend in the relationship is such that the drag coefficient increases with a decrease in the opening ratio (i.e., an increase in the contraction ratio). A similar finding was also made by Shaw (1971), who investigated the wall effect on the drag coefficient of a flat plate located within a water tunnel. Shaw noticed that, as the plate projected further into the tunnel, the velocity at the point of flow separation increased, which in turn resulted in a decrease in the pressure on the leeward side of the plate. The decrease in pressure manifested itself as an increase in the drag coefficient, which Shaw found could be expressed using a power law function in terms of the opening ratio. Similarly, Ranga Raju et al. (1983) suggested the following power law function for circular cylinders located on the bed of a channel, viz.

$$[A.16] \quad C_D = C_{Do}\left(1 - \frac{d}{B}\right)^{-1.35}$$

where C_D is the drag coefficient with contraction effects included, C_{Do} is the drag coefficient corresponding to a free-stream condition, d is the cylinder (pier) diameter and B is the channel width. It is apparent that the form of Eqs. [A.15] and [A.16] is essentially the same, with the only difference being the value of the exponent.

Figure A.2c shows the variation of φ_3 with the submergence ratio, h_1/P. It can be seen that, as the submergence ratio increases, the drag coefficient decreases. The reason for this is attributed to the existence of the free surface flow. As the submergence ratio, hence water depth, increases, the effects of the free surface on the pressure difference between the upstream and downstream faces of the object decreases. The upper range of this parameter has been extended on the basis of the trend reflected in the data. The lower range has been extended both on the basis of the trend expressed by the data and by logic related to the physics of the problem. With respect to the latter point, it has been assumed that the value of

φ_3 should approach unity (i.e., no effect due to submergence) as the submergence ratio approaches infinity. As such, the φ_3 relationship can be expressed as

[A.17] $$\varphi_3 = \frac{3.2}{(h_1/P)^3} + 1$$

Malavasi and Guadagnini (2003) observed that the drag coefficient for rectangular bridge decks increases as the flow depth increases for submergence ratios less than one and decreases as the submergence ratio becomes greater than one. The maximum drag coefficient occurs for a submergence ratio near to unity. In their work, Malavasi and Guadagnini defined submergence ratio as the water depth above the bottom of the deck relative to the deck thickness. The results of their study showed that the drag coefficient becomes constant when the submergence ratio reaches a value between 4 and 5. Analysis of Eq. [A.17] shows that, as the submergence ratio approaches a value of 5, the effects of submergence becomes negligible, which is similar to the finding of Malavasi and Guadagnini.

Figure A.2d shows the variation of φ_4 with the Froude number, Fr_1. The range of the parameter expressed by the measured data has been extended simply using the trend expressed by the data. As such, the power law fit to the data shown in the figure can be represented by

[A.18] $$\varphi_4 = 1.1(1 - Fr_1)^{15} + 1.4$$

Here, it may be observed that, as with the other φ relationships, there is a decreasing trend with an increase in the influencing parameter, which in this case is the Froude number. The results of Ranga Raju et al. (1983) and Randall and Holley (2001) on studies of bridge piers show the same trend. It may be noted that, in the present work as shown in Figure A.2d for Froude numbers greater than 0.2, the drag coefficient is constant.

A.5. Model validation and discussion

In order to provide for independent validation of the two spur dike backwater models described herein, a short series of tests was conducted in the Hydrotechnical Laboratory at the University of Saskatchewan. Two widths of flume were used in these tests so as to provide for a wider array of test conditions than was undertaken by Oak (1992). The test setup for both flumes is illustrated schematically in Figure A.3, while the test conditions are summarized in Table A.2.

For these tests, water surface levels were measured with a point gauge and flow rates with an orifice meter and by a gravimetric method. A photograph showing the model spur dike in operation is shown in Figure A4.

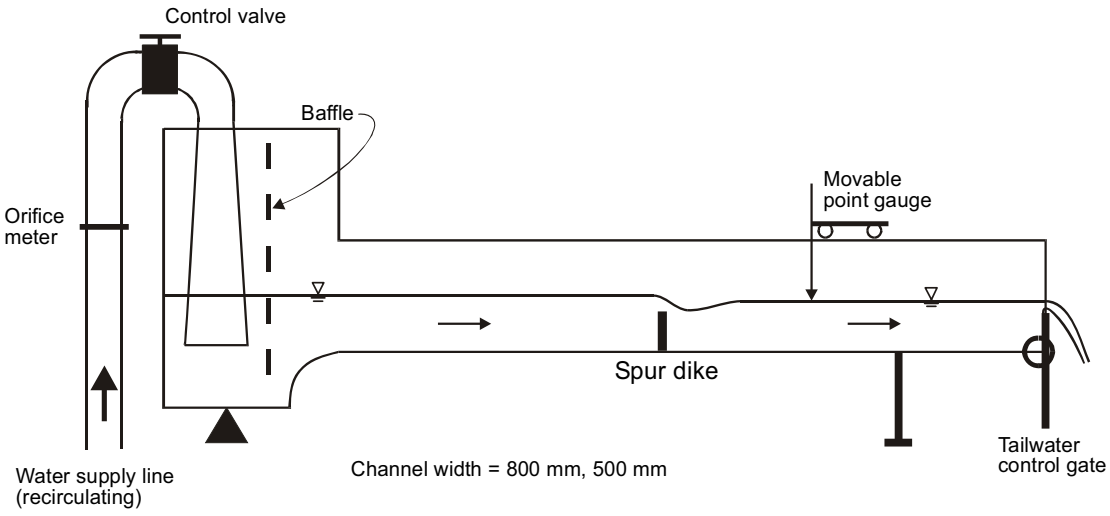

Figure A.3. Schematic illustration of the test setup used in the experiments.

Table A.2. Range of experimental parameters used in the validation experiments

Parameter	Range	Parameter	Range
Spur dike height, P (mm)	50	D/S depth, h2 (mm)	45 - 148
Spur dike length, L (mm)	200	D/S Froude number, Fr2	0.22 - 0.88
Channel width, B (mm)	500, 800	Submergence ratio, h1/P	1.22 – 3.02
Channel slope, So (m/m)	0	Discharge, Q (L/s)	7.3 – 56.7

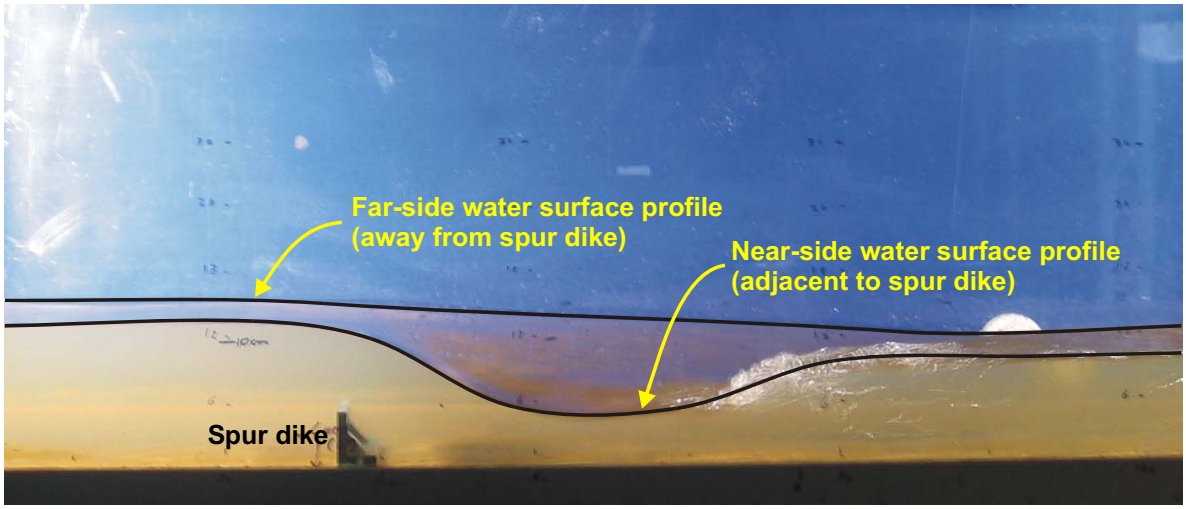

Figure A.4. Photograph showing the spur dike model in operation for one of the experiments.

As part of this verification, reference was also made to the model of Oak and Smith (1994), which was also derived using Oak's (1992) data. It is referred to as the Oak and Smith model and can be expressed as

$$[A.19] \quad \frac{h_1}{h_2} = 1 + 3.9\left(\frac{h_2}{P}\right)^{-2.4}\left(\frac{L}{B}\right)^{1.6} Fr_2^{1.5}$$

Equation [A.19] was determined using regression analysis applied to Oak's submerged spur dike data (i.e., with overtopping). It can be used to solve for the upstream depth of flow, hence backwater effect, if the downstream flow conditions are known. Strictly speaking, it is only applicable over the range of conditions tested by Oak. The other two models are represented by Eqs. [A.4] and [A.10] (i.e., the regression model) and Eqs. [A.4] and [A.11] (i.e., the multiple function model), respectively.

The results of the validation tests are shown in Figure A.5. In each case, the backwater effect (i.e., $h_1 - h_2$) determined using each of the three models has been compared with that determined by experiment. The mean relative error calculated for each of the proposed multiple function model, the regression model, and the Oak and Smith model is 9.4%, 18.9% and 42.0%, respectively. On the basis of these results, it is evident that the

proposed multiple model provides the best estimate of the backwater effect due to the spur dike. However, it is to be realized that the test conditions shown in Table A.2 go beyond that represented by Oak's (1992) data. Thus, it is not necessarily reasonable to expect that the results from the regression model and the Oak and Smith model, which are based strictly on Oak's data, should necessarily yield a good prediction for test conditions outside the range of data from which they were developed. The proposed multiple function model, however, is specifically intended to represent a broader range of each test parameter.

When the validation data set is restricted to the range tested by Oak (1992), as shown in Table A.1, the mean relative error calculated for each of the proposed multiple function model, the regression model, and the Oak and Smith model is 6.8%, 7.7% and 24.3%, respectively. These results show that both the proposed multiple function model and the regression model more-or-less perform equally well in this instance. As well, that both models perform considerably better than the Oak and Smith model, even when applied to the same data range used by Oak in his work.

It may be observed in Figure A.5 that the multiple function model provides better prediction of the backwater effect for lower backwater conditions (i.e., lower values of Δh). For higher values, the model slightly underestimates the actual backwater effect. One possible reason for the observed underestimate may be related to the determination of the effective tailwater depth in the model. During the validation tests, it was observed that, for a particular discharge and tailgate setting, removal of the spur dike from the flow resulted in a change in the tailwater depth downstream from the spur dike location. In particular, it was found that, with the spur dike removed, the downstream water level was higher than when the spur dike was present. This difference persisted for the entire length of the flume, which in some respects is a bit confounding. Given the subcritical nature of the flow and the horizontal bed (i.e., zero slope), it is evident that the local effects due to the spur dike (i.e., impacts on flow depth and velocity) must have existed for the entire distance from the spur dike location to the end of the flume. The amount of water level adjustment was noted to become smaller as the tailwater depth increased, hence as the Froude number decreased, as one would expect given the smaller kinetic effects associated with lower Froude number flow

conditions. Although the data do not exist to precisely quantify the magnitude of any error associated with determining the correct tailwater level, hence backwater effect, it is judged to be relatively small. Moreover, adjustment to the measured tailwater level would only serve to improve the apparent accuracy of the model predictions shown in Figure A.5.

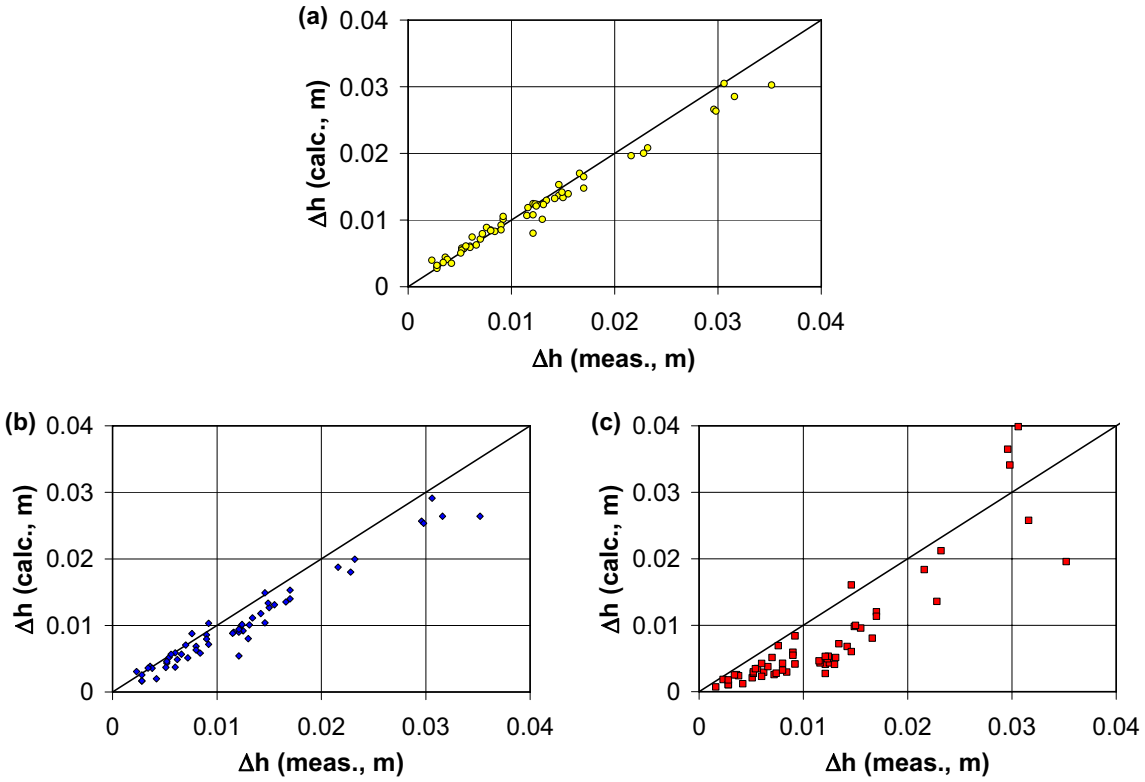

Figure A.5. Backwater prediction using a) multiple function model, b) regression model, and c) Oak and Smith model.

Another possible source of error may be related to the assumption of a momentum correction factor of unity in Eq. [A.1] (i.e., $\beta = 1$). While a β value of unity may be approximately correct for the flow approaching the spur dike, it is likely that the factor is considerably greater than unity in the reach immediately downstream. The variation in the velocity distribution in the immediate downstream reach, both vertically and laterally, is expected to be considerable because of the complex flow conditions created by the spur dike. As it was not possible to measure the tailwater depth at a location far downstream from the spur dike where the β factor would have been nearer to unity, and as velocity distributions

were not obtained as part of this study, the true momentum flux at the downstream section has invariably been underestimated. Nonetheless, if the downstream value of β were increased, it is evident from Eq. [A.1] that, for a given value of drag coefficient (or drag force), the computed upstream depth and corresponding backwater effect would increase, which in turn would result in a better correlation between the predicated and measured backwater effects.

As a final comment, it may be noted that the results of this work may be extended to spur dikes of other geometry than has been reported herein, such as spur dikes having a trapezoidal cross-section as is usual in practice. However, using a trapezoidal cross-section with an attendant rounded nose makes the structure more streamlined than is the case for a rectangular flat plate as used in this study. As such, determining the backwater effect using the results presented in this paper is likely to offer a somewhat conservative prediction (i.e., predicted backwater effect somewhat greater than that likely to occur). Until an improved predictive model is available for such situations, this is a safe approach.

A.6. Conclusions

The backwater effect due to a single spur dike in an open channel flow was studied in a laboratory flume. Analysis of the flow regime was carried out using the momentum principle, with the resistance offered by the spur dike being expressed in terms of a drag coefficient. On the basis of a series of tests conducted by Oak (1992) and several validation tests conducted as part of this study, a so-called multiple function model has been proposed for predicting the drag coefficient, which in turn allows quantification of the backwater effect due to a single spur dike in the flow. In doing this work, it has been found that, as with other bluff bodies in an open channel flow, the drag coefficient of a spur dike is a function of the structure geometry and flow condition, namely the spur dike aspect ratio, the contraction ratio, the submergence ratio and the Froude number of the flow. It was also observed that the behavior of the parameters affecting the spur dike drag coefficient is similar to that for other bluff bodies.

The results of the study show that the submergence ratio has the greatest effect on the drag coefficient, especially for flow depths near to the spur dike height. The Froude number has the least effect on the drag coefficient. It was also found that the proposed multiple function model provides better backwater prediction capability than the other two models examined, and particularly so when a wide array of test conditions is evaluated. Furthermore, considering that a spur dike with a trapezoidal cross-section is more streamlined than the two-dimensional spur dikes studied in this work (i.e. rectangular flat plates), backwater predictions made with the proposed multiple function model will be conservative.

Future work on this topic should address more specifically the nature of the backwater effect for three-dimensional spur dikes having a trapezoidal cross-section and rounded nose. As well, work is needed on assessing the impact due to an array of spur dikes, such as that often used in various types of river training and bank protection works.

A.7. Acknowledgements

Financial support for this research has been provided by a University of Saskatchewan graduate scholarship to the first author and by funding from the Natural Sciences and Engineering Research Council of Canada through a grant to the second author. This support is gratefully acknowledged. The authors also thank the anonymous reviewers for their constructive comments on the initial version of the manuscript, all of which were useful in making for an improved final product.

A.8. References

Belz, J.U., Busch, N., Engel, H., and Gasber, G. 2001. Comparison of river training measures in the Rhine catchment and their effects on flood behavior. Water and Maritime Engineering, 148(3): 123-132.

Criss, R.E., and Shock, E.L. 2001. Flood enhancement through flood control. Geology, 29: 875-878.

Dalton, C.D., and Masch, D.F. 1968. Influence of secondary flow on drag force. Journal of the Engineering Mechanics Division, ASCE, 94(EM5): 1249-1257.

Dyhouse, G.R. 1995. Myths and misconception of 1993 flood. St. Louis Division, U.S. Army Corps of Engineers Newsletter, 32(5): 6-8.

Hoerner, S.F. 1965. Fluid-dynamic drag; practical information on aerodynamic drag and hydrodynamic resistance. Brick Town, N.J., 20 chapters.

Lovelace, J.A., and Strauser, C.N. 1995. Prediction and reality concerning the 1993 Mississippi River flood: An engineers' perspective. Engineering News Record, June 5.

Malavasi, S., and Guadagnini, A. 2003. Hydrodynamic loading on river bridges. Journal of Hydraulic Engineering, ASCE, 129(11): 854-861.

Masch, F.D., and Moore, W.L. 1960. Drag forces in velocity gradient flow. Journal of the Hydraulics Division, ASCE, 86(HY7): 1-11.

Oak A.G. 1992. Backwater rise due to a submerged spur. M.Sc Thesis, University of Saskatchewan, 68 p.

Oak A.G., and Smith, C.D. 1994. Backwater effect due to overtopping a spur dike. Annual Conference of the Canadian Society for Civil Engineering, CSCE, pp. 136-145.

Pinter, N. 2004. Technical review of the Upper Mississippi River flow frequency study. Southern Illinois University, 30 p.

Pinter, N., Thomas, R., and Wlosinski, H. 2001. Assessing flood hazard on dynamic rivers. EOS, Transactions, American Geophysical Union, 82(31): 333-339.

Randall, J.C., and Holley E.R. 2001. Backwater effects of piers in sub-critical flow. FHWA, Technical Report No. TX-0-1805-1, 110 p.

Ranga Raju, K.G., Rana, O.P.S., Asawa, G.L., and Pillai, A.S.N. 1983. Rational assessment of blockage effects in channel flow past smooth circular cylinders. Journal of Hydraulic Research, IAHR, 21(4): 289-302.

Shaw, T.L. 1971. Effect of side walls on flow past bluff bodies. Journal of the Hydraulics Division, ASCE, 97(HY1): 65-79.

Shields, F.D. 1995. Fate of lower Mississippi River habitats associated with river training dikes. Journal of Aquatic Conservation: Marine and Freshwater Conservation, 5: 97-108.

Soliman, M.M., Attia, K.M., Kotb, Talaat, A.M., and Ahmad, A.F. 1997. Spur dike effects on the river Nile morphology after High Aswan Dam. Proc. of 27th IAHR Congress, Managing Water, Vol. A, pp. 805-810.

Yossef, M. F. M. 2002. The effects of groynes on rivers (literature review). Delft Cluster Report No. DC1-334-4, Delft, The Netherlands, 57 p.

Appendix B. Backwater Effect Due to the Blockage Caused by a Single Submerged Spur Dike in an Open Channel

This paper, which comprises part of the Ph.D. program reported herein, was developed on the basis of experimental results obtained by Oak (1992) and a series of experiments performed by the Ph.D. candidate. All parts of the paper including writing of the text, review of the literature, development of the theory, analysis of the results and discussion have been implemented by the Ph.D. candidate.

Dr. J.A. Kells has reviewed all parts of the work as mentioned above. This paper has been published with the following citation:

> Azinfar, H. and Kells, J.A. 2008. Backwater effect due to the blockage caused by a single, submerged spur dike in an open channel. Journal of Hydraulic Engineering, ASCE, 134(8): 1153-1157.

The manuscript presented in this appendix is identical in content to that published in the Journal of Hydraulic Engineering.

B.1. Abstract

The work reported in the paper, which is based on a laboratory study, is directed at the development of a method for predicting the backwater that may be expected to occur in response to a single, submerged spur dike located within an open channel flow. A theoretical analysis based on the momentum principle has been carried out to relate the backwater effects to the drag force exerted by the spur dike on the flow. A drag coefficient has been used to express the drag force in non-dimensional terms. Experimental data obtained in laboratory flumes for subcritical flow conditions have been used in developing predictive relationships for the spur dike drag coefficient. It is concluded that the drag coefficient is strongly correlated with the blockage created by the spur dike within the flow cross section.

B.2. Introduction

Spur dikes are hydraulic structures that project from the bank of a stream at some angle to the main flow direction. They are principally used for two purposes, namely river training and protection of the river bank from erosion. Despite their useful features, there is some concern that spur dikes may be responsible for increased flooding due to the associated backwater effect. For example, studies show that, over the past century, flood stages for given discharges at various locations along the Middle Mississippi and Lower Missouri rivers have increased by 2 m to 4 m (Criss and Shock, 2001). Pinter et al. (2001) have attributed a part of the increased stage to the construction of spur dikes. Stage increases due to spur dikes have also been reported on the Rhine River in Europe. There, it has subsequently been decided to reduce the height of the spur dikes as a way of reducing their adverse effects during times of flooding (Yossef, 2002; Belz et al., 2001). These increases in flood stage often endanger buildings, infrastructure (roadways, cables, bridges, etc.), farmland, hydraulic structures (e.g. pump stations, intakes, etc.) and people who live near the river.

To date, it appears that little work has been done with respect to developing predictive relationships for the backwater due to a spur dike in a stream. The somewhat related work that has been published with respect to backwater effects pertains to that occurring at bridge openings, where a constriction exists due to the presence of piers, abutments or both. In the

present work, an effort is made to develop a relationship for predicting the backwater effect due to the blockage caused by a single, submerged spur dike within an open channel.

B.3. Theoretical considerations

Any obstacle in a flow field exerts a drag force on the flow, which almost invariably results in some type of energy loss. In free surface flow, such as the flow in a river, the energy loss is overcome by a rise in the upstream water level, herein termed backwater. Analysis of the backwater effect due to a spur dike in a channel can be done using either an energy approach or a momentum approach. A momentum approach has been used in this work. With reference to Figure B.1, the one-dimensional linear momentum equation can be written between Section 1 upstream of the spur dike and Section 2 downstream to give

$$[B.1] \quad F_1 - F_2 - F_D - F_f + F_w = \rho Q(\beta_2 V_2 - \beta_1 V_1)$$

where F_1 is the force due to the upstream hydrostatic pressure distribution, F_2 is the force due to the downstream hydrostatic pressure distribution, F_D is the drag force due to the spur dike, F_f is the force due to boundary friction between Sections 1 and 2, F_w is the downstream component of the weight of the fluid within the control volume (i.e., between Sections 1 and 2), ρ is the fluid density, Q is the discharge, V_1 and V_2 are the average velocities at Sections 1 and 2, respectively, and β_1 and β_2 are the momentum correction factors applicable at Sections 1 and 2, respectively.

It may be assumed that the friction force is approximately equal to the downstream component of the weight of the fluid within the control volume (i.e., $F_f \approx F_w$ between Sections 1 and 2), which would be exactly true in the case of a uniform flow. Moreover, as is often the case with momentum analyses, the momentum correction factors are taken to be equal to unity (i.e., $\beta_1 = \beta_2 = 1$). Furthermore, the drag force, F_D, which is exerted by the spur dike on the flow, can be expressed as

$$[B.2] \quad F_D = C_D A_s \frac{\rho V_r^2}{2}$$

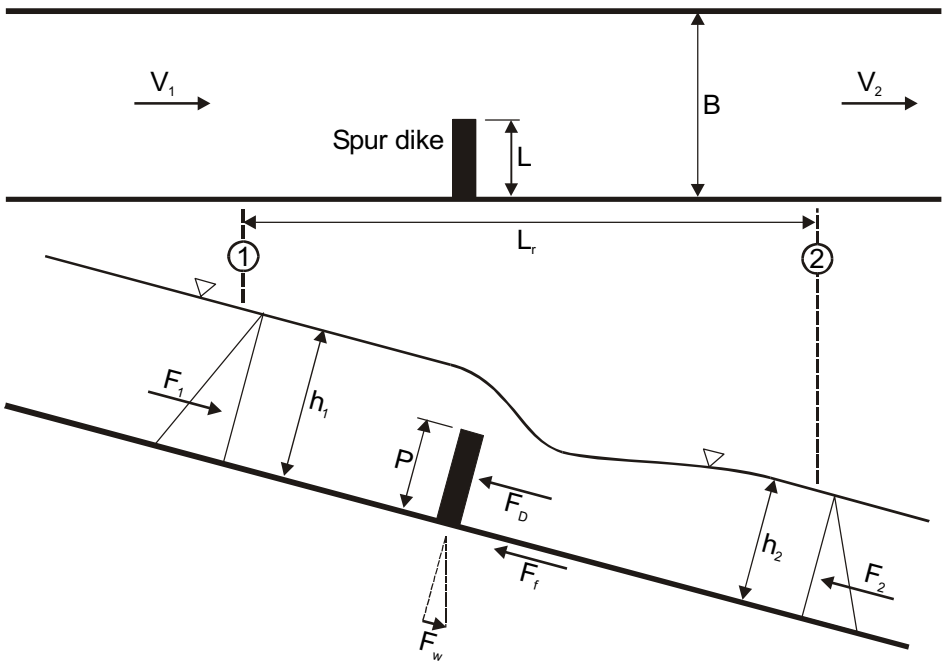

Figure B.1. Schematic illustration showing a plan and profile view of a spur dike within a control volume.

where C_D is the drag coefficient and A_s is the upstream projected area of the spur dike. For the case of a submerged spur dike, as analyzed herein, $A_s = PL$, where P is the height of the spur dike and L is the length of the spur dike perpendicular to the flow direction. The velocity, V_r, in the drag equation is a representative velocity, which for this work has been taken to be the approach velocity, V_1. On this basis, Eq. [B.1] can be revised to read

$$[B.3] \quad \frac{1}{2}\rho g B h_1^2 - \frac{1}{2}\rho g B h_2^2 - C_D A_s \frac{\rho V_1^2}{2} = \rho Q(V_2 - V_1)$$

where the hydrostatic pressure force terms have been expressed in terms of the flow depth. Here, B is the channel width, g is the acceleration due to gravity (i.e., 9.81 m/s^2), and h_1 and h_2 are the upstream and downstream flow depths, respectively. The backwater, which is the subject of this investigation, is represented by the difference between the upstream and downstream flow depths (i.e., $h_1 - h_2$).

Further manipulation of Eq. [B.3] in conjunction with the continuity equation leads to

$$[8.4] \quad 2Fr_1^2\left(\frac{h_1}{h_2}\right)^3 - \left(2Fr_1^2 - C_D A_r Fr_1^2 + 1\right)\left(\frac{h_1}{h_2}\right)^2 + 1 = 0$$

where the area ratio, A_r, herein termed the blockage ratio, is given by A_s/Bh_1 and Fr_1 is the Froude number of the approach flow. If the tailwater conditions, spur dike geometry and drag coefficient are known, Eq. [B.4] can be solved implicitly for h_1/h_2 to obtain the upstream water depth and the corresponding backwater due to the presence of the spur dike. Thus, at this juncture, the key issue requiring resolution is the determination of the spur dike drag coefficient.

Neglecting viscous effects (i.e., Reynolds number effects), which are expected to be insignificant for bluff bodies in a fully turbulent flow, and in consideration of a spur dike with a specific geometry or shape and with a specific orientation with respect to the flow direction, dimensional analysis results in the following functional relationship for the drag coefficient, viz.

$$[B.5] \quad C_D = f(F_{r1}, A_r, \frac{P}{L}, \frac{h_1}{P})$$

where P/L is the aspect ratio of the spur dike and h_1/P is the submergence ratio. The nature of the functional relationship for the drag coefficient is explored in the work reported herein.

B.4. Experiments

Two basic shapes of spur dike were evaluated in this study, namely a two-dimensional, vertical-walled spur dike (herein termed the 2-D spur dike) and a three-dimensional structure having uniformly-sloping sides (1.5H:1V) and a rounded nose (herein termed the 3-D spur dike). Moreover, only one orientation of spur dike was assessed in the present study, wherein the spur dike was normal to the channel bank hence the direction of the flow. As well, the study was solely focused on the condition of a submerged spur dike (i.e., $h_1/P > 1$). This condition is felt to be the most critical in the context of backwater

effects, as the backwater effect will be greatest during times of flooding when the spur dike is most likely to be overtopped.

Three sizes of fixed-bed flume, one of 500 mm width, one of 800 mm width and one of 1200 mm width, were used in the work. The flumes were supplied with water via a recirculating flow system within the Hydrotechnical Laboratory at the University of Saskatchewan. All of the 2-D spur dike work was done in the 500 mm and 800 mm wide flumes, while the 3-D spur dike work was done in the 800 mm and 1200 mm wide flumes. The data used in developing the backwater model included that obtained from Oak's (1992) submerged spur dike tests (720 tests for each basic shape of spur dike) as well as some 2-D test data obtained by the writers (55 tests), also for the case of a submerged spur dike. Table B.1 shows the range of parameters used in the present study.

Table B.1. Range of the experimental parameters evaluated in the study

2-D spur dikes		3-D spur dikes	
Parameter	Range	Parameter	Range
Fr_1	0.037 - 0.55	Fr_1	0.041 - 0.31
A_r	0.083 - 0.82	A_r	0.27 - 0.82
P/L	0.125 - 0.625	P/L	0.125 - 0.80
h_1/P	1.03 – 3.02	h_1/P	1.03 - 2.03
h_1/B	0.088 - 0.43	h_1/B	0.088 - 0.39

It is to be noted that, for some of Oak's tests, the length of the spur dike was equal to the width of the flume, which effectively meant that the spur dike structure was like a weir. In the case of his 3-D spur dikes, the dike length was defined as the dimension at the mid-height of the dike.

As all of the work done herein was conducted in a flume with a horizontal bed (i.e., the flume had zero slope), the assumption that $F_f = F_w$ is not valid (i.e., $F_w = 0$ in the case of a horizontal channel whereas $F_f > 0$ always). Thus, it is necessary to account for the Ff term in Eq. [B.1] and subsequent analyses. To this end, the friction force due to boundary friction at the periphery of the control volume can be represented by

[B.6] $F_f = \tau P_w L_r$

where τ is the average shear stress at the boundary of the flow (i.e., the channel boundary in contact with the flow), P_w is the wetted perimeter of the flow cross section, and L_r is the length of the reach comprising the control volume. The average shear stress along the boundary of the control volume can be determined from

[B.7] $\tau = \gamma R S_f$

where γ is the specific weight of the fluid, R is the hydraulic radius of the flow, and S_f is the energy slope of the flow. Since an H2 water surface profile occurs for subcritical flow in a horizontal channel, the values of R and S_f varied continuously throughout the length of the control volume. However, the variation in R and S_f (as well as P_w used in Eq. [B.6]) within the H2 profile was small, and thus the flow conditions at Section 2 were adopted for computation of the friction force. Manning's equation was used in computing the friction slope, with the value of Manning's n being taken to be 0.012 on the basis of a series of tests done to confirm this value for the flumes used in the study.

In the experiments, both the upstream and downstream depths of flow were measured for each spur dike geometry and flow condition. Thus, it was possible to re-analyze the data using Eq. [B.3], modified to include the friction force as given by Eq. [B.6]. Combining the two equations in conjunction with the continuity equation gives the drag coefficient as

[B.8] $$C_D = \frac{2q^2\left(\frac{1}{h_1} - \frac{1}{h_2}\right) + g\left(h_1^2 - h_2^2\right) - \frac{2\tau P_w L_r}{\rho B}}{\left(\frac{A_s}{B}\right)\left(\frac{q}{h_1}\right)^2}$$

where q is the unit discharge (i.e., Q/B). In calculating the friction force term, the reach length, L_r, was taken to be 5.5 m as reported by Oak (1992), with the portion of the reach length downstream from the spur dike being 5 m. For the data set obtained by the writers, L_r was equal to 1.5 m.

B.5. Results

Multiple variable regression analysis of the variables expressed in Eq. [B.5] using SPSS v.9 revealed that the blockage parameter is the most significant with respect to predicting the drag coefficient. In fact, the exponent on the blockage term was about an order of magnitude larger than the exponents on the other three independent variables (i.e., Froude number, spur dike aspect ratio, and submergence ratio). Given this finding, the regression analysis was performed a second time to develop a relationship between the drag coefficient and the blockage ratio alone. On the basis of this second regression analysis, equations were developed for the 2-D and 3-D spur dikes, respectively, as

[B.9] $C_D = 3.43(1 - A_r)^{-2.31}$ $R^2 = 0.94$ (2-D spur dike)

[B.10] $C_D = 2.86(1 - A_r)^{-2.27}$ $R^2 = 0.89$ (3-D spur dike)

where R^2 is the square of the correlation coefficient. Here, it may be noted that the regression has been performed on a parameter that may be referred to as the passage ratio (i.e., $1 - A_r$), which is in some ways the "inverse" of the blockage ratio. Comparison of the coefficients in Eqs. [B.9] and [B.10] suggests that the rounding of the nose of the spur dike, and possibly also the sides of the dike, serves to reduce the drag coefficient by about 17%, presumably because of a streamlining effect.

The asymptotic standard errors for the constant and exponent in Eq. [B.9] are 0.089 and 0.019, respectively, while they are 0.123 and 0.031 for the constant and exponent, respectively, in Eq. [B.10]. The mean relative error (MRE) was determined to be 13% and 32% for the 2-D and 3-D spur dikes, respectively. It may be noted that, even with inclusion of the other parameters given in Eq. [B.5] in the analysis (i.e., Froude number, spur dike aspect ratio, and submergence ratio), the MRE in each case would only be reduced by about 1%. The results for both the 2-D and 3-D spur dikes are shown plotted in Figure B.2 along with the regression equations given by Eqs. [B.9] and [B.10].

The scatter in the results may be attributed in part to experimental error, to the effects of errors in computing the bed friction, and the assumption of the momentum correction factor being equal to unity. The bed shear stress adjacent to a spur dike tip is notably greater than that of the mean value in the channel, while it is considerably smaller within the dead zones created by the spur dike (Rajaratnam and Nwachukwu, 1983). This inevitable "distortion" of the bed shear stress within the vicinity of the spur dike invariably leads to a somewhat different bed friction force from that calculated in the study. To further assess the scatter in the data, uncertainty analyses were performed on the calculated drag coefficients, C_D, using the experimentally measured parameters h_1, h_2, B, q, P_w, n, A_s, L_r and R. The results showed that the uncertainty associated with the measured parameters resulted in average percentage errors of 14% and 22% for the drag coefficients for the 2-D and 3-D spur dikes, respectively. Given that the average percentage errors from the uncertainty analyses are about the same as that of the MRE's from the regression analyses, one may conclude that the majority of the error involved in the regression analyses is due to experimental error.

Ranga Raju and Singh (1976) studied the effects of blockage on the drag coefficient of a vertical square plate placed at mid-length in a wind tunnel having a square cross-section. They observed that, as the blockage ratio increased, the base pressure behind the plate decreased while the pressure distribution on the upstream side of the plate remained constant. Their proposed equation for the drag coefficient in terms of the blockage ratio is

$$[B.11] \quad C_D = 1.8\left(1 - \frac{P}{D}\right)^{-2.32}$$

where P is the height of the plate and D is the height of the wind tunnel. In this context, h/D is analogous to A_r as used in the present study. Given the similarity in magnitude of the exponent in Eq. [B.11] to that in Eqs. [B.9] and [B.10], it can be concluded that the effect of blockage in a wind tunnel is similar to that in an open channel flow. Moreover, since the increased drag coefficient due to the increased blockage in the wind tunnel was attributed to the increased negative pressure behind the plate, it might be inferred that a similar pressure phenomenon is likely at play for the spur dike in an open channel flow. The reduced

pressure is expected to be the result of a local increase in the velocity of the flow around the object submerged within the flow.

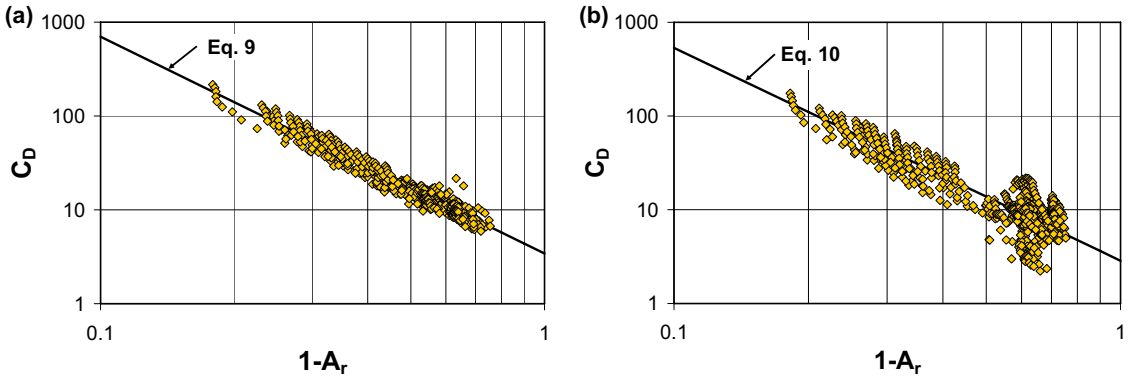

Figure B.2. Graphs of the data and regression equation for: (a) 2-D spur dike, and (b) 3-D spur dike.

B.6. Conclusions

The backwater effect due to a single spur dike in an open channel flow was studied in laboratory flumes. The analysis of the results was carried out using the momentum principle, with the resistance offered by the spur dike being expressed in terms of a drag coefficient. Using the data from a series of tests conducted by Oak (1992), and also that from a few additional tests conducted by the writers, two predictive equations are proposed for the drag coefficient applicable to a single, submerged spur dike located within an open channel flow. One equation is for a 2-D, plate-like spur dike and the other for a 3-D spur dike having a trapezoidal geometry. The proposed relationships show that the drag coefficient is mainly a function of the blockage ratio. It is also shown that the drag coefficient for a 3-D spur dike with sloping sides and a rounded nose is about 17% less than that for a 2-D spur dike in the form of a vertical, flat plate. This difference is thought to be due to the streamlining associated with the 3-D spur dike. In applying the results of this study, however, it is important to recall that they have been derived from work done in a fixed-bed flume and that they are essentially bounded by the range of experimental conditions summarized in non-dimensional form in Table B.1. Nonetheless, they do provide for a means of obtaining a first

level estimate of the backwater effect due to a single, submerged spur dike in an open channel flow.

B.7. Acknowledgements

Financial support for this research has been provided by a University of Saskatchewan graduate scholarship to the first author and by funding from the Natural Sciences and Engineering Research Council of Canada through a grant to the second author. This support is gratefully acknowledged.

B.8. References

Belz, J.U., Busch, N., Engel, H., and Gasber, G. (2001). "Comparison of river training measures in the Rhine catchment and their effects on flood behavior." Water and Maritime Eng., 148(3), 123-132.

Criss, R.E., and Shock, E.L. (2001). "Flood enhancement through flood control." Geology, 29, 875-878.

Oak, A.G. (1992). "Backwater rise due to a submerged spur." M.Sc. Thesis, University of Saskatchewan, 68 p.

Pinter, N., Thomas, R., and Wlosinski, H. (2001). "Assessing flood hazard on dynamic rivers." EOS, Transactions, American Geophysical Union, 82(31), 333-339.

Rajaratnam, N., and Nwachukwu, B. A. (1983). "Flow near groin-like structures." J. of Hydraulic Eng., ASCE, 109(33), 463-680.

Ranga Raju, K.G., and Singh, V. (1976). "Blockage effect on drag of sharp-edged bodies." J. of Wind Eng. and Industrial Aerodynamics, Elsevier, 1, 301-309.

Yossef, M. F. M. 2002. The effects of groynes on rivers (literature review). Delft Cluster Report No. DC1-334-4, Delft, The Netherlands, 57 p.

Appendix C. Uncertainty Analysis

C.1. General

There is an inherent inaccuracy or uncertainty in the measured parameters associated with the process of data acquisition as part of the experimental work. There are several factors inherent in the uncertainty, including inaccuracy of the measurement instruments and inaccuracy of readings. It is desirable to minimize the magnitude of the uncertainty and also to evaluate its magnitude for each of the measured parameters. One of the ways to minimize the uncertainty is to improve the measurement instruments or the measurement procedures. Improvement of the measurement instruments and/or procedures is usually expensive, and the extent to which this is done depends on the importance of the problem. However, in order to properly explain the results of an experiment, the uncertainties of the results should be quantified.

There are two major types of uncertainty or error involved in the results of an experiment, namely precision error and bias error. Precision error is related to the randomness of a measurement or an observation, while bias error is related to a systematic error. If a quantity is measured several times, the measured values will not necessarily be equal in value but instead they will be distributed around an average value. Precision error is proportional to the variance of the distribution curve of the samples from the average. it is usually considered to be equal to two times the standard deviation of the sample values, with a 95% level of confidence. The bias error, on the other hand, comes from a systematic source of error such as a miscalibrated scale or instrument. Bias error is generally difficult to discern, although it might be determined by comparison with a standard.

The uncertainty of the measurements of a number of independent parameters is propagated to the dependent parameter using the following equation (Coleman and Steele, 1999), viz.

$$[C.1] \quad uY = \sqrt{\sum_i \left(\frac{\partial Y}{\partial X_i} \right)^2 uX_i^{\,2}}$$

where Y is the dependent parameter, uY is the uncertainty of the dependent parameter, X_i is the i^{th} independent parameter and uX_i is the uncertainty of the i^{th} independent parameter. Equation [C.1] may be used separately for both precision and bias errors.

In most experimental programs pertaining to engineering applications, the repetition of a certain parameter is usually limited, mostly due to the large number of parameters involved in an experiment. In such circumstances, the uncertainty of a parameter can be determined using judgment. The calibration of an apparatus used to measure a certain parameter might also be a good source for determining the uncertainty of that parameter.

The main purpose of uncertainty analysis for the present work is to check if the results are affected by the embedded errors in the experimental program. In particular, it is imperative to observe how the interpretation of the results may be affected or changed due to the errors that might be involved in the experiments.

C.2. Uncertainty of the measured parameters in the present work

In the present research work, it was assumed that the uncertainty is only due to precision error. The most important parameter measured in the present study was the drag force due to a spur dike, whether operating in isolation (i.e., single spur dike) or as a part of a spur dike field. A specially-designed apparatus was fabricated to directly measure the spur dike drag force. The apparatus had three cantilever beams attached to a fixed plate at one end and a test plate (i.e., spur dike) connected to the beam by three ball joints at the other end. Two strain gauges were attached to the fixed end of each beam to detect the strains due to the normal forces exerted at the test plate end. The apparatus was calibrated using standard weights, which were correlated with the strain readings from the strain gauges. Excellent correlation (R^2= 1) was found between the strains and the mass of standard weights for each individual cantilever beam as shown in Figure 3.2.

The combined performance of the three cantilever beams was tested using three different standard weights (i.e., drag forces) placed at the various locations on the test plate.

Table 3.1 shows the results of the measurements made over the range of the measurements made. The maximum average error, over the range of the measurements made, is about 2%.

The procedure used to measure the drag force in the flume experiments gave additional insight into the determination of the drag force uncertainty. At the beginning of the experiment, the apparatus was placed in the flume and the strains were collected for a no-flow condition. At the next step, the desired discharge and flow depth were established in the flume, after which the strains were recorded. The difference between the strains in the two steps was used to determine the drag force exerted on the spur dike. Finally, the flume was drained and the strains were recorded again. In an ideal situation (i.e., no error), as the beams intended to function within the elastic region, the difference between the recorded strains in steps one and three would be equal to zero. However, it was observed that there were some differences between the readings between the two steps. For a single spur dike, the maximum error was observed to be less than 0.1 N. For the spur dike fields, on the other hand, the maximum values were about 0.2 N and 0.35 N for submerged and unsubmerged conditions, respectively. On this basis, the drag force measurement error for single spur dikes was considered to be 0.1 N. Similarly, for the submerged and unsubmerged spur dike fields, the drag force measurement errors were considered 0.2 N and 0.35 N, respectively.

Although the smallest unit on the point gauge used to measure the flow depth was 0.2 mm, it was assumed that the uncertainty of the flow depth measurement is 1.0 mm. This level of uncertainty was chosen with consideration of other factors such as human error, effect of waves in the flow, etc. The discharge was measured using a magnetic flow meter. During the reading of the discharge, it was observed that the maximum variation in the recorded discharge was 0.1 L/s, so that the uncertainty in the discharge was considered to be equal to that value. In the measurement of the spur dike dimensions, it was assumed that the linear dimensions of the plates might vary in the order of 1 mm, mostly due to the human error and also due to the effect of temperature on the measurement scales. It was also assumed that the density of water may vary by about 3 kg/m^3, mostly due to the variation in temperature and also due to the existence of dissolved materials in the water.

C.3. Uncertainty of the calculated parameters for a single submerged spur dike

The momentum equation as shown in Eq. [3.2] was applied to calculate the drag force of a single submerged spur dike. In that equation, the momentum correction factors were considered to be equal to unity. The uncertainties of the parameters shown in Eq. [3.2], including the flow depths (both upstream and uniform flow depths), discharge and the fluid density, were propagated into the calculated drag force using Eq. [C.1]. Figure C.1 represents the calculated drag force, with the uncertainties included, versus the measured drag force by the drag force measurement apparatus. It is to be noted that the calculated drag force is greater than the measured drag force. This is due to the increased bed shear stress and hence the friction force in the control volume containing the spur dike.

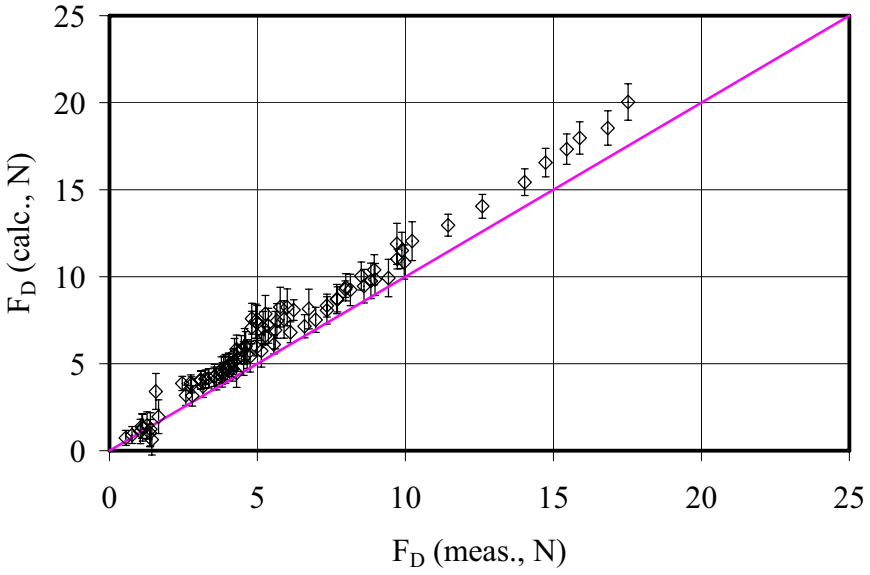

Figure C.1. Calculated drag force, with the uncertainties included, versus the measured drag force of a single submerged spur dike

The spur dike drag coefficient was calculated using Eq. [3.3] in which the representative velocity was considered to be equal to the approach velocity. In order to calculate the uncertainty of the drag coefficient, the uncertainties of the drag force, flow depth, discharge, spur dike dimensions and the fluid density were applied using Eq. [C.1]. It

should be noted that the velocity is a function of the discharge and channel width so its uncertainty is indirectly considered in the analysis.

Figure C.2 represents the calculated drag coefficient, with the uncertainties included for a single submerged spur dike, versus the passage ratio, $1-A_r$, where A_r is the blockage ratio ($=A_s/Bh_1$). It is to be noted that the uncertainty of the drag coefficient is quite small except for very small and very large drag coefficients.

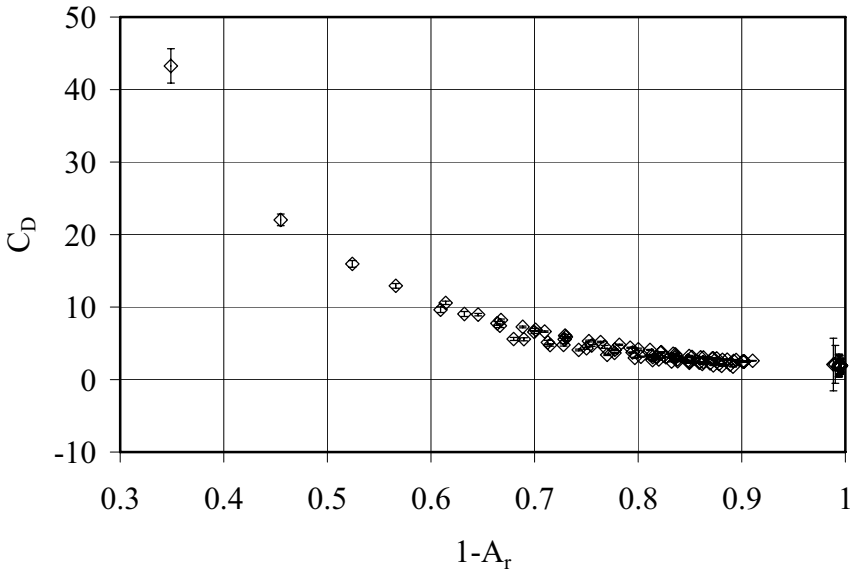

Figure C.2. Calculated drag coefficient, with the uncertainties included, versus the blockage ratio for a single submerged spur dike

C.4. Uncertainty of the calculated parameters for a single unsubmerged spur dike

Similar to the case of a submerged spur dike, the momentum equation was used to calculate the drag force of a single unsubmerged spur dike. The uncertainties of the parameters in the momentum equation including the flow depths (both upstream and uniform flow depths), the discharge and the fluid density were propagated into the calculated drag force using Eq. [C.1]. Figure C.3 represents the calculated drag force, with the uncertainties included, versus the measured drag force by the drag force measurement apparatus. Similar to submerged spur dikes, the calculated drag force is higher than the measured drag force.

The difference is attributed to the increased bed shear stress in the control volumes containing the spur dikes.

Figure C.4 represents the calculated drag coefficient of unsubmerged spur dikes, with the uncertainties included, versus the blockage ratio, A_r, and the flow depth to spur dike length ratio, h_l/L. The measured drag force by the apparatus was used to calculate the drag coefficient. In order to calculate the uncertainty of the drag coefficient, the uncertainties of the drag force, flow depth, discharge, spur dike length and the fluid density were applied using Eq. [C.1]. It is to be noted that the uncertainty is relatively high for small drag coefficients corresponding to small flow depth to spur dike length ratios. As the ratio of the flow depth to spur dike length increases, the uncertainty of the drag coefficient decreases.

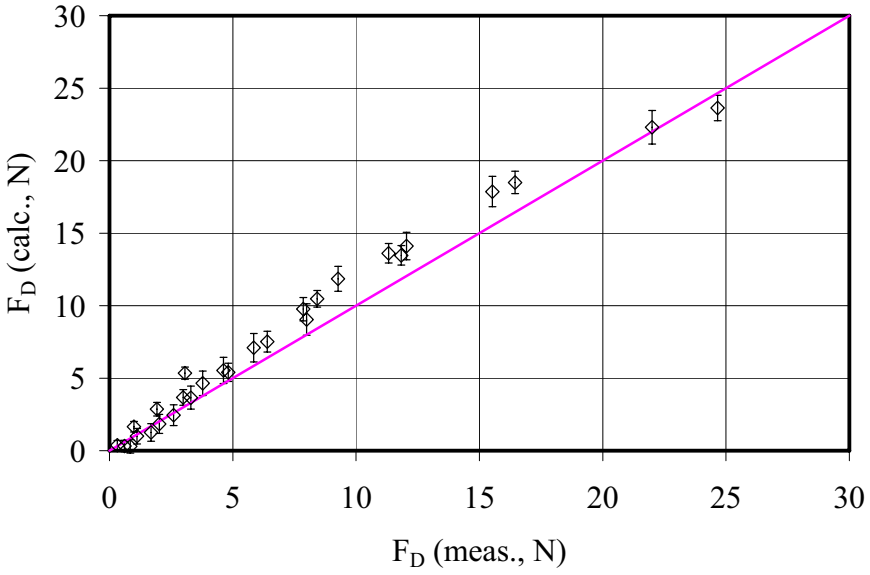

Figure C.3. Calculated drag force, with the uncertainties included, versus the measured drag force of a single unsubmerged spur dike

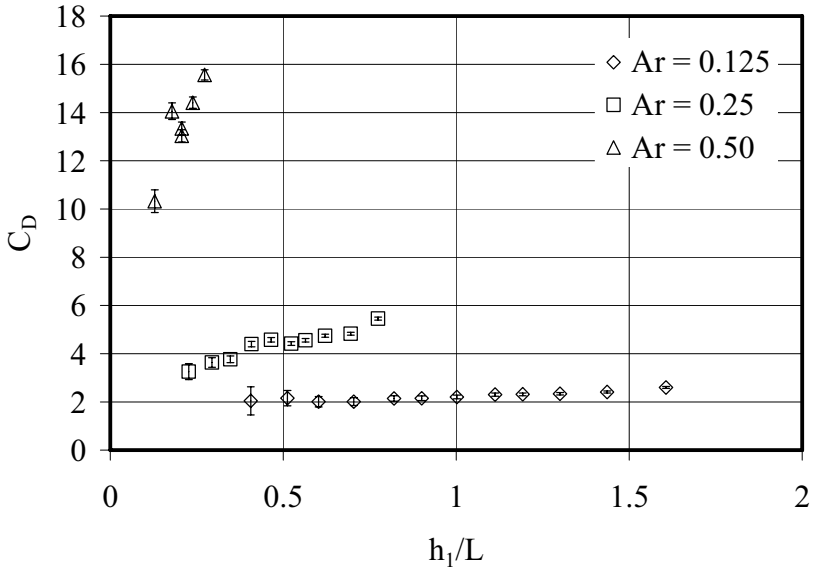

Figure C.4. Calculated drag coefficient, with the uncertainties included, versus the blockage and flow depth to spur dike length ratios for a single unsubmerged spur dike

C.5. Backwater effect calculations and corresponding uncertainty analysis for a single spur dike

The backwater effect due to a spur dike in an open channel flow is defined as the increased water level upstream of the dike over that which occurs without the dike in place. The backwater effect was measured directly in the flume experiments, and it was also calculated using Eq. [3.8]. In order to calculate the uncertainty of the backwater effect, the uncertainties of the drag force, uniform flow depth, discharge and the fluid density were used in Eq. [C.1]. Figure C.5 shows the calculated backwater effect, with the uncertainties included, versus the measured backwater effect for both submerged and unsubmerged spur dikes.

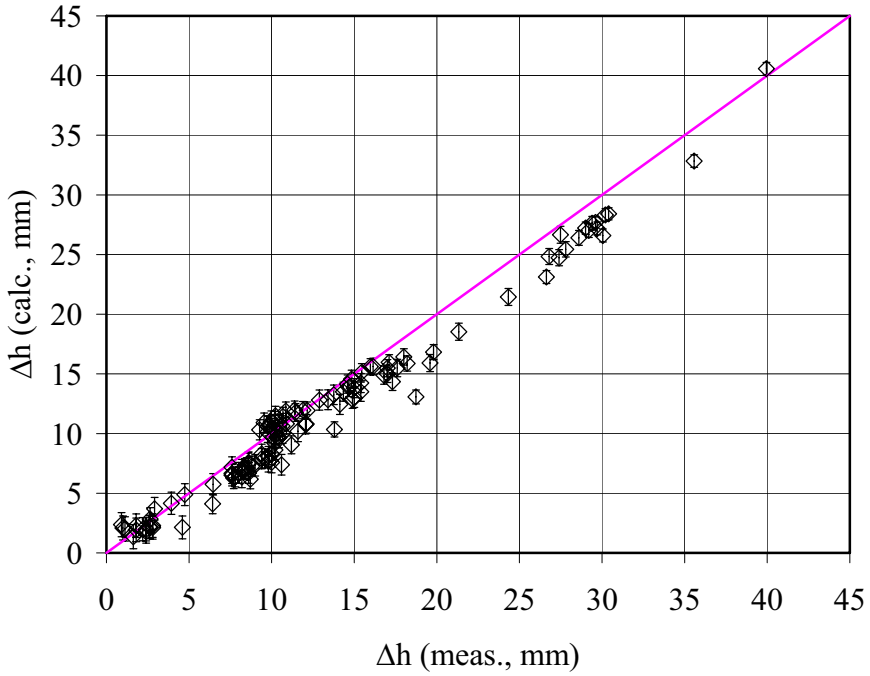

Figure C.5. Calculated backwater effect, with the uncertainties included, versus the measured backwater effect of a single spur dike in both submerged and unsubmerged flow conditions

Comparison of the above few figures in this appendix with similar figures in Chapter 3 shows that, in general, the magnitude of the uncertainties in a single spur dike does not have an impact on the interpretation of the results previously presented in Chapter 3.

C.6. Uncertainty of the relative and total relative drag forces for a spur dike field

Uncertainties associated with the relative drag force were calculated using Eq. [C.1]. In doing the analysis, the uncertainty of the drag force of each individual spur dike (i.e., F_{Di}) was determined as previously described at the beginning of this appendix. The uncertainty corresponding to the drag force due to a single spur dike, for each spur dike field arrangement, was assumed to be equal to the uncertainty of each individual spur dike in the spur dike field (i.e., $uF_D = uF_{Di}$.). On this basis, Eq. [C.1] is modified into the following equations for calculating the uncertainty of the relative drag force ($u\eta_i$) and the total relative drag force ($u\eta_t$), viz.

[C.2] $$u\eta_i = \frac{uF_D}{F_D}\sqrt{1+\eta_i^2}$$

[C.3] $$u\eta_t = \sqrt{\sum_{i=1}^{m} u\eta_i^2}$$

The variation of the relative and total relative drag forces, with the uncertainty included, for various flow conditions and spur dike configurations has been provided in Chapter 4. Two samples for spur dike fields having three spur dikes for both submerged and unsubmerged conditions are shown in Figure C.6. It is to be noted that the interpretation of the relative drag force variation with the relative spacing, which was presented in Chapter 4, is not influenced by introducing the uncertainty into the results. For example, there is a clear increase of the total relative drag force with the relative spacing even with the uncertainties attached to the results.

C.7. Backwater effect calculations and corresponding uncertainty analysis for a spur dike field

Similar to the case of a single spur dike, the backwater effect due to a spur dike field in an open channel is defined as the increased water level upstream of the most upstream spur dike over that which occurs without the dike in place. While the backwater effect was measured directly in the experiments with the physical model, it was also calculated using the following relationship, obtained from a combination of the momentum equation and the continuity equations, viz.

[C.10] $$\left(\frac{h_3}{h_2}\right)^3 - k_1\left(\frac{h_3}{h_2}\right) + k_2 = 0$$

where k_1 and k_2 are given by

[C.11a] $$k_1 = 1 + \frac{2F_{Dt}}{\rho g B h_2^2} + 2k_2$$

[C.11b] $k_2 = 2Fr_2^2$

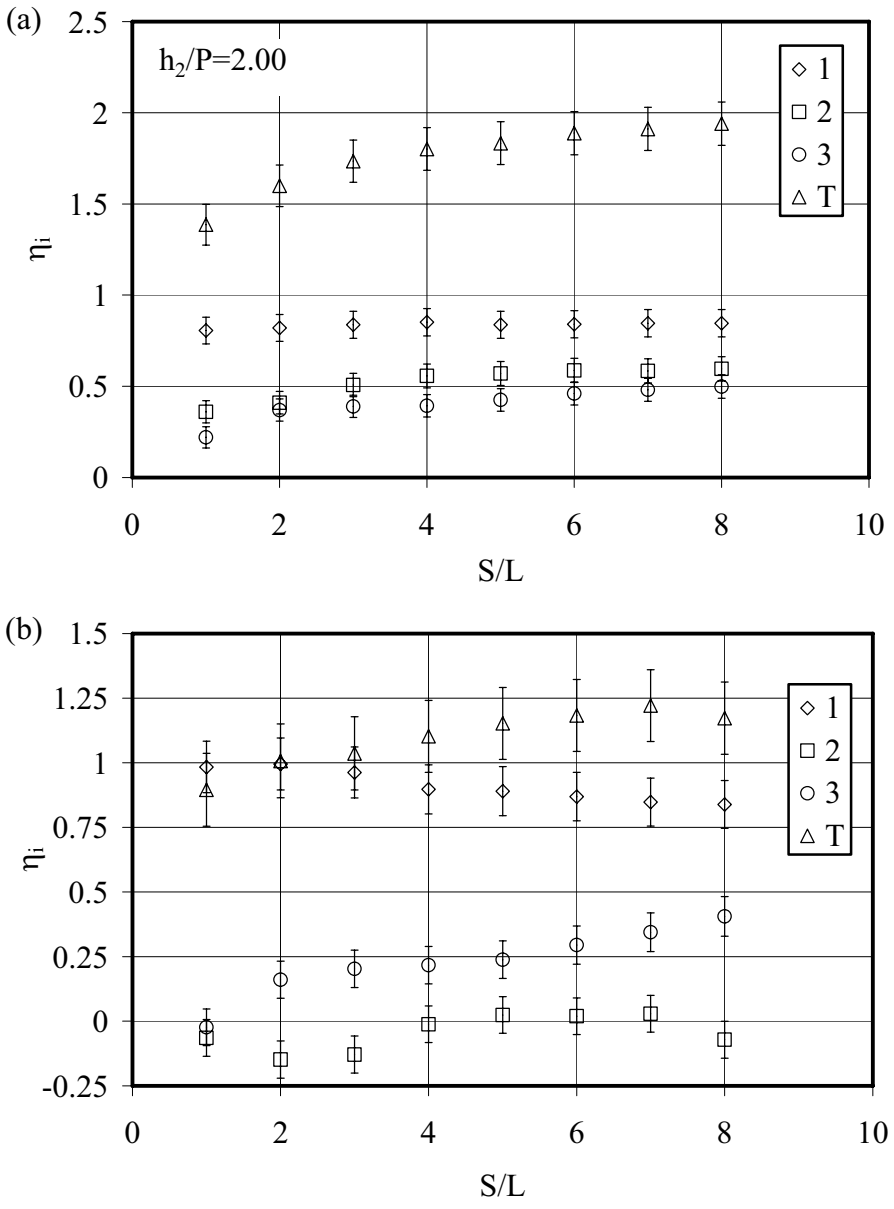

Figure C.6. Variation of the relative and total relative drag forces, with the uncertainties included, with relative spacing between spur dikes in a spur dike field having three spur dikes for: (a) submerged flow conditions, and (b) unsubmerged flow conditions

where Fr_2 is the Froude number of the uniform (or downstream) flow. Uncertainty of the backwater effect was calculated using Eq. [C.1] in which the uncertainties of the uniform

flow depth, total drag force and the Froude number were applied. The uncertainty of the total drag force was obtained using the uncertainty of the total relative drag force ($uF_{Dt} = u\eta_t F_D$). The uncertainty of the Froude number for uniform flow conditions was determined using the uncertainties of the uniform flow depth and the discharge. Figure C.8 represents the calculated backwater effect, with the uncertainties included, versus the measured backwater effect for spur dike fields. Figure C.8 shows the uncertainty of the backwater effect for spur dike fields is higher than that for single spur dikes. The higher uncertainty is probably related to the accumulated uncertainties of individual spur dikes in a spur dike field when compared to a single uncertainty of a single spur dike.

Comparison of the figures presented in this appendix for a spur dike field with similar figures in Chapter 4 shows that, in general, the inclusion of the uncertainties does not change the interpretation of the previously presented results in Chapter 4.

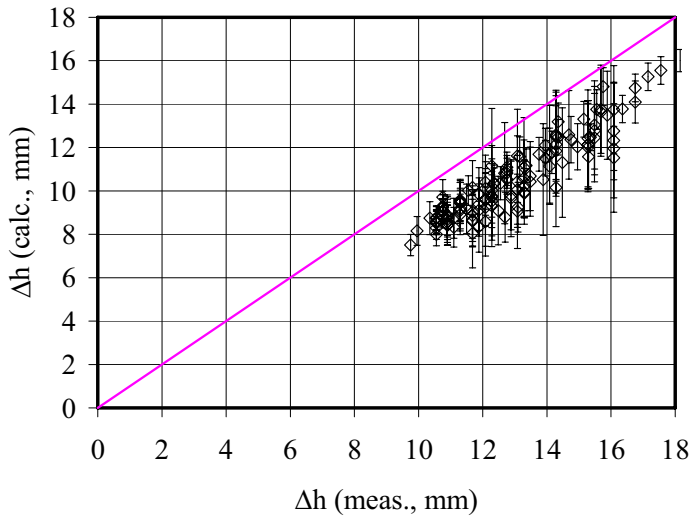

Figure C.7. Calculated backwater, with the uncertainties included, versus the measured backwater for a spur dike field

C.8. Reference

Coleman, W.H. and Steele, W.G. 1999. Experimentation and uncertainty analysis for engineers. John Wiley & Sons, Second Edition, New York, NY, USA, 275 p.